

University of Windsor

Scholarship at UWindor

Electronic Theses and Dissertations

Theses, Dissertations, and Major Papers

Winter 2014

Waste Heat Recovery Systems for Fuel Economy

Gianmarco Capano
University of Windsor

Follow this and additional works at: <https://scholar.uwindsor.ca/etd>



Part of the [Mechanical Engineering Commons](#)

Recommended Citation

Capano, Gianmarco, "Waste Heat Recovery Systems for Fuel Economy" (2014). *Electronic Theses and Dissertations*. 5015.

<https://scholar.uwindsor.ca/etd/5015>

This online database contains the full-text of PhD dissertations and Masters' theses of University of Windsor students from 1954 forward. These documents are made available for personal study and research purposes only, in accordance with the Canadian Copyright Act and the Creative Commons license—CC BY-NC-ND (Attribution, Non-Commercial, No Derivative Works). Under this license, works must always be attributed to the copyright holder (original author), cannot be used for any commercial purposes, and may not be altered. Any other use would require the permission of the copyright holder. Students may inquire about withdrawing their dissertation and/or thesis from this database. For additional inquiries, please contact the repository administrator via email (scholarship@uwindsor.ca) or by telephone at 519-253-3000ext. 3208.

Waste Heat Recovery Systems for Fuel Economy

By

Gianmarco Capano

A Thesis

Submitted to the Faculty of Graduate Studies
through Mechanical, Automotive and Materials Engineering
in Partial Fulfillment of the Requirements for
the Degree of Master of Applied Science
at the University of Windsor

Windsor, Ontario, Canada

2013

© 2013 Gianmarco Capano

Waste Heat Recovery Systems for Fuel Economy

by

Gianmarco Capano

APPROVED BY:

Randy Bowers

Department of Mechanical, Automotive & Materials Engineering

Amir Fartaj

Department of Mechanical, Automotive & Materials Engineering

Andrzej Sobiesiak, Advisor

Department head (Mechanical, Automotive & Materials Engineering)
Department of Mechanical Automotive & Materials Engineering

10/28/2013

DECLARATION OF ORIGINALITY

I hereby certify that I am the sole author of this thesis and that no part of this thesis has been published or submitted for publication.

I certify that, to the best of my knowledge, my thesis does not infringe upon anyone's copyright nor violate any proprietary rights and that any ideas, techniques, quotations, or any other material from the work of other people included in my thesis, published or otherwise, are fully acknowledged in accordance with the standard referencing practices. Furthermore, to the extent that I have included copyrighted material that surpasses the bounds of fair dealing within the meaning of the Canada Copyright Act, I certify that I have obtained a written permission from the copyright owner(s) to include such material(s) in my thesis and have included copies of such copyright clearances to my appendix.

I declare that this is a true copy of my thesis, including any final revisions, as approved by my thesis committee and the Graduate Studies office, and that this thesis has not been submitted for a higher degree to any other University or Institution.

ABSTRACT

The largest automakers strive to reduce carbon dioxide emissions to meet regulations by improving engine efficiency. A device that recovers a portion of the heat wasted in the exhaust gas could be a highly effective solution. It is believed that the most appealing technology is the Organic Rankine Cycle for its ability to recover heat from low temperature sources and its limited costs. However, Waste Heat Recovery (WHR) is still far from being employed in mass production light duty vehicles because there are still several unsolved problems. To assess the feasibility of such devices it is fundamental to develop a simulation tool able to replicate the behavior of a WHR system. This thesis discusses the main topics and pitfalls associated with the application of an Organic Rankine Cycle to recover energy in the operating of light duty vehicles. The simulation tool which was developed by the author to compare the design alternatives and quantify the potential benefits in terms of amount of energy that can be recovered, is illustrated and its functioning is explained in details. The simulation results are thoroughly examined.

DEDICATION

To my parents,

the people that taught me the meaning of love by dedicating to me, and my sister, more time than what they have dedicated to themselves.

ACKNOWLEDGEMENTS

This thesis is the culmination of a two year Double Degree Master program that was possible only with the collaboration and organization efforts of two universities, University of Windsor and Politecnico di Torino, and two leading automotive companies Fiat Group Automobile and Chrysler LLC.

Therefore I would like to express my deepest appreciation to the persons who represent these aforementioned institutions and played a decisive role in coordinating the whole program, Dr. Peter Frise, Prof. Giovanni Belingardi, Edoardo Rabino and Mohammed Malik.

I offer my sincere gratitude to my academic advisors Dr. Andrzej Sobiesiak and Prof. Ezio Spessa that have supervised my activities closely and supported me throughout my thesis with their knowledge whilst allowing me the room to work in my own way.

However, it wouldn't be possible to write this thesis without the direct technical support of Fiat and Chrysler. So I am profoundly grateful to my advisors Daniela Magnetto, Kevin Laboe and Daniel Hornback for their patience and their precious assistance that have guided me from the beginning to the final act of this project.

I would like also to express my gratitude to all the people, that do not figure as my advisors, but that have helped me in my daily activities at Fiat and Chrysler, and that with their kindness and experience have allowed me to learn and grow up as an engineer as well as a person, Mitchell Zajack, Matthew Bartlett, Timothy Scott, Antonio Mancina, Andrea Perosino, Federica Bettoja, Matteo Rostagno, Fausto Di Sciulo, Fabrizio Mattiello, Riccardo Seccardini and Marcello Canova.

A special thanks goes also to Mike Huston, Jan Stewart and Rosemarie Gignac for the tremendous help that they have provided during the time spent in Windsor.

I would like to thank my committee members, Dr. Amir Fartaj and Dr. Randy Bowers whose work have helped me to refine the thesis improving the quality of my work.

I am profoundly thankful to my parents the people that have always encouraged me morally and sustained me economically throughout my studies. Without their dedication I wouldn't have achieved any of this.

My girlfriend, Regina, deserves a special mention because she supported me despite the distance.

Finally I would like to thank my friends who shared with me this great experience, Andrea, Carlo, Gabriele, Maurizio and Yupeng, my lovely little sister, Laura.

TABLE OF CONTENTS

DECLARATION OF ORIGINALITY	iii
ABSTRACT	iv
DEDICATION	v
ACKNOWLEDGEMENTS	vi
LIST OF TABLES	x
LIST OF FIGURES	xii
LIST OF ABBREVIATIONS/SYMBOLS	xvii
NOMENCLATURE	xix
1. INTRODUCTION	1
1.1 Problem statement	1
1.2 Objectives	2
1.3 Methodology	2
1.4 Thesis Organization	3
2. REVIEW OF LITERATURE	4
2.1 Review of thermodynamics	4
2.1.1 Carnot cycle	4
2.1.2 Rankine cycle	6
2.1.3 Superheat Rankine cycle	9
2.1.4 Recuperative Rankine Cycle	11
2.1.5 Supercritical Rankine Cycle	14
2.1.6 Additional considerations	15
2.1.7 Rankine cycle summary	16
2.2 Waste Heat Recovery	17
2.2.1 WHR importance in automotive industry	18
2.2.2 WHR potential and alternatives	19

2.2.3	Thermal Electric generators WHR system.....	21
2.2.4	Organic Rankine Cycle WHR system.....	22
2.2.5	Gasoline vs diesel engines	26
2.2.6	Other considerations on WHR based on ORC in automotive industry.....	28
2.3	ORC working fluids.....	29
2.3.1	Thermodynamic and physical properties	30
2.3.2	Chemical compatibility with materials in contact.....	31
2.3.3	Safety	32
2.3.4	Environmental aspects	32
2.3.5	Availability and cost	33
2.4	ORC vs steam Rankine cycle.....	34
2.5	ORC components modeling.....	36
2.5.1	Expander	36
2.5.2	Heat exchangers	43
3.	SIMULATION TOOLS DEVELOPMENT.....	47
3.1	Preliminary model of ORC for assessing design alternatives.....	47
3.1.1	Preliminary model input data.....	47
3.1.2	Algorithm resolution.....	51
3.1.3	Data treatment.....	58
3.2	Detailed model of the WHR unit based on an ORC	58
3.2.1	Detailed model input data	60
3.2.2	Algorithm resolution.....	64
3.3	Comparison between preliminary and detailed models	102
4.	ANALYSIS AND DISCUSSION OF THE SIMULATION RESULTS	104
4.1	Preliminary analysis of ORC design alternatives.....	104
4.1.1	Operating parameters that maximize the performances.....	106
4.1.2	System layout comparison	111

4.1.3	Working fluids preliminary comparison	117
4.1.4	Considerations on the design alternatives	125
4.2	Detailed analysis of the WHR unit based on a ORC installed in a vehicle.....	126
4.2.1	Calibration of the detailed model	126
4.2.2	Steady state analysis at target operating conditions	139
4.2.3	Working fluid comparison at steady state	156
4.2.4	WHR unit integration with the engine and creation of the net power output map.....	159
4.2.5	WHR unit simulation on a standard driving cycle	165
5.	CONCLUSIONS AND RECOMMENDATIONS	175
5.1	Methodology summary	175
5.2	Preliminary model findings.....	175
5.3	Detailed model findings and results	176
5.4	Recommendations	177
	Bibliography	179
	VITA AUCTORIS	185

LIST OF TABLES

Table 4.1-1: Design point exhaust gas parameters.	104
Table 4.1-2: Components characteristics.	104
Table 4.1-3.	105
Table 4.1-4: Best performance with a standard ORC, $T_{\text{cond}} = 45\text{ }^{\circ}\text{C}$	110
Table 4.1-5: Best performance with a recuperative ORC, $T_{\text{cond}} = 45\text{ }^{\circ}\text{C}$	110
Table 4.1-6: Maximum net power output achievable with different working fluids with standard ORC (blue columns) and recuperative ORC (red columns), $T_{\text{cond}} = 35\text{ }^{\circ}\text{C}$	119
Table 4.1-7: Thermodynamic and physical properties of the organic working fluids plus water.	120
Table 4.1-8: Safety group and pollution indexes of the working fluids analyzed.	123
Table 4.1-9: Lowest pressure around the cycle of each working fluid.	124
Table 4.2-1: Measured temperatures and pressures at the inlet and outlet of each component, T boiler out = $150\text{ }^{\circ}\text{C}$	129
Table 4.2-2: Measured cycle outputs, T boiler out = $150\text{ }^{\circ}\text{C}$	129
Table 4.2-3: Detailed model simulation inputs, T boiler out = $150\text{ }^{\circ}\text{C}$	130
Table 4.2-4: Simulated temperatures and pressures at the inlet and outlet of each component, T boiler out = $150\text{ }^{\circ}\text{C}$, null pipe pressure drop.	131
Table 4.2-5: Simulated cycle outputs, T boiler out = $150\text{ }^{\circ}\text{C}$, null pipe pressure drop.	132
Table 4.2-6: Error percentage between the simulated and measured variables, T boiler out = $150\text{ }^{\circ}\text{C}$, null pipe pressure drop.	132
Table 4.2-7: Error percentage between the simulated and measured variables, T boiler out = $150\text{ }^{\circ}\text{C}$, null pipe pressure drop.	133
Table 4.2-8: Pipes characteristics of the test rig available at the CRF.	134
Table 4.2-9: Simulated temperatures and pressures at the inlet and outlet of each component, T boiler out = $150\text{ }^{\circ}\text{C}$, non-null pipe pressure drop.	134
Table 4.2-10: Simulated cycle outputs, T boiler out = $150\text{ }^{\circ}\text{C}$, non-null pipe pressure drop.	134
Table 4.2-11: Error percentage between the simulated and measured variables, T boiler out = $150\text{ }^{\circ}\text{C}$, non-null pipe pressure drop.	135
Table 4.2-12: Error percentage between the simulated and measured variables, T boiler out = $150\text{ }^{\circ}\text{C}$, non-null pipe pressure drop.	135
Table 4.2-13: Pressure drop in pipes; measured (left side) and simulated (right side).	136

Table 4.2-14: Temperatures and pressures at the inlet and outlet of each component; measured data on the left, simulation data in the middle and percentage error on the right, T boiler out = 140 °C.	137
Table 4.2-15: Cycle outputs; measured data on the left, simulation data in the middle and percentage error on the right T boiler out = 140 °C.	137
Table 4.2-16: Temperatures and pressures at the inlet and outlet of each component; measured data on the left, simulation data in the middle and percentage error on the right, T boiler out = 130 °C.	138
Table 4.2-17: Cycle outputs; measured data on the left, simulation data in the middle and percentage error on the right T boiler out = 130 °C.	138
Table 4.2-18: Temperatures and pressures at the inlet and outlet of each component; measured data on the left, simulation data in the middle and percentage error on the right, T boiler out = 120 °C.	139
Table 4.2-19: Cycle outputs; measured data on the left, simulation data in the middle and percentage error on the right T boiler out = 120 °C.	139
Table 4.2-20: Input data about the geometry of the system.	145
Table 4.2-21: Heat exchanger pressure drop effect on the net power output.	153
Table 4.2-22: Pipe diameter effect on pipe pressure drop.	155
Table 4.2-23: Working fluid tested list.	156
Table 4.2-24: Main outputs of the cycle, working fluids comparison.	157
Table 4.2-25: Minimum and maximum engine and expander rotational speeds with a speed ratio of 5.1.	161
Table 4.2-26: Exhaust gas condition that maximize the power output of the WHR unit.	164
Table 4.2-27: Driving cycle simulation results summary.	173

LIST OF FIGURES

Figure 2.1-1: Carnot cycle on T-s diagram.....	5
Figure 2.1-2: Rankine cycle system layout.....	6
Figure 2.1-3: Rankine cycle on T-s diagram.....	7
Figure 2.1-4: Rankine cycle on p-h diagram.....	8
Figure 2.1-5: Superheat Rankine cycle on T-s diagram.....	10
Figure 2.1-6: Superheat Rankine cycle on p-h diagram.....	10
Figure 2.1-7: Recuperative Rankine cycle system layout.....	12
Figure 2.1-8: Recuperative Rankine cycle on T-s diagram.....	13
Figure 2.1-9: Supercritical Rankine cycle on T-s diagram.....	15
Figure 2.2-1: Average CO ₂ emissions of main car manufacturers in Europe (2006) [16].....	18
Figure 2.2-2: Percentage of total CO ₂ emissions in Europe (2007) [15].	19
Figure 2.2-3: Energy flow of an automobile [18].	20
Figure 2.2-4: Energy distribution of a 1.3L gasoline engine at 3000 RPM [20].	20
Figure 2.2-5: Energy distribution of a 1.3l gasoline engine at a given load [20].....	21
Figure 2.2-6: Cummins WHR system with recuperative ORC [29].	23
Figure 2.2-7: Energy flow of a typical high duty and high EGR rate diesel engine [26].	24
Figure 2.2-8: BMW study on Waste Heat Recovery alternatives [33].	25
Figure 2.2-9: Three-way catalytic conversion as a function of air fuel ratio [17].	26
Figure 2.2-10: Selective Catalytic Reduction system layout [35].....	27
Figure 2.3-1: Types of working fluids: dry, isentropic and wet [39].	30
Figure 2.3-2: ASHRAE Standard 34-2007 safety classification [38].	32
Figure 2.4-1: Saturation curves on T-s diagram.	35
Figure 2.5-1: Schematic drawing of a micro turbine utilized in ORC applications [43].	37
Figure 2.5-2: Schematic drawing of a reciprocating piston type of expander [51].....	38
Figure 2.5-3: Schematic drawing of a rotary vane type of expander [10].	38
Figure 2.5-4: Schematic drawing of a rolling piston type of expander [10].	39
Figure 2.5-5: Schematic drawing of a scroll type of expander [49].....	40
Figure 2.5-6: Conceptual scheme of a scroll expander model [55].	41
Figure 2.5-7: Suction chamber of a scroll expander [55].....	42
Figure 2.5-8: Conceptual scheme of a scroll expander model [56].	43
Figure 2.5-9: Layout of the shell and tube evaporator [32].	44
Figure 2.5-10: Heat transfer model of a counter flow heat exchanger [64].	45
Figure 2.5-11: Evaporator temperature profile.	46

Figure 3.1-1: Recuperative ORC system layout for preliminary analysis.	48
Figure 3.1-2: First input window of the preliminary model.	48
Figure 3.1-3: R245fa Mollier diagram.	49
Figure 3.1-4: Second input window of the preliminary model.7	50
Figure 3.1-5: Third input window of the preliminary model.	50
Figure 3.1-6: Fourth input window of the preliminary model.	51
Figure 3.1-7: Fifth input window of the preliminary model.	51
Figure 3.1-8: Working fluid array, state 1 thermodynamic properties and definition of the range of p_2 and T_3	52
Figure 3.1-9: State 2 thermodynamic properties.	53
Figure 3.1-10: State 3 and 4 thermodynamic properties.	53
Figure 3.1-11: State 2' and 4' thermodynamic properties.	55
Figure 3.1-12: Working fluid mass flow rate, net power output and heat transfer rate in the heat exchangers.	57
Figure 3.1-13: Efficiencies.	58
Figure 3.2-1: Recuperative ORC system layout for detailed analysis.	59
Figure 3.2-2: Detailed model outside user interface.	59
Figure 3.2-3: Input window of the detailed model.	61
Figure 3.2-4: Logic blocks resolution sequence.	65
Figure 3.2-5: Working fluid switch.	66
Figure 3.2-6: Pump functional block.	67
Figure 3.2-7: Thermodynamic properties at the pump inlet and outlet.	68
Figure 3.2-8: Saturation block.	69
Figure 3.2-9: Pump efficiency and speed maps reader.	69
Figure 3.2-10: Curve fitting tool screen shot, pump efficiency map creation.	70
Figure 3.2-11: "Pump_parameters.m".	71
Figure 3.2-12: Expander functional block.	72
Figure 3.2-13: Pressure ratio across the expander.	72
Figure 3.2-14: Thermodynamic properties at the inlet and outlet of the expander.	73
Figure 3.2-15: Expander efficiency, speed and maximum volume flow rate generator.	74
Figure 3.2-16: "Expander_parameters.m".	74
Figure 3.2-17: Recuperator functional block.	77
Figure 3.2-18: Thermodynamic properties at the recuperator inlet.	78
Figure 3.2-19: Thermodynamic properties at the recuperator outlet.	78

Figure 3.2-20: Pinch point temperature difference and vapor quality verifications.	80
Figure 3.2-21: Thermodynamic properties at the condenser inlet, in the case there is no recuperator.	81
Figure 3.2-22: Boiler functional block.....	82
Figure 3.2-23: Thermodynamic properties at the boiler inlet and exhaust gas outlet temperature.	83
Figure 3.2-24: Mass flow rate of the working fluid determination.....	83
Figure 3.2-25: Boiler pinch point verification.	84
Figure 3.2-26: Mass flow rate of the working fluid final verification.	85
Figure 3.2-27: Power balance functional block.	86
Figure 3.2-28: Mass flow rate inside the components.	87
Figure 3.2-29: Power balance outputs.....	88
Figure 3.2-30:Condenser functional block.....	88
Figure 3.2-31: Thermodynamic properties at the condenser inlet and outlet.....	89
Figure 3.2-32: Condenser resolution, first part.	90
Figure 3.2-33: Condenser resolution, second part.	91
Figure 3.2-34: Heat exchanger effectiveness functional block.	93
Figure 3.2-35: Recuperator effectiveness map creation with curve fitting tool.....	94
Figure 3.2-36: Recuperator effectiveness map reader.....	95
Figure 3.2-37: C^* and NTU determination.....	95
Figure 3.2-38: Heat exchanger effectiveness determination.....	96
Figure 3.2-39: Heat exchangers pressure drop functional block.....	96
Figure 3.2-40: Determination of the pressure drop inside the heat exchangers.....	97
Figure 3.2-41: Pressure drop in the pipes functional block.	98
Figure 3.2-42: Pressure drop inside pipe 1.	100
Figure 3.2-43: General outputs plot.	101
Figure 4.1-1: Pump inlet pressure, corresponding to the saturated liquid pressure at 45 °C.	111
Figure 4.1-2: Net power output, system layout comparison, $T_{\text{cond}} = 45 \text{ }^\circ\text{C}$	112
Figure 4.1-3: Cycle efficiency, system layout comparison, $T_{\text{cond}} = 45 \text{ }^\circ\text{C}$	115
Figure 4.1-4: Working fluid mass flow rate, system layout comparison, $T_{\text{cond}} = 45 \text{ }^\circ\text{C}$	116
Figure 4.1-5: Net power output achievable with different working fluids in a recuperative ORC (left) and a standard ORC (right), $T_{\text{cond}} = 35 \text{ }^\circ\text{C}$	117
Figure 4.1-6: T-s plots of the standard ORCs that give the maximum net power output for each working fluid, $T_{\text{cond}} = 35 \text{ }^\circ\text{C}$	121

Figure 4.1-7: T-s plots of the recuperative ORCs that give the maximum net power output for each working fluid, $T_{\text{cond}} = 35 \text{ }^\circ\text{C}$.	122
Figure 4.2-1: Standard ORC test rig facility at the CRF.	128
Figure 4.2-2: Pressure drop inside the heat exchanger. Referring to the recuperator HPS and LPS mean respectively High Pressure Side and Low Pressure Side.	140
Figure 4.2-3: Boiler effectiveness map built from the experimental data furnished by the supplier.	141
Figure 4.2-4: Condenser effectiveness map built from the experimental data furnished by the supplier.	141
Figure 4.2-5: Recuperator effectiveness map built from the experimental data furnished by the supplier.	142
Figure 4.2-6: Expander efficiency map.	142
Figure 4.2-7: Pump efficiency map.	143
Figure 4.2-8: Expander volume flow rate (VFR) map.	144
Figure 4.2-9: Pump operating parameters.	146
Figure 4.2-10: Boiler operating parameters.	147
Figure 4.2-11: Expander operating parameters.	148
Figure 4.2-12: Recuperator operating parameters.	148
Figure 4.2-13: Condenser operating parameters.	149
Figure 4.2-14: Coolant fluid parameters.	150
Figure 4.2-15: Exhaust gas operating parameters.	150
Figure 4.2-16: Heat exchanger effectiveness.	152
Figure 4.2-17: Heat exchanger pressure drop.	152
Figure 4.2-18: Pipe pressure drop.	154
Figure 4.2-19: General output parameters of the WHR unit.	154
Figure 4.2-20: Exhaust gas mass flow rate map.	162
Figure 4.2-21: Exhaust gas temperature map.	162
Figure 4.2-22: Net power output of the WHR unit map, speed ratio: 5.1.	163
Figure 4.2-23: Top view of the net power output map, speed ratio: 5.1.	164
Figure 4.2-24: FTP-75 driving speed schedule [67].	166
Figure 4.2-25: HWFET driving speed schedule [67].	167
Figure 4.2-26: Net power output of the WHR unit map, speed ratio: 7.5.	168
Figure 4.2-27: Engine speed profile, FTP-75 + HWFET.	168
Figure 4.2-28: Throttle position profile, FTP-75 + HWFET.	169

Figure 4.2-29: Exhaust gas temperature profile, FTP-75 + HWFET.....	170
Figure 4.2-30: Exhaust gas mass flow rate profile, FTP-75 + HWFET.	170
Figure 4.2-31: Exhaust gas heat available profile, FTP-75 + HWFET.....	171
Figure 4.2-32: Net power output of the WHR unit, FTP-75 + HWFET.....	172
Figure 4.2-33: Total energy recovered by the WHR unit, FTP-75 + HWFET.	172
Figure 4.2-34: WHR unit total efficiency profile, FTP-75 + HWFET.	174

LIST OF ABBREVIATIONS/SYMBOLS

°C	Celsius
ALT	Atmospheric Lifetime
ASHRAE	American Society of Heating, Refrigerating and Air Conditioning Engineers
bar	Bar pressure
CFC	Chlorofluorocarbon
CO	Carbon monoxide
CO ₂	Carbon dioxide
CRF	Centro Ricerche Fiat
EGR	Exhaust Gas Recirculation
EPA	Environmental Protection Agency
Exp	Expander
FTP-75	Federal Test Procedure
GWP	Global Warming Potential
HC	Hydrocarbon
HCFC	Hydrochlorofluorocarbon
HEX	Heat Exchanger
HFC	Hydrofluorocarbons
HPS	High Pressure Side
HWFET	High Way Fuel Economy Test
Hz	Hertz
J	Joule
K	Kelvin
kg	Kilograms
kJ	Kilo Joule
km/h	Kilometer per hour
kPa	Kilo Pascal
kW	Kilo Watt
L	Liter
LPS	Low Pressure Side
m	Meter
MAX	Maximum

MFR	Mass Flow Rate
MIN	Minimum
MPH	Miles per hour
MW	Mega Watt
NEDC	New European Driving Cycle
Nm	Newton meter
NO _x	Nitrogen oxides
NSCR	Non-Selective Catalytic Reduction
ODP	Ozone Depletion Potential
ORC	Organic Rankine Cycle
Pa	Pascal
Rec	Recuperative
RPM	Revolutions Per Minute
s	Second
Stan	Standard
Sub	Sub-cooling
SUV	Sport Utility Vehicle
TE	Thermo Electric
VFR	Volume Flow Rate
W	Watt
WHR	Waste Heat Recovery
' = p	The superscript meaning “prime” is substituted by the subscript “p” in some figures derived from the software Matlab.
“ = s	The superscript meaning “second” is substituted by the subscript “s” in some figures derived from the software Matlab.

NOMENCLATURE

$\dot{Q}_{available}$	Heat transfer rate available
\dot{Q}_{ij}	Heat transfer rate between state i and j
$\dot{W}_{accessories}$	Accessories power
\dot{W}_{exp}	Expander power
$\dot{W}_{friction}$	Friction power
\dot{W}_{ij}	Power absorbed/generated between state i and i
\dot{W}_{net}	Net power
\dot{W}_{pump}	Pump power
\dot{W}_{useful}	Useful power
\dot{m}_h	Hot fluid mass flow rate
\dot{m}_c	Cold fluid mass flow rate
$\dot{m}_{exh,boil}$	Exhaust gas mass flow rate inside the boiler
\dot{m}_{exh}	Exhaust gas mass flow rate
\dot{m}_{wf}	Working fluid mass flow rate
$\Delta h_{isentropic}$	Isentropic enthalpy difference across the expander
ΔH_{vap}	Enthalpy of vaporization
Δp_{ij}	Pressure drop between state i and j
C^*	Heat capacity rate ratio
C_{max}	Maximum heat capacity rate
C_{min}	Minimum heat capacity rate
C_{source}	Heat capacity rate of the heat source
Q_{cw}	Heat ejected by the coolant
Q_{eg}	Heat ejected by the exhaust gas
Q_r	Heat ejected by the lubricant
Q_{tot}	Total heat generated by the from fuel combustion
Q_w	Heat converted into mechanical work
$X_{measured}$	General variable measured
$X_{simulated}$	General variable obtained through simulation
\dot{m}	Mass flow rate
ε_{boil}	Boiler effectiveness

ε_{cond}	Condenser effectiveness
ε_{rec}	Recuperator effectiveness
η_{carnot}	Carnot cycle efficiency
η_{cycle}	Rankine cycle efficiency
$\eta_{evaporator}$	Evaporator efficiency
η_{exp}	Expander isentropic efficiency
$\eta_{organic}$	Organic efficiency
η_{pump}	Pump efficiency
$\eta_{recovery}$	Recovery efficiency
η_{total}	Total efficiency
ΔT	Temperature difference
A	Area
$boil,in$	Boiler inlet state
$boil,out$	Boiler outlet state
$cond,in$	Condenser inlet state
$cond,out$	Condenser outlet state
cp_{exh}	Exhaust gas specific heat
cp_i	Specific heat at <i>state i</i>
D	Diameter
E	Voltage potential difference
Error	Percentage error
exp,in	Expander inlet state
exp,out	Expander outlet state
f_D	Darcy friction factor
h_i	Enthalpy per unit mass at <i>state i</i>
K_b	Bend pressure loss coefficient
$K_{b,t}$	Total pressure loss coefficient
$LMTD$	Log Mean Temperature Difference
MFR	Mass Flow Rate
NTU	Number of transfer units
p_{ad}	Internal mass flow rate expander outlet pressure

p_{cr}	Pressure at critical point
p_{ex}	External mass flow rate expander outlet pressure
p_i	Pressure at <i>state i</i>
p_{ratio}	Pressure at the expander outlet over pressure at the expander inlet
<i>Pump head</i>	Pump pressure rise
<i>pump,in</i>	Pump inlet state
<i>pump,out</i>	Pump outlet state
q	Heat
Re	Reynolds number
<i>rec,high,in</i>	Recuperator high pressure side inlet state
<i>rec,high,out</i>	Recuperator high pressure side outlet state
<i>rec,low,in</i>	Recuperator low pressure side inlet state
<i>rec,low,out</i>	Recuperator low pressure side outlet state
s_i	Entropy per unit mass <i>state i</i>
<i>State 1</i>	Pump inlet
<i>State 2</i>	Pump outlet
<i>State 2'</i>	Saturated liquid
<i>State 2_r</i>	Recuperator high pressure side outlet
<i>State 2_s</i>	Pump outlet isentropic compression
<i>State 3</i>	Expander inlet
<i>State 3'</i>	Saturated vapor
<i>State 4</i>	Expander outlet
<i>State 4_{ideal}</i>	Expander outlet isentropic expansion
<i>State 4_r</i>	Recuperator low pressure side outlet
<i>State 4_s</i>	Expander outlet isentropic expansion
T	Low temperature of a Carnot cycle
T^+	High temperature of a Carnot cycle
T_{boil}	Boiling temperature
T_c	Cold side temperature
T_{cond}	Condensation temperature
$T_{control}$	Minimum temperature at which the WHR unit is turned on

$T_{coolant,in}$	Coolant inlet temperature
$T_{coolant,out}$	Coolant outlet temperature
T_{cr}	Temperature at the critical point
$T_{environment}$	Ambient temperature
T_{evap}	Evaporation temperature
$T_{exh,in}$	Exhaust gas inlet temperature
$T_{exh,min}$	Minimum exhaust gas temperature
$T_{exh,out}$	Exhaust gas outlet temperature
T_h	Hot side temperature
T_i	Temperature at <i>state i</i>
T_{pinch}	Temperature difference at the pinch point
T_{source}	Temperature of the heat source
$T_{subcooling}$	Sub-cooling temperature at pump inlet
U	Overall heat transfer coefficient
w_{exp}	Expander work per unit mass
$w_{exp,act}$	Actual expander work per unit mass
w_{ij}	Work per unit mass between state <i>i</i> and <i>j</i>
w_{pump}	Pumping work per unit mass
α	Seebeck coefficient
β	Pump compression ratio
ξ	Inverse of the slope of the saturated vapor curve
ρ_i	Density at <i>state i</i>
ε	Heat exchanger effectiveness
ν	Kinematic viscosity

1. INTRODUCTION

The reduction of the impact that product and process have on the environment is one of the Fiat and Chrysler group's principal priorities. The research centers of the group are cooperating to reach the goal of increase the fuel economy of their products, in order to reduce carbon dioxide emissions, focusing in five key areas: optimize the fuel economy of existing engines, increase the use of alternative fuels, develop non-conventional propulsion systems, reduce vehicle energy demand and design system to cut emissions. For what concerns the latter key area, the feasibility of systems able to recover a portion of the waste heat from light duty vehicles is being assessed.

As a matter of fact, an average 35% of the energy produced in an internal combustion engine is dissipated in the exhaust gas, so a system that is able to partially recover this wasted energy could be an highly effective solution to increase the efficiency of the engine and, thus, to reduce its emissions.

Waste Heat Recovery systems are well-known in other industrial sectors, such as in power generation plants, and have lately attracted all the main automakers for the potential fuel savings that they can provide. The most attractive technologies for this purpose appears to be an Organic Rankine Cycle whose vehicle application will be treated in this thesis.

Nonetheless, despite the great innovation that these devices can bring, there are still a lot of challenges that the designers have to face before considering to introduce them in mass production vehicles. The non-stationary conditions of the exhaust gas of a vehicle, the small space under the hood, the cost of the components, the controls of the system are just a short list of the problems that have to be solved to adapt a Waste Heat Recovery system from stationary application in power generation plants.

In this scenario it is fundamental, especially in the early design stages to be able to simulate first and then test the behavior of these devices, certifying the potential fuel savings and that the system can safely operate in a vehicle.

1.1 Problem statement

As previously mentioned, simulation is a strategic action necessary in any research activities especially when innovative devices have to be introduced. It helps the decision process of selecting the proper design strategy among the multiple alternatives available.

Centro Ricerche Fiat (Fiat Research Center) and Chrysler LLC have not yet developed a simulation tool able to predict the behavior and performances of a Waste Heat Recovery unit based on Organic Rankine Cycle technology.

A flexible tool adaptable to any kind of configuration of the Waste Heat Recovery unit is then necessary. The details of the information about the WHR system are not very deep in the early design phases, so the degree of detail of the simulation tool has to be flexible. Once this model is created the following stage (not considered in the thesis) would be, the integration of such a model in a global virtual model of a vehicle and analyze the potential fuel savings.

1.2 Objectives

The first objective is to understand how the operating parameters of an Organic Rankine Cycle (working fluid type, operating pressures and temperatures, components type and more) influence the net power output of the system. In particular, the discussion about which is the working fluid most suitable for the application in WHR system based on an ORC is still open, detailed indications on this topic have to be provided.

Finally, it is fundamental to assess the net power output achievable by the system and see the percentage of heat that can be recovered and converted into useful power by the Waste Heat Recovery unit. The objective is to demonstrate with simulation that, under certain engine operating conditions, the power improvement provided by the WHR unit is 5-10% of the power output by the engine.

1.3 Methodology

The strategy adopted to give an answer to the topics listed in the paragraph above was mainly centered on the development of two simulation tools with an increase degree of accuracy.

The first simulation tool, called, for the sake of simplicity, preliminary model, is a Matlab based model built by the author to compare the possible design alternatives, focusing especially on the Organic Rankine Cycle rather than the entire Waste Heat Recovery unit. In fact, the findings obtained with this model were addressed to understand the combination of operating temperatures, pressures as well as working fluid that maximize the net power output as a function of the type of Organic Rankine Cycle selected (standard or recuperative).

The second simulation tool, called detailed model, is instead a Matlab/Simulink model developed to carry out time dependent simulations also in non-stationary operating conditions.

The degree of accuracy is much increased with respect to the previous model since the goal is to use this model to precisely predict the net power output of the cycle. It has the highest possible degree of flexibility and it is meant to be integrated in the global fuel economy simulation tool already available at Fiat and Chrysler. The validity of the outputs of the detailed model have been checked using data coming from experimental tests already carried out at Centro Ricerche Fiat.

Both simulation models have been used to compare the performances of the most commonly employed fluids in the Waste Heat Recovery industry.

However, the comparison between the working fluids was not only limited to the performances but a list of other five aspects used as term of comparison have been proposed, according to the criteria most widely accepted in literature.

1.4 Thesis Organization

The remainder of the thesis is organized in the chapters listed below:

- CHAPTER 2: contains the results of the literature survey performed by the author to explain the topic of the thesis and introduce the reader to the peculiarities of the Waste Heat Recovery industry. A theoretical background on the thermodynamic, in general, and on the Rankine Cycle, in particular, is also furnished in order to better understand the concepts explained in the following chapters.
- CHAPTER 3: a detailed explanation of the features and functioning of the two simulation models developed is provided. Especially in the detailed model particular attention has been given to the different algorithm that the program uses as function of the inputs selected by the user.
- CHAPTER 4: the simulations carried out with the two programs are explained, the results are deeply analyzed and discussed to prove the feasibility of a Waste Heat Recovery unit in automotive applications and to show the reliability of the simulation tool developed. The investigations proposed are addressed to draw a sort of ideal profile of the Waste Heat Recovery unit integrated with an engine.
- CHAPTER 5: the conclusions and the findings of the research presented throughout the thesis are outlined and summarized.

2. REVIEW OF LITERATURE

2.1 Review of thermodynamics

A certain number of thermodynamic machines use a working fluid having homogeneous and invariable chemical composition, a pure substance, that changes phase, from liquid to vapor and vice versa, inside the machine itself as a function of the local temperature and pressure. This kind of machines, operating in a range of temperatures and pressures close to the critical point of the fluid employed, are known as Steam Power Machines if their ultimate target is to generate useful power. The introduction of steam power generation systems has given a strong impulse to the industrial revolution and over the years their performances have been optimized.

Steam power generation has consistently been based on the Rankine cycle or its modification. However, in order to fully understand its operating principles, is useful to make a step backward and introduce the Carnot cycle first, since it represents the starting point for all the following analyses.

The cycles discussed in this section are not utilized in the actual power plants because are ideal cycles (totally reversible) or cycles in which just few types of irreversibility are considered. The assumptions made are summarized in the bullet list below:

- steady-state condition throughout the entire cycle
- negligible kinetic and potential energy variations
- null pressure drop inside the heat exchangers
- adiabatic transformations in the process involving exchange of work
- the fluid inside the ducts does not change its thermodynamic properties
- zero viscosity of the working fluid.

The idealized cycles represent a good approximation of the performances of many actual processes and are often used for preliminary computations.

2.1.1 Carnot cycle

The concept of thermodynamic cycle was first introduced by the French military engineer Nicolas Sadi Carnot (1769 – 1832) to determine the system which could operate at maximum efficiency using heat from a constant temperature source [1]. It is made up of two adiabatic and two isothermal transformations.

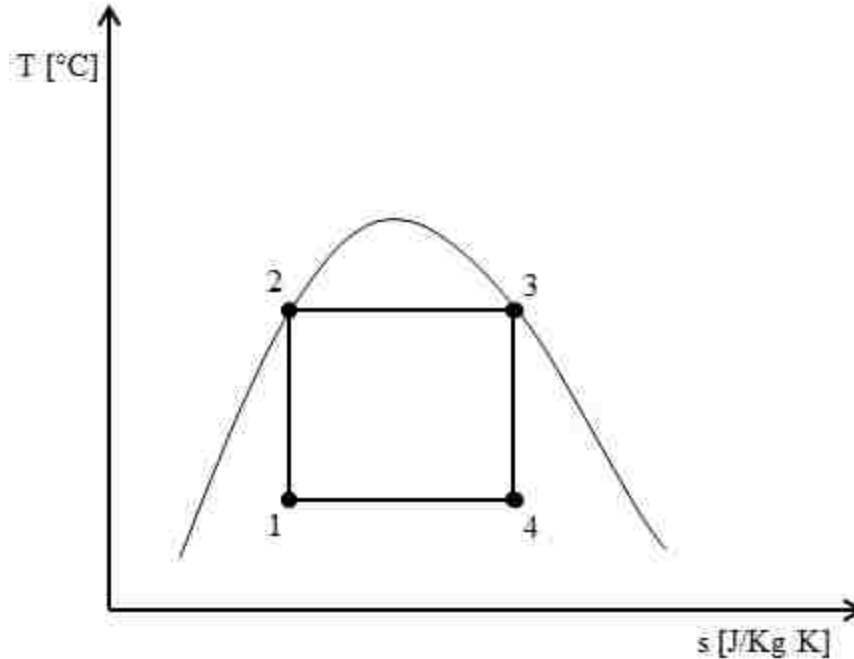


Figure 2.1-1: Carnot cycle on T-s diagram.

With reference to Figure 2.1-1 that shows the cycle on a T-s diagram, the transformations that take place are:

1 → 2: Reversible adiabatic compression (isentropic), work is done on the fluid.

2 → 3: Constant temperature evaporation, the working fluid receives heat from an external source.

3 → 4: Reversible adiabatic expansion (isentropic), the working fluid generates useful work.

4 → 1: Constant pressure and temperature condensation, the fluid, giving off heat to the environment, returns to the initial conditions.

As stated before an analysis of the Carnot cycle is representative of others, in particular the efficiency obtained by such a cycle is the highest that can be achieved by any other cycle operating within the same temperature range (T^+ and T^-). The Carnot cycle efficiency is defined as:

$$\eta_{carnot} = \frac{Q_{23} - Q_{41}}{Q_{23}} = 1 - \frac{Q_{41}}{Q_{23}} = 1 - \frac{T^-}{T^+} \quad (2.1)$$

Where $T^+ = T_2 = T_3$ is the maximum temperature reached by the fluid correspondent to the vaporization temperature and $T^- = T_4 = T_1$ is the minimum temperature or rather condensation temperature. It has been possible to make the last simplification because heat is exchanged at constant temperature. This expression gives rise to an important consideration: even though there are no irreversibilities in the cycle, the efficiency cannot be equal to 100% unless the low temperature source (T^-) was at 0K, condition never possible.

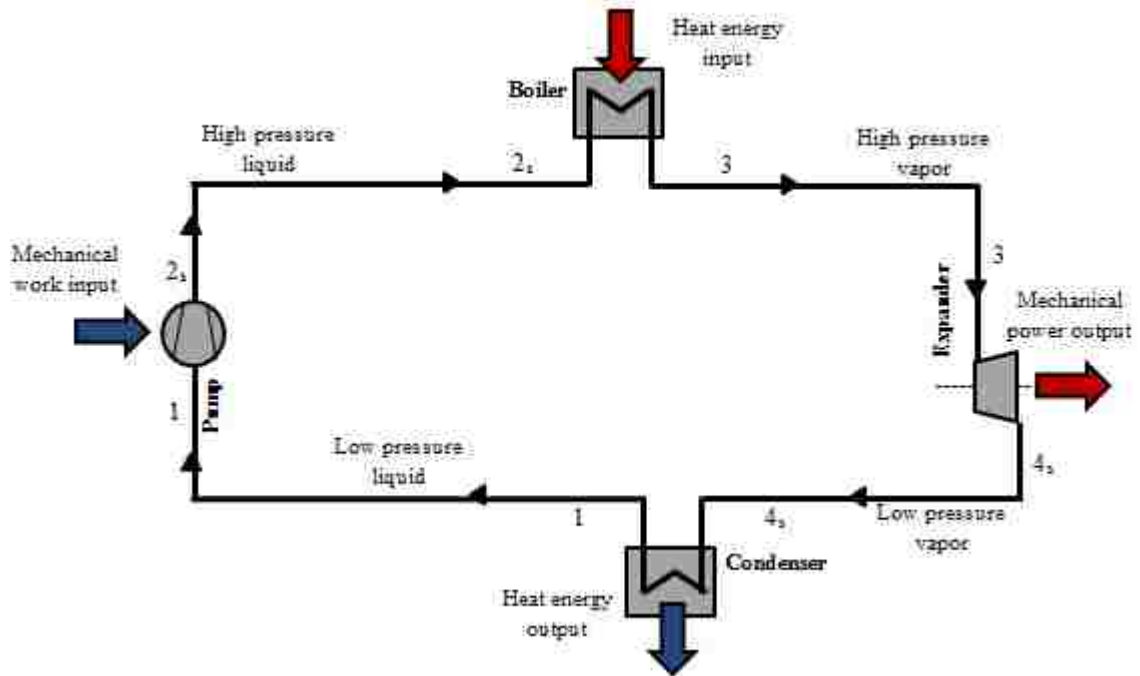


Figure 2.1-2: Rankine cycle system layout.

However, the practical attainment of the Carnot cycle is difficult, not only because of the problem of elimination of irreversibilities in actual processes, but also in view purely mechanical, there are difficulties involved in expanding and, more critically, in compressing a partially condensed wet vapor. The two-phase compression could be avoided by condensing to the saturated liquid, but this would require a subsequent process of raising the liquid to extreme pressures reversibly in order to reach the maximum temperature. For these reasons the Carnot cycle, despite of its thermodynamic advantages, has not been used in any application.

2.1.2 Rankine cycle

The standard vapor cycle, most widely known as Rankine cycle, represents a practical modification of the Carnot cycle and its operating components to overcome the limitations described in the previous paragraph. The Rankine cycle itself is named in memory of one of the founding contributors to the science of thermodynamics, William John Macquorn Rankine (1820 - 1872), a Scottish engineer and physicist who is also credited for the “Rankine” temperature scale [2]. Figure 2.1-2 shows a typical scheme of a Rankine cycle, the components utilized are a feed pump, an evaporator (or boiler), an expander and a condenser.

With reference to Figure 2.1-3 and Figure 2.1-4, that provide a visual representation of the ideal Rankine cycle diagram (1-2_s-2'-3-4_s), respectively on the T-s and p-h diagrams, the transformations that take place are described below:

1 → 2_s: Saturated liquid at low pressure and temperature is isentropically compressed (the subscript “s” indicates an isentropic transformation) up to the high pressure p_{2s}, temperature and volume changes are negligible. The work per unit mass required by the pump is equal to the enthalpy difference between point 1 and point 2_s;

$$w_{pump} = w_{12s} = \frac{p_1 - p_{2s}}{\rho_1} = (h_1 - h_{2s}) \quad (2.2)$$

2_s → 2': The high pressure sub-cooled liquid is heated up at constant pressure, until it reaches the saturation curve, point 2'.

2' → 3: Saturated high pressure liquid is vaporized at constant temperature and pressure. The heat per unit mass absorbed by the working fluid between state 3 and state 2_s is equal to:

$$q_{23} = h_3 - h_{2s} = c_p(T_{2s} - T_1) + \Delta H_{vap} \quad (2.3)$$

Where c_p is the constant pressure specific heat and ΔH_{vap} is the enthalpy of vaporization.

3 → 4_s: The saturated vapor expands isentropically from the high pressure to the low pressure. The amount of work per unit mass done by the expander is equal to:

$$w_{exp} = w_{34} = (h_3 - h_{4s}) \quad (2.4)$$

4_s → 1: The low pressure vapor condensates at constant temperature and pressure, returning to the initial conditions, the heat per unit mass released to the external environment is:

$$q_{4s1} = h_1 - h_{4s} \quad (2.5)$$

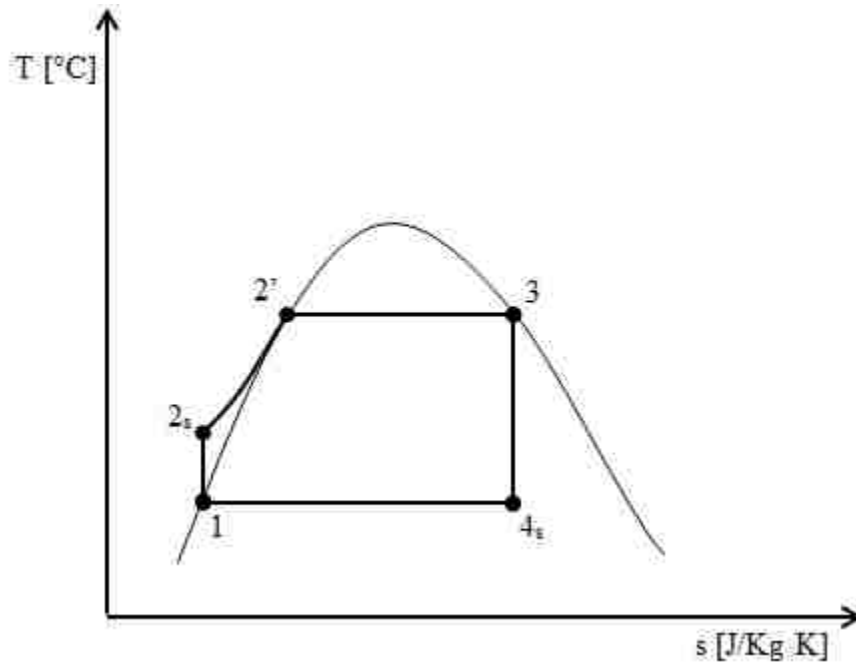


Figure 2.1-3: Rankine cycle on T-s diagram.

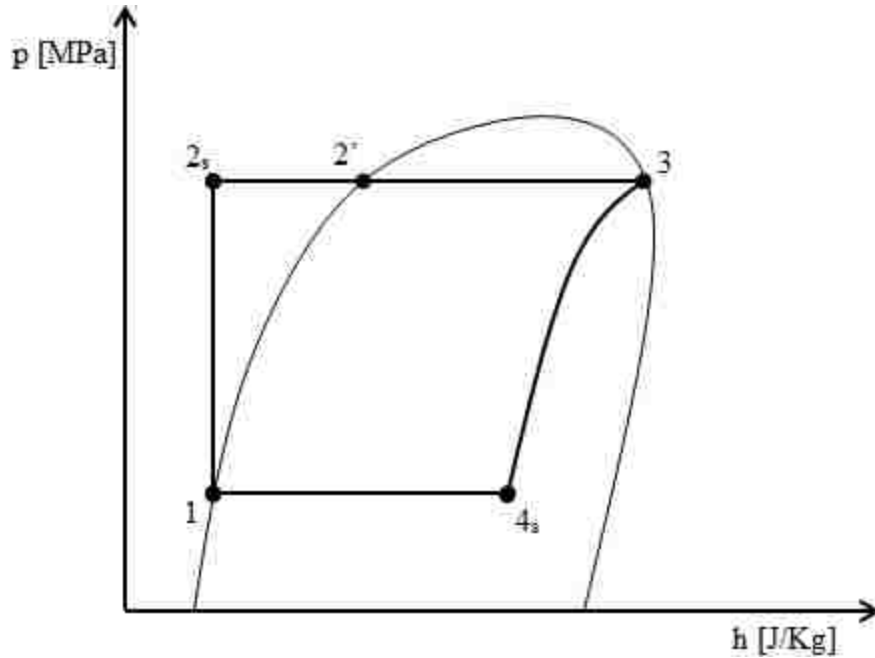


Figure 2.1-4: Rankine cycle on p-h diagram.

In order to obtain the power or heat transfer rate from Equation (2.2) to (2.5) it just takes to multiply the work/heat per unit mass by the mass flow rate of the working fluid of the cycle. Moreover, it is useful to underline that the areas underneath the T-s diagram (Figure 2.1-3) represent the heat exchanged per unity mass respectively with the hot heat source (2_s-3) and with the cold heat source (4_s-1). The difference between these two areas, thus the cycle area, represents the net output work per unity mass of the cycle.

Steam power units, if operating at steady state condition, are cyclic, hence the overall power balance can be expressed in the following manner:

$$\dot{W} = \dot{Q} + \sum_i^n h_i \dot{m}_i \quad (2.6)$$

Where \dot{W} is a power and \dot{Q} is a heat transfer rate. If an analysis of the entire cycle is performed the rightmost term of Equation (2.6) disappears, since the Rankine cycle is a closed system (work is produced without transfer of mass), giving that:

$$|\dot{W}_{34s}| - |\dot{W}_{12s}| = |\dot{Q}_{2s3}| - |\dot{Q}_{4s1}| \quad (2.7)$$

The ideal cycle efficiency is given by the ratio between the net power output and the heat flow rate occurring with the high temperature heat source.

$$\eta_{cycle} = \frac{W_{net}}{\dot{Q}_{2s3}} = \frac{W_{34s} - W_{12s}}{\dot{Q}_{2s3}} = \frac{\dot{Q}_{2s3} - \dot{Q}_{4s1}}{\dot{Q}_{2s3}} = 1 - \frac{\dot{Q}_{4s1}}{\dot{Q}_{2s3}} \quad (2.8)$$

For a given \dot{Q}_{2s3} , the lower the heat transfer rate rejected in the condenser (\dot{Q}_{4s1}), the better the efficiency. Substituting in Equation (2.8) the values of each term:

$$\eta_{cycle} = \frac{(h_3 - h_{4s}) - (h_{2s} - h_1)}{(h_3 - h_{2s})} = \frac{(h_3 - h_{2s}) - (h_{4s} - h_1)}{(h_3 - h_{2s})} \quad (2.9)$$

The last passage was possible taking into account Equation (2.7).

Considering that the pump work required is much smaller than the work generated in the expander ($h_2 \approx h_1$), Equation (2.09) can be further simplified, becoming:

$$\eta_{cycle} = \frac{(h_3 - h_{4s})}{(h_3 - h_{2s})} \quad (2.10)$$

Anyway throughout the following discussion this simplification will never be used, because it introduces a not acceptable error.

2.1.3 Superheat Rankine cycle

The Rankine cycle explained in paragraph 2.1.2, also called “saturated vapor Rankine cycle” because state 3 lays on the saturation curve, is rarely employed. In common applications, a modification of the basic Rankine cycle, known as Rankine-Hirn cycle or superheat Rankine cycle, is used in order to increase the efficiency, and, at the same time, avoid expansion in the wet region. The cycle is defined by points 1-2_s-2’-3’-3-4_s of Figure 2.1-5 and Figure 2.1-6. In those figures state 3’ corresponds to the saturated vapor condition, but the working fluid is further heated up until it reaches state 3, that still coincides with the expander inlet, but that has a temperature greater than state 3’. Basically, the working fluid is heated, at constant pressure, up to a temperature higher than the boiling temperature at the pump outlet pressure. As mentioned before the operation of the Rankine cycle at a high turbine inlet temperature in the superheat region provides two potential advantages.

First, the temperature limits between which the system operates may be increased, and the turbine expansion may be partially if not totally dry rather than wet, avoiding potential wear and failures of the turbine blades. Second, the increased temperature range provides a greater availability of the energy transferred as heat, the increase of Q_{2s3} is greater than that of Q_{4s1} and, as a consequence, the overall efficiency slightly increases. However, it has been demonstrated that, for particular kinds of fluids, the highest efficiency is achieved avoiding superheating [3]. A more detailed analysis suggests that, if the isobaric curve at the high pressure of the cycle ($p_2s = p_3$) is steeper than the one at the low pressure of the cycle ($p_4 = p_1$), the cycle efficiency increases as the expander inlet temperature (T_3) is raised in the superheat region [3].

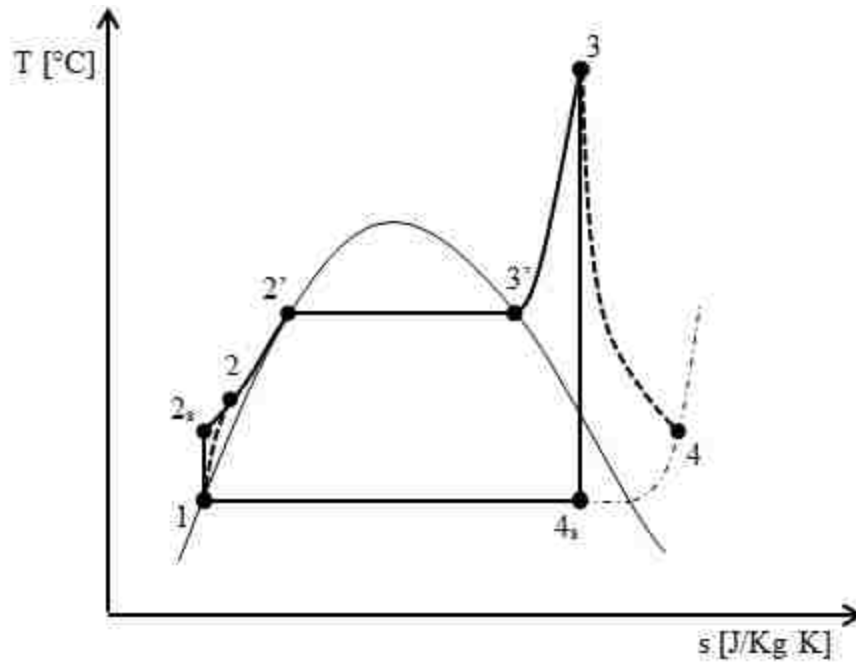


Figure 2.1-5: Superheat Rankine cycle on T-s diagram.

Operating the Rankine cycle within the superheat region produces a further deviation from the Carnot cycle since only a small portion of heat is transferred at the highest cycle temperature (T_3). The basic equations to compute the power involved in the cycle as well as the efficiencies, introduced in section 2.1.2, still hold.

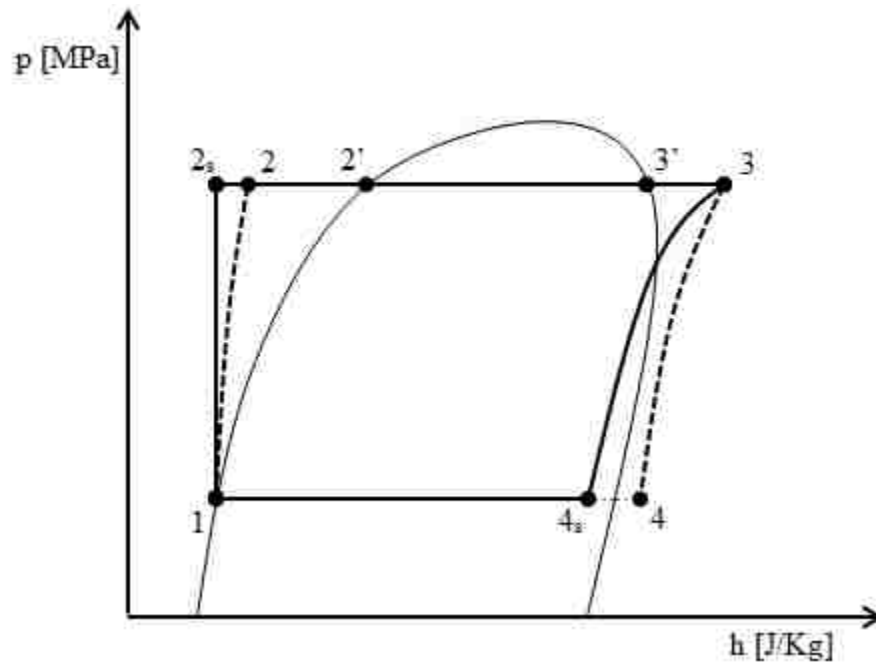


Figure 2.1-6: Superheat Rankine cycle on p-h diagram.

It is now worthy to introduce the concept of isentropic efficiency. Looking at Figure 2.1-5, and Figure 2.1-6, it can be noted that there are two additional dashed lines. As a matter of fact the cycle delimited by points 1-2-2'-3'-3-4, is a more realistic representation of a Rankine-Hirn cycle considering the transformations that actually take place in the expander and in the pump. In particular, looking at the T-s diagram, it is clear that the real expansion is not isentropic but there is an entropy increase due to intrinsic irreversibilities of the process, such as friction. Since the enthalpy of point 4 is less than that of the ideal point 4_s, the enthalpy drop across the expander is lower, hence the useful work per unit mass generated decreases. The expander isentropic efficiency is defined as the ratio between the actual work/power output and the ideal work/power output, and it is always lower than one:

$$\eta_{exp} = \frac{w_{34}}{w_{34s}} = \frac{(h_3 - h_4)}{(h_3 - h_{4s})} \quad (2.11)$$

The actual output work per unit mass of the expander is expressed according to the following equation:

$$w_{exp,act} = w_{34} = w_{34s} \cdot \eta_{exp} = (h_3 - h_{4s}) \eta_{exp} = (h_3 - h_4) \quad (2.12)$$

Making a similar consideration, the compression of the liquid in the feed pump is not isentropic. More precisely, the actual work required to compress the fluid from p₁ up to p₂ is greater than the ideal one, since the enthalpy at state 2 is greater than that of state 2_s. Thus the pump isentropic efficiency is defined as:

$$\eta_{pump} = \frac{w_{12s}}{w_{12}} = \frac{(h_1 - h_{2s})}{(h_1 - h_2)} \quad (2.13)$$

And the actual pumping work per unit mass is:

$$w_{pump,act} = w_{12} = \frac{w_{12s}}{\eta_{pump}} = \frac{(h_1 - h_{2s})}{\eta_{pump}} = \frac{p_1 - p_2}{\rho} \cdot \frac{1}{\eta_{pump}} = (h_1 - h_2) \quad (2.14)$$

Since the actual pumping work is greater than the ideal one and that the actual generated work is lower than the ideal one, the overall efficiency of the actual Rankine cycle is lower than the ideal one.

From now on the ideal cycle with isentropic compression and expansion is not considered anymore, pump and expander isentropic efficiencies will be less than one, and the subscript “act” will not be used anymore.

2.1.4 *Recuperative Rankine Cycle*

It has been explained as the efficiency of a Rankine cycle can be improved by increasing the amount of heat supplied at high temperatures, a similar effect may be obtained by decreasing the amount rejected at lower temperatures [4].

This principle is used by the recuperative Rankine cycle, also known in literature as Internal Heat Exchanger Rankine cycle, because, in the case that T_4 is remarkably higher than T_2 , a further heat exchanger is added. A schematic view of the cycle is shown in Figure 2.1-7. In this particular cycle the low pressure vapor coming out of the expander is used as heat source for heating the low temperature compressed working fluid coming out of the pump, before it reaches the boiling point.

For the sake of brevity only the T-s diagram of the recuperative Rankine cycle is reported, Figure 2.1-8. The cycle is delimited by the states 1-2-2_r-3-4-4_r, pump and expander efficiencies lower than 100% have been assumed. Looking at the schematic and at the T-s diagram it is immediately clear what is the difference with respect to the Rankine-Hirn cycle. Here the high working temperature fluid exhausted from the expander is transported to the inlet of low pressure side of a third heat exchanger, usually called recuperator or regenerator. Whereas the low temperature working fluid exported from the pump is conveyed to the inlet of the high pressure side of the recuperator. Finally the heat is transferred from the low pressure side to the high pressure side of the recuperator. The increased complexity is often justified by the increase in efficiency and hence output power generated.

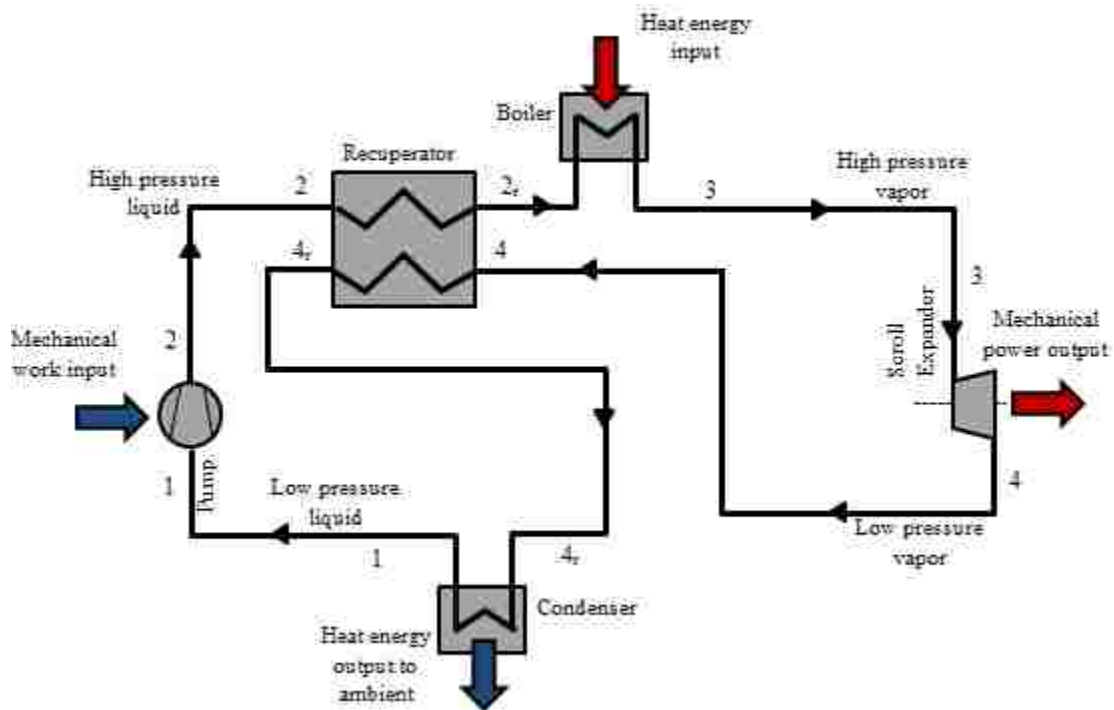


Figure 2.1-7: Recuperative Rankine cycle system layout.

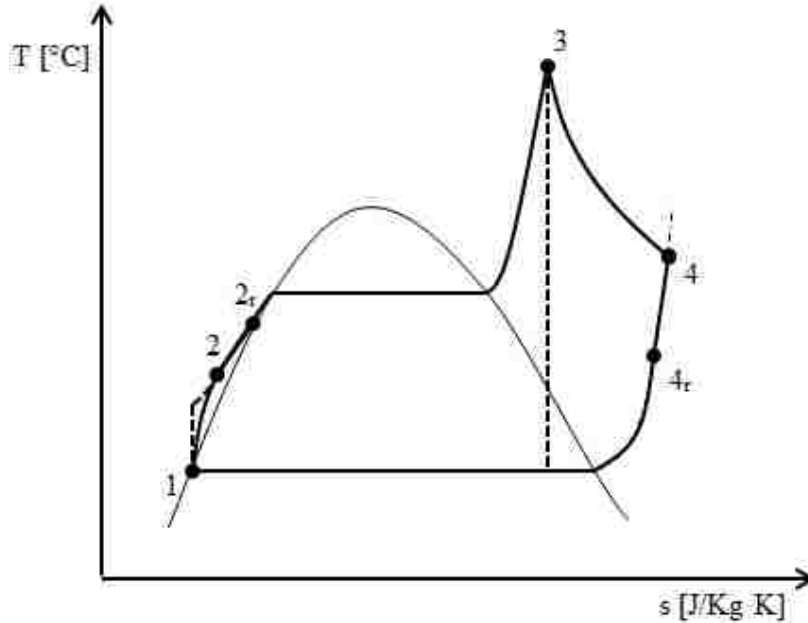


Figure 2.1-8: Recuperative Rankine cycle on T-s diagram.

The set of equations presented so far for the standard Rankine cycle should be slightly adapted.

1 → 2: There are no differences. The pumping work is still computed according to Equation (2.14).

2 → 2_r: The high pressure low temperature liquid is heated up in the internal heat exchanger, the amount of heat per unit mass exchanged is:

$$q_{22r} = h_{2r} - h_2 \quad (2.15)$$

2_r → 3: Only in this portion of the cycle the working fluid exchanges heat with the high temperature heat source, the resulting heat transfer per unit mass is:

$$q_{23} = h_3 - h_{2r} \quad (2.16)$$

3 → 4: The expansion process does not change. The work generated per unit mass is still computed with Equation (2.12).

4 → 4_r: The low pressure high temperature vapor is cooled down in the recuperator. The amount of heat given by the fluid in this transformation is equal in module, but opposite in sign, to the amount of heat received by the fluid during 2-2_r transformation:

$$q_{44r} = -q_{22r} = h_{4r} - h_4 = h_2 - h_{2r} \quad (2.17)$$

4_r → 1: The fluid releases heat to the low temperature reservoir, achieving the saturated vapor condition first, and then, completing the condensation process:

$$q_{4r1} = h_1 - h_{4r} \quad (2.18)$$

In order to better understand the advantages of the internal heat transfer, two complementary considerations can be made.

First, this internally transferred heat does not need to be supplied from outside, obviously this feature increases the thermal efficiency. Second, considering two cycles, one with an internal heat exchanger and other one without it, even though they are working between the same maximum and minimum temperatures there are differences in the average temperature at which heat is supplied to the system and in the average temperature at which heat is transferred to the environment. In the cycle with the recuperator the average temperature at which heat is supplied (from T_{2r} to T_3 of Figure 2.1-8) is higher than in the case there was no recuperator (from T_2 to T_3 Figure 2.1-8), while the average temperature at which heat is transferred to the environment (from T_{4r} to T_1) is lower than in case without recuperator (from T_4 to T_1). Both these differences result, according to Carnot, in a higher thermal efficiency of the cycle, [5]. On the other hand, if we assume that the amount of heat supplied in the evaporator remains the same, with a recuperator can be increased the mass flow rate of the working fluid that is brought to the temperature T_3 , thus increasing the power output of the cycle. According to Vaja and Gambarotta, [6], turbines or expanders with low isentropic efficiency are suitable for recuperative Rankine cycle applications. In fact a low efficiency expander leads to a temperature and enthalpy increase of the superheated vapour at the turbine outlet (state 4) and this energy is partially recovered in the recuperator. However, in most of the application is better to maximize the power output of the cycle, hence an expander with a greater efficiency has to be preferred.

2.1.5 Supercritical Rankine Cycle

In the Rankine cycle types presented so far, during the heating process (transformation 2-3) the working fluid undergoes a liquid-vapor phase transition process. However, there is a particular kind of Rankine cycle in which the working fluid, usually one with a relatively low critical temperature and pressure, can be compressed directly to its supercritical pressure and heated to its supercritical state before expansion. In other words no phase transition takes place and a supercritical compressed fluid enters the expander. This cycle is known as supercritical Rankine cycle.

Figure 2.1-9 shows the T-s diagram for such kind of Rankine cycles, it can be noted that the shape of the line that goes from point 2 to point 3 is significantly different than the previous cases and it allows obtaining a better thermal match with the high temperature heat source, resulting in a higher efficiency, [7].

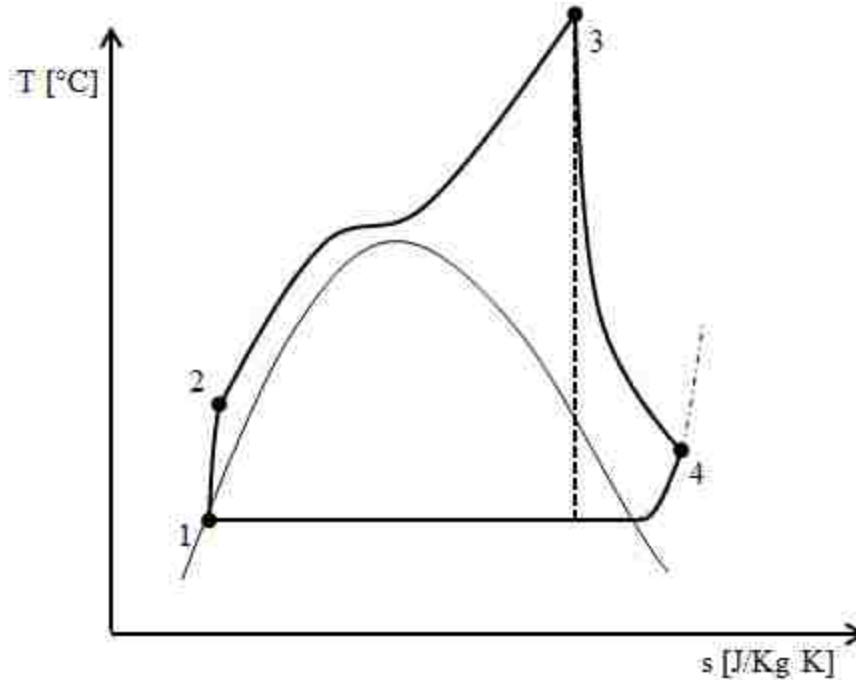


Figure 2.1-9: Supercritical Rankine cycle on T-s diagram.

2.1.6 Additional considerations

Analyzing in more details the definition of useful power, coming out from a Rankine cycle, other terms, rather than just the power generated by the expander and requested by the pump, should be included. In fact, sometimes the expander shaft must drive not only the feed pump but other accessories. The accessories are here intended as those devices that do not exchange work directly with the working fluid, such like blowers or lubrication pumps. Moreover, a given amount of power is always necessary to overcome the mechanical friction forces acting on the expander output shaft. Hence a more complete definition of useful power is [8]:

$$\dot{W}_{useful} = \dot{W}_{exp} - \dot{W}_{pump} - \dot{W}_{accessories} - \dot{W}_{friction} \quad (2.19)$$

And the organic efficiency, defined as the ratio between the useful power and the power generated by the working fluid, is:

$$\eta_{organic} = \frac{\dot{W}_{useful}}{\dot{W}_{exp} - \dot{W}_{pump}} \quad (2.20)$$

Another important efficiency, that has not been treated yet, is the evaporator efficiency ($\eta_{evaporator}$). In order to define this efficiency we should give a closer look to what happens in this component. In the evaporator, that basically is a heat exchanger, the working fluid receives heat from a source at higher temperature. However, the energy stored in the heat source is not entirely transferred to the working fluid. This is the reason why, it is useful to introduce the boiler efficiency. It is defined as the actual heat transfer rate taking place in the expander, divided by the heat transfer

rate that the system (high temperature heat source) would have if it achieves equilibrium with the external environment (assumed at 25 °C). In other words, it is the ratio of the actual heat transfer rate to the maximum potential heat transfer rate ($\dot{Q}_{available}$).

$$\eta_{evaporator} = \frac{\dot{Q}_{23}}{\dot{Q}_{available}} = \frac{\dot{Q}_{23}}{C_{source}(T_{source} - T_{environment})} \quad (2.21)$$

Where C_{source} is the heat capacity rate of the high temperature heat source expressed in J/s-K, obtained multiplying the mass flow rate of the source to the specific heat of the source itself.

This concept brings directly to the definition of a very important thermodynamic quantity that will be used later throughout the text: exergy. Exergy is the maximum amount of work that can be done by a subsystem as it approaches thermodynamic equilibrium with its surroundings by a sequence of reversible processes [9]. It is a measure of the quality of the energy of a given subsystem; the greater it is the greater is the work that potentially can be done.

The evaporator efficiency, as it is defined in Equation (2.21), is also known in the WHR industry as “recovery efficiency” and will be utilized throughout this work.

2.1.7 Rankine cycle summary

As illustrated in the in this section the Rankine cycle is a versatile power generation system due to the many different possible modifications (other possible features have been omitted such like the reheat Rankine cycle and the extraction recuperative Rankine cycle because are beyond the scope of this thesis). The output power range can go from few kW up to several MW. The flexibility and the relative simplicity have made it one of the most used power generation cycles and particularly suitable for the Waste Heat Recovery industry. As any other process, it has inherent irreversibilities such like friction-heat losses in the expander and pump, as well as pressure drops in heat exchangers and pipes that have been neglected so far.

In order to affectively improve the efficiency there are two main ways. One approach is to decrease the average low side temperature (T_{41}). However, since in most cases the low temperature cannot fall below the environment temperature, it is more common to increase the high side average temperature (T_{23}) trying to obtain a better match between the working fluid and the heat source temperatures in the evaporator, thus reducing the irreversibilities of this component.

The second approach is to increase the isentropic efficiency of the pump and the expander. Anyway the pump work in a Rankine cycle is significantly less than the expander work, so improving the efficiency of the expander provides the greatest degree of cycle efficiency improvements [10].

2.2 Waste Heat Recovery

For decades, the continuously increased fossil consumption by human's daily life and industrial production has caused many environmental problems such as global warming, ozone depletion, atmospheric pollution and so on. For these reasons energy savings has become one of the main issues that governments and researchers all over the world have to face. Therefore the need to introduce new energy conversion technologies, able to generate power without causing environmental pollution, has risen.

In particular low-medium grade heat sources have been investigated as new potential sources, because they can generate additional power without requiring extra fuel [6]. Typical examples of such a kind of sources are the solar heat, geothermal energy and waste heat that have energy available at temperature ranging from as low as 60 °C up to 600 °C. Statistical investigations indicate that the low-grade waste heat accounts for 50% of the total heat generated in industry [3], technologies that can partially recover this kind of energy, and at the same time cooling down the heat source, became popular. The most common application is a Rankine cycle which utilizes as heat source the waste heat of another thermodynamic cycle topping it. However, the water as a working fluid does not allow efficient recovery of waste heat below 370 °C, hence the low efficiency of the steam Rankine cycle using water has prevented for years the economic feasibility of these systems. In order to overcome this limitation, Rankine cycles that use organic working fluids have been developed. These fluids have lower heat of vaporization and can better follow the temperature profile of the heat source in the evaporator. Organic fluids properties will be discussed in details in section 2.3.

Due to its flexibility, there is a wide range of heat sources that can be applied to supply an Organic Rankine Cycle (ORC). As a matter of fact, selecting a suitable working fluid and, as a consequence, the shape of the saturation curve, it is possible to adapt the cycle in function of the type of heat source. Moreover, the expander of an ORC is usually less complex (one or maximum two stages) and has a higher efficiency due to the lower enthalpy drop of the organic fluids [11]. High safety and low maintenance are the other features that make ORC suitable for Waste Heat Recovery applications in power plants and industrial processes. These cycles, whose shaft power is usually converted into electric power by means of a generator, are very flexible also in terms of power output since it can range from even less than one kW up to several MWs. Literature reports several applications of ORCs bottoming power generation plants, with efficiency improvements of 5-10%, [12] and [13].

2.2.1 WHR importance in automotive industry

In industrialized countries about 25 percent of the total energy consumption is caused by transports [14]. Moreover, transportation is also one of the main sources of emissions of carbon dioxide (CO₂), as depicted Figure 2.2-2 [15]. CO₂ is a natural component of atmospheric air and it is not classified as a pollutant. However, it is one of the substances responsible for the greenhouse effect and the global climate change associated to this phenomenon. Even though road vehicles are only a portion of the overall transports, their contribution to carbon dioxide emissions is significant and must be reduced, Figure 2.2-1 shows a detailed view of the average CO₂ emissions of the main automakers. This is the reason why regulations on CO₂ emissions have become more stringent both in Europe, where manufacturer's average emissions level should not exceed 130 g/km by 2015 and a further CO₂ emission reduction to 95 g/km is specified for the year 2020 [16], and North America. In combustion of hydrocarbons Carbon dioxide (CO₂) is formed and it makes up approximately 13.7% of the exhaust gas. Hence, the amount of converted carbon dioxide is a direct index of fuel consumption. Thus the only way to reduce CO₂ emissions is to reduce fuel consumption [17].

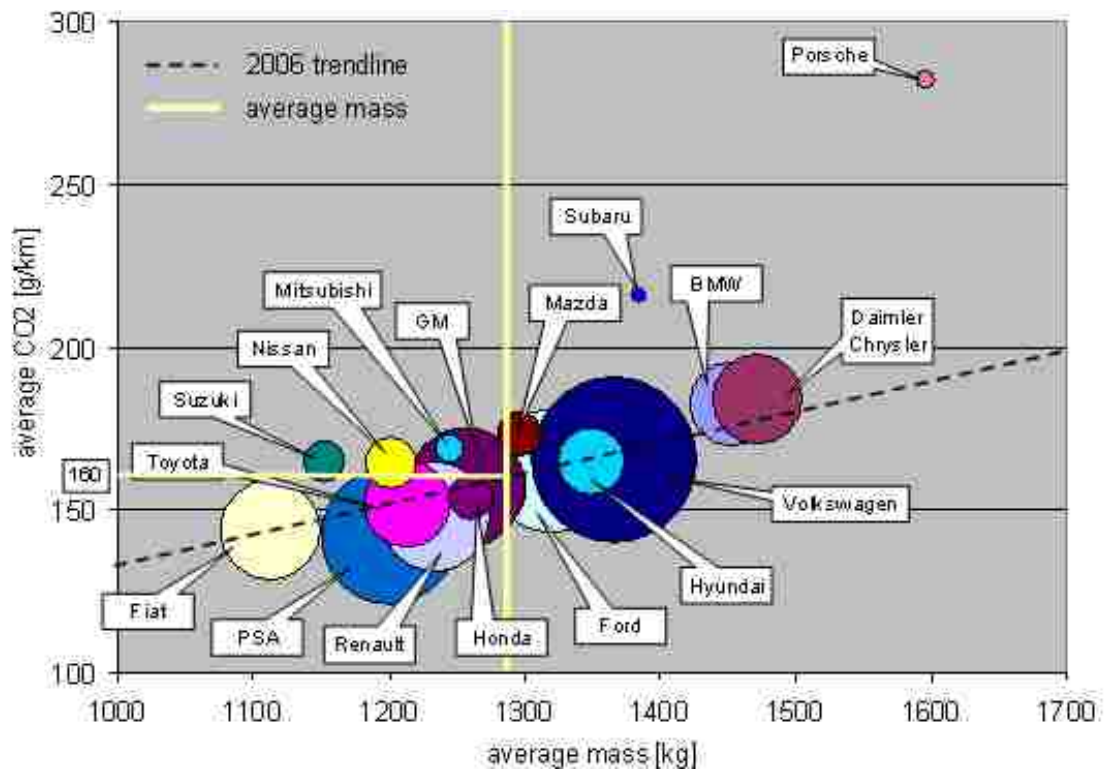


Figure 2.2-1: Average CO₂ emissions of main car manufacturers in Europe (2006) [16].

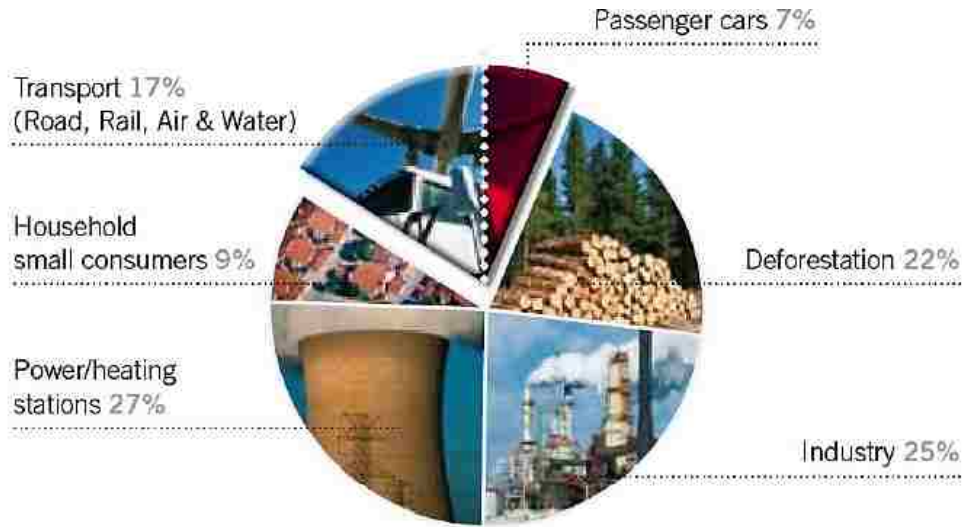


Figure 2.2-2: Percentage of total CO₂ emissions in Europe (2007) [15].

Taking into account that fuel price has risen it is clear that Waste Heat Recovery systems have a strategic importance also in automotive industry, since they are convenient from an economic as well as an environmental point of view.

2.2.2 WHR potential and alternatives

In paragraph 2.2.1 it has been shown as in the field of internal combustion engines, the research hotspot is how to further improve the fuel utilization efficiency. After Gasoline Direct Injection and Common Rail Multi-jet Diesel engines have been introduced, the challenge has become even more difficult. The maximum achievable thermal efficiency for modern engines is between 25 and 32 percent. The remaining fuel energy is lost in the form of engine waste heat discharged into the ambient. Figure 2.2-3 illustrates a common energy flow diagram for an automobile [18].

The steady state energy balance of a car is described by the equation below:

$$Q = Q_w + Q_{eg} + Q_{cw} + Q_r \quad (2.22)$$

Q is the total heat generated from fuel combustion, Q_w is the heat converted into effective mechanical work, Q_{eg} is the heat taken away by the exhaust gas, Q_{cw} is the heat reject to through the coolant (usually water), and Q_r is the remainder heat loss including the heat taken away by the lubricant.

Among these types of waste heat, the exhaust gases have the highest thermal quality, because heat is available at high temperatures, and accounts for about 22%-46% of the overall exergy of the fuel.

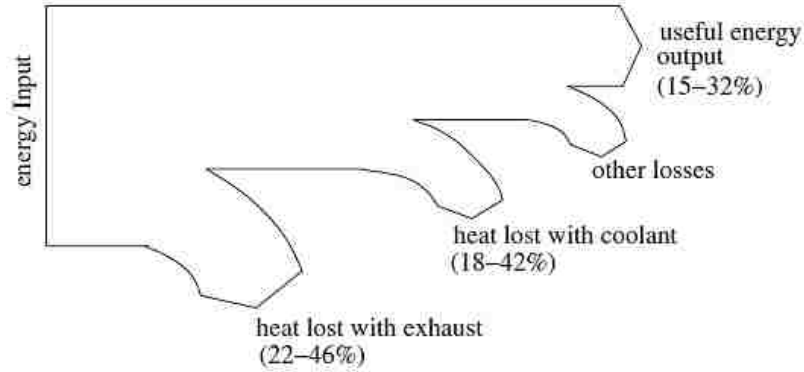


Figure 2.2-3: Energy flow of an automobile [18].

A similar percentage of energy is taken away by the radiator, however the thermal quality of cooling water is not high. Hence, if this heat were recovered, the conversion efficiency into mechanical power is low, due to the low temperature of the heat source [19]. On the other hand the temperature of lubricant is very high but its proportion in the waste heat is very small. Different studies have been carried out in order to better assess the percentage of the components of Equation (2.29). In particular Zhang et al., [20], tested a 1.3L gasoline engine concluding that the portion of heat converted into useful work (Q_w) increases when the engine load is increased for a given rotational speed, whereas this percentage does not change much changing engine speed at a given engine load. Figure 2.2-4 and Figure 2.2-5 show the results of these tests. Theoretically, except the waste heat that has to be released to the environment according to the second law of thermodynamics, the rest can be reutilized [21].

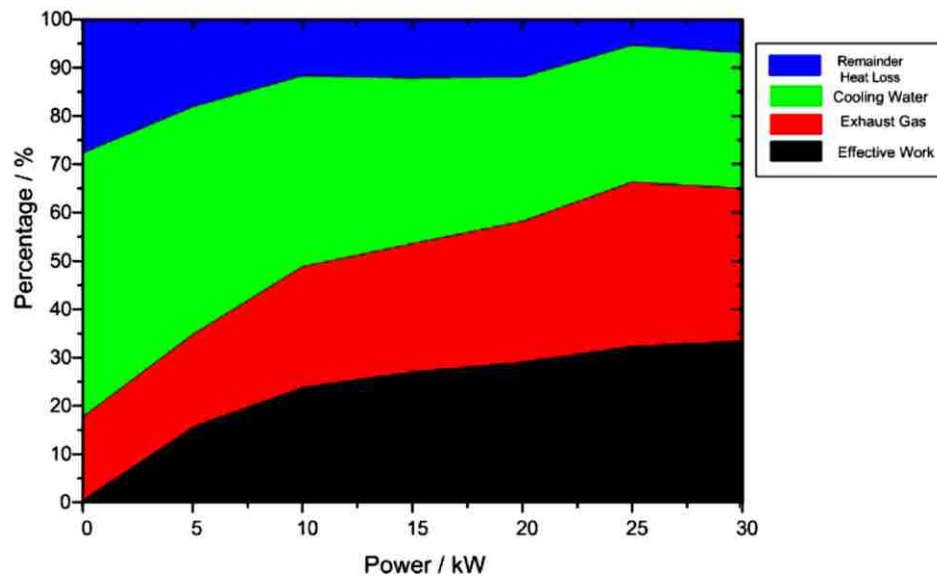


Figure 2.2-4: Energy distribution of a 1.3L gasoline engine at 3000 RPM [20].

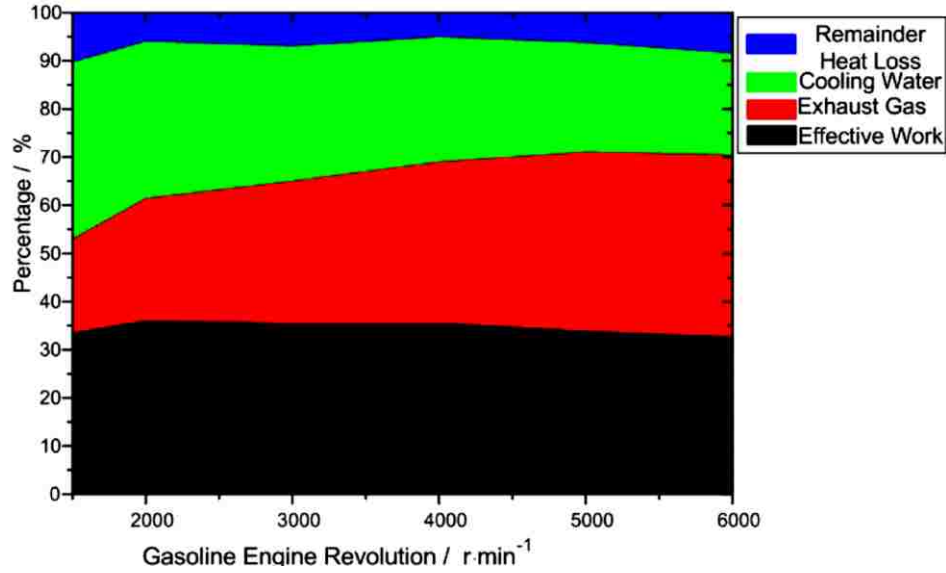


Figure 2.2-5: Energy distribution of a 1.3l gasoline engine at a given load [20].

However, almost all practical applications developed so far are focused on recovering heat from the exhaust gas (Q_{eg}) because, as previously mentioned, the thermal quality of the exhaust gas is high as well as its mass flow rate. There are mainly two ways to recover this heat. The first one is known as Thermal Electric generator (TE) and basically consists in generation of electricity using the temperature difference between exhaust gas and a cold source (usually external environment). Whereas the second one is an Organic Rankine Cycle (ORC) that uses as high temperature heat source the exhaust gas.

2.2.3 Thermal Electric generators WHR system

The thermoelectric approach is based on the properties of semiconductors materials. There are two types of semiconductors: P-type and N-type. The latter moves free electrons from the cold side to the hot side, while the other type moves them from the hot to the cold side. Combining these devices in series a Thermal Electric generator may be obtained. The voltage potential difference generated is given by:

$$E = \alpha \cdot \Delta T = \alpha \cdot (T_h - T_c) \quad (2.23)$$

Where E is the voltage, α is the Seebeck coefficient and T_h and T_c are respectively the temperature at the hot and cold side. The main limitation of this method to recover heat is that it has a very low efficiency. Special materials with a higher Seebeck coefficient are being developed to maximize this potential, [10]. If well optimized, a thermoelectric device can achieve efficiency levels that are 65-70% of the Carnot cycle efficiency. Two different kind of system configurations have been studied, whether the heat is exchanged directly or indirectly with the exhaust gas [22] and particular attention have been addressed on the design of the heat exchanger

where the semiconductor material is placed [23]. It should be also noted that TE based Waste Heat Recovery systems are highly reliable since they do not have any moving component. Nonetheless the semiconductor materials employed in this technology are too expensive for the amount of power that can be recovered.

2.2.4 Organic Rankine Cycle WHR system

The most promising technology in the WHR field is based on Organic Rankine Cycle. It has several advantages if compared to TE generators:

- more efficient
- is a well-established technology
- is cheaper
- has a higher energy utilization rate
- can generate directly mechanical power
- less backpressure.

Despite these advantages a WHR system with an ORC presents also some drawbacks if compared to TE generators:

- less reliable because it has more moving parts
- more difficult packaging
- heavier.

The first applications on vehicles were addressed to big Diesel engines, more precisely to class 8 heavy-duty truck engines. The main reason is that such engines produce a high mass flow rate and a high temperature exhaust gas stream that can be easily utilized to feed an Organic Rankine Cycle. Moreover, in trucks there are few concerns for packaging, hence the size of the heat recovery unit is not a big problem. Furthermore, these vehicles have several accessories that require a lot of current, so the power generated by Waste Heat Recovery system can be directly use to run these devices significantly reducing the fuel consumption. Advanced studies have been carried out in this car segment since the end of 70s [24] and [25], but they have become more frequent and detailed in the past five years [21], [26], [27] and [28] bringing important car manufacturers, such as Cummins and Iveco, to make advanced studies on this technology.

In particular Cummins Research and Technology department has proposed the adoption of a WHR system based on an Organic Rankine Cycle to improve engine efficiency up to 10% recovering the energy, that would otherwise be wasted, from the EGR and partially also from the exhaust gases downstream the after treatment device [29]. As stated before, Cummins confirms that the system works better for high EGR rate engines.

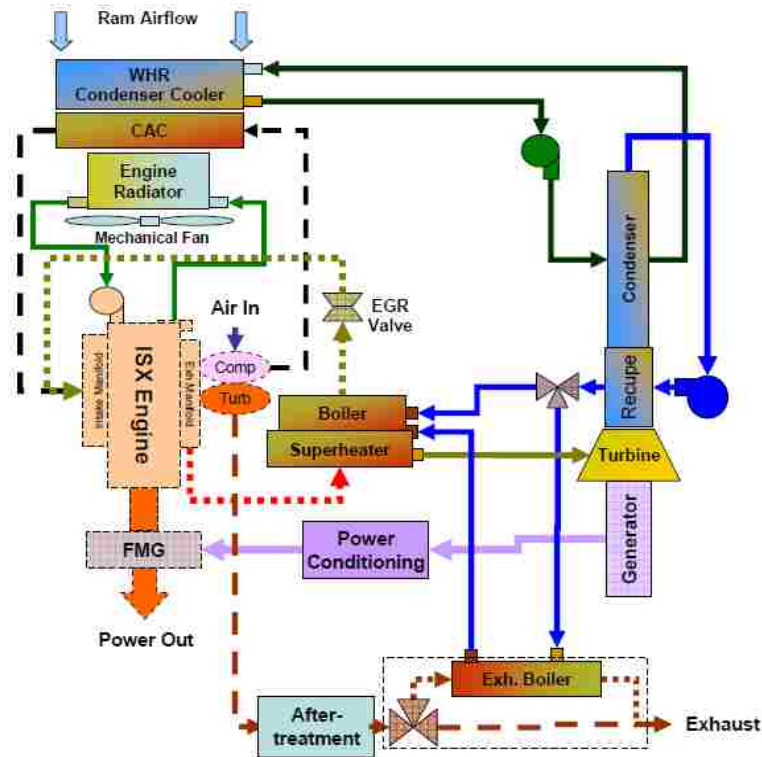


Figure 2.2-6: Cummins WHR system with recuperative ORC [29].

The architecture of the system proposed is based on a recuperative Rankine cycle. Hence the system, shown in Figure 2.2-6, includes two boilers (one that recovers heat from the EGR and another one that recovers heat from the exhaust gases), a super-heater, a turbine, a recuperator, a condenser and a feed pump. With reference to Figure 2.2-6 the working fluid is compressed in the pump, before being preheated in the high pressure side of the recuperator. Then by means of a valve the mass flow rate is divided, a portion is addressed to a heat exchanger that recovers heat from the exhaust gases another portion goes into a heat exchanger that recovers heat from the EGR gases. The two ducts converge in the super-heater that exchanges heat with the EGR, at this point the working fluid is expanded in the turbine and pre-cooled in the low pressure side of the recuperator before being condensed. An important is that in the condenser air is not used directly to condense the working fluid but another intermediate cooler (water) is adopted. This solution increases complexity and costs of the system, moreover power should be supplied to the water parasitic pump further decreasing the power output. The results obtained by Cummins through experimental tests (only using the energy coming from the EGR) show a power output generated of 19.4 kW that results in 5% improved engine thermal efficiency.

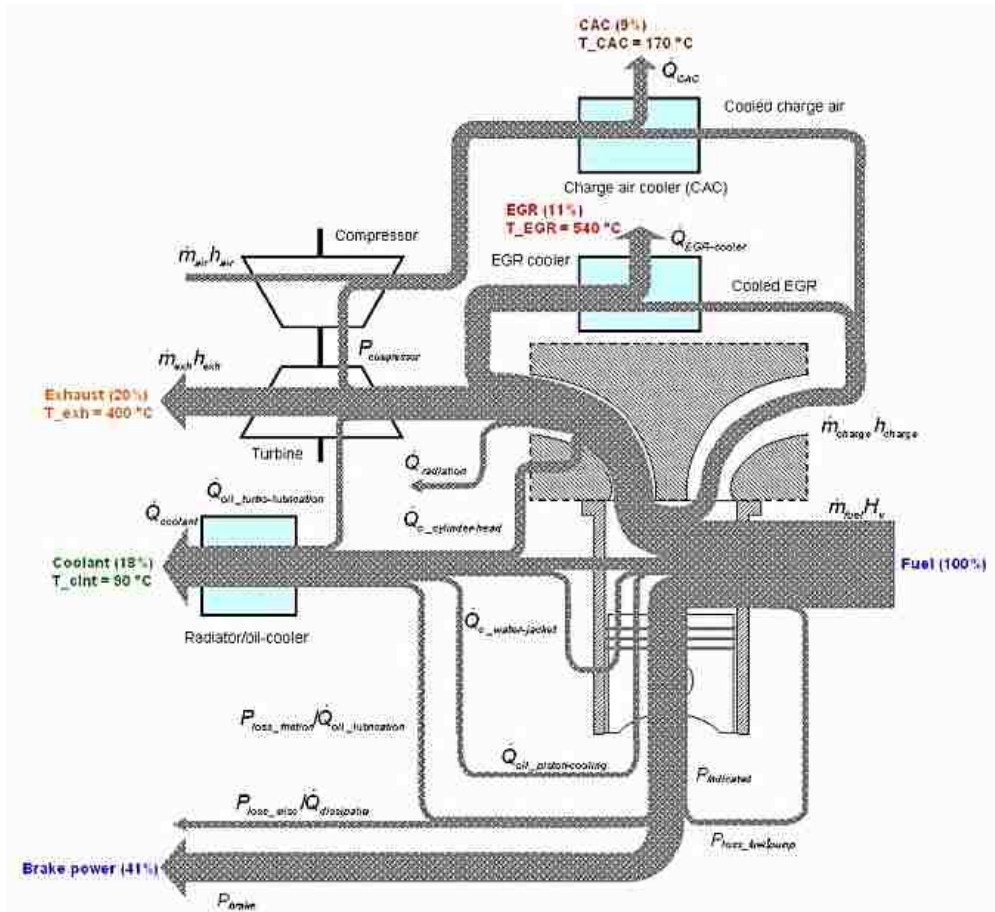


Figure 2.2-7: Energy flow of a typical high duty and high EGR rate diesel engine [26].

To sum up, the most common way to cut down the NO_x emissions in heavy-duty diesel engines is to recirculate a high percentage of exhaust gas reintroducing it into the feed pipe (high EGR rate). When this strategy is adopted the WHR system is particularly suitable because, as can be seen in [27], the EGR cooler can be replaced by the boiler of the ORC performing two tasks:

- cool down the exhaust gas, basically acting as a common EGR cooler
- heat up and vaporize the working fluid of the Organic Rankine Cycle.

This configuration is convenient since no further heat exchangers are introduced between the cylinder and the exhaust pipe, avoiding reducing the pressure of the exhaust gas portion that goes into the turbine.

Unfortunately in common European city-cars exhaust flow rate is low (engines are small) and exhaust gas temperatures are low, making the application of a heat recovery system more difficult and sometimes economically unfeasible. On the other hand North American mini-vans or big SUVs look like more suitable for WHR applications based on ORCs. They have bigger engines, the temperature of the exhaust gas is higher and the overall efficiency of the engine is generally

lower compared to those of European city-cars, making the conditions of the exhaust gas in the tailpipe more similar to those of heavy-duty trucks. More in general, the lower the exhaust flow rate and the lower the temperature of the exhaust gas the lower is the potential fuel savings, up to a certain point at which the recovery of the heat is economically unfeasible or thermodynamically impossible.

So far several configurations and alternatives of the ORC have been compared by researchers. In particular superheat Rankine cycle and recuperative Rankine cycle are the most common [20], [19], [30] and [31], whereas [32] has proposed a dual loop Waste Heat Recovery system with Organic Rankine Cycles to improve engine efficiency. The high-temperature loop recovers heat from the exhaust gas instead the low-temperature loop recovers the heat rejected by the high-temperature loop and heat coming from the engine coolant. The idea is attractive but the additional complexity of the system may become a serious limitation.

BMW, that has been the first and probably the most active Original Equipment Manufacturer (OEM) to promote the research on the WHR field, has compared different architectures of WHR units based on ORC with a WHR unit based on a TE generator [33]. The results are shown in Figure 2.2-8, where on the abscissa axis there is the heat utilization rate, thus the potential efficiency improvement, and on the ordinate axis there is the system complexity. Three possible ORC configurations were considered. 1-Loop-Rankine (A) refers to an ORC where the working fluid receives heat just from the exhaust gases, whereas in 1-Loop-Rankine (B) the working fluid is heated up also by the engine coolant. In preliminary tests carried out on a test bench by BMW using the one loop ORC that recovers heat also from the engine coolant (configuration B), a 2 kW power output has been demonstrated at a vehicle speed of 70 mph and at an engine speed of about 3200 RPM giving rise to a potential 11% efficiency improvement.

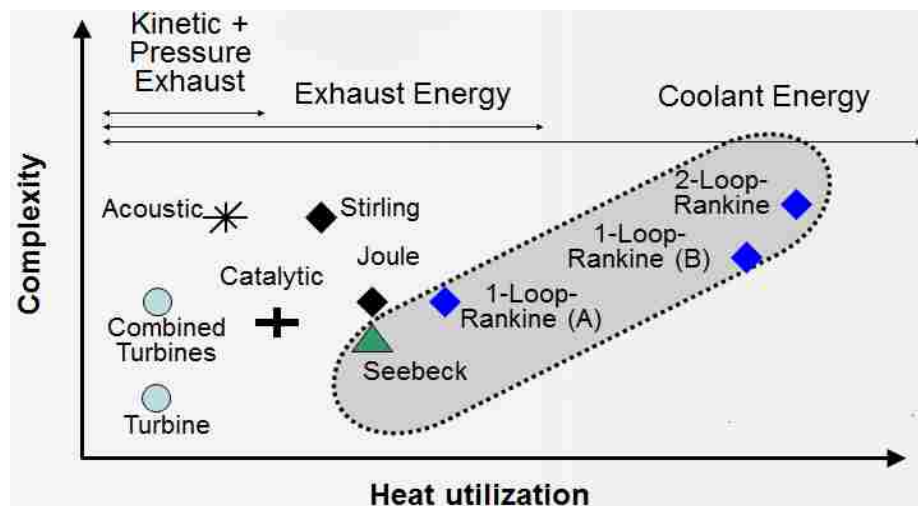


Figure 2.2-8: BMW study on Waste Heat Recovery alternatives [33].

Even Honda has given an impulse, [19]. They have proposed an ORC system to recover heat from exhaust gases of a 2L engine integrating the evaporator with the exhaust ports that are the highest-temperature section of the engine. This feature enables to capture significantly more heat in the ORC than the traditional configuration of the evaporator positioned more downstream around the exhaust pipe. The prototype of the ORC system they have designed, showed a maximum cycle thermal efficiency of 13%, recovering also a portion of heat from the engine coolant. At 100 km/h a cycle output of 2.5 kW is possible for an engine output of 19.2 kW; as a consequence the overall engine thermal efficiency rises from 28.9% to 32.7%.

2.2.5 Gasoline vs diesel engines

Another central point in the discussion is whether gasoline or diesel engines are more suitable for WHR applications. As stated before heavy-duty Diesel engines with high EGR rates represent probably the best combination. Nevertheless for light-duty engines probably the gasoline ones are more suitable. In order to understand this concept it is necessary to analyze what are the strategies to cut down the pollutants highlighting the differences between diesel and gasoline engines. The common three-way catalytic converter is meant to reduce the emissions of the three main pollutants: unburned hydrocarbons (HC), carbon monoxide (CO) and nitrogen oxides (NO_x). The three-way catalysts address carbon monoxide (CO) and hydrocarbons (HC) exhaust emissions via oxidation, while also converting nitrogen oxides (NO_x) via reduction [34]. The three-way catalysts, also known as Non-Selective Catalytic Reduction (NSCR), are most effective when the fuel supplied to the engine has an air-fuel ratio near stoichiometry. As the air-fuel ratio moves away from the stoichiometric value the conversion efficiency drops as depicted in Figure 2.2-9 [17]. Gasoline engines usually operate with an air-fuel ratio close to the stoichiometric value, thus no further after-treatment devices are needed.

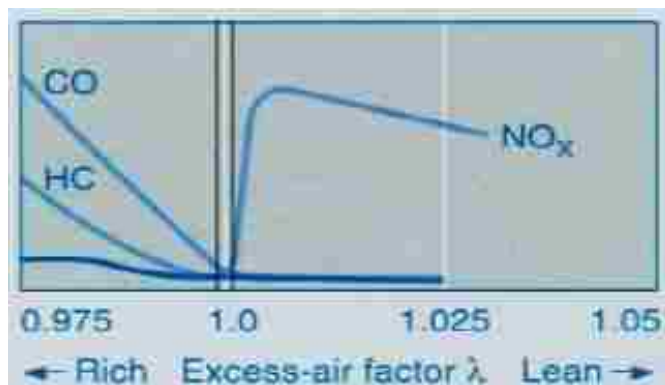


Figure 2.2-9: Three-way catalytic conversion as a function of air fuel ratio [17].

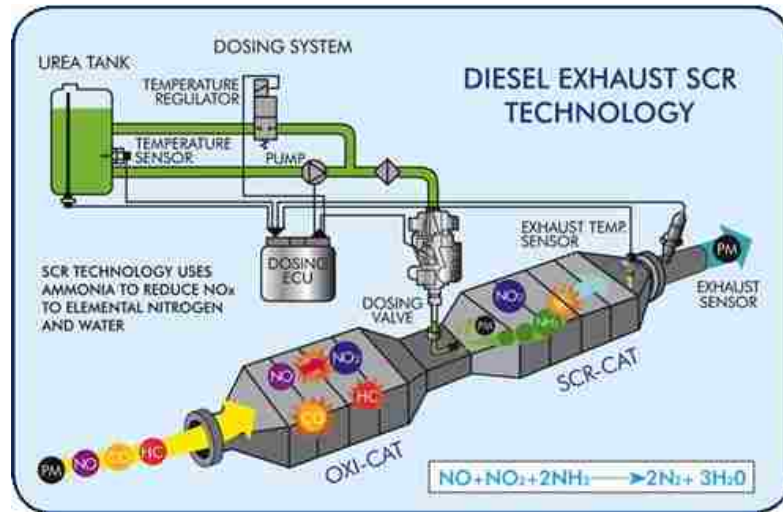


Figure 2.2-10: Selective Catalytic Reduction system layout [35].

On the other hand, in diesel engines, combustion occurs with a significant excess of air, right zone of Figure 2.2-9, making the conventional three-way catalytic conversion not efficient with NO_x , and so forcing the engineers to use other approaches to oxidize the nitrogen oxides (CO and HC are reduced effectively). There are two different strategies that can theoretically be combined together: Exhaust Gas Recirculation (EGR) and Selective Catalytic Reduction (SCR). The EGR system seeks to reduce the production of NO_x reintroducing exhaust gas cooled down into the combustion chamber in order to prevent their formation that strongly increase with increasing temperatures. In an SCR system, a liquid reducing agent composed of urea and water is combined with engine exhaust in the presence of a catalyst to convert NO_x into harmless nitrogen and water vapor, see Figure 2.2-10 [35].

The ideal chemical reactions can operate in a temperature range from 520 K to 720 K, so for Diesel engines that use this after-treatment device, it is very important that their exhaust stream has a temperature higher than 520 K, roughly 250 °C, strongly limiting the heat that can be recovered from a WHR system which must be placed upstream the catalytic converter. On the other hand the exhaust stream recirculated in light-duty vehicle with the EGR system does not have enough energy to feed an ORC, because the recirculation rate is significantly lower compared to the heavy-duty's vehicle one. Moreover, EGR system is less efficient in reducing the NO_x than SCR and, above all, it lowers engine efficiency, so more and more manufacturers are opting to use SCR technology.

Furthermore, the combustion temperature achieved in gasoline engines is higher if compared to diesel engines, meaning that in gasoline engines there is a higher energy density in the exhaust stream.

Finally, since the potential for recovering a portion of the exhaust gas energy is higher for gasoline engines, it seems advantageous to design a WHR system for this kind of light-duty vehicles.

2.2.6 Other considerations on WHR based on ORC in automotive industry

Despite the numerous advantages that the introduction of WHR systems in cars would bring, there are still some difficulties (increase weight, increased installation costs, safety hazards related to the working fluid, more complex packaging, more complex control, transient operation and increased backpressure) that to be overcome require research efforts and capital investments. In light-duty vehicles usually the hood is quite packed and is difficult to find enough room to install the components of an ORC, so the path that the pipes have to follow and the location of pump, heat exchangers and expander have to be accurately designed. The increased weight has to be taken into account when fuel savings are estimated, as well as additional costs have to be taken into account when vehicles will be sold. Moreover, the recovery of energy in the ORC is made at the expenses of the increased backpressure that reduces the energy efficiency of the in-cylinder combustion process. This is an additional problem that has to be considered in designing a WHR system especially for naturally aspirated engines rather than turbocharged ones [31]. However, the main problem is related to the control of the ORC during transient operation. All manufacturers agreed that the ORC should be designed at engine operating conditions that occur during a highway drive at constant speed and load. Vehicles driven in such conditions will have the highest efficiency increase. However, the system should be designed to operate in every situation that the vehicle may encounter without being an obstacle (for instance causing a too high back pressure), but still providing some efficiency gains. Therefore, ORC systems should include different features, such as bypass valves, reservoirs and a control system that guarantees a correct off-design point operation. The implementation of the control unit is probably the main challenge that still remains. Boretti [36] has imagined some solutions to effectively operate the system during transient time and he has simulated the performance of the engine plus heat recovery unit on an urban driving cycle as the New European Driving Cycle (NEDC).

Anyway, a key question that still remains unanswered is whether it is more convenient to use directly the mechanical power coming from the expander or to convert it into electrical power. Automakers have not yet found out which is the best alternative and there is a lack of research articles on this topic. Someone thinks that the best way is to convert the mechanical power into electrical power and store it in a battery. It can be a good solution for hybrid vehicles and for vehicles that have a lot of electric accessories to feed, for example big trucks that might even

have a fridge in it. Nevertheless this further conversion of energy introduces other losses that may reduce the potential fuel savings. Instead if the expander is mechanically coupled to the crank shaft the power generated by the WHR system is directly utilized to move the vehicle. The only problem is that it is not easy to realize this connection, since the ratio between the expander speed and the crank shaft speed would be fixed making the parameters of the ORC varying almost continuously and thus increasing the complexity of the control unit. A possible solution may be to operate the WHR system in a predefined range of engine speeds and decouple it if crankshaft speed is outside this range.

2.3 ORC working fluids

In section 2.1 it has been concluded that the most important design parameters that affect the feasibility of a Rankine cycle are the temperature in the evaporator, the temperature of superheated vapor at expander inlet and the condensing temperature [37]. However, the cycle efficiency is strictly correlated to the working fluid's normal boiling point, critical pressure, latent heat and molecular weight. The selection of the fluid that operates around the cycle is probably the most critical design choice. In Waste Heat Recovery industry to recover energy from low grade heat are commonly employed ORC, as said in section 2.2. The advantages of ORC over steam Rankine cycle become evident when an appropriate working fluid is selected. In this selection five different aspects have to be weighed:

- 1) thermodynamic and physical properties
- 2) chemical compatibility with materials in contact
- 3) environmental aspects
- 4) safety
- 5) availability and cost.

The fluids employed are classified as refrigerants, ASHRAE Standard 34-2007 [38] defines the rules to designate a refrigerant as a number according to the following rules:

- first digit on the right: number of fluorine atoms
- second digit from the right: number of hydrogen atoms plus one
- third digit from the right: number of carbons atom minus one (not used when equal to zero)
- fourth digit from the right: number of unsaturated carbon-carbon bonds in the compound (not used when equal to zero).

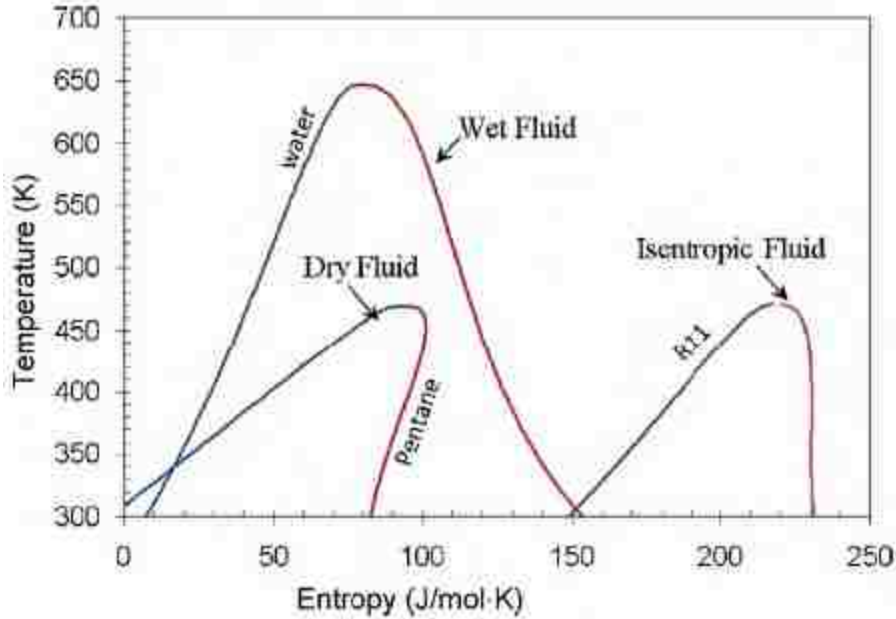


Figure 2.3-1: Types of working fluids: dry, isentropic and wet [39].

The lowercase letter that follows the refrigeration designation refers to the form of the molecule when different forms (isomers) are possible, with the most symmetrical form indicated by the number alone. As the form becomes increasingly unsymmetrical, the letters a, b, and c (lower case) are appended (for example, R-134a). If not all of the carbon bonds are occupied by fluorine or hydrogen atoms, the remainders are attached to chlorine, [40]. Every refrigerant's number is preceded by the capital letter R.

2.3.1 Thermodynamic and physical properties

The thermodynamic and physical properties are features taken into account to make a first differentiation between the fluids suitable for a given application from those that are not. Fluid density, critical temperature and pressure, latent heat and shape of the saturation curve will be discussed. In particular the working fluids are classified according to the slope of the saturation curve on the T-s diagram. There are three different types of fluid correspondent to the three possible slopes (dT/ds) of the red curve in Figure 2.3-1: wet, dry or isentropic.

Since the value of dT/ds tends to infinity for isentropic fluids, it is useful to express the fluid type as a function of the inverse of the slope ($\xi = ds/dT$). If this index is greater than zero the fluid is classified as a dry fluid, if ξ is about zero the fluid is isentropic, if ξ is smaller than zero the fluid is wet [39]. In literature, [41], is also present an empirical equation used to estimate ξ . However, the reliability of this equation is limited, large deviation may occur if it is used to estimate ξ at off-normal boiling points. So it is convenient to directly plot the saturation curve on a T-s diagram and visually establishing whether a fluid is isentropic, dry or wet.

As the name suggests, dry fluids avoid liquid formation at the expander outlet. However, if the fluid is too dry there will be an excessive superheat at the expander outlet, actually this is not always an inconvenient, since the energy left in the fluid can be recovered, by means of an internal heat exchanger (recuperator) as in a recuperative Rankine cycle, to preheat the liquid after it leaves the pump and before it enters the boiler. On the other hand with wet fluids usually a significant amount of superheat is necessary to prevent the formation of droplets at the expander outlet. In general is preferable to avoid that state 4, of figures in section 2.1, falls in the two-phase region because the formation of liquid would wear the expander lowering its performances.

Maizza and Maizza [42] have found out that fluids, with a high latent heat, high density and low specific heat, absorb more energy from the high temperature heat source thus should be preferred in WHR applications also to reduce the size of the system and the working fluid mass flow rate required. On the contrary Yamamoto [43] thinks that, since the expander inlet temperature of a low-grade heat recovery ORC is limited and that the thermal efficiency of the cycle is low, the best way to maximize the power output of the cycle is to have a high mass flow rate, hence low latent heat and high density fluids are to be preferred to increase the expander inlet flow rate. In order to answer to this questions Chen, Goswami and Stefanokos [39] have carried out a theoretical analysis that, even if it is based on some simplifying assumptions, shows how the isentropic enthalpy drop (hence work per unit mass) across the expander increases with higher latent heat when the other parameters are defined. This fact can be explained also considering that big latent heat means long line in the T-s diagram hence the total area of the cycle that is proportional to the work output (as said in section 2.1) increases. In short, fluids with high density, low specific heat and high latent heat should be preferred to maximize the expander work output.

Finally considerations about critical temperature and pressure have to be done. Condensation is a necessary process in an ORC and usually, in WHR applications, occurs at a temperature not lower than 310 K in order to reject heat to the ambient. Therefore fluids that have critical temperature below 310 K (like methane) are excluded. Moreover, the freezing point of the fluid must be below the lowest operating temperature in the cycle. The fluid must also work in an acceptable pressure range, compatible with the reliability of the entire system [39].

2.3.2 Chemical compatibility with materials in contact

Unlike water, the chemical compatibility with materials that enter in contact with organic fluids is a concern and has to be verified. Another difference from water is that organic fluids may suffer chemical deterioration and decomposition at high temperatures.

Thus the maximum operating temperature of the cycle is limited to guarantee the stability of the working fluid. In literature several studies have been carried out to assess the chemical stability of organic fluids with steel and other materials commonly employed in engines as well as their thermal stability at high temperatures and pressures [44], [45] and [46]. The working fluids used tested throughout this test are all compatible with steel in the range of temperature considered.

2.3.3 Safety

As explained before, the American Society of Heating, Refrigeration and Air Conditioning Engineers (ASHRAE) Standard 34-2007 establishes a simple means of referring to common refrigerants replace the chemical names with numbers. It also includes a safety classification that is a good estimation of the level of danger of the refrigerant. Generally, characteristics like non-corrosive, non-flammable and non-toxic are expected. However, this is not always possible and many fluids used in the past in ORCs are considered flammable under certain conditions (in presence of ignition sources or high temperature) [39]. The designer in choosing the working fluid should always be aware of the risks associated with the substance and avoid operating the fluid in conditions that may cause damage to people or devices. The safety groups are denoted by a capital letter and a number. The capital letter indicates the toxicity; A for non-toxic fluids and B for toxic fluids. Instead the following number indicates the degree of flammability; Class 1 means no flame propagation, Class 2 indicates moderate flammability, whereas Class 3 signifies refrigerant having high flammability [38] and [40], look at Figure 2.3-2 for reference.

2.3.4 Environmental aspects

Organic fluids are themselves pollutants and their impact on the environment has to be taken into account carefully. In particular there are three indexes that must be monitored before proceeding with the selection of the fluid:

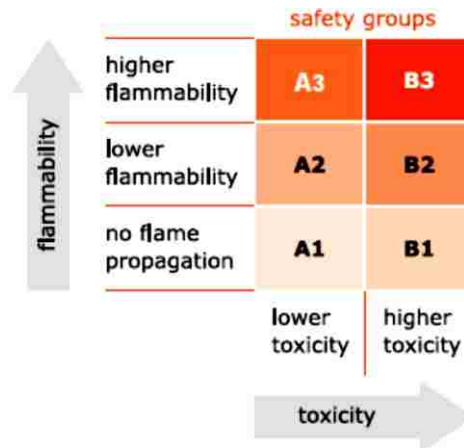


Figure 2.3-2: ASHRAE Standard 34-2007 safety classification [38].

- Ozone Depletion Potential (ODP): ratio of global loss of ozone due to a given substance over the global loss of ozone due to CFC-11 of the same mass. The ODP number can be estimated looking at the chemical composition of the fluid. Chlorofluorocarbons (CFC) have ODP numbers roughly equal to 1. Hydrochlorofluorocarbons (HCFC) have ODPs mostly in range 0.005-0.2 due to the presence of the hydrogen which makes vulnerable to reaction in the lower atmosphere, therefore reducing their chance to reach the stratosphere. Hydrofluorocarbons (HFC) have no chlorine content, so their ODP is basically zero [47].
- Global Warming Potential (GWP): is a measure of how much heat traps in the atmosphere a certain mass of a greenhouse gas compared to the heat trapped by an equal mass of carbon dioxide. It is calculated on a time interval of 20, 100 or 500 years. It is usually used along ODP index to quantify how much dangerous for the environment a fluid can be [48].
- Atmospheric Lifetime (ALT): is a measure of how long it takes to restore the equilibrium following a sudden increase or decrease of the concentration in the atmosphere of the greenhouse gas in question. It can vary from few days to several thousands of years and is very important because it helps to understand the long term impact of a greenhouse gas.

Due to environmental concerns different fluids have been already phased out (R-11, R12, R-113, R-114), while others will be phased out in 2020 or 2030 (such as R-21, R-22, R123, R124, R141b and R-142b).

2.3.5 Availability and cost

The availability and cost of the working fluids are among the considerations when selecting working fluids. Traditional refrigerants used in ORC are expensive, [39]. However, for mass production devices, as a WHR system for vehicles would be, refrigerants suppliers play an important role, since they can offer large discounts to purchase a fluid rather than another. In general the cost of refrigerants is lower if they are massive produced and hydrocarbons such as pentane are cheaper than more complex, chemically speaking, compounds. To conclude, in designing an ORC the economic aspect should always be considered when two or more working fluids have to be compared. The adoption of a fluid, that has better performances with respect to another one, must always be economically justified.

2.4 ORC vs steam Rankine cycle

The best way to understand the differences between an Organic Rankine Cycle and a steam Rankine cycle is to compare the shapes of the saturation curves of the organic fluids commonly employed in ORCs with the water one [49]. With reference to Figure 2.4-1, where the saturation curves of common organic fluids and water are plotted in the T-s diagram, the following considerations can be made:

- The slope of the saturated vapor curve (the right part of the saturation curve) is very negative for water. On the contrary the organic fluids have a saturated vapor curve that is much sharper and in some cases the slope may even become positive as happens for the pentane that is a dry fluid. Even a wet fluid as the R21 has a slope of the saturated curve that is definitely less negative than the water's one. As a consequence, for the organic fluids there is no need of a significant superheating before the expander inlet since the fluid after the expansion is very likely to stay in the vapor area. On the other hand in steam Rankine cycles the temperature at the expander inlet must be at least 450 °C to avoid the formation of droplets, this leads to high thermal stresses. The absence of liquid droplets at the end of the expansion for organic fluids reduces the risk of corrosion and wear of the expander, increasing the lifetime of the expander.
- The difference between the entropy of the saturated liquid and the saturated vapor is much smaller for organic fluids. In other words the organic saturation curve is significantly narrower. This means that also the enthalpy of vaporization is smaller, hence for the same heat transfer rate through the evaporator the organic fluid mass flow rate will be much higher than that of water, that in turn means a higher pumping power requested for a given work per unit mass.
- As a matter of fact, the size of the components is strictly correlated to the volume flow rate of the working fluid because pressure drop increases with the square of the velocity. As previously said the flow rate of the working fluid is much higher for an organic working fluid, hence to reduce the velocity and, as a consequence, the pressure drop is necessary to increase the hydraulic diameter of the pipes and of the heat exchangers.

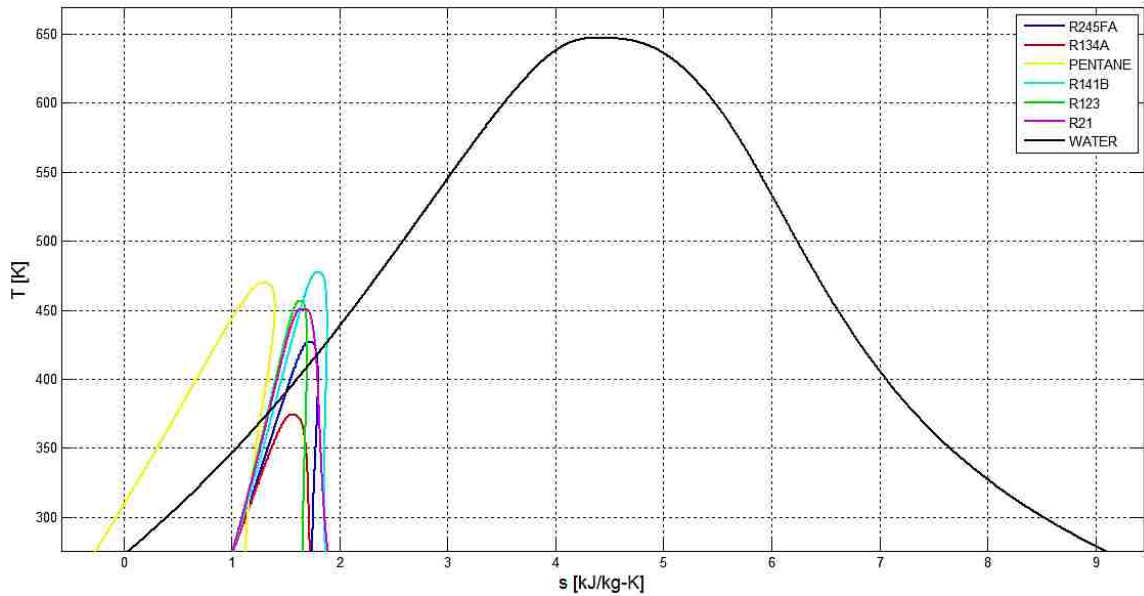


Figure 2.4-1: Saturation curves on T-s diagram.

- As previously mentioned, the critical temperature and pressure of an organic fluid are much lower than those of water. This allows the ORC to recover energy efficiently from low and medium temperature heat sources, as the exhaust gases of an internal combustion engine of a vehicle. Furthermore organic fluids enable to prevent freezing of the working fluid and air infiltration problems encountered with steam Rankine cycle due to the higher critical temperature and critical pressure of water [30].
- In steam Rankine cycle to higher thermal stresses correspond higher mechanical stresses, in fact the high pressure side of the cycle can reach pressures of about 6000-7000 kPa whereas for an ORC those pressures do not exceed 3000 kPa.
- It is generally advisable that the condensing pressure is higher than the atmospheric one in order to avoid air infiltration in the cycle. Low critical temperature organic fluids, such as R134a and R245fa, meet this requirement. However, water and other organic fluids with higher critical temperature usually have a condensing pressure lower than the atmospheric pressure.
- Economically and environmentally speaking water is very convenient if compared to the organic fluids. In fact water is cheaper and is available in huge amounts, it is not toxic, it is not flammable (safety group A1 the only organic fluid that belongs to the same group is R134a), it has a low viscosity, it is chemically stable and, above all, it is an environment friendly fluid (low GWP and null ODP).

- In steam cycles the compression ratio in the pump and the enthalpy drop across the expander are significantly higher, hence usually multi-stage expanders are employed. In ORC the enthalpy drop is lower single-stage expanders are used making the design of the expander easier [30]. Moreover, the expander for an ORC is usually more compact since the organic fluids have a higher density.

To conclude, a Rankine cycle operated with an organic working fluid is more profitable in the low and medium power ranges (less than one MW) and for heat sources with low temperatures. Since in vehicle applications the power range is of few kW and the heat source is at low or medium temperatures the ORC has to be preferred to the traditional steam Rankine cycle.

2.5 ORC components modeling

2.5.1 Expander

The component that influences the most the efficiency of an ORC is the expander. Since expander is also the most expensive component, along with the boiler, an accurate choice of this component has to be made. There are several parameters that are considered in the selection procedure such as isentropic efficiency, pressure ratio, power output, lubrication requirements, complexity, space and weight restrictions, working fluid, rotational speed range, vibrations, reliability and costs [10], [18]. For low power outputs applications, like the Waste Heat Recovery, several researches have demonstrated that positive displacement compressors can be efficiently utilized as expander. The main types of expanders available in the literature are here briefly compared.

2.5.1.1 Turbine

Turbines are dynamic machines commonly used in power generation plants at output powers higher than 100 kW [50]. In such applications efficiencies around 90% can be achieved whereas for smaller output power values the efficiency decreases significantly becoming unacceptable for power outputs around 10 kW. The most critical factor in a turbine is the tip speed the must be very high in order to have a blade Reynolds number of about 10^6 . This condition is very difficult to be achieved for small scale turbines, since the radius of the turbine itself is small, unless very high rotational speeds were used with potential reliability issues. Another problem with turbines is that the blades can be seriously damaged in the case there is formation of droplets at the end of the expansions. This is likely to happen especially for wet fluids with no high superheating.

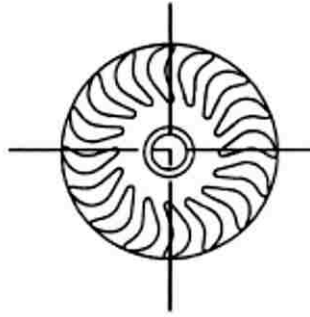


Figure 2.5-1: Schematic drawing of a micro turbine utilized in ORC applications [43].

Moreover, turbines have very small pressure ratio usually less than 2 [10], in an ORC pressure ratios up to 10 are possible so multiple stages turbines are needed which may increase significantly the complexity of the system as well as costs. Finally turbines have poor off-design performances, since in a vehicle the heat available in the exhaust gases may vary a lot during time, a turbine does not represent the best solution. For instance Yamamoto, Furuhashi, Arai and Mori [43] have tested a small turbine for an ORC proving a 46% isentropic efficiency at the reference heat input in the boiler, but if the heat input is reduced by a 25% the isentropic efficiency of the expander drops dramatically to 15%.

2.5.1.2 Reciprocating piston

Pistons are a widely used positive displacement machines. If a piston is employed in an ORC the expansion process is composed by three phases; intake, expansion and exhaust. A precise balance is required as well as an accurate timing of the valves during intake and exhaust phases in order to guarantee the correct functioning of the expander [10]. Friction losses are a major concern for this kind of expander due to the interaction that occurs between the rings the piston and the cylinder. In an ORC, where no combustion process takes place, this problem can be mitigated by dissolving a portion of lubricant in the working fluid. Other causes of irreversibilities are finite time taken by valves and heat transfer through the cylinder walls [18]. Bosch GmbH [28] has tested a reciprocating piston as an expander of a Rankine cycle for WHR application on a heavy-duty commercial vehicle. The huge amount of exhaust heat available in a heavy-duty vehicle allowed the researchers to utilize as a working fluid water and ethanol. Such expander were compared to a turbine and the results showed that in the case water were used as a working fluid a reciprocating piston gives better performances than a turbine. However, if ethanol were used, turbine and piston give approximately the same power output even if they may slightly change in function of the heat input in the cycle. Among the car manufacturers Honda R&D Co. [19] has tested an ORC having as expander a plate axial piston with an electric generator integrated.

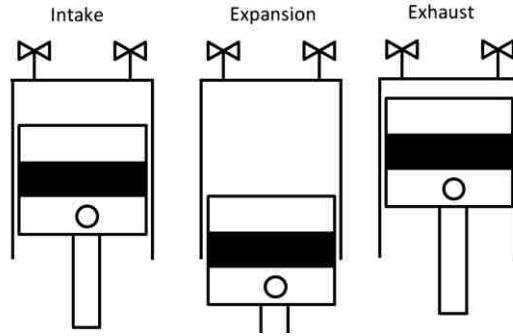


Figure 2.5-2: Schematic drawing of a reciprocating piston type of expander [51].

They opted for this solution mainly to reduce the size of the expander, with promising results in terms of performances and compactness. Nevertheless, despite the fact that reciprocating pistons are a well-established technology, the trend is to prefer other type of expanders in ORCs.

2.5.1.3 Rotary vane

A rotary vane is a positive displacement type of expander in which a high temperature high pressure vapor enters the inlet and starts to expand making the rotor move. As the rotor moves the expansion volume increases, until the expansion is completed and the vapor is exhausted. This kind of expander is robust, can withstand high pressures, it can tolerate wet expansion and has very few vibrations [10]. However, it has very high friction losses and very high leakages which strongly reduce the isentropic efficiency. Mohd, Yamada and Hoshino [52] have tested the performance of this device on an ORC with a low temperature heat source proving a maximum 48% isentropic efficiency. Rotor vane type of expander applied in an ORC has not been further investigated in literature.

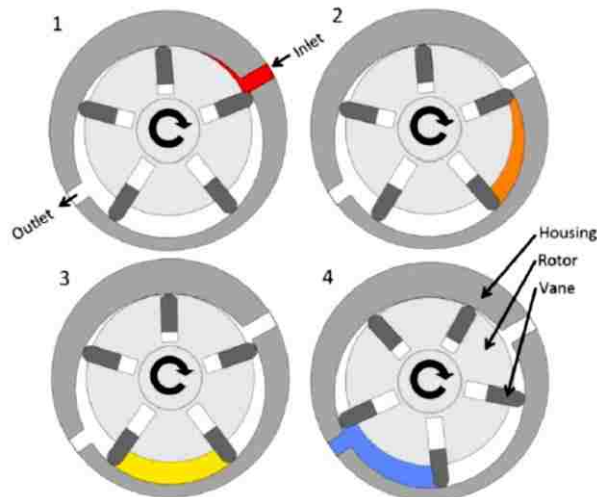


Figure 2.5-3: Schematic drawing of a rotary vane type of expander [10].

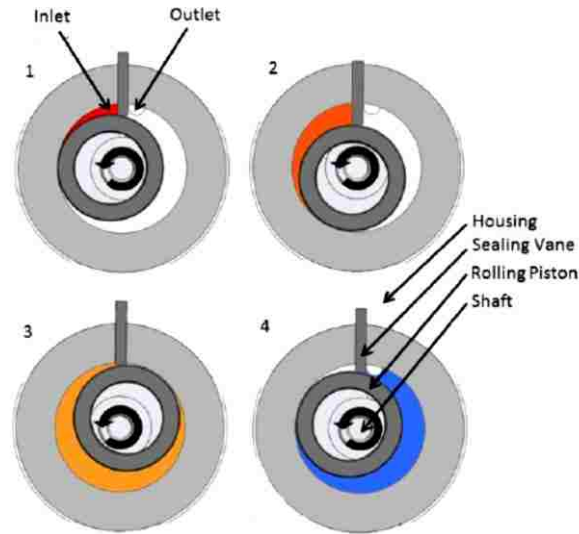


Figure 2.5-4: Schematic drawing of a rolling piston type of expander [10].

2.5.1.1 Rolling piston

Rolling piston, Figure 2.5-4, is a positive displacement type of expander, which shares several advantages and drawbacks with the rotary vane type. As a matter of fact rolling pistons can handle high pressures, have a simple construction and can tolerate wet expansion. On the other hand there are major efficiency losses due to frictions and leakage that occurs between the rolling piston and the cylinder walls, [53].

In a solar powered ORC using R245fa as a working fluid a rolling piston expander was used and tested [54]. The results reported certify a 45.2% isentropic efficiency at 800-900 RPM. However, even if friction losses are reduced if compared to a rotary vane expander, since there are less moving parts, it does not represent an attractive solution for WHR systems based on ORCs especially in vehicle applications, that's why it has not been extensively investigated in literature.

2.5.1.2 Scroll expander

Scroll expander is a positive displacement machine that, as rotary vane and rolling piston, was borne as a compressor for refrigeration and air conditioning industry but can be easily converted to expander mode with good results. As previously mentioned positive displacement type of expanders appears to be more suitable for ORCs applications with low power outputs because they are characterized by lower flow rates, higher pressure ratios and much lower rotational speeds [55]. It has a geometry that is much more complicated than that of the other positive displacement expanders thus manufacturing tolerances must be very tight; however it seems to be the best solution for ORCs applications.

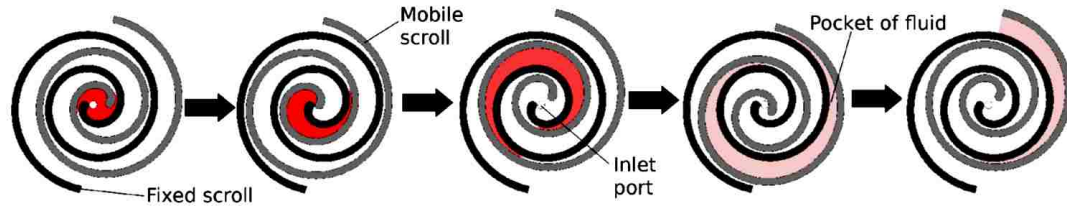


Figure 2.5-5: Schematic drawing of a scroll type of expander [49].

It can handle high pressures and wet expansion, moreover it can achieve high pressure ratios, it is reliable and it has very good off-design point performances.

With reference to Figure 2.5-5 a scroll expander is made up by two interfitting spiral-shaped scroll members. They are called fixed and orbiting scroll since the first one does not move while the second one orbits around the shaft center. The intake section is in the central region of the scroll. A portion of the vapor is trapped in a pocket that is moved toward the scroll periphery as the orbiting scroll rotates [56]. During this process the pocket volume increases according to the working fluid expansion. Generally it takes two or three shaft rotations to achieve the fully expanded state and bring the working fluid from the intake to the exhaust state. One of the main advantages of the scroll expander is that the expansion process is smooth and continuous without vibrations and pulsations, as in reciprocating piston expander.

The principal contributor to the efficiency losses is the internal leakage [55]. There are two main leakage passages in a scroll expander, known respectively as flank leakage and radial leakage [10]. The latter is due to a gap between the bottom or the top plate and the scrolls, whereas the radial leakage results from a gap between the flanks of the scrolls [57]. Several applications and studies have proven that isentropic efficiencies that range from 40% to as high as 83% can be achieved [50], [56], [58] and [59]. Moreover, good performances have been reported in literature at partial loads [60]. It has been investigated extensively in literature and so far it is the most used expander for small scale ORCs, however for automotive applications it has been tested only on stationary test rigs.

2.5.1.3 Expander modeling

In order to predict the performances of an expander in an ORC is necessary to mathematically model its behavior in order to carry out simulations. The power generated by any type of expander can be modeled according to an energy balance equation such as that presented by Wang et al. [61]:

$$\dot{W}_{exp} = \dot{m}_{wf}(h_3 - h_{4s})\eta_{exp} \quad (2.24)$$

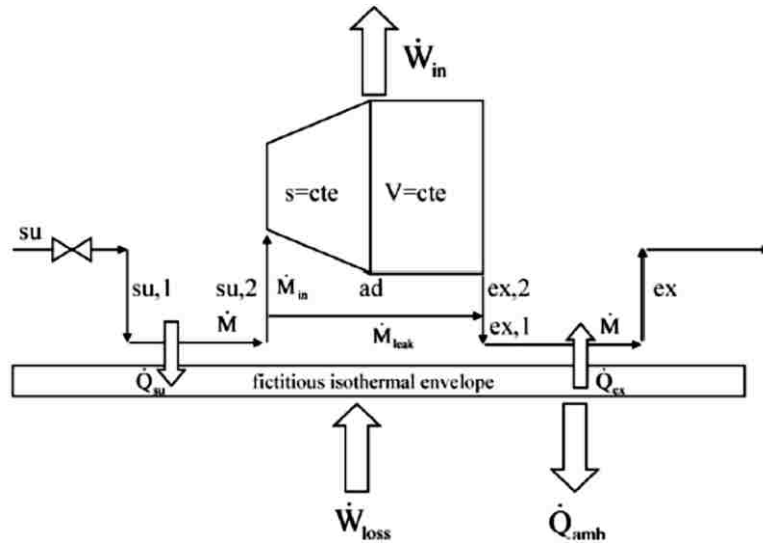


Figure 2.5-6: Conceptual scheme of a scroll expander model [55].

The subscripts refer to the states indicated in Figure 2.1-8. Instead h_{4s} is the enthalpy per unit mass that the working fluid would have at the expander outlet for an isentropic efficiency equal to one ($s_{4s}=s_3$). Basically knowing the fluid properties at the expander inlet (state 3) h_{4s} can be computed looking at the fluid properties and for a given isentropic efficiency and a working fluid mass flow rate the power generated by the expander can be computed. Nevertheless this simple equation does not give any indication of what happens inside the expander. In the following, two different ways to model a scroll expander for ORCs will be presented.

Lemort et al. [55] have proposed a semi-empirical model of a scroll expander. In particular they have decomposed the transformation that take place in the expander into six different steps.

With reference to Figure 2.5-6 the steps will be reported and briefly explained:

- 1) Adiabatic supply pressure drop: it accounts for all pressure losses encountered by the fluid from the suction line to the suction chamber. The main cause of this pressure loss is that during part of the suction process the expander suction port is blocked by the tip of the orbiting scroll, and the actual suction port area is reduced, Figure 2.5-7.
- 2) Isobaric supply cooling down: the working fluid is cooled down at constant pressure, this heat losses occur between the working fluid and the scroll, between the working fluid and the expander shell and between the shell and the outside ambient. In the model presented both supply and exhaust heat transfers are computed introducing a fictitious metal envelop at uniform temperature.
- 3) Adiabatic and reversible expansion to the pressure imposed by the built-in volume ratio of the expander.

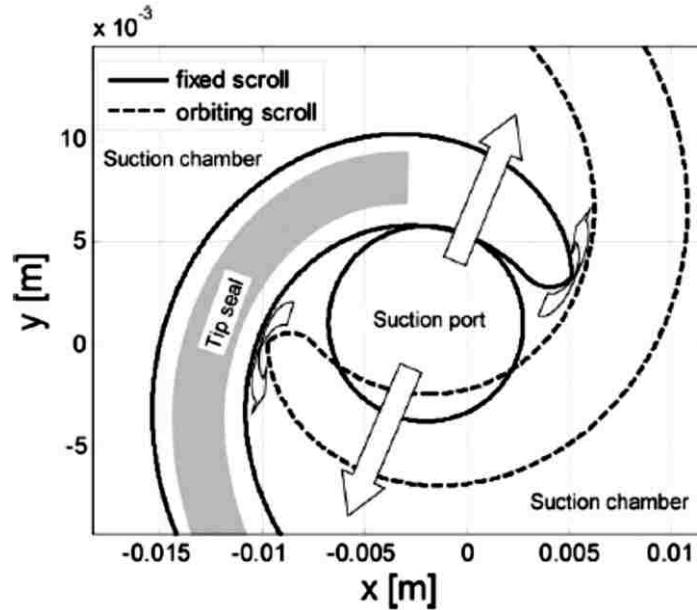


Figure 2.5-7: Suction chamber of a scroll expander [55].

Only a portion of the working fluid mass flow rate, called internal mass flow rate, enters the expander and takes part to step 3 and step 4. The remaining is leakage mass flow rate that does not participate. The internal mass flow rate generates useful power, computed as the sum of the suction, expansion and discharge powers.

- 4) Adiabatic expansion or compression at a constant volume: after the expansion has occurred the pressure of the working fluid can be either higher or lower of the system discharge pressure. This happens because the internal pressure ratio imposed by the expander is fixed. The model proposed by Lemort et al. assumes that as soon as the exhaust port is opened the internal mass flow rate slightly changes in order to compensate this pressure difference. Basically if $p_{ad} > p_{ex}$ the internal mass flow rate slightly decrease in order to make the internal mass flow rate fluid pressure equal to the discharge line pressure. Vice versa if $p_{ad} < p_{ex}$ the internal mass flow rate slightly increases. After this equilibrium is achieved the actual discharge process takes place.
- 5) Adiabatic mixing between supply and leakage flow.
- 6) Isobaric exhaust cooling down or heating up.

This model has been validated by the authors of the article and gives predictions with a maximum deviation of 2% with respect to the measurements. Unfortunately this model relies on parameters that have to be found from performance measurements. Hence it does not look like suitable for simulations that have to be carried out in early design stages, basically when a physical prototype of the machine is not yet available.

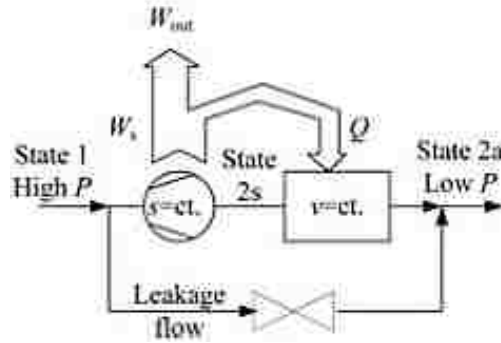


Figure 2.5-8: Conceptual scheme of a scroll expander model [56].

On the other hand Oralli et al. [56] have developed a model for a scroll expander that does not require any specific data that comes from experimental tests. The model proposed is reported in the following.

As in the model presented before, only a portion of the working fluid mass flow rate enters the scroll expander, the remaining part bypasses the expander and does not produce power. The core expansion process according to this model evolves first isentropically from state 1 to 2s of Figure 2.5-8, followed by a constant volume pressure rise from 2s to 2a. Only a portion of the power generated during the isentropic expansion can be used, in fact a portion of this power is reintroduced in the working fluid as heat and contributes to the pressure rise of the fluid from 2s to 2a.

2.5.2 Heat exchangers

In ORCs for WHR applications the core component in which actually the energy, that otherwise would have been lost, is recovered is the evaporator (or boiler). The importance of this component results evident since the more heat is captured by the evaporator the greater is the additional work that can be potentially produced by the ORC. Moreover, as mentioned in the previous sections, in an ORC there is at least one more heat exchanger, the condenser, and in recuperative ORC there is even a third one, the recuperator. The total cost of these three heat exchangers accounts for more than a half of the total cost of the components of an ORC. The main issues related to such devices are the same of the usual heat exchangers; pressure drop, heat transfer rate and temperatures at the inlet and outlet sections. In particular the pressure drop, hence friction factor, on the exhaust gas side (hot side of the evaporator) should not be too high, since, very likely, the evaporator in question is installed upstream with respect to the turbine, and so the exhaust gas has to maintain some exergy in order to expand and generate as much power as possible. Moreover, for vehicle applications, size and weight of the heat exchangers should be limited.

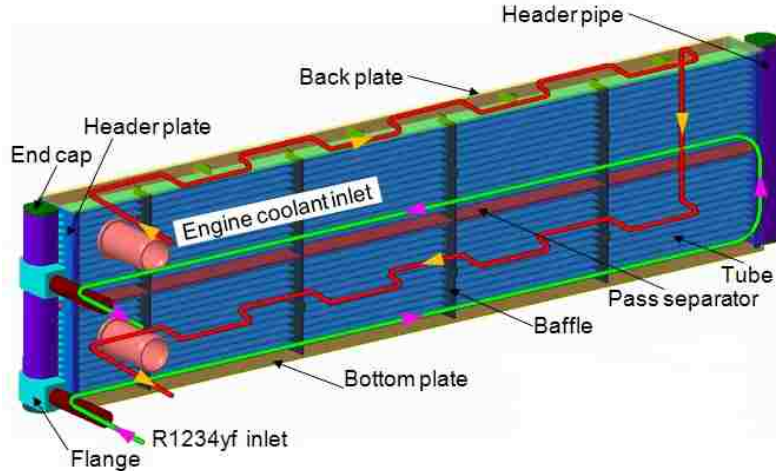


Figure 2.5-9: Layout of the shell and tube evaporator [32].

Nowadays, boiler employed are able to recover about the 50% of the heat potentially available in the exhaust gases (recovery efficiency defined as Equation (2.21)), it is a good result but it can be further improved increasing the exchanger effectiveness still considering the capital costs. In literature applications of shell and tube heat exchangers are reported, [21] and [32], as well as counter-flow heat exchangers [62] and tube and fins heat exchangers [19].

In particular, Bae et al. [32] have modified the parameters, such as baffle distance and number of passages, of a shell and tube heat exchanger in order to study the heat transfer rate and pressure drop variations of a boiler, see Figure 2.5-9. They have concluded that a two passages shell and tube heat exchanger with baffle positioned at 14.5 mm is the solution that gives the best heat transfer rate with a still acceptable pressure drop.

To analyze and model a heat exchanger, regardless the heat exchanger type, the most important parameter is the heat transfer rate that takes place in the component. Figure 2.5-10 illustrates a counter-flow heat exchanger where the subscripts “h” and “c” denote respectively the hot and cold side and the subscripts “1” and “2” denote the section of the exchanger. In this case the heat transfer rate can be computed with the following equation:

$$\dot{Q} = \dot{m}_h c p_h (T_{h1} - T_{h2}) = \dot{m}_c C p_c (T_{c2} - T_{c1}) \quad (2.25)$$

However, when modeling an ORC only the temperatures at the inlet section of both cold and hot side of the exchanger are known. In this case the heat transfer rate can be computed in different ways. The most utilized method is called ϵ -NTU, by knowing the effectiveness of the exchanger (ϵ) the heat transfer rate can be computed as follows:

$$\dot{Q} = \epsilon C_{min} (T_{h1} - T_{c2}) \quad (2.26)$$

Where C_{min} (minimum heat capacity rate) is the smallest between the $\dot{m}_h c p_h$ and $\dot{m}_c C p_c$.

The term inside the bracket is the maximum possible temperature difference, in a real heat exchanger the effectiveness is less than 1 so the outlet temperature of the cold side fluid will be always lower than the inlet temperature of the hot side fluid. This method requires that the side in which there is the minimum heat capacity rate is known; in the boiler of a WHR unit based on an ORC, the side that has the lower heat capacity rate is the hot side where the exhaust gases flow, [8] and [63]. The outlet temperature of the fluid in this side is then computed with the following equation:

$$T_{h2} = T_{h1} - \varepsilon(T_{h1} - T_{c2}) \quad (2.27)$$

Hence for the evaporator considering that the hot fluid is the exhaust gas:

$$T_{exh,out} = T_{exh,in} - \varepsilon(T_{exh,in} - T_2) \quad (2.28)$$

As a matter of fact the key parameter to apply this method is the effectiveness of the heat exchanger. This parameter is far from being constant for every operating conditions, and is function of numerous other parameters. However, according to Shah and Sekulic [64], rearranging all the variables it turns out that, for a given flow arrangement, the effectiveness of an heat exchanger is only function of two non-dimensional groups called heat capacity rate ratio (C^*) and number of transfer units (NTU). The latter is defined as the overall heat transfer coefficient multiplied by the heat transfer surface and divided by the minimum heat capacity rate:

$$NTU = \frac{UA}{C_{min}} \quad (2.29)$$

Whereas the heat capacity rate ratio is simply the ratio of the minimum heat capacity rate over the maximum one:

$$C^* = \frac{C_{min}}{C_{max}} \quad (2.30)$$

For a known heat exchanger, if effectiveness maps are available and C^* as well as NTU can be determined the effectiveness is univocally defined.

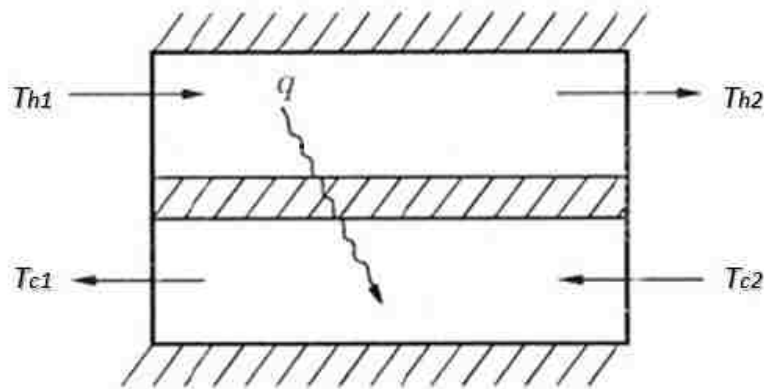


Figure 2.5-10: Heat transfer model of a counter flow heat exchanger [64].

Finally, in order to make a more complete and accurate analysis of what happens inside a heat exchanger it is important to find out the section where the minimum temperature difference between the cold fluid and the hot fluid occurs (pinch point). This concept is explained referring to the boiler. The fluids may follow two possible temperature profiles as illustrated in Figure 2.5-11. In both cases Equation (2.40) holds, however there is an important difference in the way the mass flow rate of the working fluid is computed. In the first case the pinch point occurs at the exhaust gas outlet section, left side of Figure 2.5-11. Assuming that data on the working fluid mass flow rate and specific heat are available, the working fluid mass flow rate for a given temperature at state 3 is computed as follows:

$$\dot{m}_{wf} = \frac{\dot{m}_{exh} C_{p_{exh}} (T_{exh,in} - T_{exh,out})}{(h_3 - h_2)} \quad (2.31)$$

On the other hand several articles ([5], [6] and [39]) have reported that the pinch point might occur in the section of the heat exchanger where the working fluid reaches the saturated liquid state, right side of Figure 2.5-11. In this case the working fluid mass flow rate required is given by:

$$\dot{m}_{wf} = \frac{\dot{m}_{exh} C_{p_{exh}} (T_{exh,in} - T_{exh,PP})}{(h_3 - h_{2'})} \quad (2.32)$$

Where $T_{exh,PP}$ is the temperature of the exhaust gases at the pinch point.

From this point on all the heat exchangers will be assumed to be of counter-flow type.

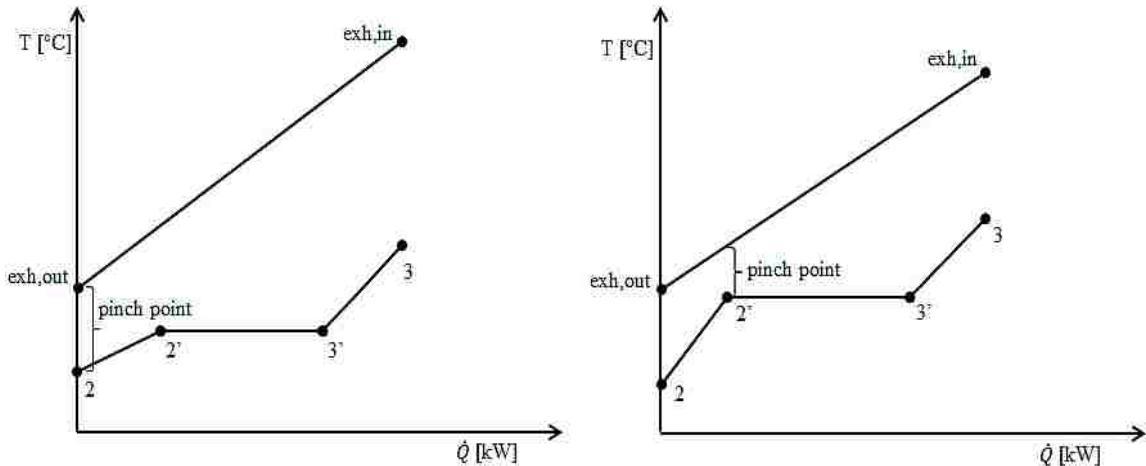


Figure 2.5-11: Evaporator temperature profile.

3. SIMULATION TOOLS DEVELOPMENT

3.1 Preliminary model of ORC for assessing design alternatives

In the early design phase the goal was to assess the feasibility of an Organic Rankine Cycle based system to recover energy from the exhaust gas of an engine, understanding how different variables influence the net power output of an ORC operating under certain constraints in stationary operating conditions. Hence, a set of energy balance equations, describing each component of an ORC, has been developed in order to compare the performance achievable with a standard ORC and a recuperative ORC by different organic fluids at various operating conditions. The thermodynamic model was built and calculated using a Matlab application with Refprop [65].

Since the ORC is meant to recover energy from the exhaust gases, the input data of the analysis were the exhaust gas temperature ($T_{exh,in}$), mass flow rate (\dot{m}_{exh}) and specific heat ($C_{p_{exh}}$) at the evaporator inlet. The preliminary model is operates with constant inputs evaluated at target vehicle operating conditions (design point).

The model developed takes into account four main variables that appear to be the most influencing in an ORC design. The first variable is the type of system layout; in fact two different mathematical models have been set up for a standard ORC and a recuperative ORC. The second variable is the type of working fluid, for instance for the recuperative ORC shown in Figure 3.1-1 six different organic working fluids have been compared. Finally the third and fourth variables were the pump compression ratio and the expander inlet temperature, basically for a given system layout and a given organic working fluid several combinations of pump compression ratio and expander inlet temperature have been used to evaluate the net power output of the system.

3.1.1 Preliminary model input data

Once the program is run it asks for several input data. In particular, in the first widow the user has to insert the pump inlet temperature, that is assumed to be equal to the condensing temperature, the maximum temperature at the expander inlet and the maximum and minimum pump compression ratio, Figure 3.1-2. These inputs are very important because they are used to define the range of compression ratio and expander inlet temperature utilized throughout the program. More specifically, the pump compression ratio is assumed to vary from the minimum pump compression ratio, that is set high enough in order that the pump provides the minimum pumping power to the working fluids to overcome the pressure drops in the heat exchangers and pipes, to as high as the maximum pump compression ratio.

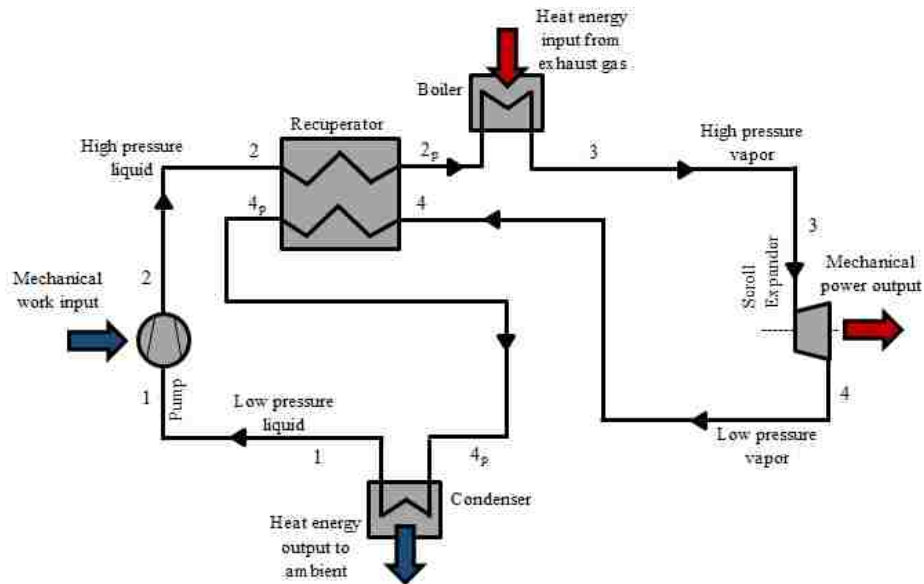


Figure 3.1-1: Recuperative ORC system layout for preliminary analysis.

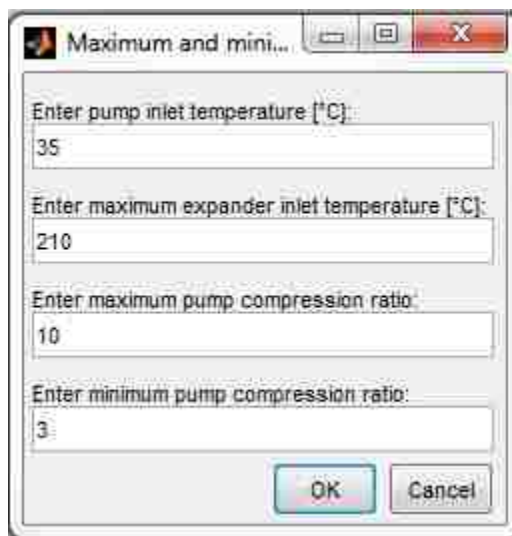


Figure 3.1-2: First input window of the preliminary model.

On the other hand, the expander inlet temperature is assumed to vary from the saturated vapor temperature of the selected working fluid at the expander inlet pressure, up to the maximum expander inlet temperature defined in the first input window, that usually corresponds to the maximum temperature that the expander can withstand without potential damages.

In order to better understand how the pump compression ratio and the expander inlet temperature are chosen an example is reported in Figure 3.1-3, where the Mollier diagram of the R245fa is plotted. By imposing that the working fluid at the pump inlet (state 1) is in the saturated liquid condition at a temperature of 35 °C the pressure at the pump inlet is univocally defined.

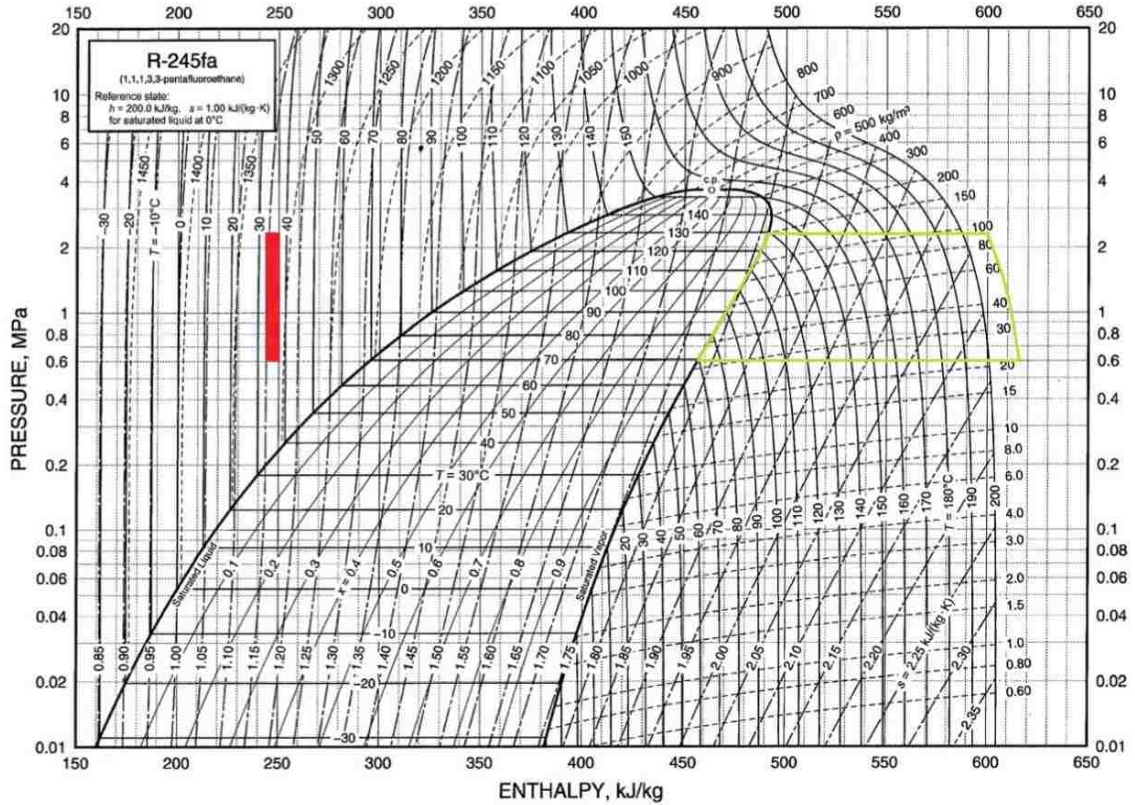


Figure 3.1-3: R245fa Mollier diagram.

Now, knowing that the pump compression ratio may vary from 3 to 10, the state 2 lays somewhere in the red segment drawn on the left side of Figure 3.1-3. For each pressure at state 2 the temperature at state 3 can vary from the temperature of the saturated vapor to the maximum expander inlet temperature, thus state 3 falls inside the area defined by the green lines in Figure 3.1-3, on the right side of the saturation curve. For each combination of state 2 and state 3, hence for each combination of pump compression ratio and expander inlet temperature, the net power output of the system is computed.

The second input window asks to the user to insert data about the exhaust gases Figure 3.1-4. Once this data are specified other parameters, mainly regarding the effectiveness and pressure drop in the heat exchangers and the isentropic efficiency of the pump and of the expander, have to be put in the model, Figure 3.1-5, Figure 3.1-6 and Figure 3.1-7. These parameters have been assumed in order to make the results more realistic, but, for the purpose of the preliminary analysis, they are not very important. The objective here is not to assess accurately the net power output of the system, but rather to compare the net power output achievable with different combinations of the pump compression ratio and expander inlet temperature in different system architectures.

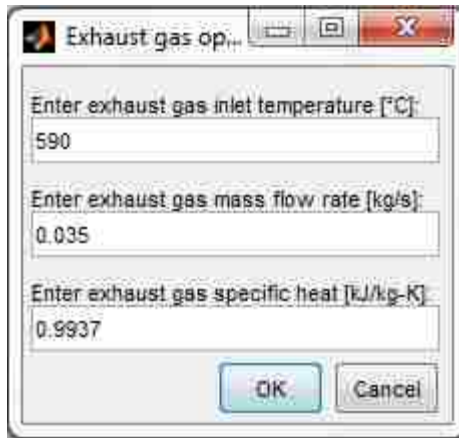


Figure 3.1-4: Second input window of the preliminary model.7

At the beginning of the program an array containing the names of the different working fluids compared is defined. The thermodynamic properties of such fluids are stored in a database called Refprop, there is a Matlab function called “refprop.m” that, interrogating this database, is able to return every kind of thermodynamic property of the fluid in question at a given state if two other properties are known. For example if temperature and pressure are known the database can be interrogated, the table of properties of the desired fluid can be read and the enthalpy, the density as well as all the other properties can be evaluated.

In the following paragraphs, the set of equations utilized to compute the fluid properties at each state around the cycle and the main outputs is presented referring to a recuperative ORC, Figure 3.1-1.

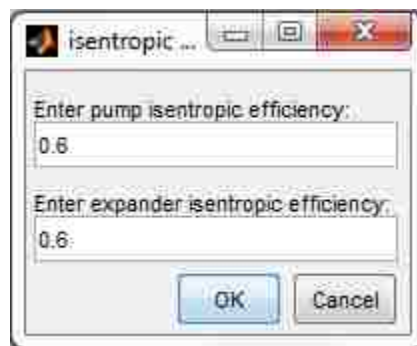


Figure 3.1-5: Third input window of the preliminary model.



Figure 3.1-6: Fourth input window of the preliminary model.

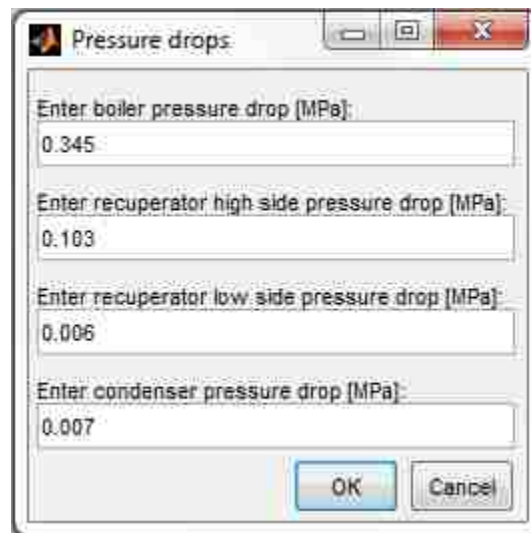


Figure 3.1-7: Fifth input window of the preliminary model.

3.1.2 Algorithm resolution

3.1.2.1 Pump

As previously mentioned the condenser outlet (pump inlet) state is taken as saturated liquid at a temperature that is about as low as we can cool the working fluid using ambient air as heat sink. Since at the saturated liquid state only one thermodynamic property is sufficient to univocally define the others. The temperature at state 1 (T_1) has been already specified in the first input window, thus the program with a “for” loop uploads from Refprop, pressure, enthalpy, entropy and density of the fluid at state 1 (p_1 , h_1 , s_1 and ρ_1) of each working fluid.

```

82 - fluid={'R245FA','R134A','PENTANE','R141B','R123','R21'};
83
84 - for k=1:length (fluid);
85 -     MaxPower (k)=0;
86 -     MaxEffTot (k)=0;
87 - end
88
89 - for k=1:length (fluid)
90
91 -     p1 (k) = refpropm('P','T',T1,'Q',0,fluid(1,k));
92 -     h1 (k) = refpropm('H','T',T1,'Q',0,fluid(1,k));
93 -     r01 (k)= refpropm('D','T',T1,'Q',0,fluid(1,k));
94 -     cp1 (k)= refpropm('C','T',T1,'Q',0,fluid(1,k));
95 -     s1 (k) = refpropm('S','T',T1,'Q',0,fluid(1,k));
96
97 -     if p1(k)*betamax>= refpropm('P','C',0,' ',0,fluid(1,k))
98 -         p2max(k)= refpropm('P','C',0,' ',0,fluid(1,k))-10;
99 -     else
100 -         p2max(k)=p1(k)*betamax;
101 -     end
102
103 -     p2min (k) = p1(k)*betamin;
104 -     p2 (k,:) = (p2min(k):(p2max(k)-p2min(k))/120:p2max(k));
105 -     T3min (k) = refpropm('T','P',p2max(k)-((deltaP_22prime*...
106 -         p2max(k)/p1(k)/betamax)...
107 -         +deltaP_2prime3),'Q',1,fluid(1,k))+10;
108 -     T3 (k,:) = (T3min(k):(T3max-T3min(k))/30:T3max);

```

Figure 3.1-8: Working fluid array, state 1 thermodynamic properties and definition of the range of p_2 and T_3 .

Then the recuperator inlet (pump outlet) pressure (p_2) is determined as:

$$p_2 = p_1 \cdot \beta \quad (3.1)$$

Where, β is the pump compression ratio. An “if” loop limits the maximum pressure at state 2 in the case that, for a certain compression ratio, the pressure at state 2 is higher than the critical one, Figure 3.1-8.

Then two other “for” loops begin, one for each possible pressure at the state 2 and the other one for each temperature at state 3. The work per unit mass requested by the pump is:

$$w_{12} = \frac{p_2 - p_1}{\rho_1} \cdot \frac{1}{\eta_{pump}} \quad (3.2)$$

Where the density of the fluid at liquid state remains constant across the pump and η_{pump} is the pump isentropic efficiency. Since the work per unit mass is equal to the pressure rise across the pump, the enthalpy at state 2 is:

$$h_2 = h_1 + w_{12} \quad (3.3)$$

```

111 - for i=1:length (p2)
112 -     for j=1:length (T3)
113
114         % Work per unit mass requested by the pump[kJ/kg]
115 -     w_pump (k,i,j) = (p2(k,i)-p1(k))/rho1(k)/eff_pump;
116 -     h2 (k,i,j)     = h1(k)+w_pump (k,i,j)*1000;
117 -     T2 (k,i,j)     = refpropm('T','P',p2(k,i),...
118         'H',h2(k,i,j),fluid(1,k));
119 -     rho2 (k,i,j)   = refpropm('D','T',T2(k,i,j),...
120         'P',p2(k,i),fluid(1,k));
121 -     cp2 (k,i,j)    = refpropm('C','T',T2(k,i,j),...
122         'P',p2(k,i),fluid(1,k));
123 -     s2 (k,i,j)     = refpropm('S','T',T2(k,i,j),...
124         'P',p2(k,i),fluid(1,k));
125 -     T_subcooling2 (k,i,j)= - T2(k,i,j) + ...
126         refpropm('T','P',p2(k,i),'Q',0,fluid(1,k));

```

Figure 3.1-9: State 2 thermodynamic properties.

Two fluids properties are necessary to completely define a state around the cycle, so once h_2 and p_2 are defined the other fluid properties at state 2 are determined using the Refprop database Figure 3.1-9.

3.1.2.2 Boiler

The pressure at the boiler outlet (p_3) is equal to the pressure at the pump outlet minus the pressure drop across the high side of the recuperator ($\Delta p_{22'}$) and boiler ($\Delta p_{2'3}$):

$$p_3 = p_2 - \Delta p_{22'} - \Delta p_{2'3} \quad (3.4)$$

```

p3(k,i,j) = p2(k,i)-(deltaP_22prime/2*(1+i/length (p2)))-...
(deltaP_2prime3/3*(1+i/length (p2)+j/length (T3)));
h3 (k,i,j) = refpropm('H','T',T3(k,j),'P',p3(k,i,j),fluid(1,k));
ro3 (k,i,j) = refpropm('D','T',T3(k,j),'P',p3(k,i,j),fluid(1,k));
cp3 (k,i,j) = refpropm('C','T',T3(k,j),'P',p3(k,i,j),fluid(1,k));
s3 (k,i,j) = refpropm('S','T',T3(k,j),'P',p3(k,i,j),fluid(1,k));

p4(k,i,j) = p1(k)+deltaP_4prime1+(deltaP_44prime/2*...
(1+j/length(T3)));
h4ideal (k,i,j) = refpropm('H','P',p4(k,i,j),'S',s3(k,i,j),fluid(1,k));
h4 (k,i,j) = h3(k,i,j) - eff_exp*(h3(k,i,j)-h4ideal(k,i,j));
T4 (k,i,j) = refpropm('T','P',p4(k,i,j),'H',h4(k,i,j),fluid(1,k));
ro4(k,i,j) = refpropm('D','T',T4(k,i,j),'P',p4(k,i,j),fluid(1,k));
cp4 (k,i,j) = refpropm('C','T',T4(k,i,j),'P',p4(k,i,j),fluid(1,k));
s4 (k,i,j) = refpropm('S','T',T4(k,i,j),'P',p4(k,i,j),fluid(1,k));
% Work per unit mass generated by the expander [kJ/kg]
w_exp(k,i,j) = (h3(k,i,j)-h4(k,i,j))/1000;

```

Figure 3.1-10: State 3 and 4 thermodynamic properties.

The temperature at the boiler outlet or expander inlet (T_3) is an independent variable and so it is already defined. Since p_3 and T_3 are determined the remaining properties of the fluid are uploaded from Refprop Figure 3.1-10.

3.1.2.3 Expander

The pressure at the expander outlet (p_4) must be equal to the pressure at the pump inlet (p_1) plus the pressure drop across the low side of the recuperator ($\Delta p_{44'}$) and condenser ($\Delta p_{4'1}$).

$$p_4 = p_1 + \Delta p_{44'} + \Delta p_{4'1} \quad (3.5)$$

The enthalpy at the expander outlet is given by:

$$h_4 = h_3 - \eta_{exp} (h_3 - h_{4,ideal}) \quad (3.6)$$

Where η_{exp} is the isentropic efficiency of the expander, defined in the third input window, and $h_{4,ideal}$ is the enthalpy that the fluid would have considering an ideal isentropic expansion from p_3 to p_4 . Taking into account that isentropic expansion means that $s_3 = s_{4,ideal}$ and that $p_4 = p_{4,ideal}$, $h_{4,ideal}$ can be determined from Refprop.

The corresponding work per unit mass produced in the expander is equal to the enthalpy drop across the expander, hence:

$$w_{34} = (h_3 - h_4) \quad (3.7)$$

Once h_4 and p_4 are obtained T_4 , s_4 , ρ_4 are determined from the fluid properties database Figure 3.1-10.

3.1.2.4 Recuperator

This component is assumed to be a counter-flow heat exchanger with a given effectiveness defined in the fourth input window. The ϵ -NTU method is used to solve this component. Since the mass flow rate is equal for both sides, the maximum temperature difference between inlet and outlet takes place in the side where the specific heat is the lowest. In general the specific heat of the working fluid at the inlet of the low pressure side of the recuperator (state 4) is higher than the specific heat at the inlet of the high pressure side of the recuperator (state 2). Hence, for a given recuperator effectiveness ϵ_{rec} , the temperature at the outlet of the low pressure side of the recuperator ($T_{4'}$) is computed as follows:

$$T_{4'} = T_4 - \epsilon_{rec} (T_4 - T_2) \quad (3.8)$$

The low side outlet pressure ($p_{4'}$) is equal to inlet pressure minus the pressure drop across the recuperator ($\Delta p_{44'}$):

$$p_{4'} = p_4 - \Delta p_{44'} \quad (3.9)$$

Finally from Refprop the correspondent enthalpy, entropy and density of the fluid are computed.

The heat extracted from the low pressure side of the recuperator is transferred to the high pressure side. Since we are making a unit mass flow rate analysis, the enthalpy drop/rise must be equal on both sides of the recuperator, allowing evaluating the enthalpy at the boiler inlet:

$$h_{2'} = h_2 + (h_4 - h_{4'}) \quad (3.10)$$

Taking into account that:

$$p_{2'} = p_2 - \Delta p_{22'} \quad (3.11)$$

$T_{2'}$, $s_{2'}$ and $p_{2'}$ are uploaded from the database. It must be pointed out that at state 2' the fluid should be sub-cooled liquid. There is a “if” loop” that in the case the state 2' computed with Equations (3.10) and (3.11) falls in the two-phase region of the Mollier diagram sets the state 2' on the saturated liquid curve still at pressure $p_{2'}$. The resulting new $h_{2'}$ is used to determine the actual enthalpy drop in the low pressure side of the recuperator that is limited, hence new $h_{4'}$ and $T_{4'}$ slightly higher are computed, Figure 3.1-11.

```

T4prime (k,i,j) = T4(k,i,j) - eff_rec*(T4(k,i,j)-T2(k,i,j));
p4prime (k,i,j) = p1(k)+deltaP_4prime1;
h4prime (k,i,j) = refpropm('H','T',T4prime(k,i,j),'P',...
    p4prime(k,i,j),fluid{1,k});
rc4prime (k,i,j) = refpropm('D','T',T4prime(k,i,j),'P',...
    p4prime(k,i,j),fluid{1,k});
cp4prime (k,i,j) = refpropm('C','T',T4prime(k,i,j),'P',...
    p4prime(k,i,j),fluid{1,k});
s4prime (k,i,j) = refpropm('S','T',T4prime(k,i,j),'P',...
    p4prime(k,i,j),fluid{1,k});
h2prime(k,i,j) = h2(k,i,j) + (h4(k,i,j) - h4prime(k,i,j));
p2prime(k,i,j) = p2(k,i) - (deltaP_22prime/2*...
    (1+i/length(p2))) * (p2max(k)/p1(k)/betamax);
if h2prime(k,i,j) > refpropm('H','P',p2prime(k,i,j),...
    'Q',0,fluid{1,k}):
    h2prime(k,i,j) = refpropm('H','P',p2prime(k,i,j),...
        'Q',0,fluid{1,k})-2;
h4prime(k,i,j) = h4(k,i,j)+h2(k,i,j)-h2prime(k,i,j);
T4prime(k,i,j) = refpropm('T','P',p4prime(k,i,j)...
    , 'H',h4prime(k,i,j),fluid{1,k});
rc4prime(k,i,j) = refpropm('D','T',T4prime(k,i,j)...
    , 'P',p4prime(k,i,j),fluid{1,k});
cp4prime(k,i,j) = refpropm('C','T',T4prime(k,i,j)...
    , 'P',p4prime(k,i,j),fluid{1,k});
s4prime(k,i,j) = refpropm('S','T',T4prime(k,i,j)...
    , 'P',p4prime(k,i,j),fluid{1,k});
end

```

Figure 3.1-11: State 2' and 4' thermodynamic properties.

Anyway, the heat per unit mass exchanged in the recuperator is equal to the enthalpy difference between inlet and outlet state in both sides:

$$q_{22'} = q_{44'} = h_4 - h_{4'} = h_{2'} - h_2 \quad (3.12)$$

3.1.2.5 Condenser

The inlet and outlet state of the condenser are already fully defined (state 4' and state 1). So we can directly compute the heat transferred per unit mass to the heat sink, usually ambient air.

$$q_{22'} = q_{44'} = h_4 - h_{4'} = h_{2'} - h_2 \quad (3.13)$$

3.1.2.6 Mass flow rate

Once the fluid properties in the points of interest around the cycle are known, the required mass flow rate of the working fluid can be estimated writing the energy balance of the boiler. Given the boiler effectiveness ($\varepsilon_{\text{boiler}}$) defined in the input windows, the boiler outlet temperature on the exhaust gas side ($T_{\text{exh,out}}$) is:

$$T_{\text{exh,out}} = T_{\text{exh,in}} - \varepsilon_{\text{boil}} (T_{\text{exh,in}} - T_{2'}) \quad (3.14)$$

Thus, the heat transfer rate taking place in the boiler is:

$$\dot{Q}_{2'3} = \dot{m}_{\text{exh}} c_{p_{\text{exh}}} (T_{\text{exh,in}} - T_{\text{exh,out}}) \quad (3.15)$$

Where, the mass flow rate and the specific heat of the exhaust gas are input data. On the working fluid side, the heat transfer rate is equal to the enthalpy rise times the mass flow rate of the working fluid (\dot{m}_{wf}) that still needs to be found Figure 3.1-12. Thus:

$$\dot{m}_{\text{wf}} = \frac{\dot{Q}_{2'3}}{(h_3 - h_{2'})} \quad (3.16)$$

3.1.2.7 Power balance

At this point since the fluid properties are computed in every state around the cycle and the working fluid mass flow rate is determined, the outputs can be computed. The power generated/requested by a component is equal to the mass flow rate multiplied by the work per unit mass generated/requested by the component Figure 3.1-11 Figure 3.1-12.

In particular, the power requested by the pump is:

$$\dot{W}_{12} = \dot{m}_{\text{wf}} \cdot w_{12} = \dot{m}_{\text{wf}} (h_2 - h_1) \quad (3.17)$$

Whereas the power generated by the expander is:

$$\dot{W}_{34} = \dot{m}_{\text{wf}} \cdot w_{34} = \dot{m}_{\text{wf}} (h_3 - h_4) \quad (3.18)$$

The net power is the difference between the power output of the expander and that of the pump:

$$\dot{W}_{\text{net}} = \dot{W}_{34} - \dot{W}_{12} \quad (3.19)$$

The heat rejection rate in the condenser is:

$$\dot{Q}_{4,1} = \dot{m}_{wf} \cdot q_{12} = \dot{m}_{wf}(h_{4'} - h_1) \quad (3.20)$$

Finally the heat transfer rate in the recuperator is:

$$\dot{Q}_{44'} = \dot{m}_{wf} \cdot q_{44'} = \dot{m}_{wf}(h_4 - h_{4'}) \quad (3.21)$$

3.1.2.8 Efficiencies

Then the only outputs that still have to be computed are the efficiencies.

The cycle efficiency is given by the ratio between the net power output and the heat flow rate occurring with the high temperature source.

$$\eta_{cycle} = \frac{\dot{W}_{net}}{\dot{Q}_{2'3}} \quad (3.22)$$

The recovery efficiency, is defined as the ratio between the actual heat transfer rate occurring in the boiler and the energy available (exergy) in the exhaust gas side at boiler inlet. The exergy, as already explained in section 2.1, is the maximum useful work possible during a process that brings the system in equilibrium with the outside environment considered at 25 °C. So:

$$\dot{Q}_{available} = \dot{m}_{exh} C_{p_{exh}} (T_{exh,in} - T_{amb}) \quad (3.23)$$

Where T_{amb} is the ambient temperature.

```

Texh_out(k,i,j) = Texh_in - eff_boil*(Texh_in-T2prime(k,i,j));
Qdot_2prime3(k,i,j) = m_exh * cp_exh*10^3*(Texh_in - Texh_out(k,i,j));

% Working fluid mass flow rate
m_fluid(k,i,j) = Qdot_2prime3(k,i,j)/(h3(k,i,j)-h2prime(k,i,j));

% Cycle outputs
% Power required by the pump [kW]
F_pump(k,i,j) = m_fluid(k,i,j)*w_pump(k,i,j);
V1(k,i,j) = m_fluid(k,i,j)*ro1(k); % [m^3/s]
% Power generated by the expander[kW]
F_exp(k,i,j) = m_fluid(k,i,j)*w_exp(k,i,j);
Volumetric_expansion_ratio(k,i,j) = ro4(k,i,j)/ro3(k,i,j);
% Boiler heat transfer rate [kW]
Qdot_boil(k,i,j) = Qdot_2prime3(k,i,j)/1000;
% Condenser heat transfer rate [kW]
Qdot_cond(k,i,j) = m_fluid(k,i,j)*(h4prime(k,i,j)-h1(k))/1000;
% Recuperator heat transfer rate[kW]
Qdot_rec(k,i,j) = m_fluid(k,i,j)*(h4(k,i,j)-h4prime(k,i,j))/1000;
% Net Power output[kW]
F_net(k,i,j) = F_exp(k,i,j) - F_pump(k,i,j);

```

Figure 3.1-12: Working fluid mass flow rate, net power output and heat transfer rate in the heat exchangers.


```

% Rankine cycle efficiency
eff_cycle (k,i,j)= P_net(k,i,j)/Qdot_boil(k,i,j);
% Recovered efficiency
eff_recovered (k,i,j)= Qdot_2prime3(k,i,j)/...
    (m_exh * cp_exh*10^3*(Texh_in - 298.15));
% Total efficiency
eff_tot (k,i,j)= eff_recovered(k,i,j) * eff_cycle(k,i,j);

```

Figure 3.1-13: Efficiencies.

Thus the recovery efficiency is:

$$\eta_{recovery} = \frac{\dot{Q}_{2'3}}{\dot{Q}_{available}} \quad (3.24)$$

Finally the total efficiency is:

$$\eta_{total} = \eta_{cycle} \eta_{recovery} \quad (3.25)$$

3.1.3 Data treatment

The three “for” loops used allow to repeat the computations presented in the previous paragraph for different working fluids, different compression ratios and different expander inlet temperatures; the fluid properties at each state around the cycle are stored in four dimensional matrixes for every possible combination of variables considered. A different set of equations have been developed for the standard ORC (with no recuperator) and the results stored in similar big matrixes.

The preliminary model just described has been very useful for a first comparison of the main design alternatives.

3.2 Detailed model of the WHR unit based on an ORC

Once the influence of the most important variables of an ORC have been studied a detailed model of the system has been developed. This model has to replicate as accurately as possible the behavior of the WHR unit, giving also to the user the flexibility to adapt the model to different configurations, for example switching from standard to recuperative ORC. A three steps strategy has been followed:

- implement the model in Matlab/Simulink environment
- calibrate the model according to experimental tests data coming from a test rig available at the Fiat Research Center (CRF)
- carry out simulations and analyze the results to assess the potential fuel savings.

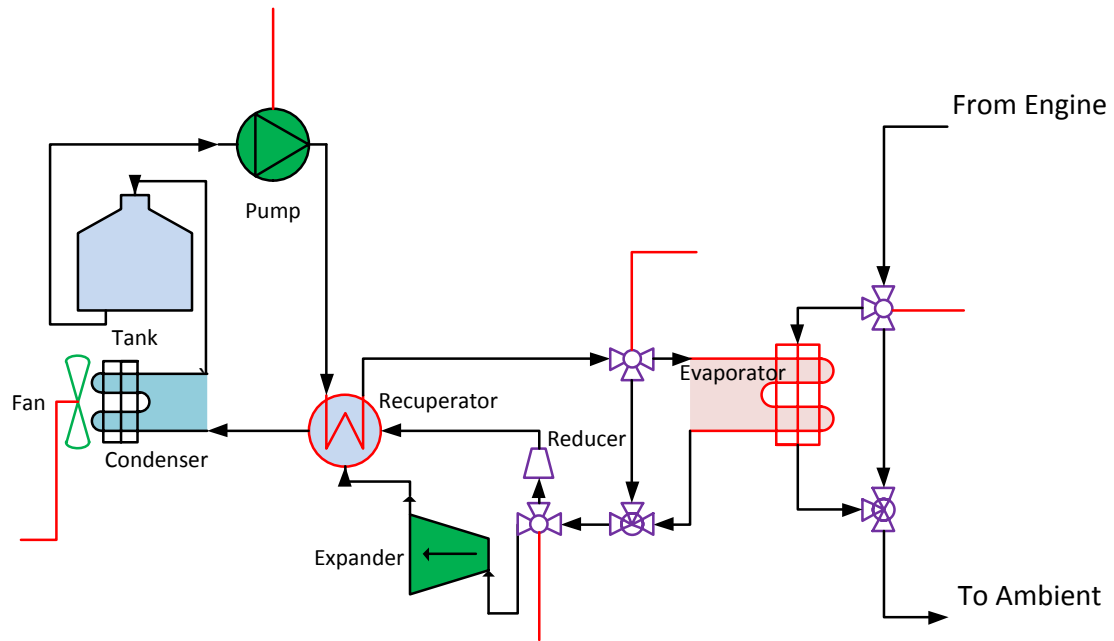


Figure 3.2-1: Recuperative ORC system layout for detailed analysis.

The control aspects of the WHR unit, as well as the final choice of the components, were parallel activities carried out by Chrysler, so the model has been adapted and modified as the design of the system was becoming more defined.

That said, the model will be explained highlighting the possible alternatives that can be selected by the user.

A sketch of the layout of the system and its components is shown in Figure 3.2-1.

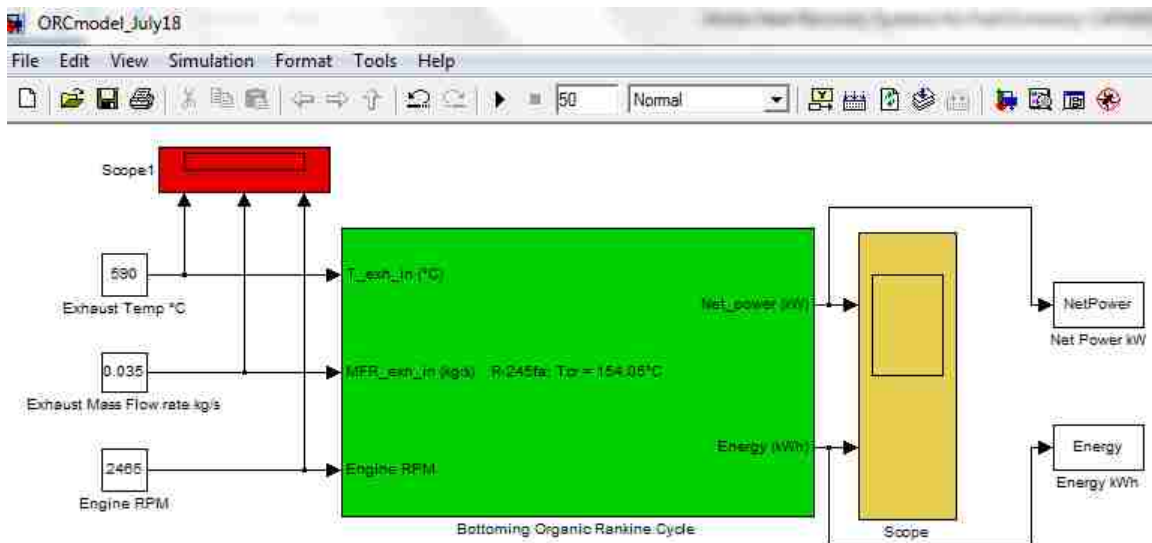


Figure 3.2-2: Detailed model outside user interface.

3.2.1 Detailed model input data

The outside user interface of the model is shown in Figure 3.2-2. The data the user is required to input are those regarding the exhaust gas:

- temperature
- mass flow rate
- average specific heat.

The calibration of the model has been done in stationary operating conditions since the test rig available was not able to test the performances of an ORC during transient conditions. This is the reason why the input data of the exhaust gas were initially assumed constant.

By double clicking on the green block of Figure 3.2-2 the user opens a window, shown in Figure 3.2-3, that requests details about the ORC and its components.

The first six inputs are pup-up menus in which the user is required to choose:

- 1) the working fluid adopted from a list of available ones (first menu)
- 2) whether there is the recuperator or not (second menu)
- 3) if the pressure drop in the pipes are assumed constant and equal to the initial value or not (third menu)
- 4) if the efficiency of the pump and the efficiency of the expander are assumed constant and equal to the initial value or not (fourth menu)
- 5) if the effectiveness of the heat exchangers are assumed constant and equal to the initial value or not (fifth menu)
- 6) if the pressure drop in the heat exchangers have to be assumed constant and equal to the initial value or not (sixth menu).

Parameters	
Working fluid	R245fa
Does the Organic Rankine Cycle have the recuperator?	Yes
Do you want to assume the pressure drop in the pipes constant and equal to the initial value?	No
Do you want to assume the expander and pump efficiencies constant and equal to the initial value?	No
Do you want to assume the effectiveness of the heat exchangers constant and equal to the initial value?	No
Do you want to assume the pressure drop of the heat exchangers constant and equal to the initial value?	No
Organic Rankine cycle operating parameters [T_subcooling target (°C), T_exp_in (°C)]	
	[5 210]
Recuperator characteristics [Recuperator effectiveness initial, Recuperator pinch point (°C), Recuperator low pressure drop initial (kPa), Recuperator high pressure drop initial (kPa)]	
	[0.80 10 0.3 0.1]
Boiler characteristics [Boiler effectiveness initial, T_pinch_point (°C), T_exh_min (°C), Boiler pressure drop initial (kPa)]	
	[0.9 10 100 19]
Is the expander mechanically connected to the engine shaft?	Yes
Expander characteristics [Expander efficiency initial, Gear ratio, Pressure ratio max, Pressure ratio min, P_expander max (kPa), Expander VFR max (m ³ /s), Expander VFR min (m ³ /s)]	
	[0.6 5.45 8 2 2100 0.0095 0.004]
Condenser characteristics [Condenser effectiveness initial, Condenser pinch point (°C), T_coolant_fluid_in (°C), Condenser pressure drop initial (kPa)]	
	[0.2 5 30 1]
Pump characteristics [Pump efficiency initial, Pump head nom (kPa), Pump head min (kPa), Pump head max (kPa), Pump VFR max (m ³ /s), Pump VFR min (m ³ /s), Pump motor efficiency]	
	[0.6 2100 800 2800 0.00009 0.00002 0.8]
Minimum gas temperature where the ORC is turn on (T_minimum>T_boiling+T_pinch_boiler)	
	160
Mean specific heat value of the exhaust gas (kJ/kg-K)	
	0.9937
Pipe diameters (m) [D1, D2, D3, D4, D5, D6]	
	[0.0127 0.0127 0.0254 0.0254 0.0254 0.0127]
Pipe length (m) [L1, L2, L3, L4, L5, L6]	
	[0.8 0.4 0.8 1 0.8 1]
N° of 90° bends [B1, B2, B3, B4, B5, B6]	
	[2 1 2 4 2 3]
Initial pressure drop in the pipes (kPa) [Pdrop pipe1, Pdrop pipe2, Pdrop pipe3, Pdrop pipe4, Pdrop pipe5, Pdrop pipe6]	
	[0 0 0 0 0]
Coolant fluid	50-50 Ethylene-Glycol
Boiler pressure drop curve coefficients [boil0, boil1, boil2]	
	[97.703 -3655.3 38953]
Recuperator low pressure drop curve coefficients Pressure drop curve coefficients [rech0, rech1, rech2]	
	[0.1219 -9.788 303.89]
Condenser pressure drop curve coefficients [cond0, cond1, cond2]	
	[0.4197 7.8931 117.75]
Recuperator high pressure drop curve coefficients Pressure drop curve coefficients [rech0, rech1, rech2]	
	[-0.4918 87.505 3158.6]
Exhaust gas pressure drop curve coefficients [exh0, exh1, exh2]	
	[-0.04209 16.447 0]

Figure 3.2-3: Input window of the detailed model.

Unless detailed data about pump, expander and heat exchangers are available the input to the fourth, fifth and sixth pop-up menus of Figure 3.2-3 should be “No”. However, if data from the suppliers of such components are available and the user wishes to select the “Yes” option, the maps that have to be available are respectively:

- Pump efficiency and pump speed as a function of the pump pressure rise and volume flow rate. Expander efficiency and expander speed as a function of the pressure ratio across the expander and the volume flow rate.
- Effectiveness of each heat exchanger as a function of the number of transfer units (NTU) and of the heat capacity rate ratio (C^*), defined in paragraph 2.5.2.
- Pressure drop in each heat exchanger as a function of the mass flow rate.

After this first group of inputs almost all the others are of numerical type. The desired sub-cooling temperature, needed to avoid cavitation in the pump, at the condenser outlet and the expander target inlet temperature have to be defined.

Then for what concerns the recuperator, the boiler and the condenser the program needs to know:

- heat exchanger effectiveness
- pressure drop inside the component
- minimum temperature difference at the pinch point.

If in the fifth and sixth pop-up menus the answer was “No” the first two parameters are just initial values assumed at time instant equal to zero, otherwise they are constant values and they do not change throughout the whole simulation period.

For what concerns the expander an important distinction has to be made. In a WHR unit for vehicle application the power output can be mechanical or electrical. In the first case the expander has to be connected to the engine shaft by means of a pulley belt system, whereas in the latter the expander is connected to an electric generator, very often integrated inside the expander itself, that usually provides a current that recharges a battery. The difference is that in the case mechanical power is used the expander speed is given for a given engine speed and cannot be changed, on the opposite the expander speed is defined by the volume flow rate in the case electric power is used. Immediately below the pop-up menu where the distinction just explained is made, the expander characteristics have to be specified:

- the isentropic efficiency at initial time instant
- the gear ratio, basically the speed ratio between the engine shaft and the expander
- minimum and maximum pressure ratio across the expander
- minimum and maximum volume flow rate (VFR) inside the expander.

For the efficiency the same considerations done for the heat exchangers effectiveness and pressure drops hold, if in the fourth pop-up menu the answer was “No” the expander efficiency is just the value assumed at the time instant equal to zero of the simulation.

Finally, the pump parameters required are:

- the isentropic efficiency at initial time instant

- the nominal pump head (pressure rise) across the component
- minimum and maximum pressure rise the pump is able to provide
- minimum and maximum VFR that the pump is able to compress
- the efficiency of the driving system of the pump (usually an electric motor).

While the nominal pump head value is set equal to the desired performance of the pump the other parameters are easy to be found in every catalogue of pumps. Nonetheless the maximum and minimum volume flow rate could not be provided but they can be assumed equal to the maximum and minimum speed of the machine, expressed in round per second, multiplied by the swept volume of the pump.

Then scrolling down the input parameters needed (Figure 3.2-3), there is the minimum temperature of the exhaust gas at which the WHR unit is turned on, taken into account only when a variable exhaust gas temperature profile is inserted as an input, and the specific heat of the exhaust gas whose value is assumed to be constant throughout the boiler.

Moving down there are inputs about the geometry of the system that play an active role in the program only in the case the answer to the third pop-up menu was “No”. The length of each pipe and the diameter of each pipe should be input and are used to estimate the distributed and concentrated pressure losses. Here the name given to the pipes is presented:

- pipe 1: from the pump outlet to the recuperator high pressure side inlet
- pipe 2: from the recuperator high pressure side outlet to the boiler inlet
- pipe 3: from the boiler outlet to the expander inlet
- pipe 4: from the expander outlet to the recuperator low pressure side inlet
- pipe 5: from the recuperator low pressure side outlet to the condenser inlet
- pipe 6: from the condenser outlet to the pump inlet.

In the case the recuperator is not used pipes 2 and 5 do not exist, they are simply not taken into account in the program, and pipe 1 goes from the pump outlet to the boiler inlet and pipe 5 from the expander outlet to the condenser inlet.

Furthermore the number of tight (90°) bends in each pipe is used to estimate the concentrated pressure losses. So, more in general, the number of tight bends should also include the other possible concentrated pressure losses for example a thermocouple or other instrumentations to measure the pressure or mass flow rate typically employed in a test rig. In other words, the number of tight bends in a pipe corresponds to the total number of concentrated pressure losses regardless their the type. Under the geometry information there is a box in which the initial values of the pressure drop in each pipe are defined. If the answer in the third pop-up menu was “Yes” they will be used throughout the whole simulation period.

The next input is again a pop-up menu in which the user can select the coolant fluid used in the condenser, in order to estimate its specific heat and hence the mass flow rate of the coolant fluid required.

The last five arrays that have to be defined, still referring to Figure 3.2-3, are the coefficients of the pressure loss curves inside each heat exchanger. These curves are approximated with a second order polynomial equation that usually fits well the experimental results. From left to right the three coefficients that have to be inserted are the constant term the coefficient that multiplies the mass flow rate and the coefficient that multiplies the mass flow rate at the second power.

It must be clarified that some parameters may not be taken into account as a function of the option selected by the users in the first six pop-up menus. If for example the WHR unit does not include a recuperator, the recuperator characteristics are not taken into account at all, but the users has to input anyway some values, even all zeros, to make the model run.

3.2.2 Algorithm resolution

The internal structure of the program, that can be visualized looking under the mask of the green block of Figure 3.2-2, is organized into a series of functional blocks that execute Matlab instructions to carry out different tasks. Each block uses output of other blocks, so there is an unique sequence of resolution of the program, shown in Figure 3.2-4. It has been found out that the expander inlet temperature, that coincides with the boiler outlet temperature under the hypothesis of null heat losses in the pipes, strongly influence the efficiency and hence the power output of the cycle. So the control strategy adopted is that of varying the rotational speed of the pump, that is driven by an electric motor and not by the expander, in order to supply the cycle exactly with the mass flow rate of the working fluid that can be brought at the desired expander inlet temperature, set by the user in the initial input window. However, in order to evaluate this mass flow rate the boiler inlet temperature is necessary, this is not a straightforward process because of the potential presence of the recuperator. So the first three functional blocks (pump, expander and recuperator) are solved with a per unit mass analysis that is used to determine the thermodynamic properties (pressure, temperature and enthalpy) at the boiler inlet and outlet. Then the mass flow rate of the working fluid that can be heated up to the desired expander inlet temperature is computed in the exhaust gas heat exchanger (or boiler) functional block. At this point an energy balance analysis of each component is carried out, evaluating also the mass flow rate flowing in the bypass pipes. The condenser functional block is solved. At last, three different functional blocks are solved at the same time; the outputs of these blocks at a given time instant (n) are used as an input for the simulation at the following time instant (n+1).

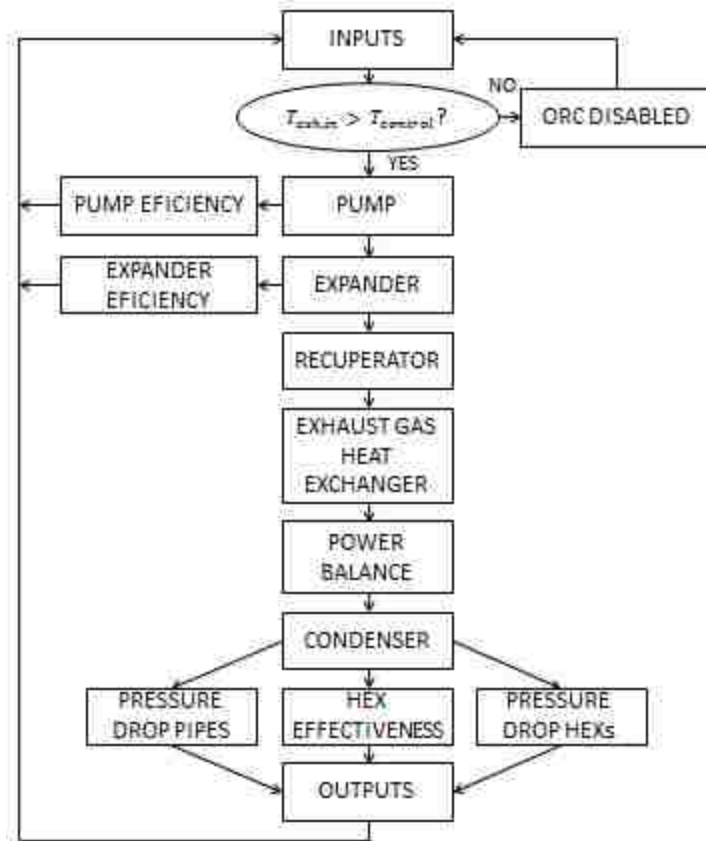


Figure 3.2-4: Logic blocks resolution sequence.

In the following the model implemented is explained in details starting from the most general case, hence when the heat exchanger effectiveness, pressure drop in the pipes and in the heat exchangers are not assumed constant, and highlighting how it responds to other combinations of inputs of the pop-up menus 2 to 6 presented in paragraph 3.2.1.

Before doing that it is worth to spend few words on how the working fluid type selected affects the model, as a matter of fact the first thing that the program does, even before starting to solve the functional blocks is to assign a number to the working fluid selected. As previously mentioned, the working fluid type is only used as an input for the command “refpropm.m” that reads files containing the properties of the working fluid considered. These files are named with the extended name of the fluid, however different working fluids have different length of their names. Since Simulink requires that the length of a string must be specified and cannot change, some countermeasures had to be taken. The simplest solution appeared to be that of assigning a number with double digits to each working fluid. A proper switch, as the one showed in Figure 3.2-5, assigns to the variable “Working_fluid” exactly the number correspondent to the working fluid selected by the user in the input window.

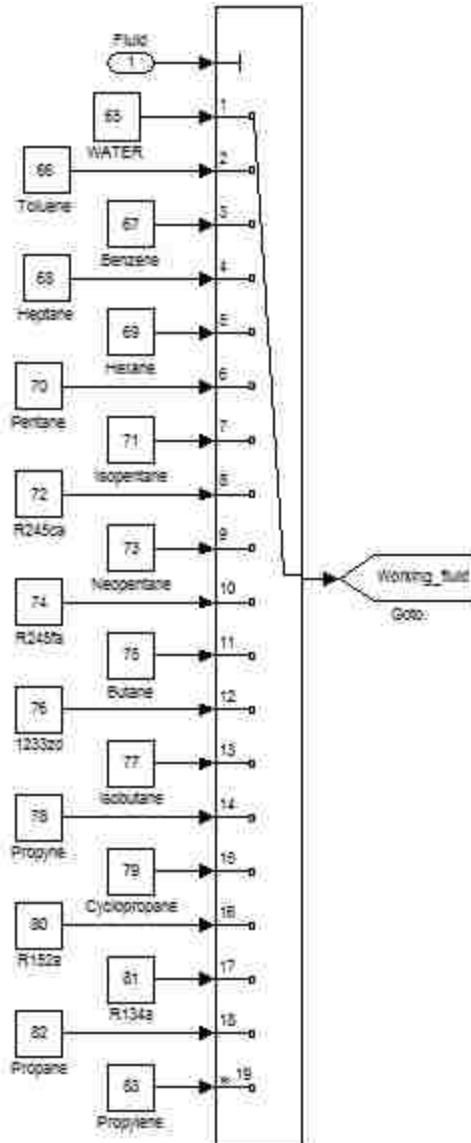


Figure 3.2-5: Working fluid switch.

Now, anytime the command “refprop.m” is used, the variable “Working_fluid” is converted by the command “char” from a number with two digits to a single letter. Finally, just renaming the file containing the fluid property table, exactly with the same letter that the command char returns, the program runs fine.

Once this complex, but necessary, procedure has been explained we can move on analyzing in detail each functional block following the logic resolution sequence.

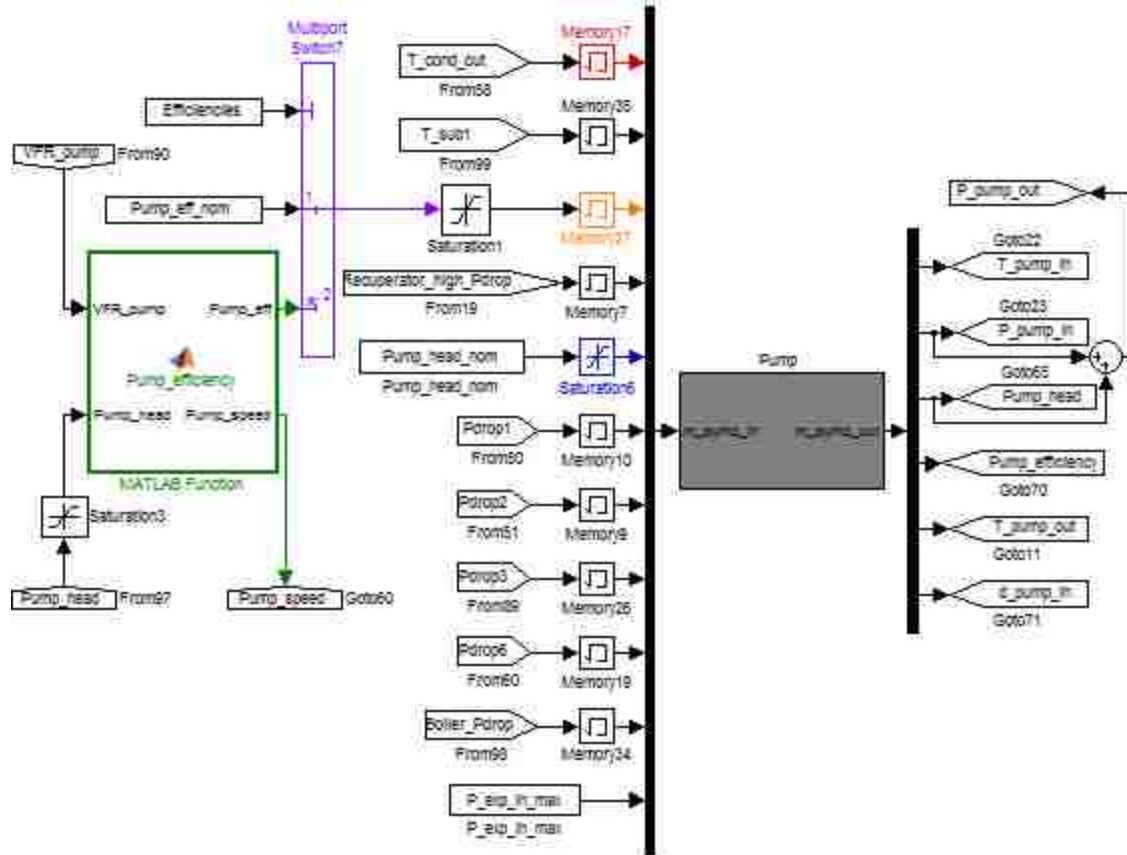


Figure 3.2-6: Pump functional block.

3.2.2.1 Pump

The first functional block solved is the pump, Figure 3.2-6. As mentioned before, the mass flow rate of the working fluid flowing inside this component is still unknown so a per unit mass analysis is carried out.

The first step is to determine the thermodynamic properties of the fluid at the pump inlet. The pump inlet pressure is computed from the condenser outlet pressure minus the pressure drop taking place in the pipe connecting the condenser outlet to the pump inlet (pipe 6). During the first time instant of the simulation the pressure drop in pipe 6 is assumed equal to zero and then in the following time instants the pressure drop is assumed equal to that computed in the previous time instant, this approach is made possible by the block “memory” of Simulink, like the red one of Figure 3.2-6. On the other hand, since the pressure drop in a pipe is assumed to be an isothermal transformation, the temperature at the pump inlet is equal to the temperature at the condenser outlet. It must be pointed out that the initial pump inlet temperature is equal to the target condensing temperature minus the target sub-cooling temperature, so it is just an estimation.

In the following instants the pump inlet temperature and pressure are computed starting from the outputs of the condenser block of the previous time instant. Anyway, once temperature and pressure are determined the values of density and enthalpy at the pump entrance are uploaded from Refprop database. At this point the pump outlet pressure is estimated; three different limitations to such value have to be considered:

- The pressure at the expander inlet cannot be higher than a given value.
- The machine pump head range.
- The pressure at the pump outlet must be lower than the critical one of the working fluid employed.

The last condition is considered by the user selecting an appropriate value to the nominal pump head in the initial input window (paragraph 3.2.1). The second limitation is considered inside the saturation blocks, like the blue one in Figure 3.2-6, that limits the value of the nominal pump head; it must be greater than the minimum pump head and lower than the maximum pump head values imposed in the input window, see Figure 3.2-8. Finally, the first condition is considered inside the pump block by setting the pump outlet pressure equal to the minimum between the pressure at the pump inlet plus the nominal pump head value and the maximum pressure that the expander can withstand plus the pressure drop values in the boiler, in the recuperator and in the pipes 1, 2 and 3.

```

21  ** Thermodynamic properties at pump inlet
22 -  P_cond_out = refpropm('P','T',(T_pump_in+T_sub)...
23      + 273.15,'O',0,char(Working_fluid));
24 -  P_pump_in = P_cond_out - Pdrop6;
25 -  h_pump_in = refpropm('H','T',T_pump_in+273.15,...
26      'P',P_pump_in,char(Working_fluid));
27 -  d_pump_in = refpropm('D','T',T_pump_in+273.15,...
28      'P',P_pump_in,char(Working_fluid));
29
30  ** Thermodynamic properties at pump outlet
31 -  P_pump_out = min(P_exp_in_max + Recuperator_high_Pdrop...
32      + Boiler_Pdrop + Pdrop1...
33      + Pdrop2 + Pdrop3 ,P_pump_in + Pump_head);
34 -  h_pump_out = h_pump_in + (((P_pump_out - P_pump_in)...
35      *1e3)/(d_pump_in*Pump_efficiency));
36 -  T_pump_out = refpropm('T','P',P_pump_out,'H',...
37      h_pump_out,char(Working_fluid));
38 -  T_pump_out = T_pump_out -273.15;

```

Figure 3.2-7: Thermodynamic properties at the pump inlet and outlet.

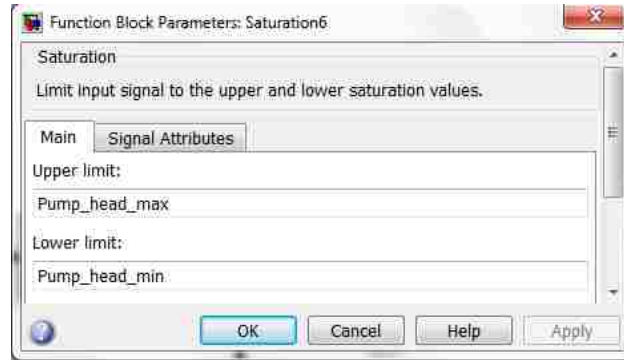


Figure 3.2-8: Saturation block.

Once the pressure at the pump outlet is known the enthalpy at the pump outlet is computed by means of Equation (3.2) and (3.3). Finally the temperature is determined with Refprop. The true pump head (pressure rise) is finally computed as the pump outlet pressure minus the pump inlet pressure. Figure 3.2-7 illustrates the main part of the Matlab script inside the pump block.

Focusing our attention on the inputs of the pump block, the Matlab function block in the green box of Figure 3.2-6 deserves particular attention. This block from the true pump head and the volume flow rate values returns the pump efficiency and the pump rotational speed required. Inside the Matlab function block there is a Matlab script that reads the performance maps of the pump in question and uploads the desired values, basically the same approach as the one used with “refpropm.m” explained in section 3.1. Double clicking on the block called “Pump_efficiency” the Matlab instructions shown in Figure 3.2-9 appear. The function “Pump_parameters.m” is used to read the maps of the components previously created with the procedure explained in the following. Data coming from experimental tests carried out on the real component used are gathered and grouped in four different arrays: pump volume flow rate, pump head, pump speed and pump isentropic efficiency.

```

1 function [Pump_eff, Pump_speed] = ...
2   Pump_efficiency (VFR_pump, Pump_head)
3
4   coder.extrinsic('Pump_parameters');
5
6   % Initialisation of the output parameters
7   Pump_eff = 0;
8   Pump_speed = 0;
9
10  % Outputs
11  [Pump_eff, Pump_speed] = Pump_parameters (VFR_pump, Pump_head);

```

Figure 3.2-9: Pump efficiency and speed maps reader.

In order to create the efficiency and speed maps, the “curve fitting” tool available with Matlab has been utilized. First, the isentropic efficiency array has been plotted as a function of the volume flow rate and of the pump pressure rise. Figure 3.2-10 shows a screen shot of the curve fitting tool, where the black dots correspond to the experimental data. The program is able to generate a surface that interpolates these data minimizing the standard deviation. Among the possible solutions, in the example reported, a linear interpolation has been chosen, purple box of Figure 3.2-10. In other words, the curve fitting tool allows the user to create a surface that interprets in an accurate way the experimental point plotted on the diagram. The pump efficiency map is created, it is saved and the same procedure repeated for the pump speed map. Once the pump efficiency and speed maps are both saved, the “Pump_parameters.m” file simply uploads these maps and reads them in order to return the efficiency and rotational speed values that correspond to the pump head and volume flow rate analyzed, as illustrated in Figure 3.2-11. However, the pump efficiency value determined in this way is used as an input of the pump block only if the pump and expander efficiency are not assumed constant in the input window, and whether the performance maps of the component are available or not. In order to exclude the results coming from the “Pump_efficiency” block, the purple multiport switch of Figure 3.2-6 has been added so that in the case the isentropic efficiency of the pump is assumed constant the switch stops the value coming from the pump efficiency map. Anyway, the pump efficiency value determined at a given time instant is used to estimate the efficiency of the machine during the following time instant, by means of the orange memory block in Figure 3.2-6.

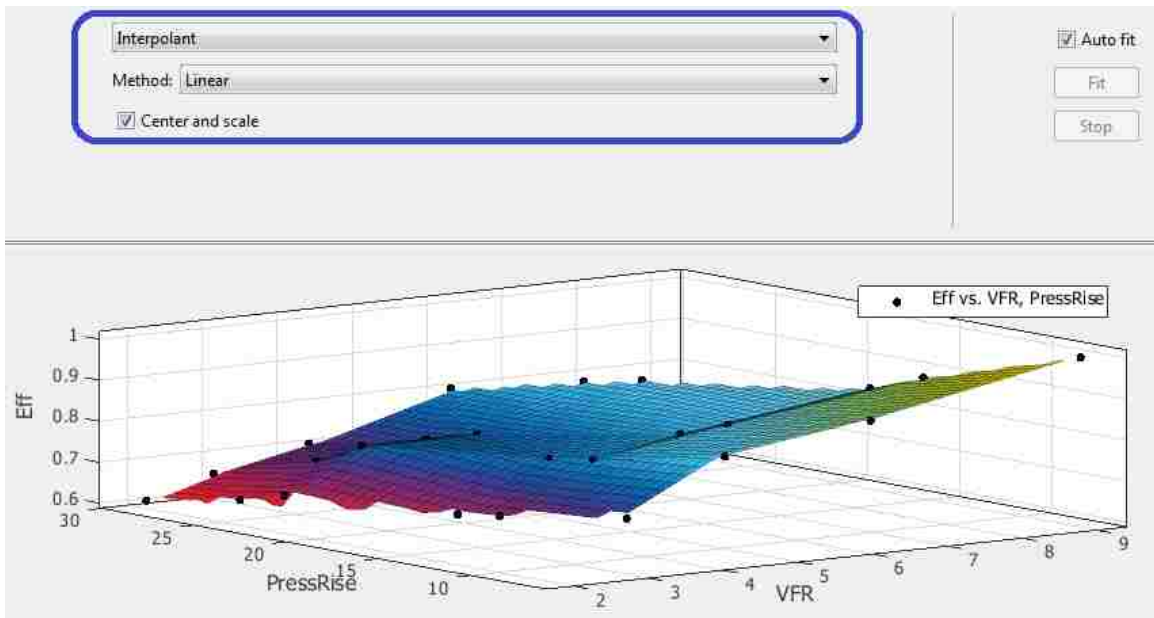


Figure 3.2-10: Curve fitting tool screen shot, pump efficiency map creation.

```

1   function [Pump_efficiency,Pump_speed] = ...
2       Pump_parameters (VFR_pump, Pump_head)
3
4       % Initialisation of the output parameters
5 -   Pump_efficiency = 0;
6 -   Pump_speed = 0;
7
8 -   Pump_head_bar = Pump_head/100;
9
10      % Outputs
11 -   load Pump_efficiency_map
12 -   Pump_efficiency = fitresult (VFR_pump,Pump_head_bar);
13
14 -   load Pump_speed_map
15 -   Pump_speed = fitresult (VFR_pump,Pump_head_bar);

```

Figure 3.2-11: "Pump_parameters.m".

On the other hand, the pump speed is not used as an input for further analyses but its behavior is tracked because it corresponds to the rotational speed of the electric motor that will drive it.

To conclude the examination of this block, the outputs considered are:

- temperature, pressure and density at the pump inlet
- temperature and pressure at the pump outlet
- actual pump head and actual pump efficiency.

3.2.2.2 Expander

The per unit mass analysis continues in the expander block shown in Figure 3.2-12.

As in the case of the pump block, the first step is to determine the thermodynamic properties of the fluid at the expander inlet. The expander inlet temperature is assumed constant, except in some special cases explained later, and comes from the input window. Indeed, the expander inlet pressure is equal to the pump outlet pressure minus the pressure losses inside the heat exchangers and pipes between the pump and the expander. Once this first step is accomplished a first estimation of the expander outlet pressure is done. For a given target condensing temperature the pressure at the expander outlet is equal to the pressure of the saturated vapor at the condensing temperature plus the pressure drops that take place into the low pressure side of the recuperator and in pipes 4 and 5.

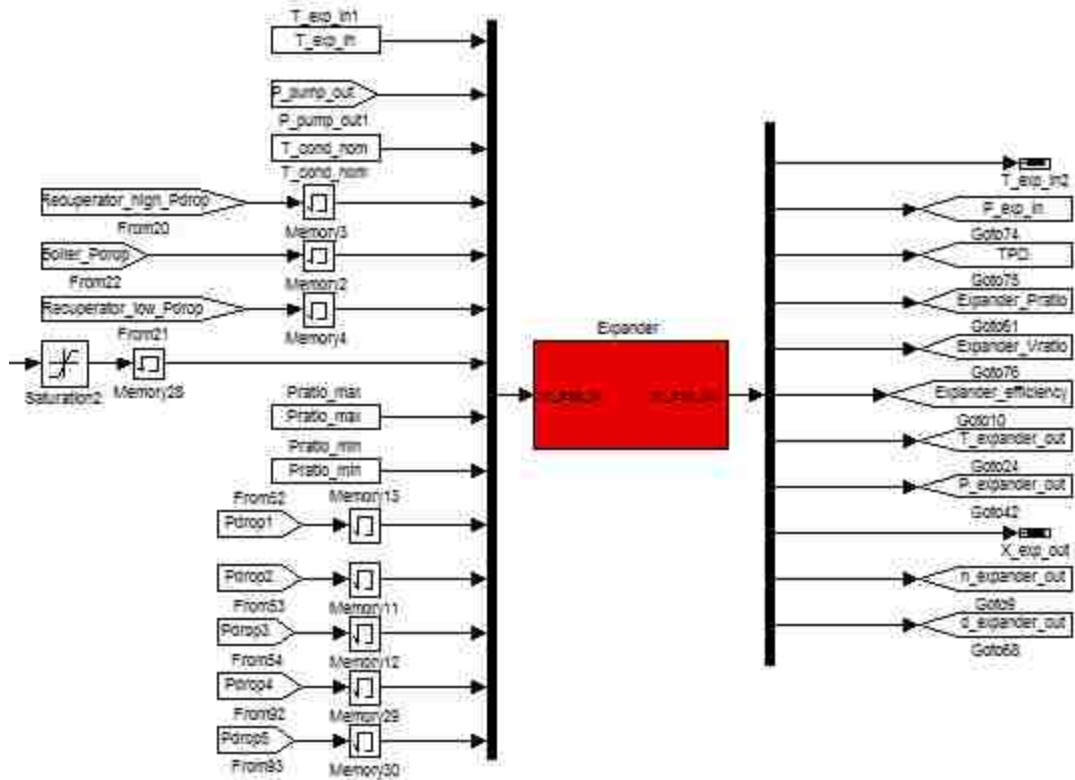


Figure 3.2-12: Expander functional block.

Then the resulting pressure ratio across the expander is computed and the program checks if it falls within the operating range of the machine. If, for example, the pressure ratio computed is higher than the maximum one, the program sets the actual pressure ratio equal to the maximum possible and calculates the new pressure at the expander outlet that as well as the new condensing temperature, obviously, will be higher than those previously computed. The Matlab script portion of the expander block that executes this procedure is shown in Figure 3.2-13.

```

37  %% Expander pressure ratio
38 -  P_exp_in      = P_pump_out - Recuperator_high_Pdrop...
39 -             - Boiler_Pdrop - Pdrop1 - Pdrop2 - Pdrop3;
40 -  P_condensation = refpropm('P','T',T_cond+...
41 -             273.15,'Q',1,char(Working_fluid));
42 -  P_exp_out     = P_condensation + ...
43 -             Recuperator_low_Pdrop + Pdrop4 + Pdrop5;
44
45 -  Pratio = P_exp_in/P_exp_out;
46 -  Pratio = min(Pratio ,Pratio_max);
47 -  Pratio = max (Pratio, Pratio_min);
48
49 -  P_exp_out = P_exp_in / Pratio;

```

Figure 3.2-13: Pressure ratio across the expander.

```

49 %% Thermodynamic properties at expander inlet
50 % and outlet with maximum superheating
51 - h_exp_in      = refpropm('H','T',T_exp_in+...
52               273.15,'P',P_exp_in,char(Working_fluid));
53 - d_exp_in     = refpropm('D','T',T_exp_in+...
54               273.15,'P',P_exp_in,char(Working_fluid));
55 - s_exp_in     = refpropm('S','T',T_exp_in+...
56               273.15,'P',P_exp_in,char(Working_fluid));
57
58 - h_exp_out_is  = refpropm('H','P',P_exp_out,...
59               'S',s_exp_in,char(Working_fluid));
60
61 - h_exp_out_real = h_exp_in - Expander_eff*...
62               (h_exp_in - h_exp_out_is);
63 - T_exp_out_real = refpropm('T','P',P_exp_out,...
64               'H',h_exp_out_real,char(Working_fluid));
65 - d_exp_out_real = refpropm('D','P',P_exp_out,...
66               'H',h_exp_out_real,char(Working_fluid));
67 - Q_exp_out_real = refpropm('Q','P',P_exp_out,...
68               'H',h_exp_out_real,char(Working_fluid));

```

Figure 3.2-14: Thermodynamic properties at the inlet and outlet of the expander.

Once the pressure at the expander outlet is known, it takes just to determine the expander outlet enthalpy to fully define all the other fluid properties. By means of the fluid properties database the expander inlet entropy is determined, then knowing that in the ideal case of isentropic expansion the expander outlet entropy is equal to expander inlet entropy, the expander outlet enthalpy ideal is determined still using the “refpropm.m” function with the expander outlet pressure already computed and the entropy at the expander inlet. Once the enthalpy at the expander outlet in the ideal case is known using Equation (3.6), basically the definition of isentropic efficiency, the real enthalpy at the expander outlet is computed. Then temperature, density and quality of the vapor at the expander outlet are uploaded from the fluid properties database and finally the volume ratio and the expander power density are determined, see Figure 3.2-14.

Giving a closer look to the inputs of the system it can be noted that the condensing temperature is assumed equal to the greater between the condensing temperature in the previous time instant and the nominal condensing temperature. The latter is assumed 10 degrees greater than the inlet temperature of the coolant fluid flowing in the condenser (input value set by the user), that usually coincides with the coolant fluid of the engine.

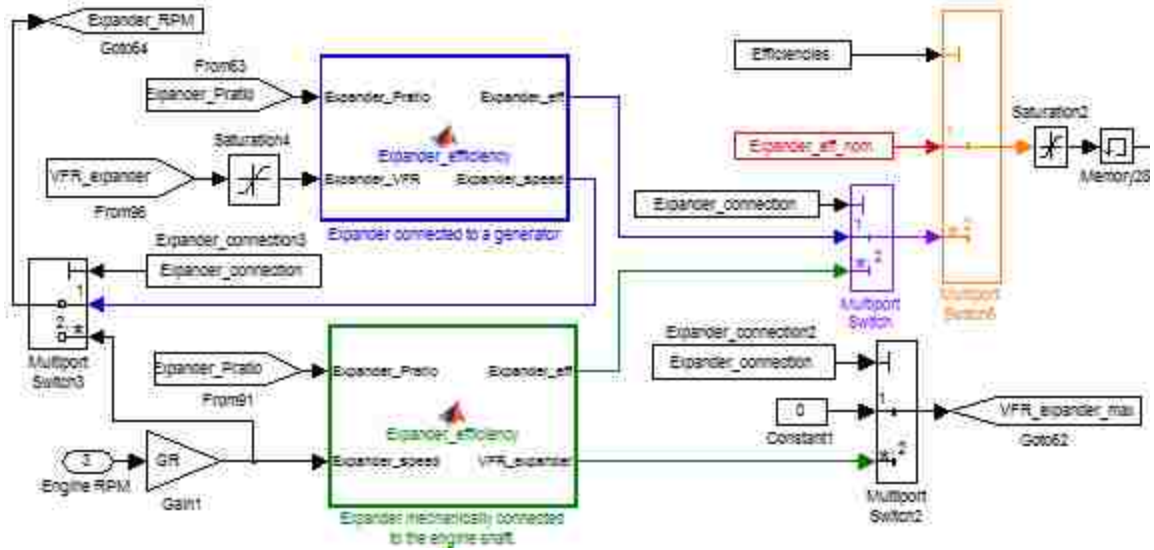


Figure 3.2-15: Expander efficiency, speed and maximum volume flow rate generator.

Nonetheless, Figure 3.2-12 does not show the port at which the seventh input is connected. That input port corresponds to the isentropic efficiency of the expander; two Matlab function blocks and two switches are employed to determine that input value, as illustrate in Figure 3.2-15. As previously explained in paragraph 3.2.1, there are two main important decisions that the user of the software have to make regarding the expander. The first one is whether or not the expander isentropic efficiency is to be assumed constant or not. In the case it is not, and hence the expander characteristics are known, there are two other possible alternatives; the expander might be mechanically connected to the engine shaft or it can be geared to an electric generator. In short, there are three possible ways in which the expander efficiency is estimated, as a function of the choices made by the user. In any case, the efficiency during the initial time instant is assumed equal to the nominal one.

```

1 function [VFR_exp, Expander_efficiency] =...
2     Expander_parameters (Expander_Pratio, Expander_speed)
3
4     % Initialisation of the output parameters
5     VFR_exp = 0;
6     Expander_efficiency = 0;
7
8     % Outputs
9     load Expander_VFR_map
10    VFR_exp = fitresult(Expander_Pratio, Expander_speed);
11
12    load Expander_efficiency_map
13    Expander_efficiency = fitresult(Expander_Pratio, VFR_exp);

```

Figure 3.2-16: "Expander_parameters.m".

In order to utilize the correct value of efficiency there is a system of a couple of switches that addresses only the correct efficiency into the expander block input port, the two switches are highlighted in the purple and orange boxes of Figure 3.2-15. The control port input of each switch depends on the choices made by the user of the software. With reference to Figure 3.2-15, the three possible combinations are highlighted:

- Expander efficiency assumed constant (red): the control port input of the orange switch is equal to 1.
- Expander efficiency assumed not constant and expander mechanically connected to the engine shaft (green box): the control port input of both switches is equal to 2.
- Expander efficiency assumed not constant and expander connected to an electric generator (blue box): the control port input of the purple switch is equal to 1, whereas the control port input of the orange switch is equal to 2.

Whereas in the first case it is easy to understand that the position of the purple switch does not influence the outcome of this portion of software, it is more interesting to look at the peculiarities and the differences inside the two boxes correspondent to the second and third cases. In order to make these estimations, performance maps of the expander were created starting from experimental data by means of the Matlab curve fitting tool with a procedure similar to that used for the pump performance maps. In total three different maps have been created combining four different arrays:

- volume flow rate vs expander pressure ratio and expander speed
- expander speed vs expander pressure ratio and volume flow rate
- expander efficiency vs expander pressure ratio and volume flow rate.

With that in mind, the procedure followed to determine the expander efficiency at a given time instant is here reported first for the case the expander is mechanically connected to the engine shaft. Once we know the engine RPM, the expander rotational speed is univocally determined for a given transmission ratio. So the inputs of the box are the pressure ratio at that time instant (coming from the outputs of the expander block) and the engine expander rotational speed. Inside the green box there is a Matlab script in which a function called “Expander_parameters.m” is used to read the performance maps, previously created.

This function has been appropriately designed to this application, and executes the following instructions (see also Figure 3.2-16):

- 1) Uploads and reads the map that gives the volume flow rate inside the expander as a function of the pressure ratio across the expander and the expander rotational speed.

- 2) Uploads and reads the map that gives the expander efficiency as a function of the of the pressure ratio across the expander and the expander volume flow rate.

The two outputs of the green box are the expander efficiency and the maximum volume flow rate inside the expander. The first output goes into the purple switch, whereas the second one goes into a different switch. It is a relevant data only in the case the expander is mechanically connected to the engine shaft, and will be used later in the program to determine the mass flow rate inside the expander bypass pipe.

On the other hand if the expander is connected to an electric generator the blue box is the one that matters. In this case the expander speed expressed in RPM is an output parameter rather than an input parameter. In fact along with the expander pressure ratio there is the volume flow rate inside the expander as input. Basically the main difference is that while in the previous case the expander speed was function of the engine speed, so the volume flow rate was constrained to that speed, in the case now examined the expander speed is function of the volume flow rate of the working fluid inside the expander and of the pressure ratio across the expander. The volume flow rate inside the expander is not constrained by other external factors provided that the resulting expander speed stays within the operating range of the machine.

Thus inside the blue box of Figure 3.2-15 there is another function called “Expander_parameters2.m” that executes the following instructions:

- 1) Uploads and reads the map that gives the rotational speed of the expander as a function of the pressure ratio across the expander and the volume flow rate.
- 2) Uploads and reads the map that gives the expander efficiency as a function of the of the pressure ratio across the expander and the expander volume flow rate.

The second instruction of both the blue and the green boxes read the same map, whereas the difference lays in the first instruction where the map read by the program changes.

Finally the last thing that should be noted is that the expander speed is also computed in this portion of the program, a further switch distinguish between the case in which the expander speed is equal to the engine speed multiplied by the speed ratio or whether the expander speed is that coming out the blue box.

3.2.2.3 Recuperator

The recuperator functional block, illustrated in Figure 3.2-17, is the last one in which the per unit analysis is carried out. The pressure and temperature at the outlet of the pump and of the expander along with other parameters of the heat exchanger such as its effectiveness pressure drop in both sides and its effectiveness are the main inputs of this functional block. As a matter of fact the user

is able to choose in the input window, described in paragraph 3.2.1, whether or not the Rankine cycle uses the recuperator, so there are two different blocks correspondent to each different case:

- green box of Figure 3.2-17: case with the recuperator
- light blue box of Figure 3.2-17: case without the recuperator.

All the inputs go into both boxes, but only the outputs coming from the box correspondent to the user selection are considered thanks to the presence of a switch.

Now the equations inside each box are shown starting from the case where the recuperator is present. As usual the first step is to determine the thermodynamic properties at recuperator inlet, see Figure 3.2-18. The temperature at the low pressure side inlet is equal to the expander outlet temperature, whereas the pressure is equal to that at the expander outlet minus the pressure drop inside pipe 4. On the other hand the temperature at the high pressure side inlet is equal to the temperature at the pump outlet, whereas the pressure at the high pressure side inlet is equal to the pressure at the pump outlet minus the pressure drop inside pipe 1.

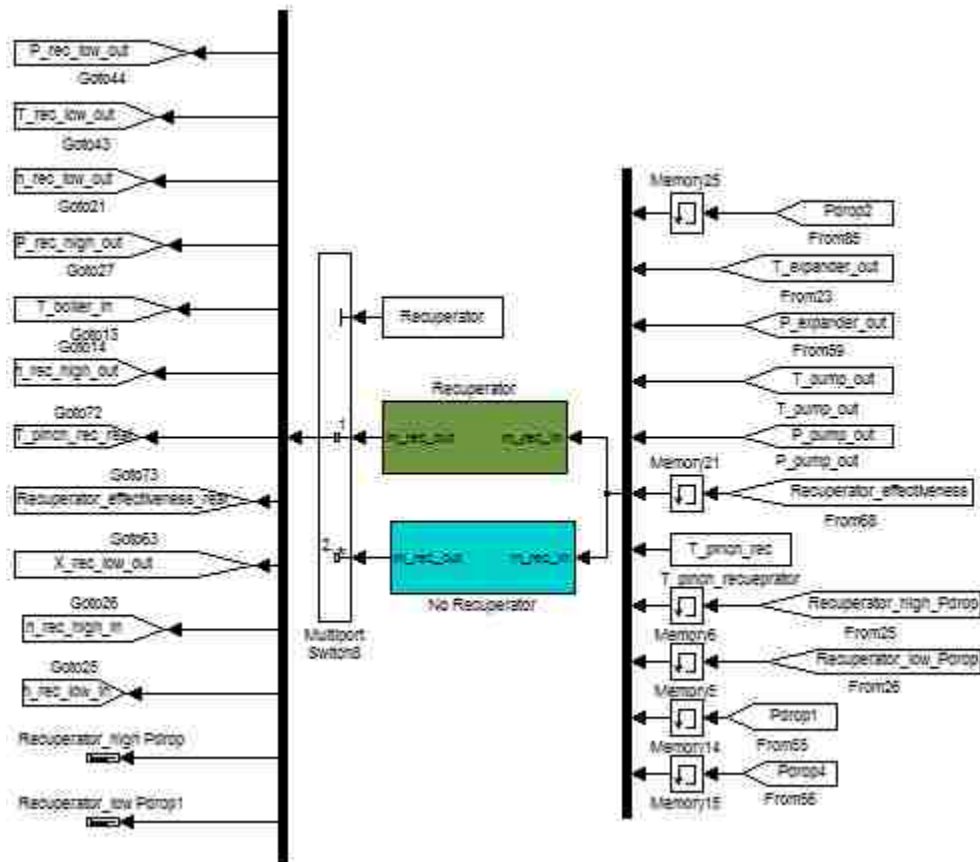


Figure 3.2-17: Recuperator functional block.

```

26     %% Thermodynamic properties at the inlet of the low side and
27     % high side of the recuperator
28 -   T_rec_high_in = T_pump_out;
29 -   P_rec_high_in = P_pump_out - Pdrop1;
30 -   h_rec_high_in = refpropm('H','T',T_rec_high_in+273.15,'P',...
31       P_rec_high_in, char(Working_fluid));
32
33 -   T_rec_low_in = T_exp_out;
34 -   P_rec_low_in = P_exp_out - Pdrop4;
35 -   h_rec_low_in = refpropm('H','T',T_rec_low_in+273.15,'P',...
36       P_rec_low_in, char(Working_fluid));

```

Figure 3.2-18: Thermodynamic properties at the recuperator inlet.

Then solving the component according to the ϵ -NTU method the temperature at the outlet of the low pressure side of the recuperator has been computed with the same formula used in the preliminary model, Equation (3.8). Taking into account that the pressure at the low pressure side outlet of the recuperator is equal to the inlet pressure minus the pressure drop inside the heat exchanger also the enthalpy at the low pressure side outlet can be computed by means of Refprop. Since, in general, the assumption that the mass flow rate of the working fluid flowing in both sides of the recuperator is the same holds, the enthalpy drop in the low pressure side must be equal to the enthalpy rise in the high pressure side. The outlet pressure of the high pressure side can be determined as the inlet pressure minus the pressure losses inside the component. Finally also the temperature at the high pressure side outlet of the recuperator is determined using Refprop (see Figure 3.2-19).

Then there is a double “if” loop used to make some verifications. In particular the first “if” checks that at the outlet of the high pressure side of the recuperator there is no vapor formation.

```

42     %% Thermodynamic properties at the outlet of the low side and
43     % high side of the recuperator
44 -   T_rec_low_out = T_rec_low_in - Recuperator_eff*(T_rec_low_in...
45       -T_rec_high_in);
46 -   P_rec_low_out = P_rec_low_in - Recuperator_low_Pdrop;
47 -   h_rec_low_out = refpropm('H','T',T_rec_low_out+273.15,'P',...
48       P_rec_low_out, char(Working_fluid));
49
50 -   h_rec_high_out = h_rec_high_in+(h_rec_low_in-h_rec_low_out);
51 -   P_rec_high_out = P_rec_high_in - Recuperator_high_Pdrop;
52 -   T_rec_high_out = refpropm('T','P',P_rec_high_out,'H',...
53       h_rec_high_out, char(Working_fluid)); % [°C]
54 -   T_rec_high_out = T_rec_high_out - 273.15;

```

Figure 3.2-19: Thermodynamic properties at the recuperator outlet.

The second "if" checks that the temperature difference at the pinch point, that usually is at the inlet section of the high pressure side, is not lower than the minimum temperature difference at which the heat exchanger can operate. It is important to note that in the case there was vapor formation in the high pressure side of the recuperator some countermeasures have to be taken. Chrysler people have thought that a bypass pipe around the low pressure side of the recuperator is appropriate in order to reduce the heat given to the high pressure side and avoid to have the working fluid partially vaporized at the high pressure side outlet. In any case, enthalpy at the recuperator low pressure side outlet does not change, the only thing that may change is the mass flow rate of the working fluid inside the low pressure side. If this happens the assumption just made about the enthalpy drop that has to be equal in both sides does not hold anymore, however carrying out some simulations, it has been seen that the portion of mass flow rate flowing in the bypass pipe is so small that it can be approximated equal to zero. The actions taken to make the verifications just explained are illustrated in Figure 3.2-20.

All the considerations made for the case with the recuperator do not hold in the case there is no recuperator, and the outputs of the light blue box of Figure 3.2-17 pass through the switch. Basically that box acts as it was transparent. It computes the properties at the recuperator inlet as the other block and then, it simply sets the required outputs equal to the correspondent conditions at the recuperator inlet. This is true admitting what already stated in paragraph 3.2.1, that if there is no recuperator in the cycle pipes 2 and 5 do not exist; the inlet conditions compute in the light blue box coincide with the conditions at the condenser inlet. Figure 3.2-21 shows the Matlab script inside the box in question.

To conclude temperature pressure and enthalpy at the recuperator outlet are then grouped, along with other parameters, and showed as the functional block outputs. They will be very important inputs for the following component solved (the boiler) and for the condenser.

```

70 -   if (h_rec_high_out <= h_sat_liq);
71 -       T_pinch_calc = T_rec_low_out - T_rec_high_in;
72 -       if (T_pinch_calc < T_pinch_rec);
73 -           T_rec_low_out    = T_pinch_rec + T_rec_high_in;
74 -           Recuperator_eff1 = (T_rec_low_in-T_rec_low_out)...
75 -               / (T_rec_low_in-T_rec_high_in);
76 -           T_pinch_recl    = T_pinch_rec;
77 -           h_rec_low_out    = refpropm('H','T',T_rec_low_out,...
78 -               +273.15,'P',P_rec_low_out,char(Working_fluid));
79 -           h_rec_high_out    = h_rec_high_in+(h_rec_low_in-...
80 -               h_rec_low_out);
81 -           T_rec_high_out    = refpropm('T','P',P_rec_high_out,...
82 -               'H',h_rec_high_out,char(Working_fluid));
83 -           T_rec_high_out    = T_rec_high_out - 273.15;
84 -       else
85 -           T_pinch_recl    = T_pinch_calc;
86 -           Recuperator_eff1 = Recuperator_eff;
87 -       end
88 -   else
89 -       h_rec_high_out = refpropm('H','P',P_boiling,'Q',0,...
90 -           char(Working_fluid));
91 -       T_rec_high_out = refpropm('T','P',P_rec_high_out,'H',...
92 -           h_rec_high_out,char(Working_fluid));
93 -       T_rec_high_out = T_rec_high_out - 273.15;
94 -       T_pinch_calc    = T_rec_low_out - T_rec_high_in;
95 -
96 -       if (T_pinch_calc < T_pinch_rec)
97 -           T_rec_low_out    = T_pinch_rec + T_rec_high_in;
98 -           Recuperator_eff1 = (T_rec_low_in-T_rec_low_out)/...
99 -               (T_rec_low_in-T_rec_high_in);
100 -           T_pinch_recl    = T_pinch_rec;
101 -           h_rec_low_out    = refpropm('H','T',T_rec_low_out+...
102 -               273.15,'P',P_rec_low_out,char(Working_fluid));
103 -           h_rec_high_out    = h_rec_high_in+(h_rec_low_in-...
104 -               h_rec_low_out);
105 -           T_rec_high_out    = refpropm('T','P',P_rec_high_out,...
106 -               'H',h_rec_high_out,char(Working_fluid));
107 -           T_rec_high_out    = T_rec_high_out - 273.15;
108 -       else
109 -           T_pinch_recl    = T_pinch_calc;
110 -           Recuperator_eff1 = Recuperator_eff;
111 -       end
112 -   end

```

Figure 3.2-20: Pinch point temperature difference and vapor quality verifications.

```

25  ** Thermodynamic properties at the inlet of the low
26  % side and high side of the recuperator
27 -  T_rec_high_in = T_pump_out;
28 -  P_rec_high_in = P_pump_out - Pdrop1;
29 -  h_rec_high_in = refpropm('H','T',T_rec_high_in...
30      +273.15,'P',P_rec_high_in,char(Working_fluid));
31
32 -  T_rec_low_in = T_exp_out;
33 -  P_rec_low_in = P_exp_out - Pdrop4;
34 -  h_rec_low_in = refpropm('H','T',T_rec_low_in+...
35      273.15,'P',P_rec_low_in,char(Working_fluid));
36
37  ** Thermodynamic properties at the outlet of the low
38  % side and high side of the recuperator equal to the
39  % inlet properties
40 -  T_rec_low_out = T_rec_low_in;
41 -  P_rec_low_out = P_rec_low_in;
42 -  h_rec_low_out = h_rec_low_in;
43
44 -  h_rec_high_out = h_rec_high_in;
45 -  P_rec_high_out = P_rec_high_in;
46 -  T_rec_high_out = T_rec_high_in;

```

Figure 3.2-21: Thermodynamic properties at the condenser inlet, in the case there is no recuperator.

3.2.2.4 Boiler or exhaust gas heat exchanger

The fourth component solved is the boiler. Now that the boiler inlet temperature is known the required mass flow rate of the working fluid can be figured out. Figure 3.2-22 shows the boiler functional block. Among the inputs of this block we can recognize:

- exhaust gas mass flow rate, specific heat and inlet temperature
- temperature of the working fluid at boiler inlet and the desired temperature of the working fluid at the boiler outlet
- pressure drop inside the boiler, boiler effectiveness, minimum temperature difference at the pinch point
- maximum and minimum volume flow rate of the pump.

The latter plays an important role in the case the heat available in the exhaust gas is so much that the mass flow rate that can be brought at the desired boiler outlet temperature exceeds the maximum mass flow rate that the pump can supply.

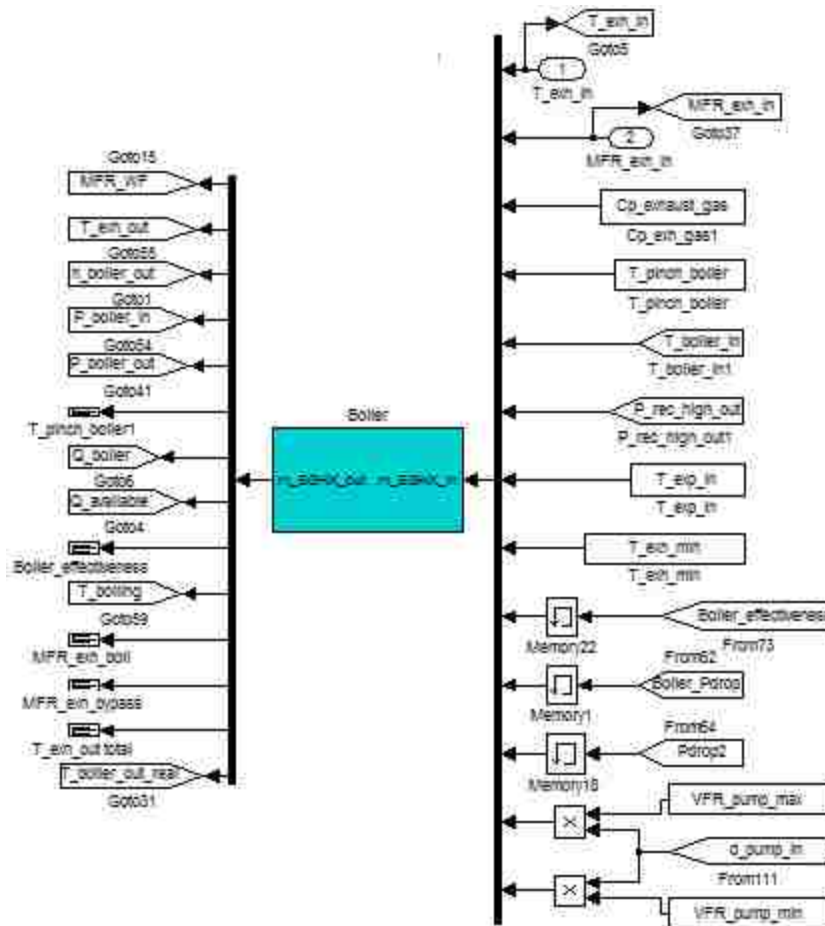


Figure 3.2-22: Boiler functional block.

In the opposite scenario may happen that the heat available in the exhaust gas is so low that the mass flow rate that can be brought at the desired boiler outlet temperature is lower than the minimum mass flow rate that the pump can supply. Anyway, looking the Matlab script inside the boiler block, the thermodynamic properties at the boiler inlet are determined starting from those at the outlet of the recuperator high pressure side. Then the boiling temperature is computed as the temperature of the saturated liquid at the boiler inlet pressure, the implicit assumption is that the pressure loss inside the heat exchanger occurs entirely during the evaporation process. Then still using the ϵ -NTU method the temperature of the exhaust gas at the boiler outlet section is computed using Equation (3.14). If this temperature is lower than the exhaust gas minimum temperature (set in the input window) a portion of the mass flow rate of the exhaust gas will bypass the boiler in order that once it is mixed up with the portion of mass flow rate that flows inside the boiler the average temperature of the whole mass flow rate of the exhaust gas is equal to the minimum exhaust gas temperature allowed. So if this is the case, the mass flow rate of the exhaust gas that flows in the boiler is given by Equation (3.26):

```

42      %% Thermodynamic properties at the boiler inlet
43 -   P_boiler_in = P_rec_high_out - Pdrop2;
44 -   h_boiler_in = refpropm ('H','T',T_boiler_in+273.15,...
45 -     'P',P_boiler_in,char(Working_fluid));
46 -   T_boiling   = refpropm ('T','P',P_boiler_in,'Q',0,...
47 -     char(Working_fluid));
48 -   T_boiling   = T_boiling - 273.15;
49
50      %% Verification of the heat exchanger efficiency
51 -   T_exh_out_calc = T_exh_in-(Boiler_eff*(T_exh_in-...
52 -     T_boiler_in));
53 -   if (T_exh_out_calc < T_exh_min)
54 -     MFR_exh_boil = MFR_exh_in * (T_exh_in - ...
55 -     T_exh_min)/(T_exh_in - T_exh_out_calc);
56 -   else
57 -     MFR_exh_boil = MFR_exh_in;
58 -   end

```

Figure 3.2-23: Thermodynamic properties at the boiler inlet and exhaust gas outlet temperature.

$$\dot{m}_{exh,boil} = \dot{m}_{exh} \cdot \frac{(T_{exh,in} - T_{exh,min})}{(T_{exh,in} - T_{exh,out})} \quad (3.26)$$

Where $T_{exh,out}$ is the outlet temperature of the exhaust gas computed using the ϵ -NTU method, that will coincide with the outlet temperature of the portion of exhaust gas actually flowing inside the boiler, that will be mixed with the portion of exhaust gas bypassing the boiler that still is at the temperature that there was at the inlet of the boiler. Figure 3.2-23 shows the Matlab script the executes the procedure just explained.

At this point knowing the inlet and outlet temperatures of the exhaust gas as well as its heat capacity, the heat transfer rate inside the boiler can be computed and since the enthalpy rise in the working fluid side is known the mass flow rate of the working fluid can be determined (see Figure 3.2-24). Scrolling down the script there is a double “if” loop in which it is verified that the pinch point temperature difference is not lower than the minimum one allowed to make the heat exchanger operate properly. However, unlike the recuperator where the pinch point section is known here it can be in two different positions: or at the working fluid inlet section or where the working fluid achieves the saturated liquid state.

```

64      %% Mass flow rate of the working fluid
65 -   P_boiler_out = P_boiler_in - Boiler_Pdrop;
66 -   h_boiler_out = refpropm('H','T',T_boiler_out+273.15,'P',...
67 -     P_boiler_out,char(Working_fluid));
68 -   MFR_WF_calc = MFR_exh_boil*Cp_exh_in*(T_exh_in-...
69 -     T_exh_out_calc)/((h_boiler_out-h_boiler_in)*1e-3);

```

Figure 3.2-24: Mass flow rate of the working fluid determination.

This is the reason why a double “if” loop is necessary (see Figure 3.2-25).

```

74  %% Pinch point calculation
75  h_sat_liq = refpropm('H','T',I_boiling+273.15,...
76  'Q',0,char(Working_fluid));
77  T_exh_sat_liq = I_exh_in - (MFR_WF_calc*(h_boiler_out...
78  -h_sat_liq)*1e-3)/(MFR_exh_boil*Cp_exh_in));
79
80  if (T_exh_sat_liq-I_boiling) < (T_exh_out_calc-...
81  I_boiler_in)
82  T_exh_pinch = T_exh_sat_liq;
83  T_pinch_calc = T_exh_pinch-I_boiling;
84  if (T_pinch_calc > T_pinch_boiler)
85  T_pinch_boiler1 = T_pinch_calc;
86  Boiler_eff1 = Boiler_eff;
87  else
88  T_pinch_boiler1 = T_pinch_boiler;
89  Q_WF_pinch = MFR_exh_boil*Cp_exh_in*...
90  (T_exh_in-(T_boiling+T_pinch_boiler1));
91  MFR_WF_calc = Q_WF_pinch/((h_boiler_out...
92  -h_sat_liq)*1e-3);
93  T_exh_out_calc = I_exh_in-(MFR_WF_calc*...
94  ((h_boiler_out-h_boiler_in)*1e-3)/...
95  (MFR_exh_boil*Cp_exh_in));
96  Boiler_eff1 = (I_exh_in-I_exh_out_calc)...
97  /(I_exh_in-I_boiler_in);
98  end
99  else
100 T_exh_pinch = T_exh_out_calc;
101 T_pinch_calc = T_exh_pinch-I_boiler_in;
102 if (T_pinch_calc > T_pinch_boiler)
103 T_pinch_boiler1 = T_pinch_calc;
104 Boiler_eff1 = Boiler_eff;
105 else
106 T_pinch_boiler1 = T_pinch_boiler;
107 Q_WF_pinch = MFR_exh_boil*Cp_exh_in*...
108 (T_exh_in-(T_boiler_in+T_pinch_boiler1));
109 MFR_WF_calc = Q_WF_pinch/((h_boiler_out...
110 -h_boiler_in)*1e-3);
111 T_exh_out_calc = T_boiler_in+T_pinch_boiler1;
112 Boiler_eff1 = (T_exh_in-I_exh_out_calc)...
113 /(I_exh_in-I_boiler_in);
114 end
115 end

```

Figure 3.2-25: Boiler pinch point verification.

```

119  % MFR of the exhaust gas and working fluid final verification
120  T_exh_out      = T_exh_out_calc;
121
122  if MFR_WF_calc > MFR_pump_max
123      MFR_WF      = MFR_pump_max;
124      Q_boiler    = MFR_WF * (h_boiler_out-h_boiler_in)*1e-3;
125      MFR_exh_boil = Q_boiler/ Cp_exh_in/ (T_exh_in-T_exh_out);
126      T_boiler_out1 = T_boiler_out;
127  elseif MFR_WF_calc < MFR_pump_min
128      MFR_WF      = MFR_pump_min;
129      h_boiler_out = h_boiler_in + MFR_exh_boil * ...
130          Cp_exh_in * (T_exh_in-T_exh_out)*1e+3/MFR_WF;
131      T_boiler_out1 = refpropm ('T','P', P_boiler_out,...
132          'H',h_boiler_out, char(Working_fluid));
133      T_boiler_out1 = T_boiler_out1 - 273.15;
134  else
135      MFR_WF      = MFR_WF_calc;
136      T_boiler_out1 = T_boiler_out;
137  end

```

Figure 3.2-26: Mass flow rate of the working fluid final verification.

Whether the pinch point is at the working fluid inlet section or at the saturated liquid section the procedure remains unvaried, see Figure 3.2-25 for details. The temperature difference at the pinch point section is put equal to the minimum one, set by the user in the main input window, as a consequence a new exhaust gas temperature at the pinch point section is determined, and a new heat transfer rate is determined as well. This heat transfer rate divided by the enthalpy rise of the working fluid from the pinch point section to the outlet section gives the new mass flow rate of the working fluid.

The last verification that still has to be done is to check that the mass flow rate of the working fluid computed is within the operating range of the pump, Figure 3.2-26. Actually, it should be clarified that the pump has limitations on the maximum and minimum volume flow rate (practically maximum and minimum rotational speed multiplied by the swept volume), that has to be converted in limitations on the maximum and minimum mass flow rate multiplying them by the density at the pump inlet.

The very last step is to compute the actual heat transfer rate and the heat available whose ratio gives the so called recovery (or recovered) efficiency. In particular the heat available is equal to:

$$\dot{Q}_{available} = \dot{m}_{exh} C_{p_{exh}} (T_{exh,in} - T_{exh,min}) \quad (3.27)$$

Where the \dot{m}_{exh} is the total mass flow rate of the exhaust gases that can be equal or greater than the actual mass flow rate flowing inside the boiler.

To conclude the most important output of this functional block is definitely the mass flow rate of the working fluid that is a very important input for the following functional blocks.

3.2.2.5 Power balance

The Power balance functional block, Figure 3.2-27, is the fifth solved.

The outputs of this block are important and are the ones that the user looks at:

- power consumed by the pump
- power generated by the expander
- heat transfer rate in the recuperator
- mass flow rate in the pump, in the expander and in both sides of the recuperator
- mass flow rate in the bypass pipes around the expander and around the low pressure side of the recuperator
- volume flow rate in the pump and in the expander.

The first step is to determine the mass flow rate flowing inside all the other components, that might be equal or lower than that flowing in the boiler, as illustrated in Figure 3.2-28. In particular the mass flow rate in the pump and in the high side of the recuperator must be equal to that flowing in the boiler. On the other hand the mass flow rate inside the low pressure side of the recuperator is calculated at the end of the script, whereas the mass flow rate inside the expander is function of the connection type. In particular in the case the expander was mechanically connected to the engine shaft the volume flow rate inside the expander is limited.

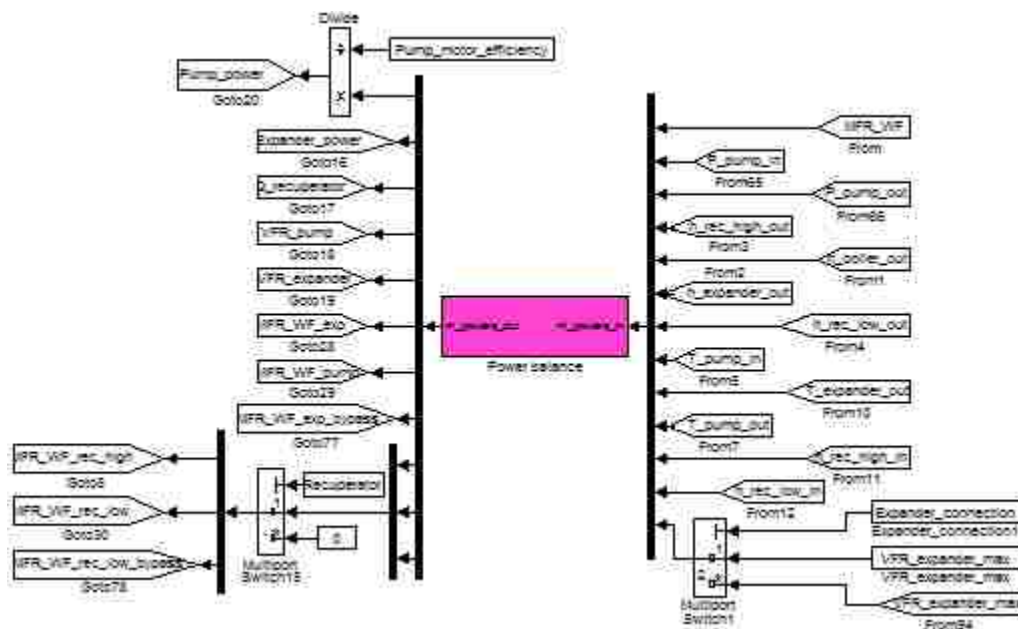


Figure 3.2-27: Power balance functional block.

```

24  %% Enthalpy at the pump inlet and outlet
25 - h_pump_in = refpropm('H','T',T_pump_in+273.15,...
26     'P', P_pump_in,char(Working_fluid));
27 - h_pump_out = refpropm('H','T',T_pump_out+273.15,...
28     'P', P_pump_out,char(Working_fluid));
29
30  %% Density at the pump inlet and at the expander outlet
31 - d_pump_in = refpropm('D','T',T_pump_in+...
32     273.15,'H', h_pump_in,char(Working_fluid));
33 - d_expander_out = refpropm('D','T',T_expander_out+...
34     273.15,'H', h_expander_out,char(Working_fluid));
35
36  %% Mass flow rate in the components
37 - MFR_WF_exp = min (MFR_WF, VFR_expander...
38     * d_expander_out);
39 - MFR_WF_exp_bypass = MFR_WF - MFR_WF_exp;
40 - MFR_WF_pump = MFR_WF;
41 - MFR_WF_rec_high = MFR_WF;

```

Figure 3.2-28: Mass flow rate inside the components.

This is the reason why the mass flow rate inside the expander is set equal to the minimum between the mass flow rate inside the boiler and the maximum volume flow rate inside the boiler multiplied by the density at the expander outlet. In order to determine the maximum volume flow rate, in the bottom right zone of Figure 3.2-27, there is a switch that behaves in this way:

- Expander mechanically connected, the expander maximum volume flow rate comes from the green box of Figure 3.2-15.
- Expander connected to a generator, the expander maximum volume flow rate is a constant value and comes from the input window.

Once the mass flow rate inside the expander is computed, the mass flow rate inside the bypass pipe around the expander is equal to the mass flow rate inside the boiler minus the mass flow rate inside the expander. The portion of mass flow rate that bypasses the expander goes through a reducer that is something like a nozzle in which the diverging walls make the pressure of the working fluid drop in order to make it equal to the expander outlet pressure.

Finally the remaining outputs are computed (look at Figure 3.2-29 for reference). The power requested by the pump, the power generated by the expander and the heat transfer rate inside the recuperator are all computed multiplying the enthalpy drop or rise across the component by the mass flow rate inside the component itself. A particular mention deserves the power absorbed by the pump because the value obtained multiplying the mass flow rate by the enthalpy rise is then divided by the efficiency of the motor that drives the pump, in order to obtain the true power consumed.

```

45 %% Outputs
46 - Pump_power      = MFR_WF_pump*(h_pump_out-h_pump_in)*1e-3;
47 - Expander_power = MFR_WF_exp*(h_expander_in-...
48     h_expander_out)*1e-3;
49 - Q_recuperator   = MFR_WF_rec_high*(h_rec_high_out-...
50     h_rec_high_in)*1e-3;
51
52 - MFR_WF_rec_low  = Q_recuperator / ((h_rec_high_out-...
53     h_rec_high_in)*1e-3);
54 - MFR_WF_rec_low_bypass = max (0,MFR_WF - MFR_WF_rec_low);
55
56 - VFR_pump        = MFR_WF_pump/d_pump_in;
57 - VFR_expander1   = MFR_WF_exp/d_expander_out;

```

Figure 3.2-29: Power balance outputs.

Then the mass flow rate inside the low pressure side of the recuperator is calculated as the heat transfer rate inside the recuperator divided by the enthalpy drop in the low pressure side. Subtracting the value obtained from the mass flow rate of the working fluid inside the boiler the mass flow rate flowing inside the bypass pipe around the low pressure side of the recuperator can be figured out.

The outputs concerning the mass flow rate inside the recuperator are filtered in a switch outside the Matlab script, if there is no recuperator it simply sets all these values equal to zero.

3.2.2.6 Condenser

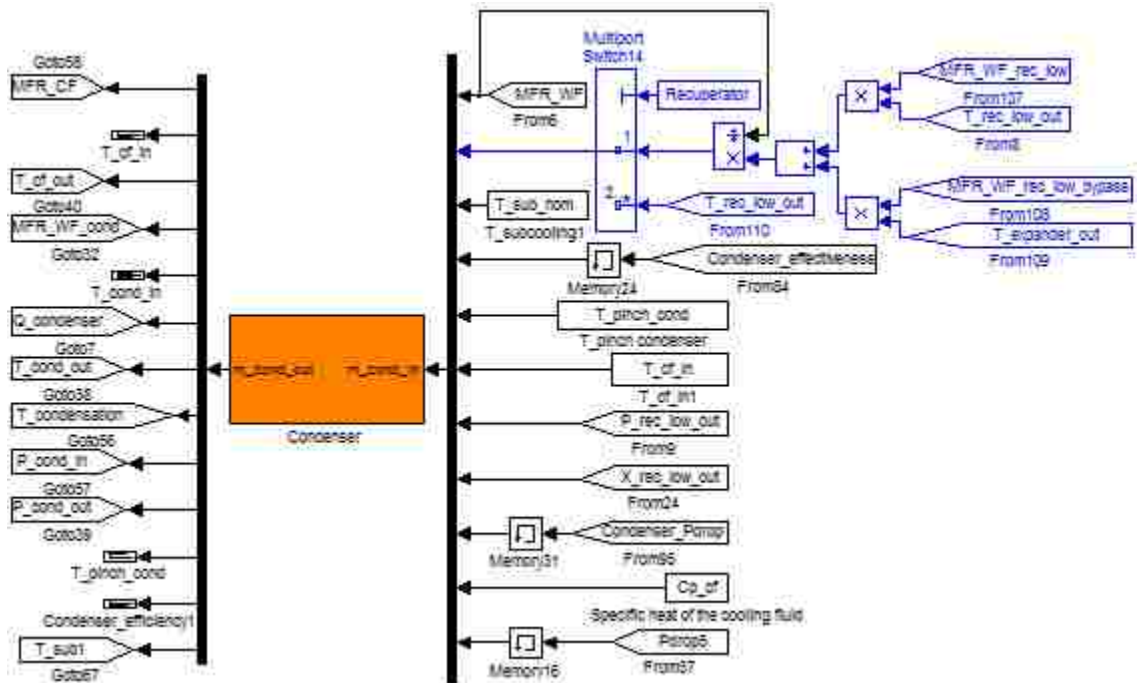


Figure 3.2-30: Condenser functional block.

The condenser is the sixth functional block solved. It must be solved after the “Power balance” functional block because in order to compute the temperature at the expander inlet the mass flow rate of the working fluid flowing inside the low pressure side of the recuperator and in the bypass pipe has to be known. With reference to Figure 3.2-30 the blue boxes’ task is to calculate the temperature at the condenser inlet equal to the temperature at the low pressure side of the recuperator outlet. If there is the recuperator the condenser inlet temperature is computed in the following way Under the assumption that the heat capacity of the working fluid does not change a lot between the two temperatures considered:

$$T_{cond,in} = \frac{\dot{m}_{rec,low} \cdot T_{rec,low,out} + \dot{m}_{rec,low,bypass} \cdot T_{rec,low,in}}{\dot{m}_{boil}} \quad (3.28)$$

With clear meaning of the subscripts. Otherwise if there is no recuperator the condenser inlet temperature is equal to the recuperator outlet temperature than in turns is equal to the recuperator inlet temperature that in turns it is equal to the expander outlet temperature.

Anyway, beside the condenser inlet temperature the other input parameters are:

- heat exchanger effectiveness, pressure drop and pinch point minimum temperature difference
- inlet temperature and specific heat of the coolant fluid.

The inlet temperature of the coolant fluid is the maximum between the ambient temperature plus 5 degrees and the coolant minimum temperature, both these values have been set by the user in the main input window.

```

36  % Thermodynamic properties at the condenser inlet
37 - MFR_WF_cond = MFR_WF;
38 - T_cond_in   = T_rec_low_out;
39 - P_cond_in   = P_rec_low_out - Pdrop5;
40 - h_cond_in   = refpropm('H','T', T_cond_in+273.15,...
41 -             , 'P', P_cond_in, char(Working_fluid));
42
43  % Thermodynamic properties at the condenser outlet
44 - P_cond_out = P_cond_in - Condenser_Pdrop;
45 - T_liq_sat  = refpropm('T','P',P_cond_out, 'Q',0,...
46 -             char(Working_fluid));
47 - T_liq_sat  = T_liq_sat - 273.15;
48
49 - T_cond_out = max(T_liq_sat - T_sub_nom, T_cf_in + ...
50 -             + T_pinch_cond);
51 - T_sub      = T_liq_sat - T_cond_out;
52 - h_cond_out = refpropm('H','T',T_cond_out + ...
53 -             273.15, 'P',P_cond_out ,char(Working_fluid));

```

Figure 3.2-31: Thermodynamic properties at the condenser inlet and outlet.

Looking at Figure 3.2-31 that shows the inside of the condenser block it can be seen that firstly the thermodynamic properties at the condenser inlet are determined. After that, the pressure at the condenser outlet is set equal to the pressure at the condenser inlet minus the pressure drop inside the condenser. Then the condensing temperature is determined from Refprop as the saturated liquid temperature at the condenser outlet pressure, under the assumption that the pressure drop inside the heat exchanger takes place entirely before the sub-cooling process. The temperature at the condenser outlet is the maximum between the coolant inlet temperature plus the condenser pinch point minimum temperature difference (that are both inputs imposed by the user) and the condensing temperature minus the target sub-cooling temperature. Once pressure and temperature at the condenser outlet are determined the actual sub-cooling at the condenser outlet is calculated as well as the enthalpy at the condenser outlet.

```

59      %% Condenser resolution (eps-NUT method modified)
60 -    T_cf_out_calc = T_cf_in + Condenser_eff * (...
61      T_cond_in - T_cf_in);
62 -    if (X_cond_in > 1)
63 -        h_cond_sat_vap = refpropm('H','T',T_liq_sat +...
64      273.15,'Q',1,char(Working_fluid));
65 -        MFR_CF      = MFR_WF_cond * (h_cond_in-...
66      h_cond_out)*1e-3/(Cp_cf*(T_cf_out_calc-T_cf_in));
67 -        T_cf_pinch   = T_cf_in + (MFR_WF_cond * ...
68      (h_cond_sat_vap-h_cond_out)*1e-3/(Cp_cf*MFR_CF));
69 -        T_pinch_calc = T_liq_sat - T_cf_pinch;
70 -        if (T_pinch_calc > T_pinch_cond)
71 -            T_cf_out      = T_cf_out_calc;
72 -            Condenser_eff1 = Condenser_eff;
73 -            T_pinch_cond1 = T_pinch_calc;
74 -        else
75 -            T_cf_pinch   = T_liq_sat - T_pinch_cond;
76 -            MFR_CF      = MFR_WF_cond *...
77      (h_cond_sat_vap- h_cond_out)*1e-3/...
78      (Cp_cf * (T_cf_pinch - T_cf_in));
79 -            T_cf_out      = T_cf_in +( MFR_WF_cond *...
80      (h_cond_in - h_cond_out)*1e-3/...
81      (Cp_cf*MFR_CF));
82 -            Condenser_eff1 = (T_cf_out- T_cf_in)/...
83      (T_cond_in - T_cf_in);
84 -            T_pinch_cond1 = T_pinch_cond;
85 -        end
86 -    else

```

Figure 3.2-32: Condenser resolution, first part.

However, to fully define and explain what happens inside the condenser, information about the outlet temperature of the coolant fluid and of its mass flow rate have to be computed. The assumption made is that there is a pump that can provide the condenser with as much coolant fluid as it needs to condensate and sub-cooling the mass flow rate of the working fluid flowing inside the condenser.

The method adopted to solve the component is the ϵ -NTU method, given that the largest portion of heat transfer occurs during the condensation process (usually around 80%).

This assumption is important because only during the condensation process the coolant fluid has the minor heat capacity rate, whereas while the vapor is cooled down to the saturated vapor state and when the liquid is sub-cooled the working fluid has the minor heat capacity rate. Since the ϵ -NTU method is used to compute the outlet temperature of the fluid that has the minor heat capacity rate inside an heat exchanger, if the assumption just made did not hold it would have been impossible to directly compute the outlet temperature of the coolant fluid. Instead the condenser should have been divided into three zones with three different effectiveness, procedure that results longer and more difficult since very seldom there are available data so detailed about a heat exchanger.

```

87 - MFR_CF      = MFR_WF_cond * (h_cond_in-...
88 -         h_cond_out)*1e-3/(Cp_cf*(T_cf_out_calc-T_cf_in));
89 - T_cf_pinch  = T_cf_in + (MFR_WF_cond * ...
90 -         (h_cond_in-h_cond_out)*1e-3/(Cp_cf*MFR_CF));
91 - T_pinch_calc = T_liq_sat - T_cf_pinch;
92 - if (T_pinch_calc > T_pinch_cond)
93 -     T_cf_out      = T_cf_out_calc;
94 -     Condenser_eff1 = Condenser_eff;
95 -     T_pinch_cond1  = T_pinch_calc;
96 - else
97 -     T_cf_pinch     = T_liq_sat - T_pinch_cond;
98 -     MFR_CF         = MFR_WF_cond * (h_cond_in-...
99 -         h_cond_out)*1e-3/(Cp_cf * (T_cf_pinch ...
100 -         - T_cf_in));
101 -     T_cf_out       = T_cf_in +( MFR_WF_cond *(...
102 -         h_cond_in - h_cond_out)*1e-3/...
103 -         (Cp_cf*MFR_CF));
104 -     Condenser_eff1 = (T_cf_out- T_cf_in)/...
105 -         (T_cond_in - T_cf_in);
106 -     T_pinch_cond1  = T_pinch_cond;
107 - end
108 - end

```

Figure 3.2-33: Condenser resolution, second part.

Anyway, with reference to Figure 3.2-32 and Figure 3.2-33, once the coolant fluid outlet temperature is estimated for the first time there is a double “if” loop that verifies that the specifications about the minimum temperature difference at the pinch point are met, distinguishing the case in which at the condenser inlet the working fluid is entirely at vapor state or in the case the fluid is partially condensed. In the first case the pinch point should be at the section of the heat exchanger where the working fluid is at the saturated vapor state, while in the second case the pinch point section is at the working fluid section. If the pinch point temperature difference is lower than the minimum one a new (lower) coolant fluid outlet temperature is computed, a new (higher) mass flow rate of the coolant fluid is computed as well as the real condenser effectiveness that will be lower than the input one.

The output of the condenser functional block, especially temperature and pressure at the condenser outlet section are used as input for the pump functional block during the following time instant.

3.2.2.7 Heat exchanger effectiveness

The heat exchanger effectiveness functional block, shown in Figure 3.2-34, is the first one presented among the three blocks solved simultaneously by Simulink. This block does not provide any useful output for the simulation at a given time instant but its outputs are used as inputs for the simulation in the following time instant. The goal of this functional block is hence to estimate the real effectiveness of the heat exchanger at a given time instant in order to provide a more accurate input for the next time instant, it is basically an iterative process that enables to refine the effectiveness value estimated.

Recalling what already explained in paragraph 2.5.2, the heat exchanger effectiveness is function of two different non-dimensional numbers: the heat capacity rate ratio (C^*) and the number of transfer unit (NTU). The only problem is that the NTU cannot be determined before that the heat exchanger blocks are solved because there are no information about the internal geometry heat exchangers and so the NTU has computed with an inverse process starting from the heat transfer rate:

$$NTU = \frac{\dot{Q}_{hex}}{LMTD \cdot C_{min}} \quad (3.29)$$

Where \dot{Q}_{hex} is the heat transfer rate inside the heat exchanger and LMTD is the log mean temperature difference computed as:

$$LMTD = \frac{\Delta T_1 - \Delta T_2}{\ln(\Delta T_1/\Delta T_2)} \quad (3.30)$$

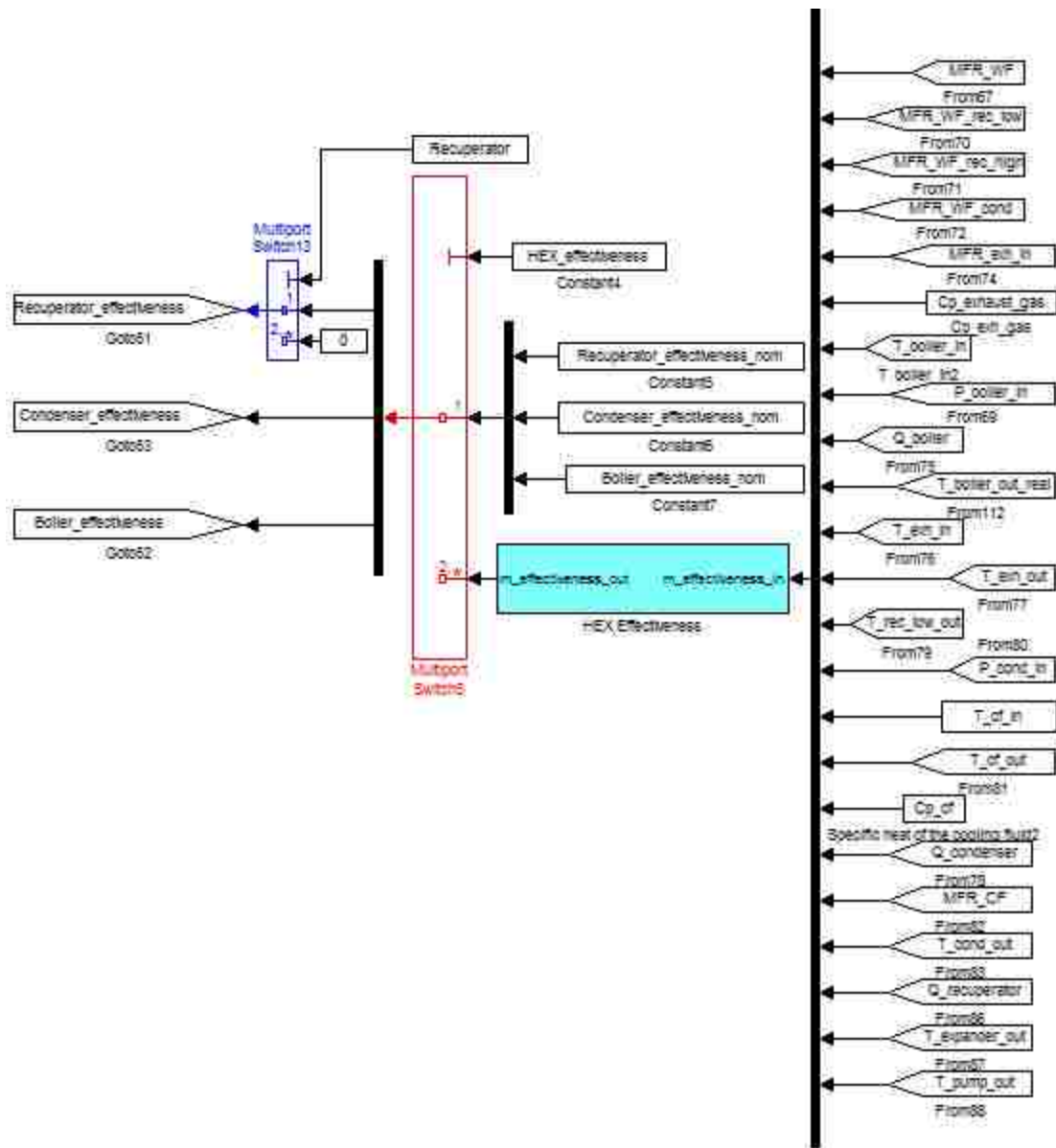


Figure 3.2-34: Heat exchanger effectiveness functional block.

Where ΔT_1 and ΔT_2 are the temperature differences between cold fluid and hot fluid at the two extreme sections of a heat exchanger.

Since data about the heat exchanger effectiveness were available, the following procedure has been adopted. First of all, similar to that done for the expander and pump efficiency maps, the curve fitting tool of Matlab has been used. The points correspondent to the experimental data have been plotted, and then they have been approximated by a surface. The equation of this surface has been already taken from the literature since the shape of such a curve follows a given trend that is similar for similar type of heat exchangers.

In particular for a counter-flow type heat exchanger Shah and Sekulic [64] indicate to use the equation below:

$$\varepsilon = \frac{1 - \exp[-NTU(1 - C^*)]}{1 - C^* \exp[-NTU(1 - C^*)]} \quad (3.31)$$

To this equation few coefficients have been added in order to let the curve fitting tool adapt this theoretical surface with the surface that has the same general trend but that fits in the best possible way the experimental results. The final equation used is underlined in red in Figure 3.2-35, where x and y are respectively NTU and C^* , whereas a , b and c are the three coefficients added. Once similar maps have been created for each heat exchanger analyzed (boiler, condenser and recuperator) and saved in a file, a Matlab function able to upload and read the desired map has been created for each heat exchanger, Figure 3.2-36.

Coming back to the heat exchanger effectiveness block it has as inputs all the parameters necessary to compute C^* and NTU , so:

- Temperatures at the inlet and outlet of each heat exchanger
- Heat transfer rate inside each heat exchanger
- Mass flow rate of both fluids inside each heat exchanger

For each heat exchanger the program repeats the same procedure, showed in . It first calculates the heat capacity rate of each fluid then it calculated the heat capacity rate ratio C^* as the ratio between the minimum to the maximum heat capacity rate. Then the log mean temperature difference is determined and NTU computed using Equation (3.29). The last step is to use the functions previously created to evaluate the expected effectiveness, Figure 3.2-38.

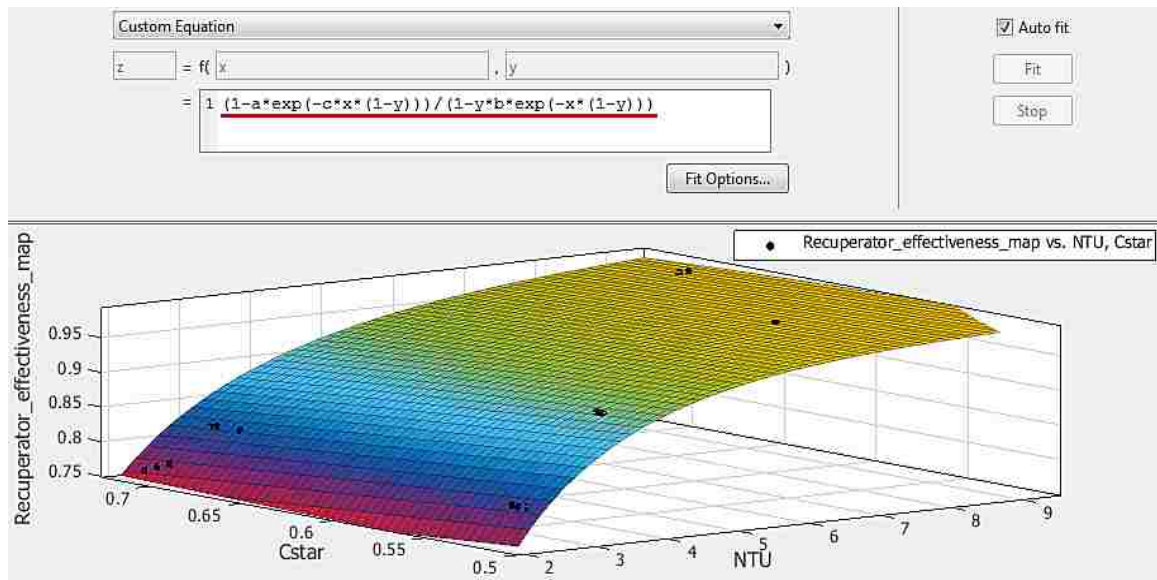


Figure 3.2-35: Reciprocator effectiveness map creation with curve fitting tool.

```

1 function y = Recuperator_effectiveness (NTU_rec, Cstar_rec)
2
3     % Initialisation of the output parameters
4     y = 0;
5
6     % Outputs
7     load Recuperator_effectiveness_map
8
9     y = fitresult(NTU_rec,Cstar_rec);

```

Figure 3.2-36: Recuperator effectiveness map reader.

```

46 %% Boiler
47 Cp_boil_in = refpropm ('C','T', T_boil_in+273.15,...
48     'P', P_boil_in, char(Working_fluid));
49 C_WE_boil = Cp_boil_in * 10^-3 * MFR_WE;
50 C_exh     = MFR_exh * Cp_exhaust_gas;
51 Cstar_boil = C_exh/C_WE_boil;
52 LMTD_boil = ((T_exh_in-T_boil_out)-(T_exh_out-...
53     T_boil_in))/log((T_exh_in-T_boil_out)/...
54     (T_exh_out-T_boil_in));
55 NTU_boil  = Q_boiler / LMTD_boil / C_exh;
56
57 %% Condenser
58 Cp_cond_in = refpropm ('C','T', T_cond_in+...
59     273.15, 'P', P_cond_in,char(Working_fluid));
60 C_WE_cond = Cp_cond_in * 10^-3 * MFR_WE_cond;
61 C_cf      = MFR_CF * Cp_cf;
62 Cstar_cond = C_WE_cond/C_cf;
63 LMTD_cond = ((T_cond_in-T_cf_out)-(...
64     T_cond_out-T_cf_in))/log((T_cond_in-...
65     T_cf_out)/(T_cond_out-T_cf_in));
66 NTU_cond  = Q_condenser / LMTD_cond / C_cf;
67
68 %% Recuperator
69 C_rec_low = Q_recuperator / (T_rec_low_in...
70     - T_cond_in);
71 C_rec_high = Q_recuperator / (T_boil_in -...
72     T_rec_high_in);
73 Cstar_rec = C_rec_low/C_rec_high;
74 LMTD_rec  = ((T_rec_low_in-T_boil_in)-...
75     (T_cond_in-T_rec_high_in))/log((T_rec_low_in-...
76     T_boil_in)/(T_cond_in-T_rec_high_in));
77 NTU_rec   = Q_recuperator / LMTD_rec / C_rec_low;

```

Figure 3.2-37: C^* and NTU determination.

However, two switches are necessary to filter the data coming out the light blue box of Figure 3.2-34, because of the different combinations that the user can choose from the input window.

```

79  ** Outputs
80  Boiler_eff      = Boiler_effectiveness (NTU_boil, Cstar_boil);
81  Recuperator_eff = Recuperator_effectiveness (NTU_rec, Cstar_rec);
82  Condenser_eff   = Condenser_effectiveness (NTU_cond, Cstar_cond);

```

Figure 3.2-38: Heat exchanger effectiveness determination.

The first switch that acts on the data is the red one, two possible alternatives are possible:

- If the user wishes to treat the heat exchanger effectiveness as a constant, the output data of the light blue box are not considered and the output of the functional block are set equal to the effectiveness values defined in the input window.
- If the heat exchanger effectiveness are not assumed constant the values extrapolated from the maps pass through the switch.

Then another distinction has to be done, so the blue switch comes into play:

- If the recuperator is not present the recuperator effectiveness is put equal to zero.
- If the recuperator is present the recuperator effectiveness coming out of the red switch passes through the blue switch.

Once the output data have passed through these two switches, they are used as an input of the correspondent functional block for the simulation in following time instant.

3.2.2.8 Pressure drop inside the heat exchangers

The pressure drop inside the heat exchangers is the simplest functional block, Figure 3.2-39.

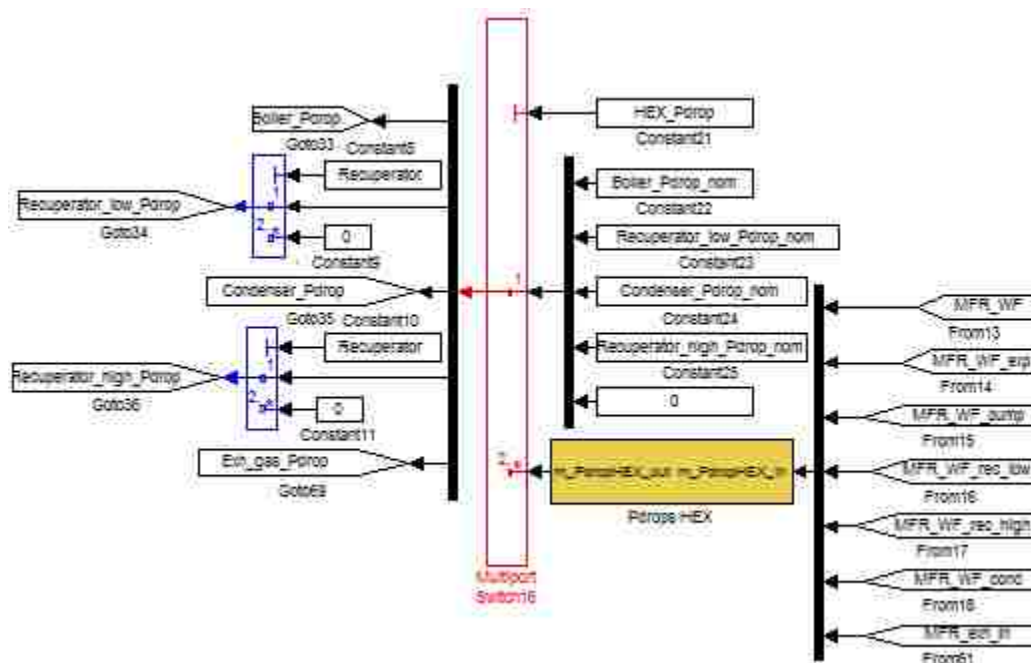


Figure 3.2-39: Heat exchangers pressure drop functional block.

```

13  ** Pressure drop inside the heat exchangers
14 - Boiler_Pdrop      = boill2 * MFR_WE^2 + boill1 *...
15     MFR_WE + boill0;
16 - Recuperator_low_Pdrop = rec12 * MFR_WE_rec_low^2 +...
17     rec11 * MFR_WE_rec_low + rec10;
18 - Condenser_Pdrop    = cond2 * MFR_WE_cond^2 +...
19     cond1 * MFR_WE_cond + cond0;
20 - Recuperator_high_Pdrop = rech2 * MFR_WE_rec_high^2 ...
21     + rech1 * MFR_WE_rec_high + rech0;
22 - Exhaust_gas_Pdrop  = exh2 * MFR_exh_in^2 +...
23     exh1 * MFR_exh_in + exh0;

```

Figure 3.2-40: Determination of the pressure drop inside the heat exchangers.

The same considerations done for the heat exchanger effectiveness holds; it cannot be estimated before solving the other functional blocks because the mass flow rate is not known. So this functional block calculates a posteriori the pressure drop at a given time instant to estimate the expected pressure drop inside the heat exchanger in the following time instant. It relies on the fact that the user has available the pressure drop curve as a function of the mass flow rate inside each heat exchanger. These curves are usually well approximated by a second order polynomial equation whose coefficients are input data required in the initial input window. So if these curves are known the only inputs required in the functional block are the mass flow rate of the fluid inside the heat exchangers. Then just multiplying the proper coefficient with the proper power of the mass flow rate the pressure drop can be computed, Figure 3.2-40.

As in the case of the heat exchanger effectiveness also for the pressure drop the outputs have to be filtered by some switches. In particular there are three switches: one red and two blue in Figure 3.2-39. The red switch is the first one, it sets the values of the pressure drop inside each heat exchanger equal to the initial values in the case the user has selected the option of considering the pressure drop inside the heat exchangers constant in the input window. On the other hand the two blue switches sets the pressure drop in both sides of the recuperator equal to zero in the case there is no recuperator in the system.

Still, the data that have passed through the switches are used as an important input for the simulation in the following time instant.

3.2.2.9 Pressure drop inside the pipes

The last functional block presented is the one that computes the pressure drop inside the pipe, Figure 3.2-41. The pressure drop inside the pipes is assumed equal to initial value until it is estimated in this block for the first time during the initial time instant.

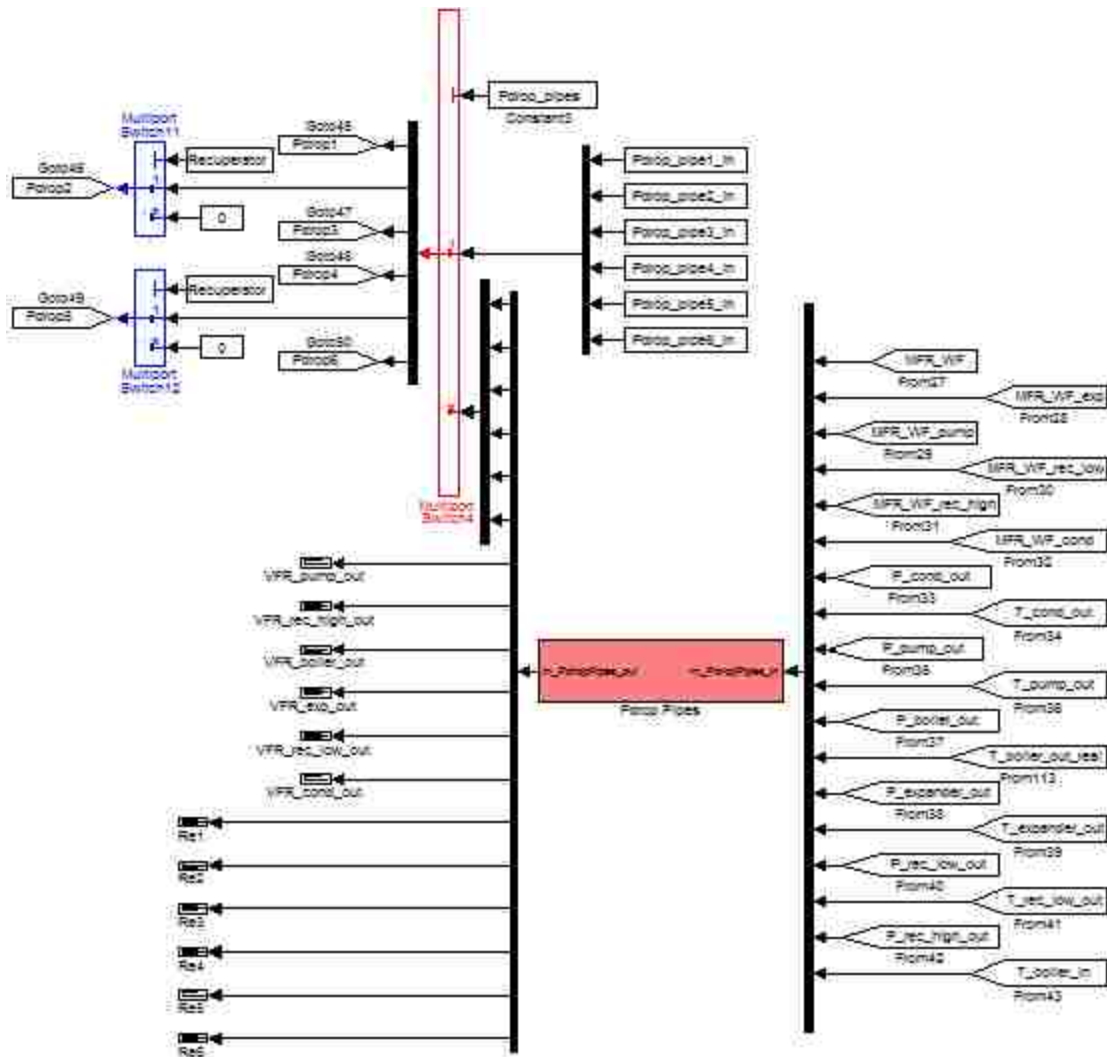


Figure 3.2-41: Pressure drop in the pipes functional block.

The inputs of this functional block are pressure, temperature and mass flow rate at the outlet of each component, or, in other words, at the inlet of each pipe. Also the information about the geometry of the pipes (diameter, length and number of tight bends), inserted by the user in the input window, go into this functional block.

Looking inside the box, the first action taken is to determine the density and kinematic viscosity at the inlet of each pipe. Then, dividing the mass flow rate by the density, the volume flow rate inside each pipe is found. At this point the Reynolds number in each pipe is calculated, with the following equation:

$$Re = 4 \cdot \frac{\dot{V}}{(\pi D \nu)} \quad (3.32)$$

Where at the numerator there is the volume flow rate, while D is the pipe inside diameter and ν is the kinematic viscosity. It has been obtained from the definition of Re number substituting the velocity of the fluid with the volume flow rate divided by the cross section of the pipe

Now, under the assumption of smooth pipes, the Darcy friction factor is computed as a function of the Re number. In particular three different equations can be used [66]:

If $Re < 4000$:

$$f_D = \frac{64}{Re} \quad (3.33)$$

If $4000 < Re < 10^5$

$$f_D = \frac{0.3164}{Re^{0.25}} \quad (3.34)$$

If $Re > 10^5$

$$f_D = 0.0032 + \frac{0.221}{Re^{0.237}} \quad (3.35)$$

At this point, all the data necessary to compute the distributed pressure losses are available, however also the concentrated pressure losses, modeled as 90° bends, have to be taken into account. In order to do that there of the bend pressure loss coefficient (K_b) has to be estimated. In general in literature [64] there are available charts that give K_b as a function of:

- bend deflection angle
- radius of curvature of the bend to the internal diameter of the pipe ratio
- Reynolds number.

However, since these charts are complex and too many variables have to be taken into account, an approximation has been done in order to assess a reasonable value of the bend pressure loss coefficient and consider it constant. Considering a bend deflection angle equal to 90° , a radius of curvature of the bend to the internal diameter of the pipe ratio around 1 and a Reynolds number ranging from 10^4 to 10^5 a reasonable value for K_b appeared to be 0.4 and that was the constant value assumed for the computation of the pressure drop inside the pipes.

Finally, it should be noted that the part of pipe that is affected by the bend is the one after the bend. We can also say that the concentrated losses inside a pipe are cumulative, because each bend further increases the bend pressure loss coefficient. So if there are n bends it is necessary to divide the pipe length into $n+1$ sections and for each of those compute a different total pressure drop coefficient ($K_{b,t}$), defined as:

$$K_{b,t} = K_b + f_D \frac{4L}{D} \quad (3.36)$$

Where K_b is the already presented bend pressure drop coefficient, and the other term is the distributed pressure drop coefficient. The first section will have a K_b equal to zero, all the other sections will have a K_b equal to the constant value assumed (in this case 0.3 for pipes on the vapor side because they usually have a higher Reynolds number and 0.4 for all the other pipes) multiplied by the number of bends before the section. However, it must be pointed out that for different pipe diameters, type of concentrated loss, Reynolds number range and pipe length a different K_b should be selected.

Figure 3.2-42 shows the Matlab script used to calculate the pressure drop inside pipe 1, the one that goes from the pump outlet to the recuperator high pressure side inlet. The “if” loop of Figure 3.2-42 distinguish between the case where there are no bends in the pipe so K_b is always equal to zero and there is no need to divide the pipe into different sections from the case where there are some bends. Whereas, the “for” loop is necessary in the case there are some bends to make K_b increase section by section. The same equations are set for the other pipes and the pressure drop inside each pipe is then computed. Exactly as happened in the pressure drop inside the heat exchanger functional block three different switches are necessary to filter the data coming out the pink box of Figure 3.2-41. The red switch is the first one, it sets the values of the pressure drop inside each pipe equal to the initial value in the case the user wants to consider constant the pressure losses inside the pipes. On the other hand the two blue switches sets the pressure drop of pipe 2 and 5 equal to zero in the case there is no recuperator in the system.

```

107 %% Pdrop between pump outlet and recuperator high side inlet
108 - Rel = VFR_pump_out*4/(pi*D1*ki_pump_out);
109 - if Rel <= 4000
110 -     f1 = 64/Rel;
111 - elseif Rel >= 10^5
112 -     f1 = 0.0032+(0.221/Rel^0.237);
113 - else
114 -     f1 = 0.3164/Rel^0.25;
115 - end
116 - if B1 > 0
117 -     for i =1:(B1+1)
118 -         Pdrop1 = Pdrop1 + ((Kb1*(i-1)+f1 * L1/(B1+1))...
119 -             /D1)*d_pump_out * (VFR_pump_out)^2 * 8 /...
120 -             (D1^4 * pi^2))*10^-3;
121 -     end
122 - else
123 -     Pdrop1 = (f1 * L1 /D1 ) * d_pump_out * ...
124 -         (VFR_pump_out)^2 * 8 / (D1^4 * pi^2)*10^-3;
125 - end

```

Figure 3.2-42: Pressure drop inside pipe 1.

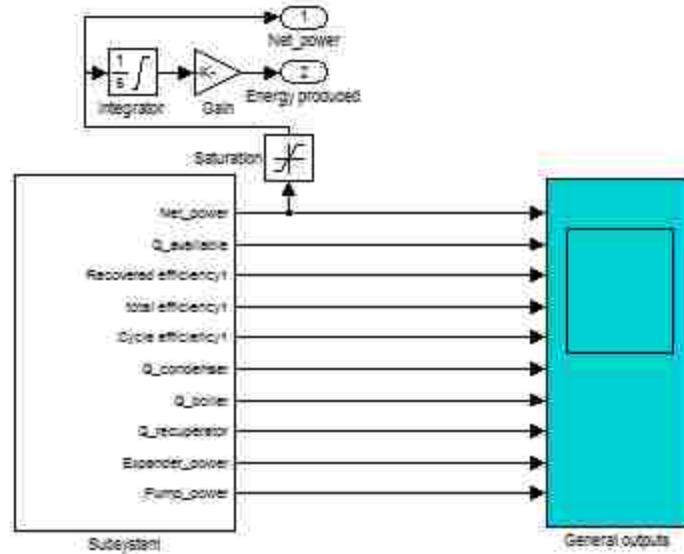


Figure 3.2-43: General outputs plot.

Finally the outputs of this functional block at time instant n are an input for the other functional blocks at time instant $n+1$.

3.2.2.10 Data treatment

The outputs of each functional block are stored files and plotted by means of graphs. It is very important for the user of the program to be able to monitor all the results. There two main different blocks where all the main variable of the cycle are plotted.

The first one is called “General outputs” and it is shown in Figure 3.2-43.

It plots all the main outputs of interest:

- net power output of the cycle
- heat available in the exhaust gas
- recovery efficiency
- Rankine cycle efficiency
- total efficiency
- heat transfer rate in the condenser
- heat transfer rate in the boiler
- heat transfer rate in the recuperator
- expander power output
- power requested by the pump.

The definitions used to compute these values are those introduced throughout the thesis.

Inside the white box on the left of Figure 3.2-43 there is a system of switches that automatically turns off the WHR unit, setting equal to zero all the outputs except for the heat available in the exhaust gas, in case the inlet temperature of the exhaust gas is lower than a value defined in the input window by the user. Moreover, the net power output of the system and its integral over time are stored and sent to the outside user interface, shown in Figure 3.2-2

Along with the general outputs are also plotted in another block, called output diagnostic, all the parameters that characterize each component, in the case the user wants to investigate in deeper details the functioning of each component. For example the pump parameters plotted are:

- volume flow rate inside the pump
- temperature, pressure and density at the pump inlet
- pump head (pump pressure rise)
- pump isentropic efficiency
- temperature at the pump outlet
- power request by the pump
- pump rotational speed

For the sake of brevity the outputs plotted for the other components are not listed, anyway they correspond to the main outputs of the functional blocks presented in paragraphs from 3.2.2.1 to 3.2.2.6.

3.3 Comparison between preliminary and detailed models

The structure of the two models developed to analyze the behavior of a Waste Heat Recovery unit based on an Organic Rankine Cycle technology has been thoroughly explained in sections 3.1 and 3.2. Here the author wants to clearly specify and highlight the differences between the two models. Despite many equations and the general structure of the two programs are similar there are many substantial differences.

First of all, as already mentioned, the purpose of the two models is quite different. While the preliminary model was meant to give indications on how the net power output of the system varies as a function of the most critical variables of an ORC. Being more interested on the trend of variation rather than on the numeric values coming out of the model. On the contrary the detailed model has as ultimate goal that of being integrated in a Matlab/Simulink model of the overall vehicle and see how much fuel savings it can generate in a driving cycle.

Hence it has to replicate the real conditions occurring in a WHR system based on a ORC technology, in order to assess as accurately as possible the net power output and all the other operating parameters of the system.

As a matter of fact the detailed model is also a more flexible tool. It can predict the behavior of the WHR unit with different layouts (standard or recuperative), with different working fluids and with different degrees of accuracy simply by selecting the proper input in the initial input window.

Going into more concrete aspects the detailed model includes also some features not contemplated by the preliminary model, they are listed here:

- sub-cooling before the pump inlet
- bypass pipes around the expander, around the recuperator low pressure side and around the exhaust gas side of the boiler
- minimum temperature difference at the pinch point verification in the heat exchanger
- possibility to select the fluid acting as a coolant in the condenser
- estimation of the mass flow of the coolant required in the condenser
- distributed and concentrated pressure losses inside the pipes
- possibility to assume variables pump and expander isentropic efficiencies
- possibility to assume variable pressure drops inside heat exchangers
- time dependent simulations with the possibility of defining variable exhaust gas temperature and mass flow rate
- possibility to assess the rotational speed of both pump and expander
- distinction between the case in which the expander is connected to the engine shaft or to an electric generator.

4. ANALYSIS AND DISCUSSION OF THE SIMULATION RESULTS

4.1 Preliminary analysis of ORC design alternatives

In section 3.1, the methodology employed and the objectives sought in the preliminary analysis have been accurately explained. Here, in the current section, the results obtained by means of the preliminary model are illustrated and thoroughly analyzed.

Even though the purpose of this analysis was another, the inputs data have been chosen in order to accomplish a simulation that replicates, at least with good approximation, the operating conditions of a real WHR system. Table 4.1-1 shows the input parameters of the exhaust gas of the 3.6L V-6 Chrysler gasoline engine. They were evaluated at target vehicle operating condition (design point), correspondent to a highway drive at constant vehicle speed (70 Mph) with engine rotating at 2465 RPM and generating a torque of 125 Nm. In this conditions the power delivered by the engine is of 29 kW.

EXHAUST GAS PARAMETERS	
Exhaust gas temperature at boiler inlet [°C]	590
Exhaust gas flow rate [kg/s]	0.035
Average exhaust specific heat [kJ/kg-K]	0.9937

Table 4.1-1: Design point exhaust gas parameters.

Table 4.1-2 illustrates the other inputs describing the performances of the components used in the WHR system. Obviously in the case a standard ORC is analyzed the parameters of the recuperator are not considered.

While the parameters of Table 4.1-1 derive directly from experimental tests carried out on the engine in question, those of Table 4.1-2 regarding the heat exchangers, come from initial indications provided by suppliers.

COMPONENTS PERFORMANCE	
Condenser Effectiveness ϵ_{cond}	90%
Boiler Effectiveness ϵ_{boiler}	85%
Recuperator Effectiveness ϵ_{recup}	87%
Pump Isentropic Efficiency η_{pum}	60%
Expander Isentropic Efficiency η_{exp}	60%
Condenser Pressure Drop $\Delta p_{4'1}$ [kPa]	7
Boiler Pressure Drop $\Delta p_{2'3}$ [kPa]	345
Recuperator High Pressure Side Drop $\Delta p_{22'}$ [kPa]	103
Recuperator Low Pressure Side Drop $\Delta p_{44'}$ [kPa]	6

Table 4.1-2: Components characteristics.

On the other hand, the conservative isentropic efficiency values assigned to the pump and to the expander were suggested by experimental tests carried out in a test rig mounted at Fiat Research Center (CRF).

For what concerns the range of variability of the pump compression ratio and of the expander inlet temperature they have been defined arbitrarily by the author, and summarized in Table 4.1-3. More specifically, the pump compression ratio is assumed to vary from as low as 3 to as high as 10. The expander inlet temperature is assumed to vary from the saturated liquid vapor temperature, of the selected working fluid, at the expander inlet pressure, up to 210 °C, maximum temperature that the expander can withstand. Obviously the lower bound of the expander inlet temperature is not reported in Table 4.1-3 because it varies for each working fluid.

RANGE OF VARIABILITY OF THE PUMP COMPRESSION RATIO AND OF THE EXPANDER INLET TEMPERATURE	
Minimum Pump Compression Ratio	3
Maximum Pump Compression Ratio	10
Maximum Expander Inlet Temperature [°C]	210

Table 4.1-3

The condensing temperature imposed were either 35 °C or 45 °C as a function of the scope of the analysis, the results obtained with the two different condensing temperatures are compared. Finally, simulations have been carried out for the working fluids listed in Table 4.1-7, except water. Those working fluids have been chosen among the ones commonly employed in ORCs especially because they are particularly different one from another, some are dry some others are wet, some are cheap some others are expensive. Anyway their characteristics allowed the author to make a complete analysis that can be extended to other fluids.

Moreover, it is fundamental to underline that, since the pump compression ratio has been chosen as an input, rather than the pump pressure rise, only fluids that have a pump inlet pressure high enough have been tested. For instance water and ethanol have a significantly higher critical temperature and pressure than the fluids listed in Table 4.1-7, so at the pump inlet temperature selected (35 °C or 45 °C) they have a pressure very low. Hence, even though the fluid is compressed in the pump and its pressure is multiplied by a factor of ten, the working fluid is not able to overcome the pressure losses inside the heat exchangers and produce useful work. This limitation is avoided in the detailed model, where the parameter chosen to characterize the pump performances is the pressure rise, also known as pump head. In the detailed model the pressure at the pump outlet is not a multiple of the pressure at the pump inlet, but it is the pressure at the pump inlet plus the desired pump pressure rise, the latter can be controlled by selecting a proper pump and by varying its rotational speed.

In short, the choice of using as an input of the preliminary model the pump compression ratio penalizes too much the working fluids with a high critical pressure. Countermeasures have been taken to overcome this limitation in the detailed analysis; the pump model adheres more to the reality because the pump pressure rise is the characterizing parameter.

That said, the different comparisons made are summarized in the bullet list below:

- 1) For a given condensing temperature, system layout and working fluid the combination of compression ratio and expander inlet temperature that maximizes the net power output has been investigated.
- 2) For a given condensing temperature, working fluid, pump compression ratio and expander inlet temperature the performances achievable with the two different system layouts (recuperative and standard) have been compared.
- 3) For a given combination of system layout and condensing temperature, the maximum net power outputs achievable with different working fluids have been compared.

The results obtained and the considerations done are reported in the following paragraphs.

4.1.1 Operating parameters that maximize the performances

In order to assess the pump compression ratio and the expander inlet temperature that maximize the net power output simulations have been carried out just for a condensing temperature equal to 45 °C since the results do not change for changing condensing temperature. Moreover, only for the purpose of theoretically studying the influence of these two factors, the maximum compression ratio has been set equal to 25, even if it is unrealistic or it is economically unfeasible to realize. Running the preliminary model and searching among the possible combinations of pump compression ratios and expander inlet temperature the one that returns the highest net power output the results shown in Table 4.1-4 and Table 4.1-5, respectively for a standard ORC and a recuperative ORC, have been found out.

The results reported in the table are easy to be interpreted, in the columns the maximum net power output achievable with a given working fluid is reported along with other operating parameters. Each row of the tables refer to a different working fluid among those considered in the preliminary analysis. In both tables the fluid that gives the maximum net power output is highlighted with bold characters.

From the previous sections subscripts 1 and 2 of the tables analyzed refer to the state of the working fluid respectively at the pump inlet and outlet, the meaning of the other symbols is shortly defined here:

- T_{evap} : evaporation temperature
- $T_{\text{exp,in}}$: expander inlet temperature
- P_2/P_1 : pump compression ratio
- P_{critical} : critical pressure
- $P_2 - P_1$: pump pressure rise
- wf MFR: mass flow rate of the working fluid
- $T_{\text{exh,out}}$: exhaust gas outlet temperature

Looking at Table 4.1-5 that refers to a recuperative ORC, with an internal heat exchanger (recuperator) included, it appears evident that for a recuperative ORC the higher the expander inlet temperature the greater is the net power output. In fact the expander inlet temperature that gives the maximum power output is equal to the maximum one imposed (210 °C) for every working fluid with the only exception of the R134a. In order to make a more accurate comparison the amount of superheat given to the working fluid should be considered. So comparing the evaporating temperature to the expander inlet temperature, it comes out that the R134a has the greatest difference between evaporating temperature and expander inlet temperature, hence it receives a great amount of superheat. The expander inlet temperature is lower if compared to that of the other fluids only because the evaporating temperature is significantly lower. So it can be stated that for a recuperative ORC no matter what kind of working fluid is adopted, a great amount of superheat is to be preferred paying attention not to overcome the maximum temperature that the expander can withstand and that one the working fluid can withstand without becoming unstable. This happens because even if at the expander outlet the working fluid is still at high temperatures, a portion of the heat left in the working fluid is used in the recuperator to pre-heat the high pressure liquid coming out of the pump, increasing the overall efficiency of the cycle. On the other hand the interpretation of the optimal expander inlet temperature for a standard ORC Table 4.1-4 is more complex. In general we see that the expander inlet temperatures are lower for R245fa, R134a and Pentane, whereas they remain unchanged and still equal to 210 °C for the other three working fluids analyzed. However, looking also at the evaporating temperatures we can see that the R134a still receives a great amount of superheat. Theoretically, for dry and isentropic fluids in a recuperative ORC no superheat gives a better net power output, instead, for wet working fluids a significant amount of superheat should be preferred.

The finding partially agrees with the theory, in fact the wet working fluids considered, R134a and R21 give the best net power output with a significant amount of superheat, even if in the case of the R134a not the maximum possible. On the other hand, only pentane that is a dry fluid gives the best results with only a very small amount of superheat; all the other isentropic and dry working fluids (R245fa, R141b and R123) give the greatest net power output with a non-negligible amount of superheat, so before selecting the desired expander inlet temperature for a standard ORC an accurate analysis should be carried out to see the most convenient one.

Now focusing the attention on the pump compression ratio column we can see that there is no an optimal value valid for all the working fluids. So in order to understand better this phenomenon the analysis should be extended also to the pump outlet pressure and to the critical pressure columns. In particular if we compare the just mentioned columns of both tables (Table 4.1-4 and Table 4.1-5) it is easy to notice how the optimal pressure at the pump outlet is very close to the critical pressure, just slightly lower, no matter the fluid selected or the type of ORC. That corresponds to that theoretically predictable since increasing the pump outlet pressure the area defined by the cycle plotted on a T-s diagram that is proportional to the net power output, increases. So basically the higher the pump outlet pressure the greater the net power output. However, there are two very important limitations. The first one, already mentioned, is the critical pressure of the working fluid; the pressure at the pump outlet has to be lower than this value with a certain margin of safety, from the data acquired with the simulation 10 kPa is sufficient, however, if the risk of having a supercritical ORC wants to be avoided, 100 kPa appears more adequate. Actually, the most stringent limitation usually is another that has not been considered here: the maximum pressure that the expander can withstand, usually around 2000-2500 kPa for a scroll expander. If it was taken into account no one of the performances reported in Table 4.1-4 and Table 4.1-5 could have been achieved, since the P_2 reported are 1000 to 2000 kPa over the usual limit of an expander.

Finally, even if it was not the objective of this analysis the working fluid that seems to provide the greatest net power output is the R141b. More interesting is the analysis of the correspondent efficiencies, that can give an indication on the maximum performances achievable with different working fluids and with the component operating parameters defined in Table 4.1-2.

- For a standard ORC the maximum cycle efficiency is around 9 to 12% and the maximum recovery efficiency, defined in Equation (3.24), is around 80%.
- For a recuperative ORC the maximum cycle efficiency is higher, ranging from 13% to 15%, whereas the recovery efficiency is slightly lower around 70% because the temperature at the boiler inlet of the working fluid is higher since the high pressure liquid is heated up in the recuperator.

In any case the net power output for a given working fluid as well as the total efficiency, defined as the products of the two efficiencies mentioned above, is always higher for recuperative ORCs. To conclude, the objective here was to understand which pump pressure ratio and expander inlet temperature maximize the net power output rather than assess the net power output achievable itself. It has been found out that the higher the compression ratio, and in turns the expander inlet pressure, the higher is the net power output, no matter the layout of the system nor the working fluid type. On the other hand the expander inlet temperature that gives the maximum net power output is the highest possible for a recuperative ORC (no matter the working fluid) and for a standard ORC with wet working fluids. However, for dry or isentropic working fluids the optimal expander inlet temperature may vary from the condition in which no superheat is provided to the condition where a significant amount of superheat is given. For each kind of working fluid an analysis is suggested to understand which is the best expander inlet temperature.

STANDARD ORC													
	Max Net Power output [kW]	Tevap [°C]	Temp in [°C]	P2/P1	P2 [kPa]	P critical [kPa]	P1 [kPa]	P2-P1 [kPa]	wf MFR [kg/s]	Recovery Efficiency	Cycle Efficiency	Efficiency Tot	Texh out [°C]
R245fa	1.539	153.9	187.2	12.4	3641.0	3651.0	294.5	3346.5	0.055	81.59%	9.60%	7.83%	129.0
R134a	0.972	100.9	180.1	3.5	4049.3	4059.3	1159.9	2889.4	0.057	81.50%	6.07%	4.95%	129.5
Pentane	1.818	196.3	199.7	24.7	3360.0	3370.0	136.1	3223.9	0.028	81.59%	11.34%	9.25%	129.0
R141b	2.052	197.8	210.0	25.0	3908.8	4212.0	156.4	3752.4	0.051	81.51%	12.81%	10.44%	129.5
R123	1.861	183.5	210.0	20.1	3651.8	3661.8	181.7	3470.1	0.062	81.54%	11.61%	9.47%	129.3
R21	1.977	178.1	210.0	15.1	5171.2	5181.2	343.2	4828.0	0.056	81.33%	12.37%	10.06%	130.5

Table 4.1-4: Best performance with a standard ORC, $T_{\text{cond}} = 45\text{ }^{\circ}\text{C}$.

RECUPERATIVE ORC													
	Max Net Power output [kW]	Tevap [°C]	Temp in [°C]	P2/P1	P2 [kPa]	P critical [kPa]	P1 [kPa]	P2-P1 [kPa]	wf MFR [kg/s]	Recovery Eff	Cycle Eff	Eff Tot	T exh out [°C]
R245fa	1.896	153.1	210.0	12.4	3641.0	3651.0	294.5	3346.5	0.062	71.16%	13.55%	9.64%	187.9
R134a	1.325	100.8	199.6	3.5	4049.3	4059.3	1159.9	2889.4	0.074	73.60%	9.16%	6.74%	174.1
Pentane	2.152	194.4	210.0	24.7	3360.0	3370.0	136.1	3223.9	0.031	71.34%	15.35%	10.95%	186.9
R141b	2.219	193.9	210.0	24.3	3794.1	4212.0	156.4	3637.7	0.055	74.81%	15.10%	11.30%	167.3
R123	2.111	182.1	210.0	20.1	3651.8	3661.8	181.7	3470.1	0.071	73.43%	14.63%	10.74%	175.1
R21	2.065	172.9	210.0	14.1	4826.1	5181.2	343.2	4482.9	0.058	77.08%	13.64%	10.51%	154.5

Table 4.1-5: Best performance with a recuperative ORC, $T_{\text{cond}} = 45\text{ }^{\circ}\text{C}$.

4.1.2 System layout comparison

The previous paragraph has already furnished few indications about the comparison between the two possible system layouts (recuperative or standard), however to make a complete and extensive analysis the power output as well as the other operating parameters, have to be compared in the whole range considered of expander inlet temperature and pump compression ratio. In the present paragraph the net power output and other parameters are plotted in 3d graphs for all the possible combinations of pump compression ratio and expander inlet temperature of each working fluid; the condensation temperature used to derive these pictures is equal to 45 °C. Figure 4.1-2 shows the net power output of the cycle achievable by each working fluid with a standard ORC, blue surfaces, and with a recuperative ORC, red surfaces. It immediately results evident how the red surfaces are above the blue ones for almost every operating conditions. So the recuperative ORC appears to be a better solution. However, there are different combinations of expander inlet temperature and pump compression ratio in which the blue surfaces are over the red ones.

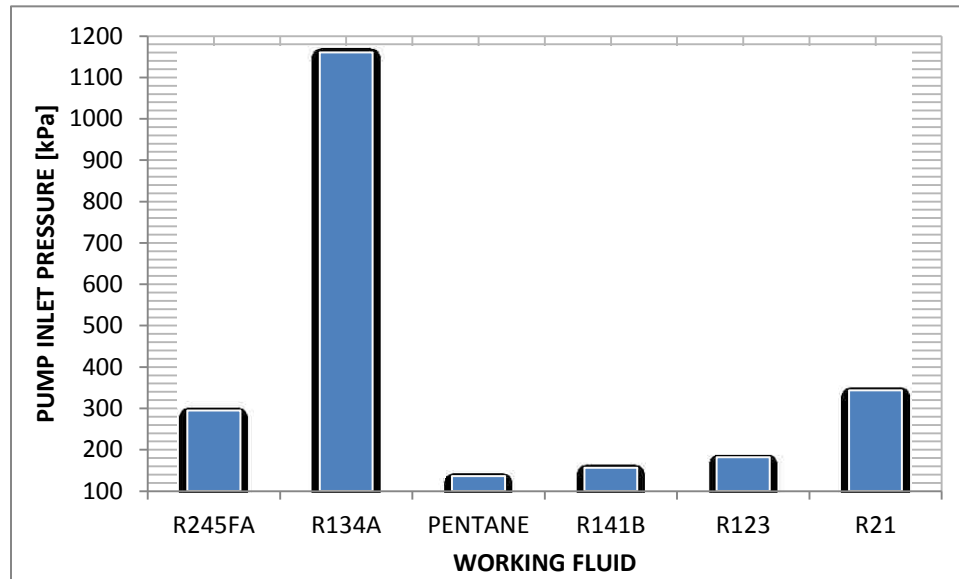


Figure 4.1-1: Pump inlet pressure, corresponding to the saturated liquid pressure at 45 °C.

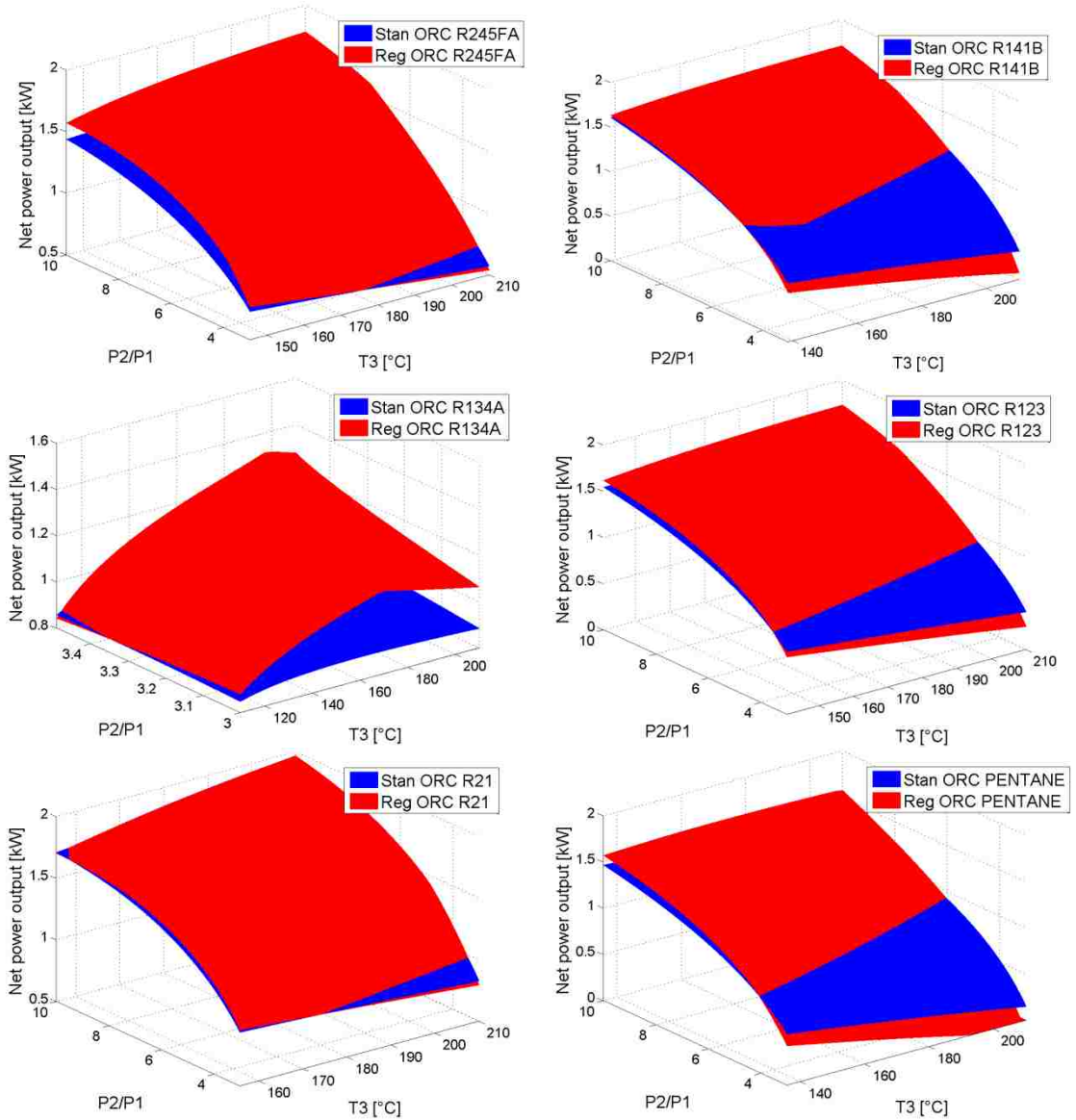


Figure 4.1-2: Net power output, system layout comparison, $T_{\text{cond}} = 45 \text{ }^{\circ}\text{C}$.

In particular these areas are significant for Pentane and R141b. Giving a closer look it results evident that the zones in which the blue surfaces prevail have a low pump compression ratio (P_2/P_1). This could be explained considering that the pressure losses, that negatively affect the power output, in a recuperative ORC are greater than the pressure losses in a standard ORC since there is a further heat exchanger, the recuperator. For low compression ratios these further pressure losses are more influencing up to the point that they overcome the benefits of the recuperation.

The validity of this consideration is confirmed comparing the pressure at the pump inlet (P_1) of the six working fluids considered, this parameter is only function of the fluid saturation curve since it is the pressure of the saturated liquid at the selected condensing temperature (45 °C). Looking at Figure 4.1-1 it results that the three working fluids on the right column of Figure 4.1-2 (R141b, R123, and Pentane) have the lowest pump inlet pressure. Those fluids are also the ones in which the net power output of the standard ORC is greater than the net power output of the recuperative ORC for a wider range of pump compression ratios (blue surface over the red surface of Figure 4.1-2). In fact, for a certain pump compression ratio, to a lower pressure at the pump inlet corresponds a lower pressure at the pump outlet. In turns the pressure losses inside the heat exchangers represent a greater percentage of the pump outlet pressure making the cycle efficiency, hence the net power output, of a recuperative ORC drop. For example let's compare the performances of R245fa and Pentane for a pump compression ratio equal to 5 and a expander inlet temperature equal to 210 °C. The pump inlet pressure of R245fa is equal to 1475 kPa obtained multiplying the pump inlet pressure of Figure 4.1-1 to the pump compression ratio selected. Repeating the same procedure the Pump outlet pressure of the Pentane is equal to 680 kPa. The total pressure losses considered for a recuperative ORC are 461 kPa from Table 4.1-2; respectively 31% of the pump outlet pressure for the R245fa and 67% of the pump outlet pressure for the Pentane. On the other hand if a standard ORC is used the total pressure losses inside the heat exchangers are equal to 352 kPa, respectively 23% (R245fa) and 51% (Pentane) of the pump outlet pressure. For the R245fa the reduction of this percentage (from 31% to 23%) is lower than that of the Pentane (from 67% to 51%), meaning that Pentane has a greater benefit in terms of reduction of pressure losses in employing a standard ORC if compared to the R245fa. In fact, looking at the correspondent charts of the net power output for the two working fluids considered, at an expander inlet temperature of 210 °C and a pump compression ratio of 5 there are two different situations: in the R245fa charts a recuperative ORC gives greater net power output, whereas in the Pentane chart a standard ORC gives a greater net power output. In short, in the operating conditions considered in the case Pentane were used, the introduction of the recuperator generates an increase in pressure loss that is so high, in terms of percentage of the pump outlet pressure, to hide the benefits of the recuperation and to make the net power output decrease rather than increase; so a standard ORC should be preferred. On the opposite, for R245fa, the increase in pressure loss does not influence too much the net power output of the cycle so the adoption of a recuperative ORC with the recuperator still increases the net power output.

Actually, it should be underlined that the difference between the net power output of a standard and a recuperative ORC for low values of expander inlet temperature is very small. In some cases (R134a and R21), even at high values of compression ratio, a standard ORC gives a higher net power output. This was expected from what stated in the previous paragraph (4.1.1), since the recuperator gives the best benefits when there is a high temperature at the expander outlet.

The considerations made above are summed up in the bullet list below:

- The net power output of a recuperative ORC (red surfaces of Figure 4.1-2) in general is greater than the net power output of a standard ORC (blue surfaces).
- For low compression ratios might happen that the net power output of standard ORCs is higher than that of recuperative ORCs, due to the greater pressure losses that characterize a recuperative ORC.
- The range of compression ratios in which the net power output of a standard ORC is higher than that of recuperative ORC is a function of the fluid properties and in particular of the pump inlet temperature assumed equal to the pressure of the saturated liquid at the selected condensing temperature. The lower this pressure the bigger the range.

Nonetheless, it results evident that the overall greatest net power output achievable is achieved for every working fluid with the recuperative system layout. So if the pump compression ratio and expander inlet temperature can be chosen arbitrarily by the designer, a recuperative ORC is advisable since it can provide the maximum possible net power output for a given working fluid. Figure 4.1-3 illustrates the cycle efficiency as a function of the pump compression ratio and the expander inlet temperature. The light blue surfaces correspond to recuperative ORCs whereas the yellow ones correspond standard ORCs. The plots of Figure 4.1-3, as predictable, have the same shape of the net power output plots of Figure 4.1-2. Actually the difference between the surfaces is more accentuated if compared to that of the net power output, in fact the zone in which a standard ORC has a better efficiency than a recuperative ORC is smaller than the area in which a standard ORC gives a greater net power output than a recuperative ORC, for a given working fluid. This difference can be easily noted looking at the R21 and R134a plots, for high values of P_2/P_1 and low values of expander inlet temperature (T_3) the net power output of a standard ORC is greater however the cycle efficiency is lower. This fact is easily explained recalling that the cycle efficiency is calculated as the net power output of the cycle divided by the heat introduced in the cycle during the evaporation of the working fluid, that in a WHR unit corresponds to the heat given by the exhaust gas. However, this heat absorbed by the working fluid may vary in absolute value from fluid to fluid and especially from a system layout to another.

More precisely, in a standard ORC the boiler inlet temperature is lower than in a recuperative ORC, with a standard ORC more heat can be extracted from the exhaust gas (the recovery efficiency is higher). Hence in the general case where the cycle efficiency of a standard ORC is lower than in a recuperative ORC the greater amount of heat introduced makes the net power output difference less accentuated.

Anyway, beside this clarification, all the other considerations done for the net power output plots hold.

Finally in Figure 4.1-4 the mass flow rate of the working fluid is depicted for the same range of pump compression ratios and expander inlet temperatures.

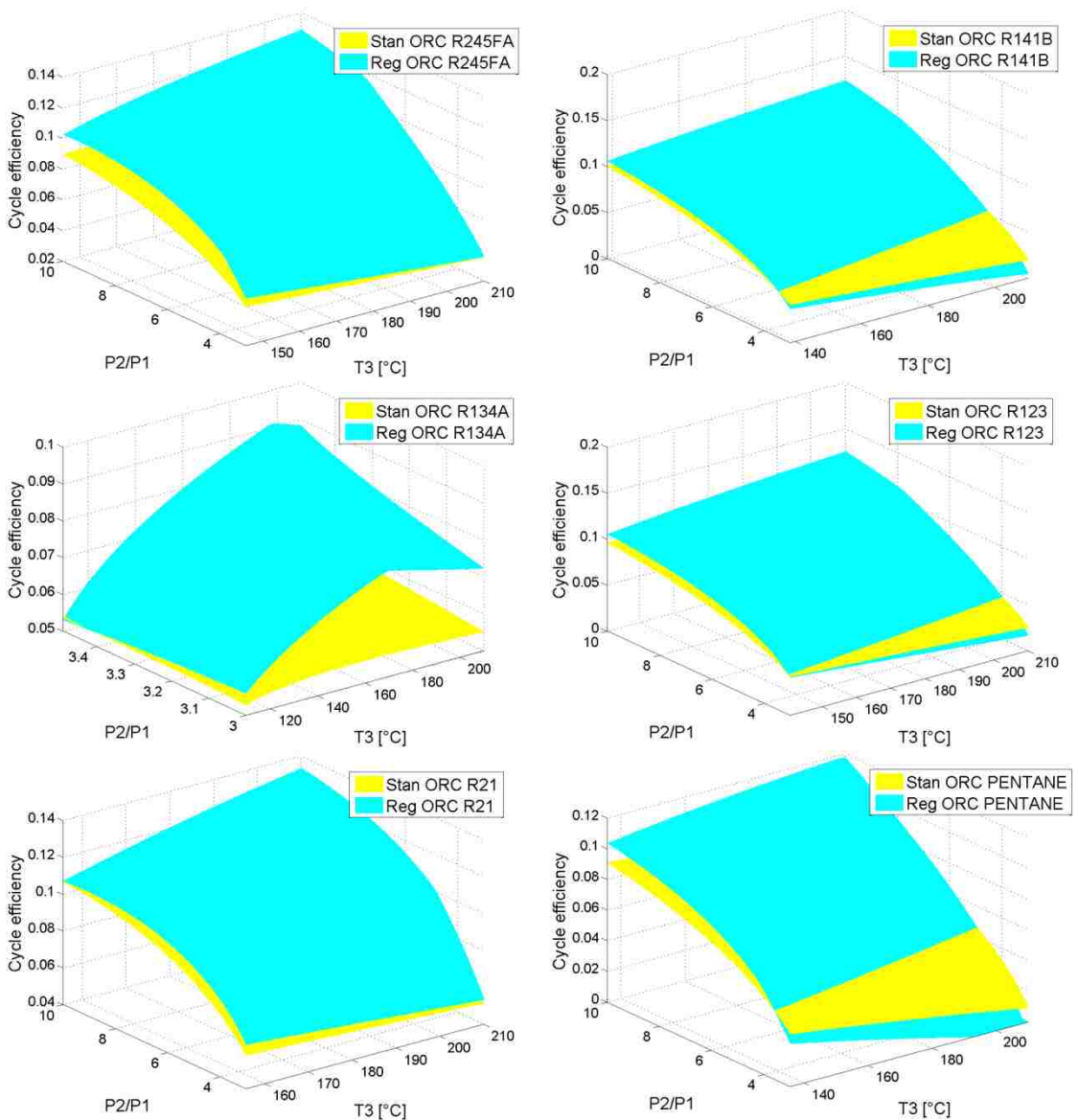


Figure 4.1-3: Cycle efficiency, system layout comparison, $T_{cond} = 45$ °C.

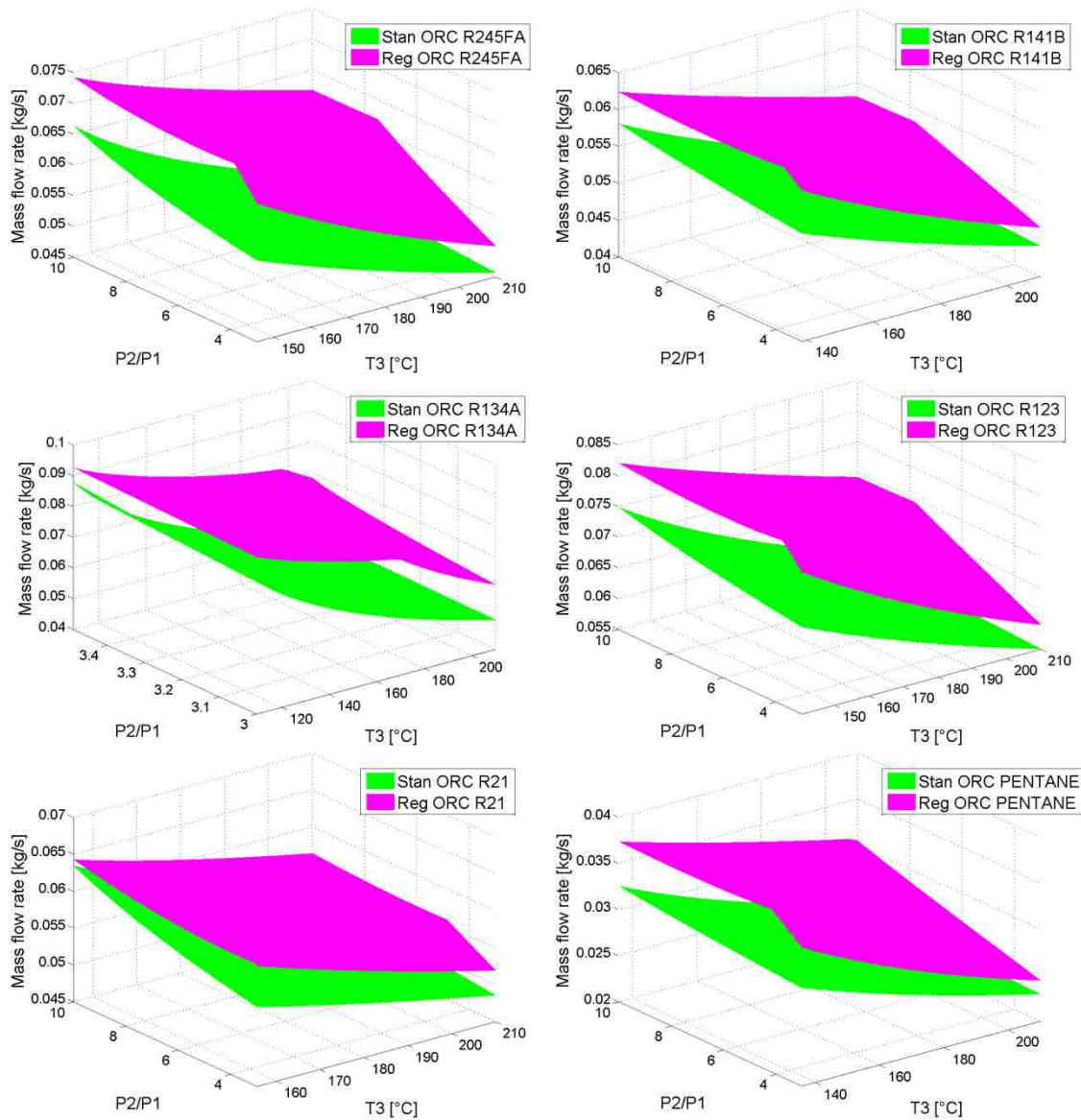


Figure 4.1-4: Working fluid mass flow rate, system layout comparison, $T_{\text{cond}} = 45^\circ\text{C}$.

Looking at the charts two main considerations that hold for every working fluid can be done:

- Recuperative ORCs have to be supplied with more mass flow rate than standard ORCs no matter what working fluid is selected nor which combination of P_2/P_1 and T_3 .
- For a given P_2/P_1 , the lower the temperature at the expander inlet (T_3) the higher the mass flow rate of working fluid required.

The latter can be explained simply considering that, for a given boiler inlet temperature, the lower the expander inlet temperature the lower the enthalpy rise between across the boiler. With that in mind, for a given heat transfer rate in the boiler, the lower the enthalpy rise the higher the mass flow rate of the working fluid required to extract the same amount of heat from the exhaust gas.

A similar explanation can be done to the first consideration made. In particular as previously said the boiler inlet temperature of a standard ORC is lower than the boiler inlet temperature of a recuperative ORC so the enthalpy rise across the boiler with a standard ORC is higher and as a consequence the mass flow rate of the working fluid should be lower with respect to that of a recuperative ORC. However, this is true if the heat transfer rate inside the boiler of a standard ORC were the same as that one of a recuperative ORC. Since we have already said that the heat transfer rate inside the boiler is higher for standard ORCs the explanation to this phenomenon is a little more complex. From a recuperative ORC point of view there are two differences that affects the mass flow rate. From one side the enthalpy rise across the boiler is lower, so a greater mass flow rate is expected, but from another side the heat transfer rate is lower, so a lower mass flow rate is expected. Since in the charts of Figure 4.1-4 the mass flow rate of the working fluid in a recuperative ORC is higher than that in a standard ORC, it is evident that the contribution that prevails is that of the lower enthalpy drop. So the decrease in enthalpy rise is greater than the decrease in heat transfer rate. The greater amount of mass flow rate required is a small disadvantage of the recuperative ORC with respect to the standard ORC since the pipe and components dimensions have to be bigger, adding complexity to the system.

4.1.3 Working fluids preliminary comparison

The last analysis carried out by means of the preliminary model is the comparison of the working fluids considered in terms of absolute performances. 3d graphs, similar to those presented in the previous paragraph, are shown in the following. The are two plots (one for standard and another for recuperative ORC) for each operating parameter (e.g. net power output) in which the results obtained with different working fluids are reported together.

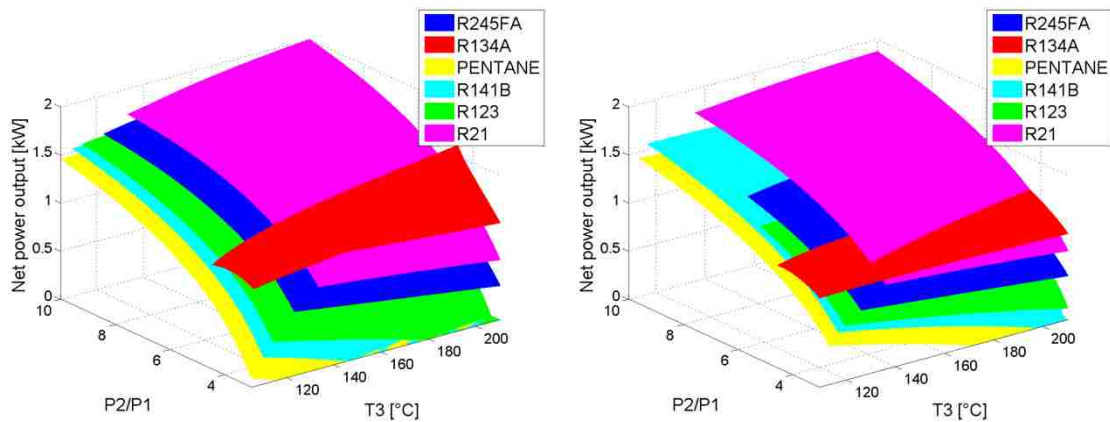


Figure 4.1-5: Net power output achievable with different working fluids in a recuperative ORC (left) and a standard ORC (right), $T_{\text{cond}} = 35 \text{ }^{\circ}\text{C}$.

The range of pump compression ratio (P_2/P_1) used goes from 3 to 10 or from 3 to the pump compression ratio that makes the pump outlet pressure stay below the critical pressure of the working fluid considered. On the other end the expander inlet temperature (T_3) as usual goes from the saturated vapor temperature at the expander inlet pressure up to 210 °C. In practice the lower bound of T_3 is different for each working fluid.

Figure 4.1-5 shows the net power output comparison, on the left side the results obtained with a recuperative ORC are reported and on the right side the ones obtained with a standard ORC. The first thing that appears evident is that there is a working fluid whose pump compression ratio range is limited and cannot go over 5, it is the red one (R134a) this is due to its high pressure at condensation temperature, so multiplying this pressure by the compression ratio the pump outlet pressure quickly becomes higher than the critical temperature. That said, let's analyze more accurately the picture on the left side. The working fluid that gives the best performances throughout almost the whole range of variability of the two independent variables considered is the R21. Looking at the physical properties of this fluid, reported in Table 4.1-7, it turns out that it has the second highest latent heat and the lowest specific heat among the working fluids tested. As explained in paragraph 2.3.1 these are the conditions that a working fluid should have to obtain a high net power output.

Actually for low values of the compression ratio R134a is able to provide a net power output even greater and in particular if the maximum possible T_3 is used the net power output plot of the R134a presents a pronounced peak. Excluding R134a from the ranking the second best working fluid (in terms of net power output) appears to be R245fa followed by R123, R141b and Pentane. This ranking is substantially different from that emerged in Table 4.1-5 where R141b was the fluid that gave the greatest net power output, this is because the maximum pump compression ratio considered in the analysis reported in this paragraph is limited to 10 whereas in Table 4.1-5 the limit was significantly higher (25). However, since in a WHR unit the practical maximum compression ratio is not higher than 10 this limitation is necessary and in the detailed model there will be an even more stringent one.

Anyway, the conclusions drawn in paragraph 4.1.1 are confirmed: for each working fluid the maximum net power using a recuperative ORC is obtained with the maximum possible expander inlet temperature and maximum pump compression ratio.

More complex are the results reported on the right side of Figure 4.1-5. The best working fluid still is the R21, except in the case the cycle is operated at small compression ratios and a high expander inlet temperatures, conditions in which R134a remains the best working fluid. However, the second best is difficult to be determined.

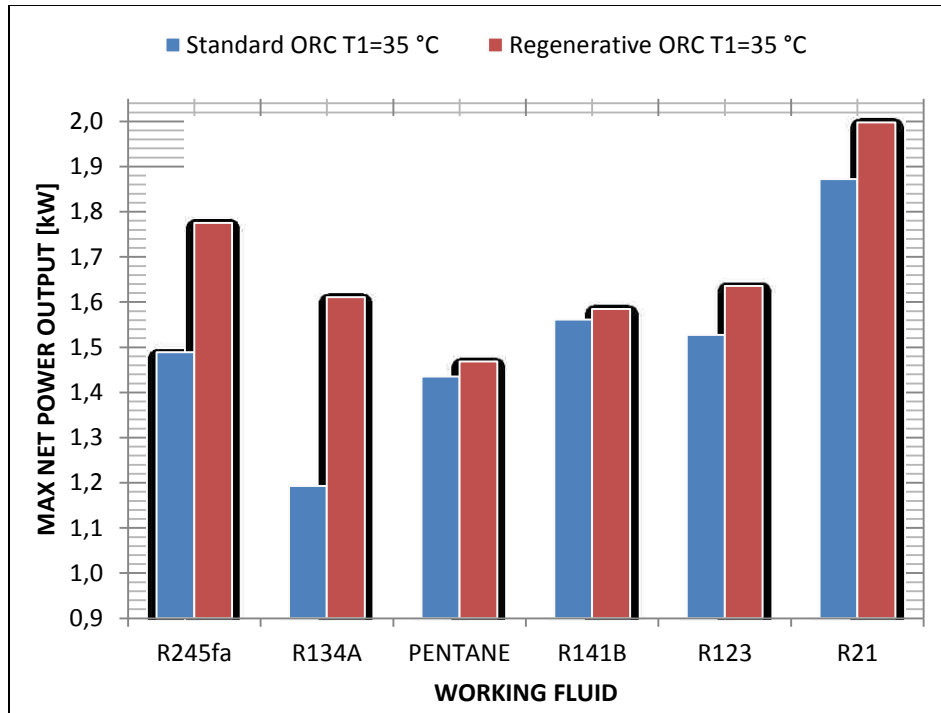


Table 4.1-6: Maximum net power output achievable with different working fluids with standard ORC (blue columns) and recuperative ORC (red columns), $T_{cond} = 35$ °C.

More precisely, for high pump compression ratios and low expander inlet temperatures R141b and Pentane prevail over R245fa. On the contrary, at medium to high expander inlet temperatures and high compression ratios R245fa is the second best followed by R141b and Pentane. Finally for low compression ratios R245fa is still the second best, but followed by R123.

Table 4.1-6 compares the maximum net power outputs achievable by the working fluids analyzed, no matter the combination of pump compression ratio and expander inlet temperature. In absolute value the maximum net power output is achieved with R21 recuperative ORC, followed by R21 standard ORC and R245fa recuperative ORC. Furthermore, the table above underlines the benefits of the introduction of the recuperator in terms of increase in maximum net power output. Pentane and R141b do not have great benefits (e.g. Pentane goes from 1.44 kW to 1.47 kW, less than 2% increase) so the adoption of a recuperative ORC for such fluids is not suggested whereas R245fa and R134a have great advantages in using a recuperative ORC, their maximum net power output respectively grows of 19.4% and 35.3%, making the R134a pass from the less appealing working fluid if a standard ORC is used to the fourth best behind R21, R245fa and R123 with a recuperative ORC. Anyway, with the boundary conditions imposed the net power output of the R21 with a recuperative ORC is around 2 kW that corresponds to an increase of 6.8% of the engine power, considering a power delivered by the engine of 29 kW.

The plots on T-s diagrams of the cycles that give the net power outputs reported on Table 4.1-6 are illustrated in Figure 4.1-6 and Figure 4.1-7. On the top of each plot the combination of P_2/P_1 and T_3 that give the maximum net power output is reported.

	Name	Type	Molecular weight	T_{cr} (K)	P_{cr} (MPa)	Vapor Cp (J/kg-K)	Latent heat (kJ/kg)	ξ (J/kg-K ²)
R-21	Dichlorofluoromethane	HCFC	102.92	451.4	5.18	339.85	216.17	-0.78
R-123	2,2-Dichloro-1,1,1-trifluoroethane	HCFC	152.93	456.8	3.66	738.51	161.82	0.26
R-134a	1,1,1,2-Tetrafluoroethane	HFC	102.03	374.2	4.06	1211.51	155.42	-0.39
R-141b	1,1-Dichloro-1-fluoroethane	HCFC	116.95	477.5	4.21	848.37	215.13	0.00
R-245fa	1,1,1,3,3-Pentafluoropropane	HFC	134.05	427.2	3.64	980.90	177.08	0.19
R-601	Pentane	HC	72.15	469.7	3.37	1824.12	349.00	151
R-718	Water	-	18.00	647.1	22.06	1943.17	2391.79	-17.78

Table 4.1-7: Thermodynamic and physical properties of the organic working fluids plus water.

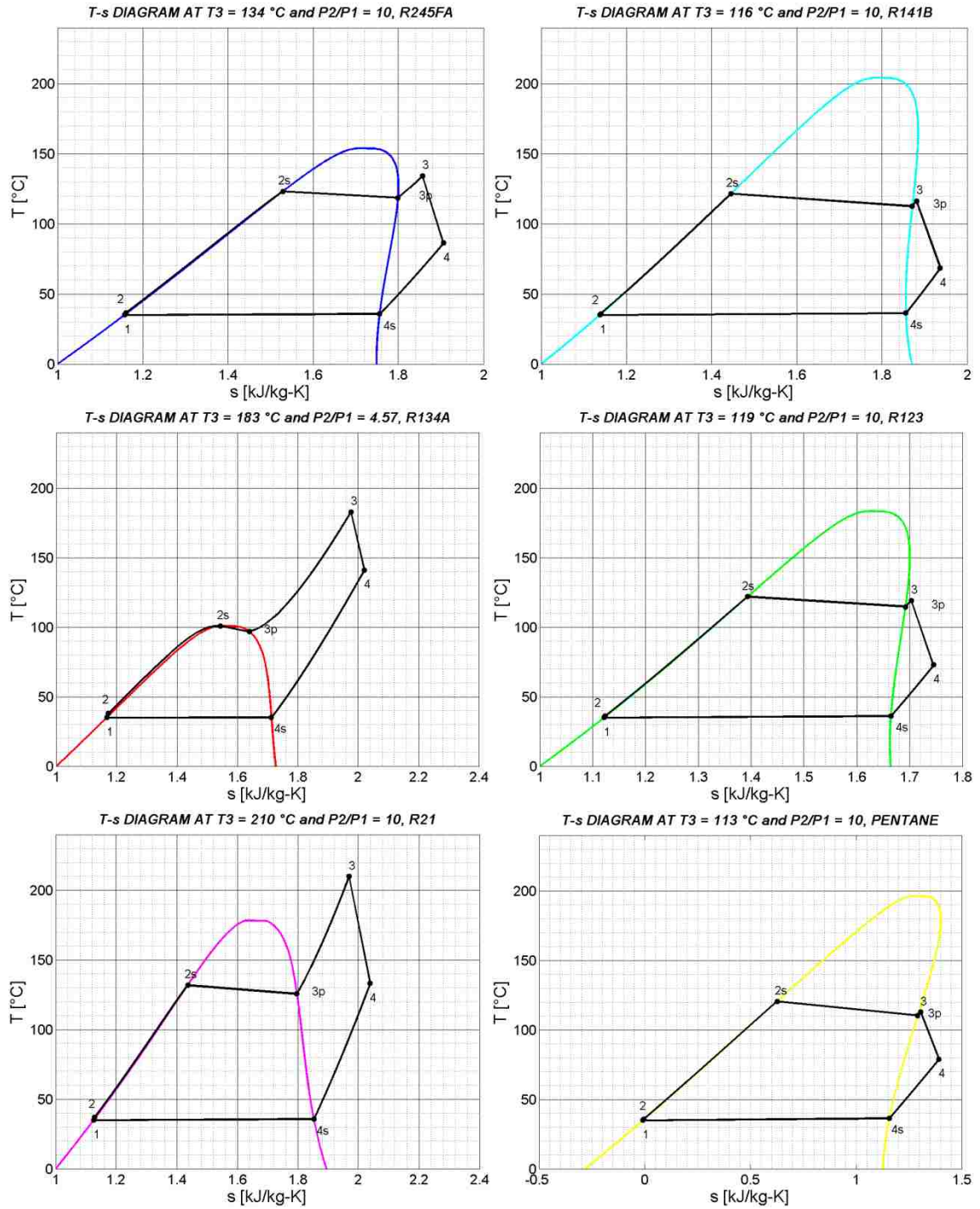


Figure 4.1-6: T-s plots of the standard ORCs that give the maximum net power output for each working fluid, $T_{\text{cond}} = 35\text{ }^\circ\text{C}$.

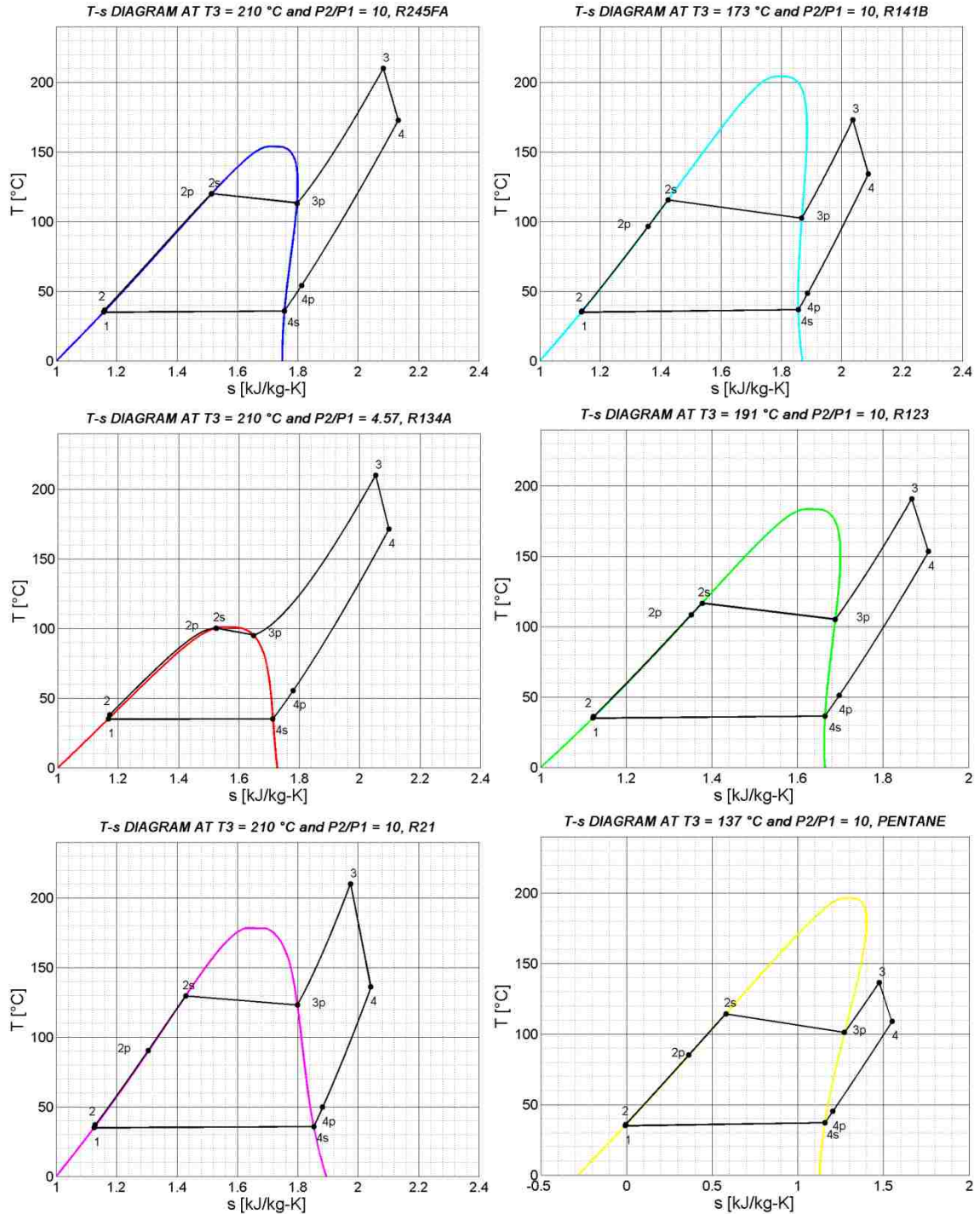


Figure 4.1-7: T-s plots of the recuperative ORCs that give the maximum net power output for each working fluid, $T_{\text{cond}} = 35\text{ }^{\circ}\text{C}$.

Once again from the pictures above it is clear how for every working fluid in a recuperative ORC a significant amount of superheat is preferable, whereas for four, out of six, working fluids a low amount of superheat is more suitable in a recuperative ORC.

Nonetheless, in order to compare and decide which working fluid is the most suitable for the application in a ORC for a WHR unit, two other major factors, along with the net power output, play a very important role: environmental pollution regulations and pressure at the pump inlet.

Table 4.1-8 shows the safety groups and the three principal indexes, already presented in paragraph 2.3.4, that quantify the impact that the working fluids have on the environment. Looking at the regulations already in place, the refrigerants with ODP around 1 have already been phased out. All the six working fluids analyzed meet this requirement, however the regulations in terms of ODP will become more stringent in the next years. More precisely the fluids with ODP greater than zero, like R21, R123, and R141b, will be banned in 2020 or 2030. Even if in literature are reported different applications of such working fluids in ORCs, in the present work has been preferred not to consider them suitable for the application because a WHR system for a vehicle has to be designed imagining a medium to long term usage of the device, and it makes poor sense to design all the components for a working fluid that will be banned within 6 years. Given that, the three working fluids remaining after this first skimming are R134a, R245fa and Pentane (or R601). None of them have safety groups particularly dangerous. In this case of application the designer should be more worried by the flammability rather than the toxicity so safety groups A1 and B1 are acceptable because they are not flammable, look at paragraph 2.3.3 for reference.

	Name	Safety group	ODP	GWP (100 yrs)	Atmospheric lifetime (yrs)
R-21	Dichlorofluoromethane	B1	0.04	151	1.7
R-123	2,2-Dichloro-1,1,1-trifluoroethane	B1	0.02	77	1.3
R-134a	1,1,1,2-Tetrafluoroethane	A1	0	1430	14
R-141b	1,1-Dichloro-1-fluoroethane	A2	0.12	725	9.3
R-245fa	1,1,1,3,3-Pentafluoropropane	B1	0	1030	7.6
R-601	Pentane	-	0	4 ± 2	12 ± 3

Table 4.1-8: Safety group and pollution indexes of the working fluids analyzed.

Now the second requirement comes into play; the lowest pressure around the cycle still has to be higher than the ambient pressure in order to avoid infiltration of air inside the pipes in the case of there was a non-perfect sealing. The section in which the pressure is the lowest is definitely that of the pump inlet. Since in the preliminary model the pump inlet state corresponds to the saturated liquid state at the selected condensing temperature, it just takes to look at the fluid properties tables and determine the pressure of the saturate liquid at the lowest condensing temperature possible (35 °C) of the three refrigerants remaining. The results are summarized in Table 4.1-9.

	Saturated liquid pressure at 35 °C [kPa]
R-134a	887.0
R-245fa	211.7
Pentane	97.7

Table 4.1-9: Lowest pressure around the cycle of each working fluid.

Taking into account that the ambient pressure is around 101.3 kPa it results evident that Pentane does not meet the requirement just imposed hence the only two working fluids remaining in the list are R134a and R245fa. Not by chance this two refrigerants are the most widely used also in the air conditioning systems and in different other applications so their availability is high and their cost is fair. It must be said that if a saturated liquid temperature of 45 °C was chosen for the Pentane its pressure would be higher than the ambient one but the net power output of the cycle would be slightly lower.

Finally, in order to decide which is the most suitable working fluid, we can go back and look at Table 4.1-6. R245fa definitely gives better performances, moreover it does not represent a compromise for what concern the Global Warming Potential (GWP of Table 4.1-8) and the Atmospheric Lifetime since both these indexes are lower than those of the R134a even if they are not low in absolute value.

To some up, the criterion adopted to rank the working fluid has been the following:

- zero ODP in order to meet the regulations that will be introduced in 2020
- pump inlet pressure higher than ambient pressure
- performances
- GWP and safety considerations.

Among the fluid that have failed to meet the first requirement the one that gives the greatest net power output has been put first. The resulting ranking is shown in the bullet list below:

- 1) R245fa
- 2) R134a
- 3) Pentane or (R601)
- 4) R21
- 5) R123
- 6) R141b.

4.1.4 Considerations on the design alternatives

The indications given in this section will constitute the bases for the analyses reported in the section 4.2. The recuperative ORC seems to be the best choice especially if fluids like R134a and R245fa are used. Beside that it has been found out that the simplest way to increase the net power output of the cycle is to make the pump outlet pressure as high as possible. The limitations to this pressure are basically three:

- pump characteristics
- critical pressure of the working fluid
- maximum pressure that the expander can withstand.

The latter has not been treated in this section but it will be considered in the following one. For what concerns the expander inlet temperature for a recuperative ORC it should be as high as possible, whereas for a standard ORC a more detailed investigation of the working fluid employed is necessary to determine the best expander inlet temperature. It has also been showed how with a recuperative ORC higher efficiencies in absolute value can be achieved, if proper pump compression ratios and expander inlet temperatures are picked. However, the mass flow rate of the working fluid required by a recuperative ORC is always higher than that of a standard ORC. Finally a brief comparison of six organic working fluids has been illustrated. These working fluids have been chosen among the most commonly employed in literature and especially because they belong to different families (wet isentropic and dry) so the differences could be discovered. Even though a more complete analysis will be carried out with the detailed model, the working fluids ranking reported, furnishes a good indication of which can be the refrigerants more interesting for a WHR system application. In particular, R245fa has been indicated, by almost all the carmakers dealing with research in this field, as the most promising working fluid along with ethanol that has not been analyzed so far because of the limitation of the preliminary model explained at the beginning of section 4.1. Anyway by means of the detailed model the performances obtained with ethanol, water, R245fa and R134a will be thoroughly examined.

4.2 Detailed analysis of the WHR unit based on a ORC installed in a vehicle

The detailed model of a Waste Heat Recovery unit developed in Matlab/Simulink environment was explained in section 3.2. This flexible simulation tool was built to investigate the behavior of the device estimating the potential power output of the system in stationary conditions, as well as the fuel savings in an homologation driving cycle. As already mentioned, the detailed model is a flexible tool that can be adapted to multiple operating conditions and system layout configurations; it will be used by the simulation teams of Fiat and Chrysler that will integrate this Matlab/Simulink model, of the WHR unit, in a Simulink model of the overall vehicle to which the WHR unit is destined. However, the first step to accomplish in order to check the validity of the detailed model is to compare its results to those coming from experimental tests. That was possible because at the Fiat Research Center (CRF) in Turin there is an already working test rig of an ORC.

The remaining of this section will be divided into five parts:

- 1) calibration of the model with experimental data already available
- 2) steady state simulation at target operating conditions and sensitivity analysis
- 3) steady state comparison of different working fluids at target operating conditions
- 4) WHR unit integration with the engine and creation of the net power output map
- 5) simulation of the behavior of the system into a homologation driving cycle and assessment of the potential fuel savings.

4.2.1 Calibration of the detailed model

The test rig available at CRF, as already said, was used to check the validity of the results obtained with the detailed model. The technical characteristics of the test rig are reported in the list below:

- standard ORC (no recuperator)
- scroll expander integrated with an electric generator, the maximum pressure at the expander inlet is 1500 kPa
- boiler electrically heated (the working fluid is not heated nor vaporized by the exhaust gas of an engine), maximum temperature at the boiler outlet is 150 °C
- water cooled condenser
- volumetric pump, maximum pressure rise of 1700 kPa
- working fluid R245fa.

The procedure followed was to collect the data of tests already performed, adapt the inputs of the detailed model in order to exactly replicate the operating conditions of the tests and finally check if the outputs of the model coincide with the results of the tests.

Measurement stations of temperature and pressure are placed upstream and downstream of each component. A mass flow rate measurement station is placed at the pump outlet. The power output is measured as the electric load transmitted to a resistor. The tests, whose results were utilized, have been performed following a two steps procedure:

- The boiler has been warmed up until the desired temperature at the boiler outlet is reached.
- The data coming from the measurement stations were acquired each second for a period of two minutes.

Hence, after the data acquisition process, Excel tables were generated containing the following data for each second of the acquisition period:

- temperature in [$^{\circ}\text{C}$] before and after each component
- pressure in [kPa] before and after each component
- the heat transfer rate exchanged in the boiler and in the condenser [kW]
- the mechanical power produced by the expander and absorbed by the pump [kW]
- the mass flow rate of the working fluid measured after the pump [kg/s].

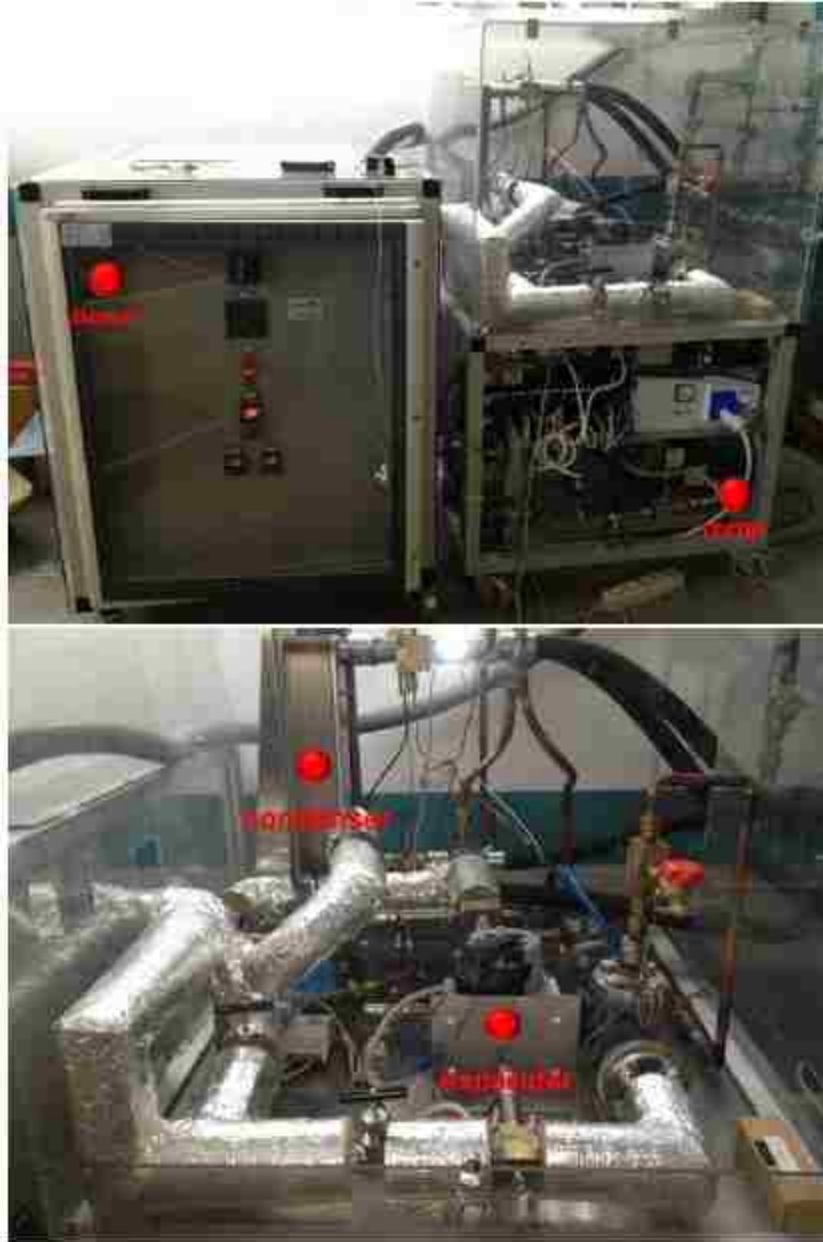


Figure 4.2-1: Standard ORC test rig facility at the CRF.

Some other parameters of interest were evaluated from those measured:

- ORC cycle efficiency
- pump and expander isentropic efficiencies.

In order to compare the results stored in such tables with the results of the model a time average of these parameters has been done. The experimental data available referred to four different expander inlet temperatures:

- 120 °C
- 130 °C

- 140 °C
- 150 °C.

4.2.1.1 Expander inlet temperature 150 °C comparison

In the first comparison performed the expander inlet temperature was the highest possible achievable by the instrumentation, 150 °C. The results of the experimental tests available are illustrated in Table 4.2-1 and Table 4.2-2.

	T [°C]	P [kPa]
Pump inlet	22.5	145
Pump out	24.1	1326
Boiler inlet	23.5	1322
Boiler outlet	151.5	1304
Expander inlet	149.4	1289
Expander outlet	107.3	200
Condenser inlet	105.0	169
Condenser outlet	23.7	150

Table 4.2-1: Measured temperatures and pressures at the inlet and outlet of each component, T boiler out = 150 °C.

MFR WF [kg/s]	0.048
Net power [kW]	1.43
Pump efficiency	0.36
Expander efficiency	0.75
Cycle efficiency	9.74%
Boiler power [kW]	14.68
Expander power [kW]	1.55
Pump power [kW]	0.117
Condenser power [kW]	12.92
Coolant inlet temp [°C]	21.3
Coolant outlet temp [°C]	22.3

Table 4.2-2: Measured cycle outputs, T boiler out = 150 °C.

From these results the input parameters necessary to carry out the simulation with the detailed model have to be extrapolated to replicate the conditions in which the tests were carried out. To this purpose, in the first six pop-up menus of the initial input window, shown in Figure 3.2-3, the answers were respectively:

- “R245fa”, the working fluid adopted
- “No”, there is no recuperator
- “No”, initially the pressure drop in the pipes was not considered
- “Yes”, constant expander and pump efficiency

- “Yes”, constant heat exchanger effectiveness
- “Yes”, constant heat exchanger pressure drop.

In particular, the pressure drop inside the pipes was assumed equal to zero in the first simulation. Moreover, in the remaining two pop-up menus distributed in the input window the answers were:

- “No” to the one asking if the expander was mechanically connected to the engine shaft.
- “Water” to the one where the coolant fluid in the condenser had to be selected.

$T_{\text{subcooling}}$	5 [°C]	Standard value assumed
$T_{\text{exp,in}}$	149.4 [°C]	Equal to the measured value
ϵ_{boiler}	0.745	Computed with the definition of effectiveness, from the measured temperatures at the boiler inlet and outlet
ΔP_{boiler}	18.25 [kPa]	Computed as the pressure at the boiler inlet minus the pressure at the boiler outlet measured
$T_{\text{pinch,boiler}}$	10 [°C]	Standard value assumed
$T_{\text{exh,min}}$	100 [°C]	Standard value assumed
η_{expander}	0.754	Equal to the measured value
$P_{\text{exp,max}}$	1500 [kPa]	Expander specification
$P_{\text{ratio,exp}}$ Min-Max	2-8	Component specification
Exp VFR Min-Max	0.003 0.0095 [kg/s]	Component specification
$\epsilon_{\text{condenser}}$	0.011	Computed with the definition of effectiveness, from the measured temperatures at the condenser inlet and outlet
$T_{\text{pinch,condenser}}$	2 [°C]	Component specification
$\Delta P_{\text{condenser}}$	17.25 [kPa]	Computed as the pressure at the condenser inlet minus the pressure at the boiler outlet measured
$T_{\text{coolant,in}}$	21.3 [°C]	Equal to the measured value
η_{pump}	0.361	Equal to the measured value
Pump Head nom	1181 [kPa]	Compute as the pressure at the pump outlet minus the pressure at the pump inlet measured
Pump Head Min-Max	700-1700 [kPa]	Component specification
Pump VFR Min-Max	$2 \cdot 10^{-5}$ - $9 \cdot 10^{-5}$ [m ³ /s]	Component specification

Table 4.2-3: Detailed model simulation inputs, T boiler out = 150 °C.

Then, the other input parameters set up are reported and explained in Table 4.2-3; it is important to underline that not all the input parameters shown in Figure 3.2-3 were necessary because of the answers provided in the pop-up menus.

The boiler effectiveness selection was the biggest hurdle to be overcome before launching the simulation. Before explaining how the heat exchanger effectiveness was chosen, a short preamble is necessary. As a matter of fact, in the test rig, the heat transfer rate taking place in the boiler is

the key parameter since no exhaust gas exists. On the contrary, in the detailed model the key parameters of the boiler are the inlet temperature and the mass flow rate of the exhaust gas as well as the boiler effectiveness. So, it should be found a way to select fictitious values for the boiler effectiveness, exhaust gas inlet temperature and mass flow rate that give exactly the heat transfer rate measured in the boiler. Moreover, since in the test rig there is no exhaust gas, the selection of its mass flow rate and inlet temperature is uniquely addressed to obtain the value of the heat transfer rate measured. Given that, the author has chosen to keep the exhaust gas mass flow rate and inlet temperature equal to those correspondent to the target vehicle operating conditions already utilized in the preliminary analysis (see Table 4.1-1). Once the mass flow rate and the expander inlet temperature were determined, the only parameter that miss to compute the definition of heat exchanger effectiveness is the exhaust gas outlet temperature. Basically, for the mass flow rate and inlet temperature of the exhaust gas arbitrarily assumed, we should find the exhaust gas outlet temperature that we would have if the heat transfer rate taking place in the boiler were exactly equal to the one measured in the experimental test. Hence, the fictitious exhaust gas outlet temperature was calculated with the equation below:

$$T_{exh,out} = T_{exh,in} - \frac{\dot{Q}_{boiler}}{Cp_{exh}\dot{m}_{exh}} \quad (4.1)$$

Where Cp_{exh} is the average specific heat of the exhaust gas assumed equal to that reported in Table 4.1-1. The resulting boiler effectiveness is thus:

$$\epsilon_{boiler} = \frac{T_{exh,in} - T_{exh,out}}{T_{exh,in} - T_{boil,in}} \quad (4.2)$$

Where $T_{boil,in}$ is the temperature at the boiler inlet of the working fluid, that is taken from the measured values of Table 4.2-1.

	T [°C]	P [kPa]
Pump inlet	23.4	168
Pump out	25.0	1349
Boiler inlet	25.0	1349
Boiler outlet	149.4	1331
Expander inlet	149.4	1331
Expander outlet	105.7	186
Condenser inlet	105.7	186
Condenser outlet	23.4	168

Table 4.2-4: Simulated temperatures and pressures at the inlet and outlet of each component, T boiler out = 150 °C, null pipe pressure drop.

Now that all the input parameters necessary to run the detailed model have been set up, the simulation is launched and the results obtained have to be compared to those coming from the

experimental tests. Since it is a steady state simulation (the input conditions of the exhaust gas are constant) the output values after a certain amount of iterations (usually no more than three) are constant. This is the reason why the tables referring to the simulation results contain only an unique value correspondent to the output value of the variable in question after 10 seconds of simulation of the 50 total.

MFR WF [kg/s]	0.049
Net power [kW]	1.51
Pump efficiency	0.36
Expander efficiency	0.75
Cycle efficiency	10.32%
Boiler power [kW]	14.64
Expander power [kW]	1.63
Pump power [kW]	0.1182
Condenser power [kW]	13.13
Coolant inlet temp [°C]	21.3
Coolant outlet temp [°C]	22.3

Table 4.2-5: Simulated cycle outputs, T boiler out = 150 °C, null pipe pressure drop.

Table 4.2-4 and Table 4.2-5 show the results coming from the simulation. However, in order to assess how close these results are to those measured with the test rig other tables have been generated containing the error, expressed in percentage, introduced with the simulation:

$$Error = \frac{X_{simulated} - X_{measured}}{X_{measured}} \cdot 100 \quad (4.3)$$

Where X is a general variable among those considered. Table 4.2-6 and Table 4.2-7 illustrate the results obtained. Focusing on Table 4.2-6 it is clear how the simulation gives accurate approximations, especially for what concerns the temperatures around the cycle. On the contrary the simulated pressures slightly deviate from the measured ones in particular those at condenser inlet, at condenser outlet and at pump inlet with error that can go to as high as 15%.

	T	P
Pump inlet	+4.0%	+15.5%
Pump out	+3.8%	+1.7%
Boiler inlet	+6.3%	+2.0%
Boiler outlet	-1.4%	+2.1%
Expander inlet	0.0%	+3.3%
Expander outlet	-1.5%	-6.8%
Condenser inlet	+0.6%	+10.4%
Condenser outlet	-1.2%	+11.7%

Table 4.2-6: Error percentage between the simulated and measured variables, T boiler out = 150 °C, null pipe pressure drop.

Moving to Table 4.2-7 it can be seen that the mass flow rate of the working fluid, the coolant outlet temperature and the heat transfer rate taking place in the heat exchangers have a percentage error of less than 2%. Expander and pump efficiencies as well as coolant inlet temperature are input parameters so they are not relevant for this analysis. Finally, the simulated pump power is close to the measured one however the expander power and as a consequence the net power output bring an error of more than 5%. More precisely, the simulated expander power and the net power are higher with respect to the correspondent measured values. Since the interest usually lays on the net power output the results obtained with the detailed model appears to be quite reliable.

MFR WF	+1.3%
Net power	+5.7%
Pump efficiency	0.0%
Expander efficiency	0.0%
Cycle efficiency	+6.0%
Boiler power	-0.3%
Expander power	+5.4%
Pump power	+1.4%
Condenser power	+1.6%
Coolant inlet temp	0.0%
Coolant outlet temp	0.0%

Table 4.2-7: Error percentage between the simulated and measured variables, T boiler out = 150 °C, null pipe pressure drop.

However, the causes of these differences have to be investigated. In particular looking at the tables of the experimental tests two assumptions made in this first simulation do not hold:

- null temperature drop in pipes
- null pressure drop in pipes.

For what concern the first assumption listed the detailed model is not designed to consider these losses, mainly because they are particularly hard to predict unless an estimation of the temperature drop per unit length of the pipe is made. On the other hand the pressure drop in the pipes can be considered in the detailed model simply by selecting the “Yes” option in the proper pop-up menu and knowing the length, diameter and number of concentrated losses of each pipe. So, the length of the pipes of the test rig have been measured and the number of concentrated losses have been counted, look Table 4.2-8. Using these values as inputs of the detailed model and considering the pressure drop in the pipes different from zero the results obtained with the detailed model are expected to be closer to those measured.

	Bends	Measurement stations	Total concentrated losses	Length [m]	Diameter external [m]	Diameter internal [m]
Pipe1	9	3	12	2.5	0.017	0.0125
Pipe3	8	2	10	3	0.027	0.0209
Pipe4	4	2	6	1.4	0.027	0.0209
Pipe6	5	2	7	1.5	0.017	0.0125

Table 4.2-8: Pipes characteristics of the test rig available at the CRF.

	T [°C]	P [kPa]
Pump inlet	23.4	164
Pump out	25.0	1345
Boiler inlet	25.0	1344
Boiler outlet	149.4	1326
Expander inlet	149.4	1313
Expander outlet	108.1	207
Condenser inlet	108.1	186
Condenser outlet	23.4	168

Table 4.2-9: Simulated temperatures and pressures at the inlet and outlet of each component, T boiler out = 150 °C, non-null pipe pressure drop.

MFR WF [kg/s]	0.049
Net power [kW]	1.41
Pump efficiency	0.36
Expander efficiency	0.75
Cycle efficiency	9.62%
Boiler power [kW]	14.64
Expander power [kW]	1.53
Pump power [kW]	0.118
Condenser power [kW]	13.24
Coolant inlet temp [°C]	21.3
Coolant outlet temp [°C]	22.3

Table 4.2-10: Simulated cycle outputs, T boiler out = 150 °C, non-null pipe pressure drop.

Table 4.2-9 and Table 4.2-10 show the results obtained, whereas Table 4.2-11 and Table 4.2-12 illustrate the correspondent percentage errors.

Comparing the two tables above with Table 4.2-6 and Table 4.2-7 it can be seen how the percentage errors are reduced. Given the uncertainty that characterizes the experimental tests and that a mathematical model of a system, even if it is accurate, introduces several approximations, a percentage error equal or less than 5% is assumed to be acceptable. With that in mind the results of the simulation with non-null pressure losses in pipes appear to be even more reliable than the simulation in which the pressure drop in pipes were neglected; net power output, cycle efficiency

and expander power had an error percentage greater than the defined threshold of 5% now with non-null pressure drop in pipes all these values have an error significantly higher than the threshold.

	T	P
Pump inlet	+4.0%	+12.9%
Pump out	+3.8%	+1.4%
Boiler inlet	+6.3%	+1.7%
Boiler outlet	-1.4%	+1.7%
Expander inlet	0.0%	+1.9%
Expander outlet	+0.7%	+3.6%
Condenser inlet	+2.9%	+10.4%
Condenser outlet	-1.2%	+11.7%

Table 4.2-11: Error percentage between the simulated and measured variables, T boiler out = 150 °C, non-null pipe pressure drop.

MFR WF	+1.3%
Net power	-1.5%
Pump efficiency	0.0%
Expander efficiency	0.0%
Cycle efficiency	-1.2%
Boiler power	-0.3%
Expander power	-1.2%
Pump power	+1.4%
Condenser power	+2.5%
Coolant inlet temp	0.0%
Coolant outlet temp	+0.1%

Table 4.2-12: Error percentage between the simulated and measured variables, T boiler out = 150 °C, non-null pipe pressure drop.

However, it must be pointed out that now all these parameters are lower than the measured ones whereas with null pressure drop in pipes all these parameters were higher. In other words, the expander power output, the cycle efficiency and the net power output are overestimated if the pressure drop in the pipes is considered null and they are underestimated if the pressure drop in pipes is considered non-null. Nonetheless, in the latter case the simulated values are closer to the measured one, since their error percentage are all lower than 2%.

Analyzing in deeper details Table 4.2-9 and Table 4.2-11 we found out that there are the same weaknesses encountered assuming null pressure drop in pipes; the pressure at condenser inlet, at condenser outlet and pump inlet are all overestimated by 10% or more. These errors are big and they have to be monitored carefully in the next comparisons between measured values and simulated values to see if the program always overestimates the above mentioned pressures.

Finally a comparison between the pressure drop in pipes measured and simulated is presented in Table 4.2-13.

	Pdrop [kPa]		Pdrop [kPa]
Pipe 1	4.20	Pipe 1	1.30
Pipe 3	15.18	Pipe 3	13.10
Pipe 4	31.02	Pipe 4	20.70
Pipe 6	4.94	Pipe 6	3.76

Table 4.2-13: Pressure drop in pipes; measured (left side) and simulated (right side).

The pipe pressure drop simulated is always lower than that measured, making the simulated values not very reliable. Despite of that the general trend of the pipe losses is respected; they are higher in pipes 3 and 4 (working fluid at vapor phase) and lower in pipe 1 and 6 (working fluid at liquid phase).

Even though the pipe pressure losses are not very well approximated, according to the author, it makes sense to considering them non-null because it is a more conservative assumption and especially because doing that the net power output simulated is closer to the measured one. Anyway, if there are no information about the geometry of the system assuming a null pressure drop in pipes reliable indications about the net power output value can be obtained, the user has only to keep in mind that these values are slightly overestimated.

Given that the geometry of the test rig is known, in the following paragraph, where the comparison between the experimental tests and the simulations continues, the pressure drop in pipes will be considered non-null.

4.2.1.2 Expander inlet temperature 120 °C, 130 °C and 140 °C comparison

In this paragraph the comparison between the experimental tests and the simulation results is performed for others expander inlet temperatures, to see if the considerations done in the previous paragraph are confirmed.

For the sake of brevity tables similar to Table 4.2-3, reporting the inputs imposed in the program to run the simulation for other expander inlet temperatures are not reported. Anyway, the procedure followed to obtain the values that have been put as input of the program is exactly the same described in the previous paragraph.

Table 4.2-14 through Table 4.2-19 show the comparison between the experimental data and the data coming from the simulation for the other expander inlet temperatures that have been tested. On the rightmost columns of each table the percentage error is also reported. Looking at the tables two major observations can be done:

- The expander power, the cycle efficiency, the net power output and the other cycle outputs predictions are accurate and the percentage error stays always well below the 5% threshold adopted.
- The lower the expander inlet temperature the higher is the percentage error, in other words the higher is the inaccuracy of the model.

	Measured data		Simulation data		Error	
	T [°C]	P [kPa]	T [°C]	P [kPa]	T	P
Pump inlet	22.3	144	23.8	167	+6.8%	+15.9%
Pump out	23.9	1336	25.4	1359	0.0%	+1.7%
Boiler inlet	23.3	1332	25.4	1358	+9.3%	+1.9%
Boiler outlet	141.4	1296	139.0	1322	-1.7%	+2.0%
Expander inlet	139.0	1282	139.0	1309	0.0%	+2.1%
Expander outlet	96.3	196	97.2	206	+1.0%	+4.9%
Condenser inlet	94.3	166	97.5	186	+3.4%	+12.4%
Condenser outlet	23.5	149	23.8	170	+1.3%	+14.6%

Table 4.2-14: Temperatures and pressures at the inlet and outlet of each component; measured data on the left, simulation data in the middle and percentage error on the right, T boiler out = 140 °C.

	Measured data	Simulation data	Error
MFR WF [kg/s]	0.047	0.048	+1.7%
Net power [kW]	1.36	1.33	-1.7%
Pump efficiency	0.36	0.36	0.0%
Expander efficiency	0.75	0.75	0.0%
Cycle efficiency	9.73%	9.60%	-1.3%
Boiler power [kW]	13.94	13.89	-0.4%
Expander power [kW]	1.47	1.45	-1.4%
Pump power [kW]	0.117	0.119	+2.0%
Condenser power [kW]	12.26	12.57	+2.6%
Coolant inlet temp [°C]	21.3	21.3	0.0%
Coolant outlet temp [°C]	22.2	22.3	+0.2%

Table 4.2-15: Cycle outputs; measured data on the left, simulation data in the middle and percentage error on the right T boiler out = 140 °C.

- Pressures at pump inlet, at condenser inlet and at condenser outlet are not well approximated and they are higher of more than the 10% of the measured values, as already noticed in the previous paragraph.
- Temperatures at pump and boiler inlets are approximated with a percentage error that goes from 5% to 10%.

According to the author, the last two points of the list above, could be the causes that lead the program to underestimate the net power with respect to the measured one, despite the pressure

drop in the pipes is lower with respect to the measured one. More in general the program seems to overestimate the low pressures of the cycle (those that the working fluid has from the expander outlet to the pump inlet). Furthermore the program underestimates the pressure losses in the pipes. There might be a cancellation between these two errors that leads to a good approximation of what have been called cycle outputs. As a matter of fact a higher low pressure of the cycle leads to lower net power outputs, whereas a lower pressure loss in the pipes leads to a higher net power output.

	Measured data		Simulation data		Error	
	T [°C]	P [kPa]	T [°C]	P [kPa]	T	P
Pump inlet	22.4	144	24.1	168	+7.5%	+16.7%
Pump out	24.1	1328	25.7	1352	0.0%	+1.8%
Boiler inlet	23.4	1324	25.7	1351	+9.8%	+2.0%
Boiler outlet	131.3	1292	128.8	1319	-1.9%	+2.1%
Expander inlet	128.8	1280	128.8	1307	0.0%	+2.1%
Expander outlet	86.1	196	87.1	206	+1.2%	+5.2%
Condenser inlet	84.5	166	87.1	188	+3.2%	+13.2%
Condenser outlet	23.6	149	24.1	172	+2.0%	+15.4%

Table 4.2-16: Temperatures and pressures at the inlet and outlet of each component; measured data on the left, simulation data in the middle and percentage error on the right, T boiler out = 130 °C.

	Measured data	Simulation data	Error
MFR WF [kg/s]	0.047	0.048	+1.9%
Net power [kW]	1.25	1.23	-2.0%
Pump efficiency	0.36	0.36	0.0%
Expander efficiency	0.73	0.73	0.0%
Cycle efficiency	9.38%	9.23%	-1.6%
Boiler power [kW]	13.34	13.28	-0.4%
Expander power [kW]	1.37	1.35	-1.6%
Pump power [kW]	0.117	0.119	+2.3%
Condenser power [kW]	11.76	12.07	+2.6%
Coolant inlet temp [°C]	21.5	21.5	0.0%
Coolant outlet temp [°C]	22.4	22.4	+0.1%

Table 4.2-17: Cycle outputs; measured data on the left, simulation data in the middle and percentage error on the right T boiler out = 130 °C.

To conclude the digression on the pressure drop in the pipes, a value of the bend pressure loss coefficient slightly lower than the one reported in the previous paragraphs has been selected, because the algorithm adopted to compute the pressure drop in the pipes seems to penalize too much the pipes with a small diameter and a high number of concentrated losses. Since this is the case of the test rig, the best solution was to select a bend pressure loss coefficient equal to 0.1 for the vapor side pipes and 0.2 for the liquid side pipes.

Despite the weaknesses highlighted above the detailed model should be considered a good simulation tool mainly because all the principal cycle outputs are approximated with high accuracy.

	Measured data		Simulation data		Error	
	T [°C]	P [kPa]	T [°C]	P [kPa]	T	P
Pump inlet	23.3	147	25.1	175	+7.8%	+19.2%
Pump out	24.4	1315	26.2	1343	0.0%	+2.1%
Boiler inlet	23.7	1311	26.2	1342	+10.7%	+2.4%
Boiler outlet	121.6	1282	118.5	1313	-2.5%	+2.4%
Expander inlet	118.5	1266	118.5	1302	0.0%	+2.8%
Expander outlet	76.3	196	77.3	210	+1.4%	+7.3%
Condenser inlet	74.7	165	77.3	192	+3.5%	+16.2%
Condenser outlet	24.0	152	25.1	179	+4.7%	+17.8%

Table 4.2-18: Temperatures and pressures at the inlet and outlet of each component; measured data on the left, simulation data in the middle and percentage error on the right, T boiler out = 120 °C.

	Measured data		Simulation data		Error	
MFR WF [kg/s]		0.047		0.049		+2.5%
Net power [kW]		1.16		1.14		-2.3%
Pump efficiency		0.48		0.48		0.0%
Expander efficiency		0.69		0.69		0.0%
Cycle efficiency		9.08%		8.91%		-1.9%
Boiler power [kW]		12.82		12.76		-0.5%
Expander power [kW]		1.25		1.22		-2.0%
Pump power [kW]		0.085		0.088		+2.9%
Condenser power [kW]		11.33		11.64		+2.7%
Coolant inlet temp [°C]		22.1		22.1		0.0%
Coolant outlet temp [°C]		23.1		23.1		+0.2%

Table 4.2-19: Cycle outputs; measured data on the left, simulation data in the middle and percentage error on the right T boiler out = 120 °C.

4.2.2 Steady state analysis at target operating conditions

Once the model has been calibrated and the reliability of its results has been verified, simulation of the behavior of the WHR system in operating conditions, that could not be reached with the test rig already available at the CRF, were carried out. The most interesting simulation was definitely the one carried out at the vehicle operating conditions (design point) already defined in Table 4.1-1, that will be referred to as target operating conditions. As previously underlined, to make an accurate assessment of the potential power output achievable detailed information about the components that will be employed are necessary.

To this purpose the first step was to gather the data coming from the suppliers of the components and then translate them into usable input for the detailed model.

For what concerns the heat exchangers the supplier of these components has furnished several data from whom it has been possible to draw the pressure drop curve as a function of the mass flow rate flowing and the heat exchanger effectiveness curve as a function of the heat capacity rate ratio and number of transfer unit for each heat exchanger (boiler, condenser and recuperator). Figure 4.2-2 shows the pressure drop curve of each heat exchanger. The trends shown are curve fits into experimental data points provided by the supplier of the heat exchangers. Whereas, Figure 4.2-3 through Figure 4.2-5 show the effectiveness maps built with the curve fitting tool of Matlab as explained in paragraph 3.2.2.1.

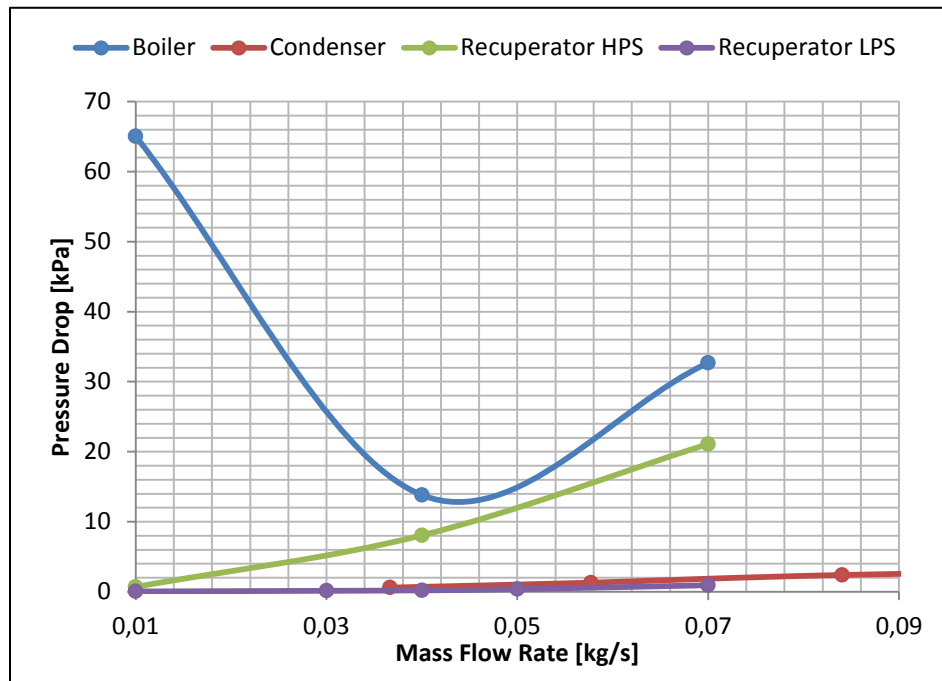


Figure 4.2-2: Pressure drop inside the heat exchanger. Referring to the recuperator HPS and LPS mean respectively High Pressure Side and Low Pressure Side.

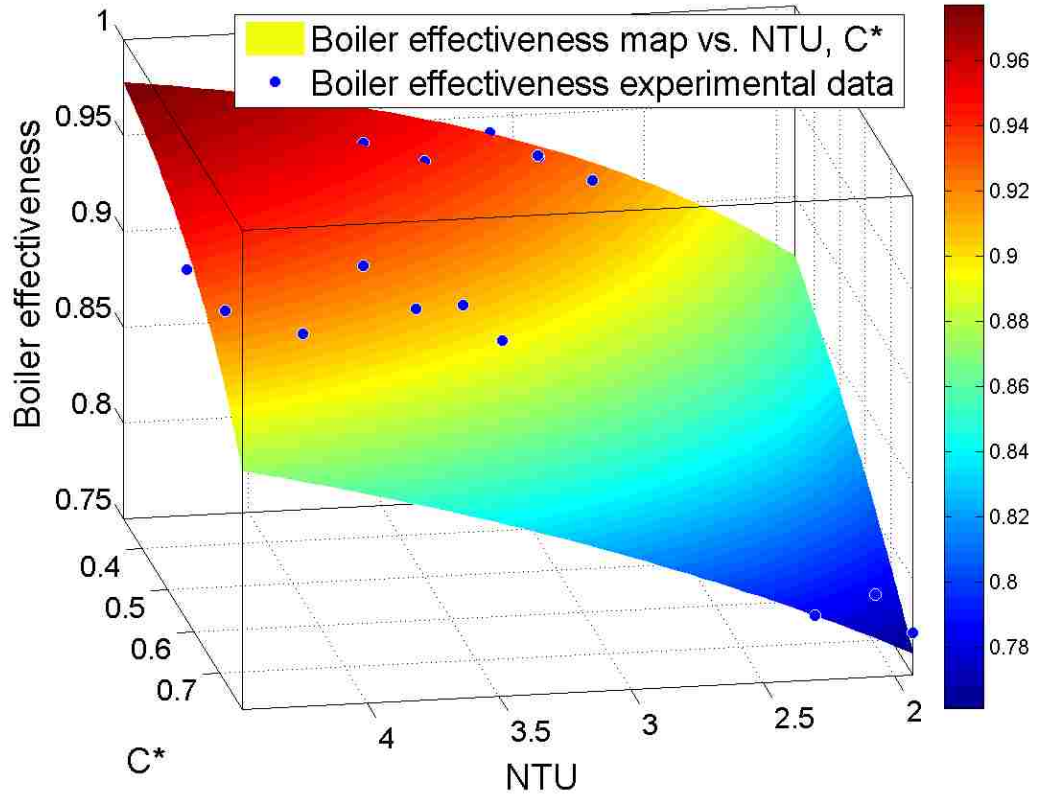


Figure 4.2-3: Boiler effectiveness map built from the experimental data furnished by the supplier.

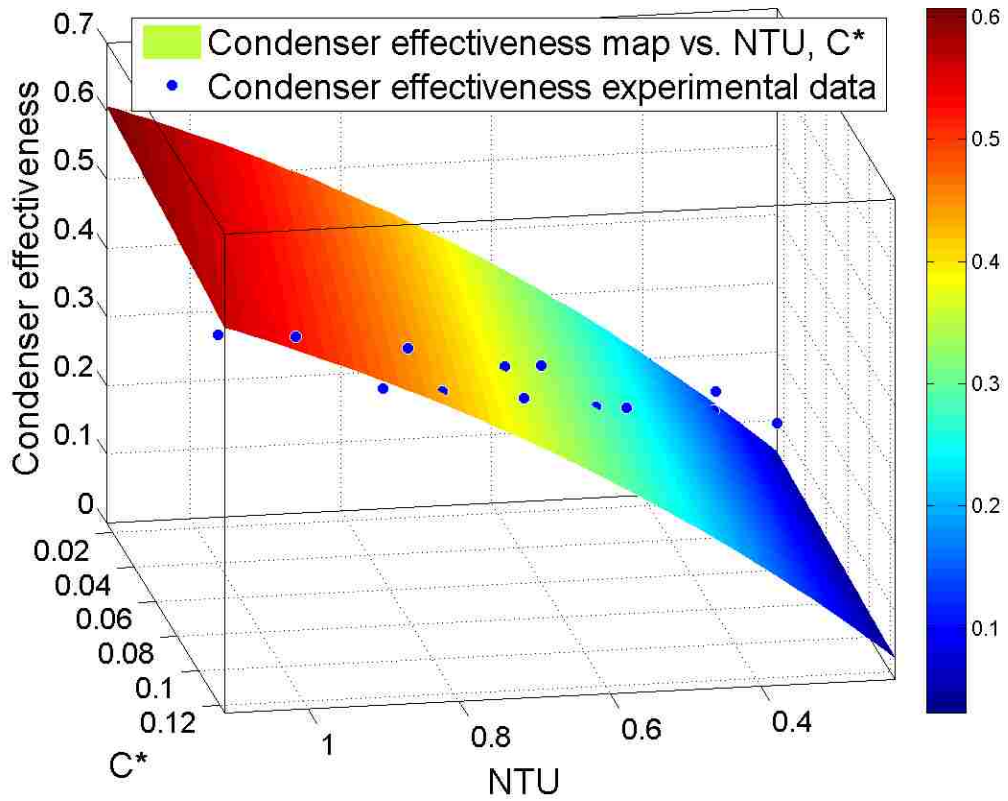


Figure 4.2-4: Condenser effectiveness map built from the experimental data furnished by the supplier.

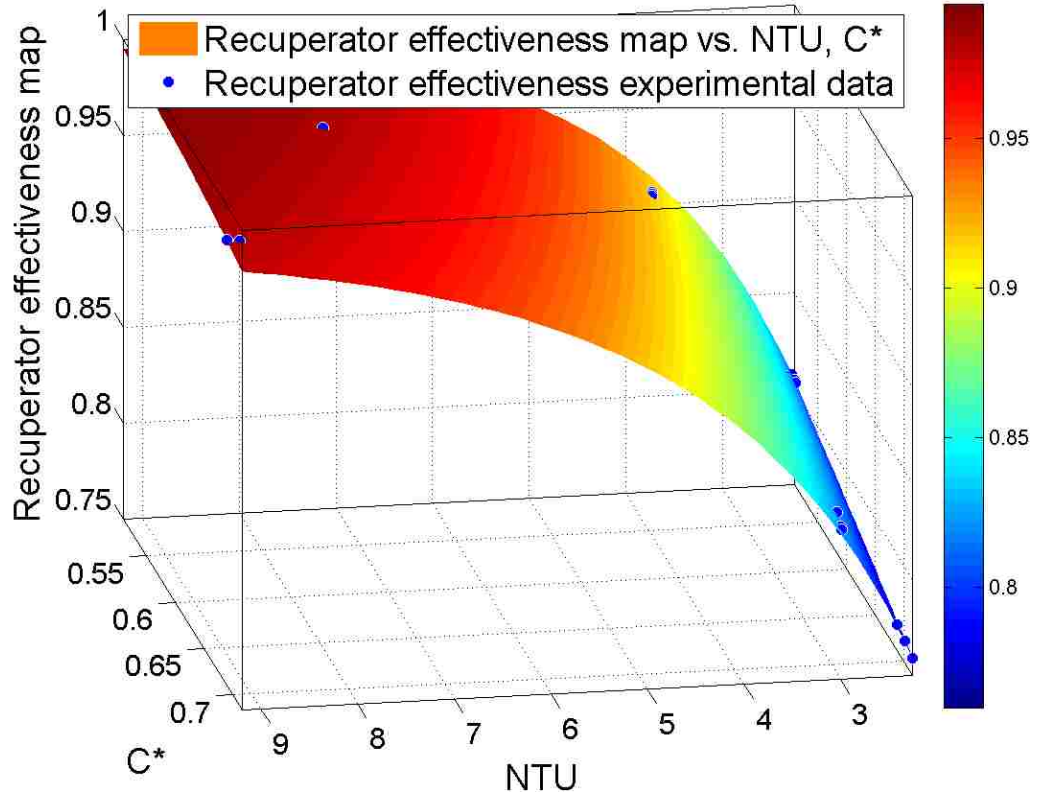


Figure 4.2-5: Recuperator effectiveness map built from the experimental data furnished by the supplier.

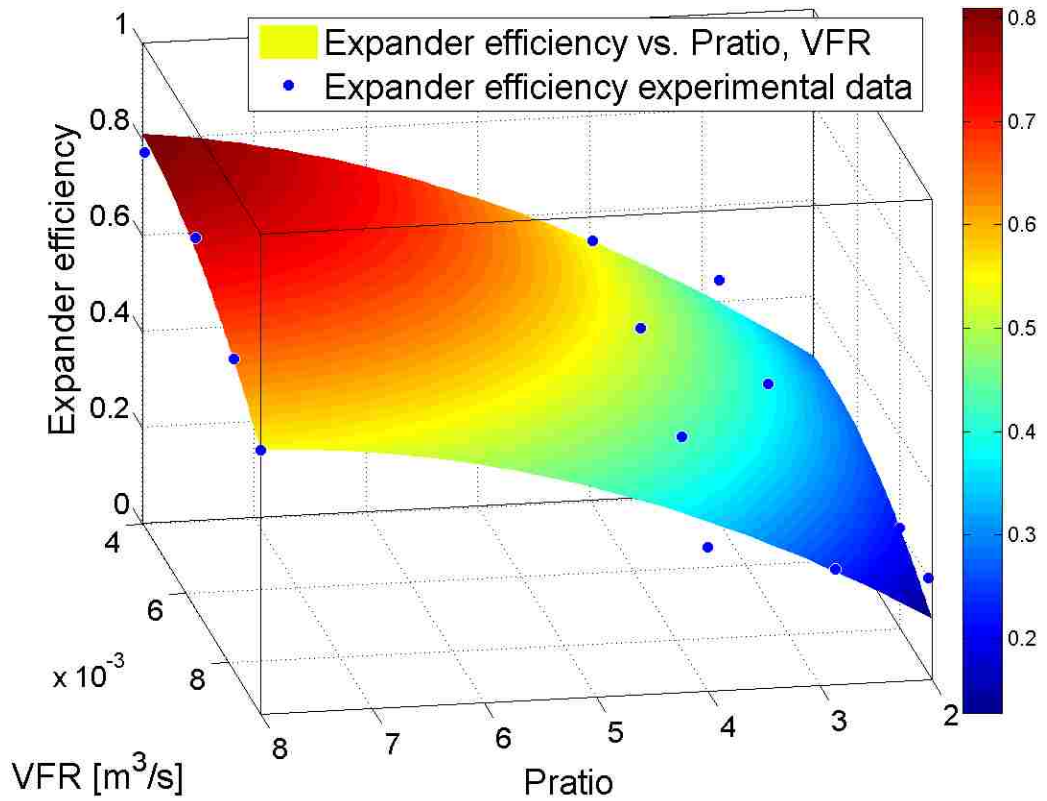


Figure 4.2-6: Expander efficiency map.

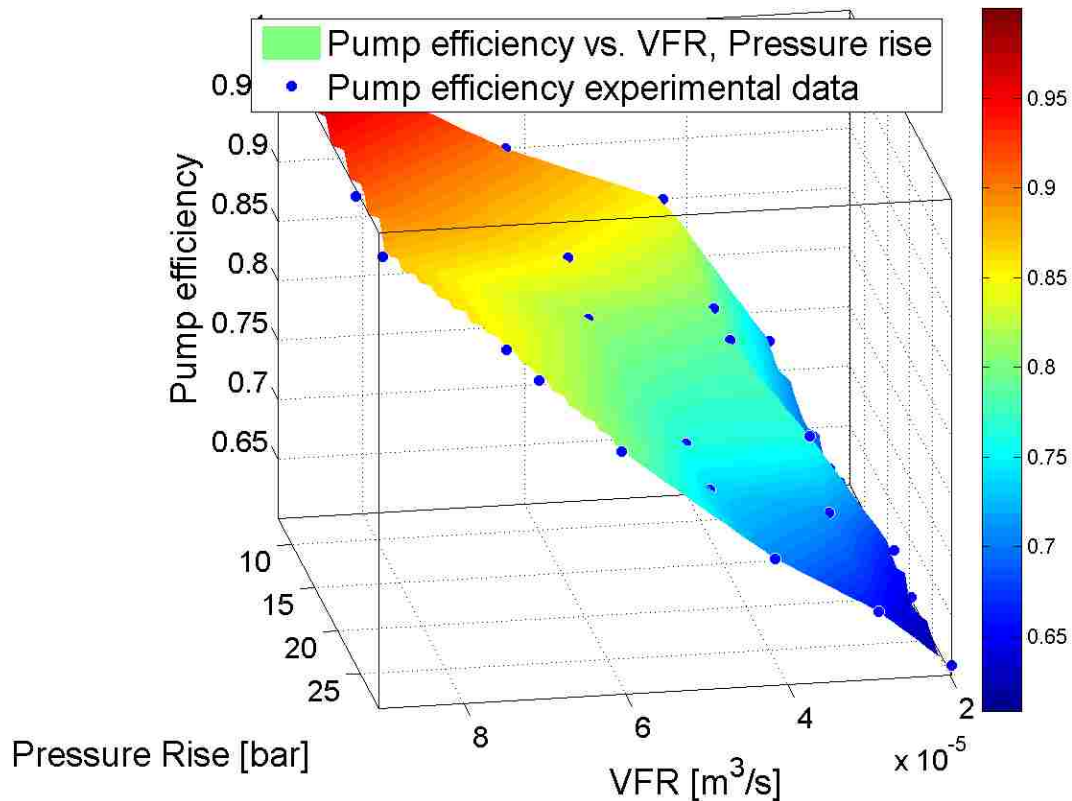


Figure 4.2-7: Pump efficiency map.

On the other hand specific data on the pump and expander that will be used in the real WHR unit were still unavailable, nonetheless performance curves of machines similar to that ones have been used in the detailed model. Figure 4.2-6 and Figure 4.2-7 show the efficiency maps respectively of the expander and of the pump. Speed maps for both machines have also been built, but here, for the sake of brevity, they are not reported. It should be also remarked that for what concerns the expander if it is mechanically connected to the engine shaft the volume flow rate map, as the one shown in Figure 4.2-8, rather than the speed map of the machine is used.

Anyway, looking at the efficiency map of the expander it is evident how the most optimum performances are obtained for high pressure ratios and that isentropic efficiencies higher than the 60% assumed in the preliminary analysis can be achieved. The same consideration holds for the pump efficiency, an isentropic efficiency significantly higher than 60% can be achieved. So it appears more precise to consider the isentropic efficiencies of the machines function of the conditions at which they operate. However, it still remains to be confirmed that the performance curves utilized in the detailed model, and reported in the figures above, correspond to those of the real components.

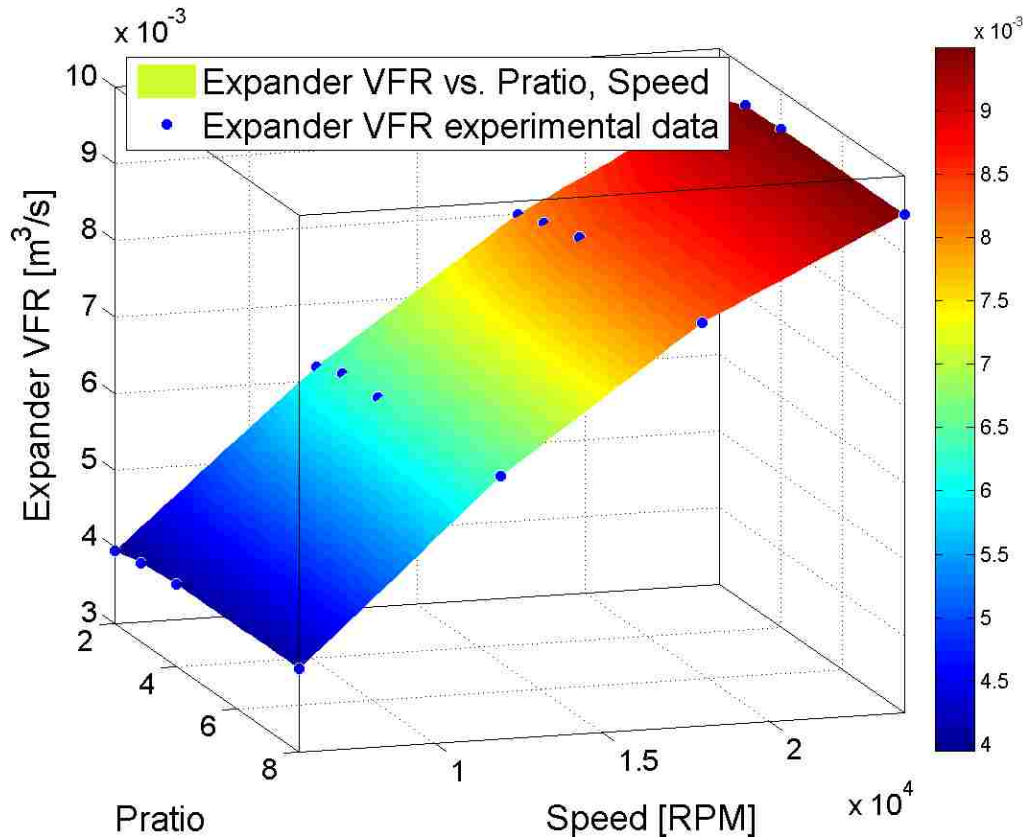


Figure 4.2-8: Expander volume flow rate (VFR) map.

Beside the performance maps of the components extensively explained, the other input parameters used for the simulation follow the strategy that has been indicated by the preliminary analysis as the one that can return the highest net power output:

- recuperative ORC
- highest possible temperature at the expander inlet ($210\text{ }^{\circ}\text{C}$)
- highest possible pressure at the expander inlet (2100 kPa)
- R245fa as working fluid.

The initial input window depicted in Figure 3.2-3 exactly contains the input parameters, set by the author, to carry out the simulation that replicates in the best possible way the behavior of the WHR system at the operating conditions of interest. As already anticipated, pump and expander efficiency, heat exchangers effectiveness, pressure drop in pipes and pressure drop in the heat exchangers are all assumed variable and not equal to the initial value and the maps and curves available have been integrated in the model. So the answer to the pop-up menus (explained in paragraph 3.2.1) from the third to the sixth was “No”. Among the other inputs, the initial values of efficiency, effectiveness and pressure drop of the components do not affect too much the results since these values are estimated through correspondent performance maps.

More influencing are the assumptions made about the geometry. As a matter of fact, at this stage of the design process (we should recall that the automaker is still far from applying this kind of device in production vehicles) there are no information about the pipes geometry so it is difficult to assess the length of the pipes and the number of concentrated losses. To compute the number of concentrated losses, the author has arbitrarily assumed a geometry that has the minimum possible number of tight bends and meets a series of requirements, typical of an ORC:

- Pump intake from the lowest point of the tank (interposed between the condenser and the pump) in order to be sure that only liquid comes into it.
- Condenser and expander inlet/outlet direction is downward to be sure that the liquid drops go down.

Once this rough sketch of the geometry was done, to number of tight bends computed in each pipe has been added another concentrated loss that corresponds to the measurement stations installed in the device. A greater length has been assigned to the pipes with more bends. Finally the diameter of the pipes on the vapor side (pipe 3, 4 and 5) has been set equal to one inch whereas that of the remaining pipes is equal to half an inch. Table 4.2-20: Input data about the geometry of the system. sums up the inputs about the geometry of the system.

Pipe N°	1	2	3	4	5	6
Bends N°	2	1	2	4	2	3
Pipe Length [m]	0.8	0.4	0.8	1	0.8	1
Pipe Diameter [m]	0.0127	0.0127	0.0254	0.0254	0.0254	0.0127

Table 4.2-20: Input data about the geometry of the system.

Once all the input parameters have been described and inserted in the model the simulation can be run (50 seconds was the duration selected), and the results obtained are reported in the following pages.

Figure 4.2-9 shows the pump most important operating parameters as a function of time:

- Pump isentropic efficiency, at the initial time instant, is equal to the initial value selected in the input window (0.6) then progressively it becomes equal to the value that the program reads from the map (0.8).
- Pressure rise given to the fluid (around 1900 kPa at steady state conditions), it is selected in order that considering all the pressure losses in the pipes and in the boiler, the pressure at the expander inlet is the maximum that the expander can withstand.
- Power absorbed by the pump (around 0.15 kW), even including the efficiency of the motor that has to transmit the power to the pump.
- Pump speed (around 1900 RPM at steady state), read from the tables.

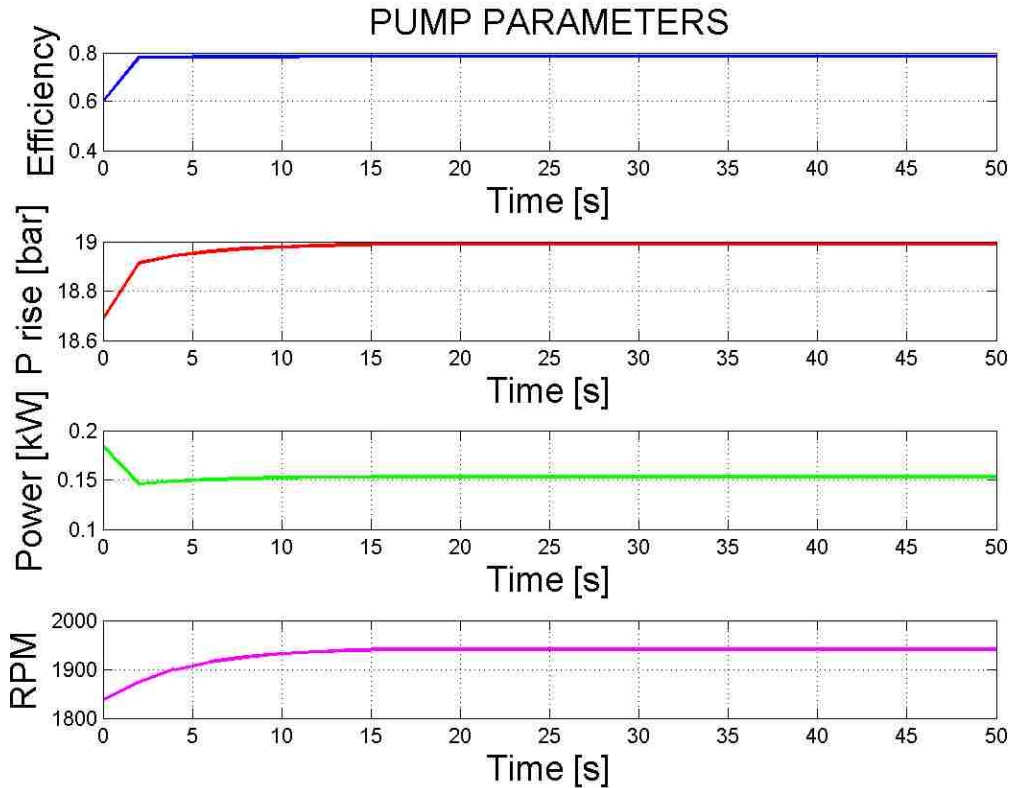


Figure 4.2-9: Pump operating parameters.

From this first picture presented it is clear that, even if the simulation is at steady state conditions (the exhaust gas inlet parameters do not change during time), it takes a certain amount of time, inversely proportional to the simulation frequency, for the output parameters to achieve a constant value. The reasons to explain this phenomenon are mainly two:

- The detailed model works with an iterative process, at the end of each simulation instant some inputs values for the following one are recalculated.
- The initial values selected are seldom equal to the real ones.

The simulation frequency selected was of 1 Hz, so basically one per second. If a higher frequency were selected the output would have achieved faster the steady state value and similar graphs could be obtained with shorter simulation periods. With that in mind the remaining outputs are shown. Figure 4.2-10 illustrates the boiler operating parameters:

- Inlet temperature (110 °C)
- outlet temperature, (210 °C) equal to the maximum possible temperature at the expander inlet set as an input
- boiling temperature (around 125 °C)
- heat transfer rate in the boiler.

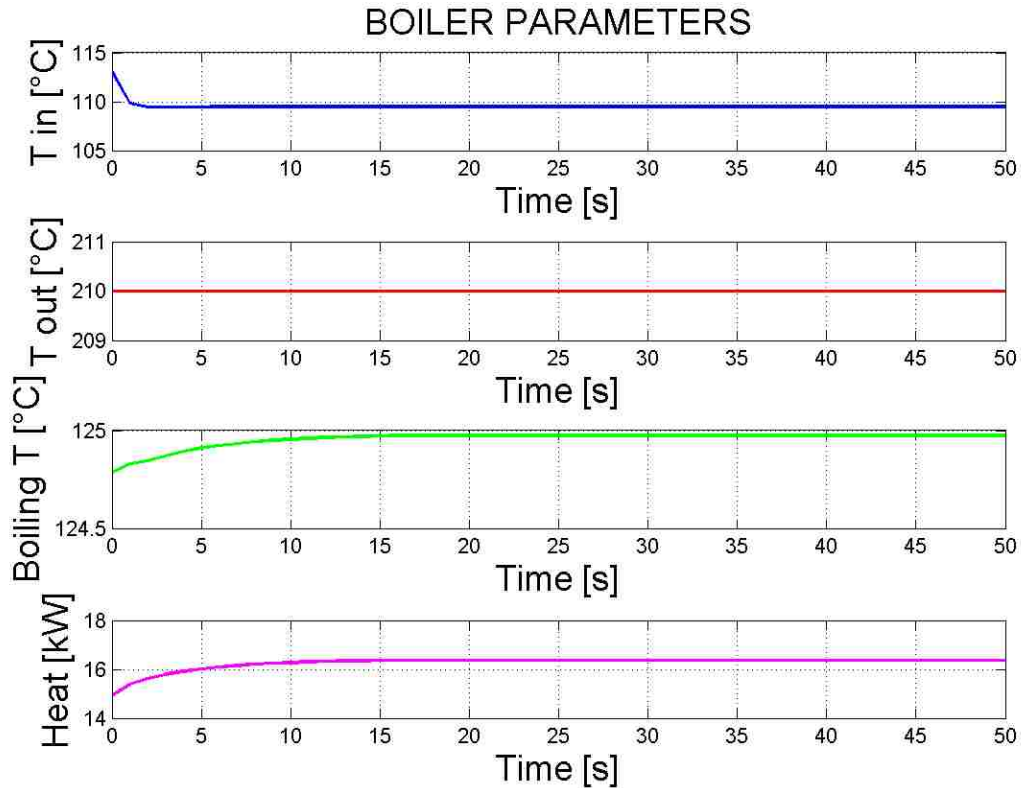


Figure 4.2-10: Boiler operating parameters.

The latter is the most important because it indicates the amount of heat that is extracted from the exhaust gas. It is slightly higher than 16 kW, so the exhaust gas of the engine analyzed can be categorized as a low grade heat source, according to the definition furnished in section 2.2.

On the other hand the expander operating parameters are illustrated in Figure 4.2-11:

- Expander efficiency is around 0.75. It is greater than the initial value and greater than the one assumed in the preliminary analysis.
- Pressure ratio across the expander (around 8).
- Net power output. It is slightly greater than 2.5 kW, it is a very promising result even though the real component very likely will generate less power.
- Expander speed. The reason why the expander operates at such high efficiencies is that the speed ratio between the engine shaft and the expander has been chosen in order that the expander operates at a speed that gives a high value of isentropic efficiency (5.45). In particular giving an engine speed of 2465 RPM the expander speed is 13434 RPM. Provided that the expander can safely work at the speed indicated in the point above, the combination of speed and pressure ratio is the one that gives the best isentropic efficiency for the machine selected.

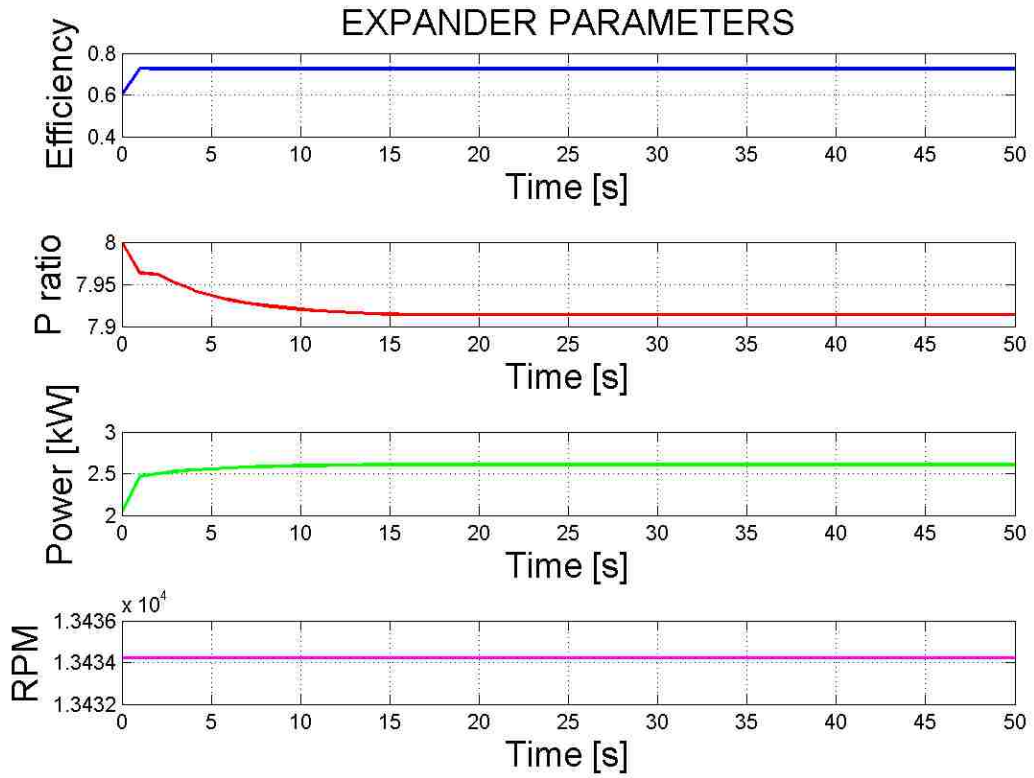


Figure 4.2-11: Expander operating parameters.

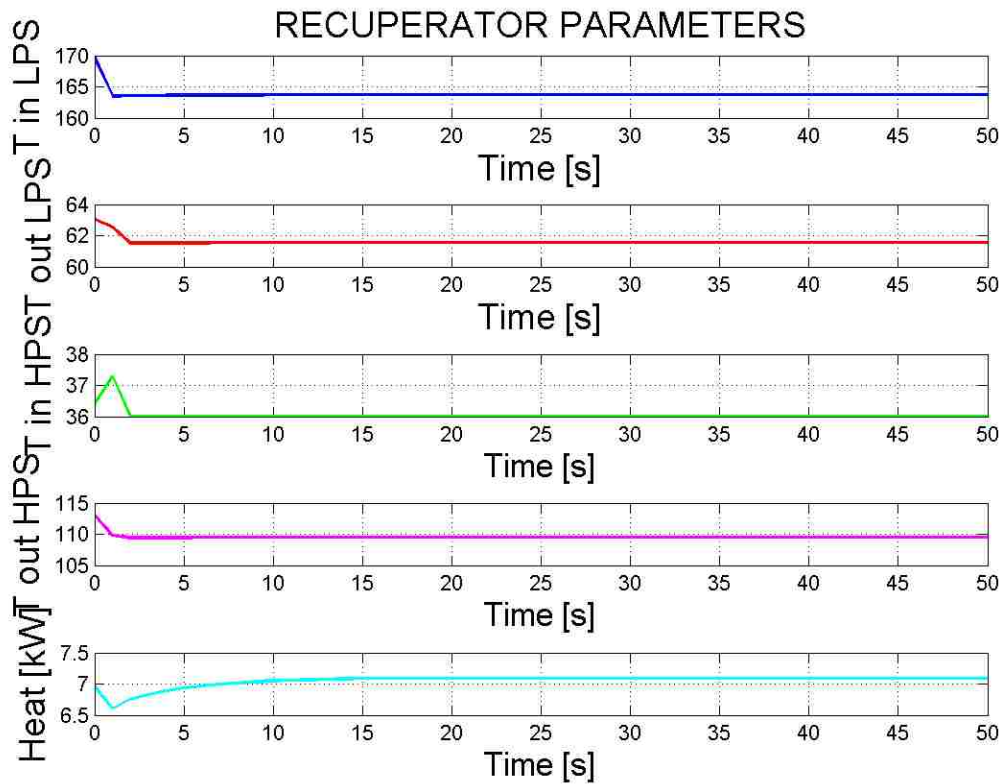


Figure 4.2-12: Recuperator operating parameters.

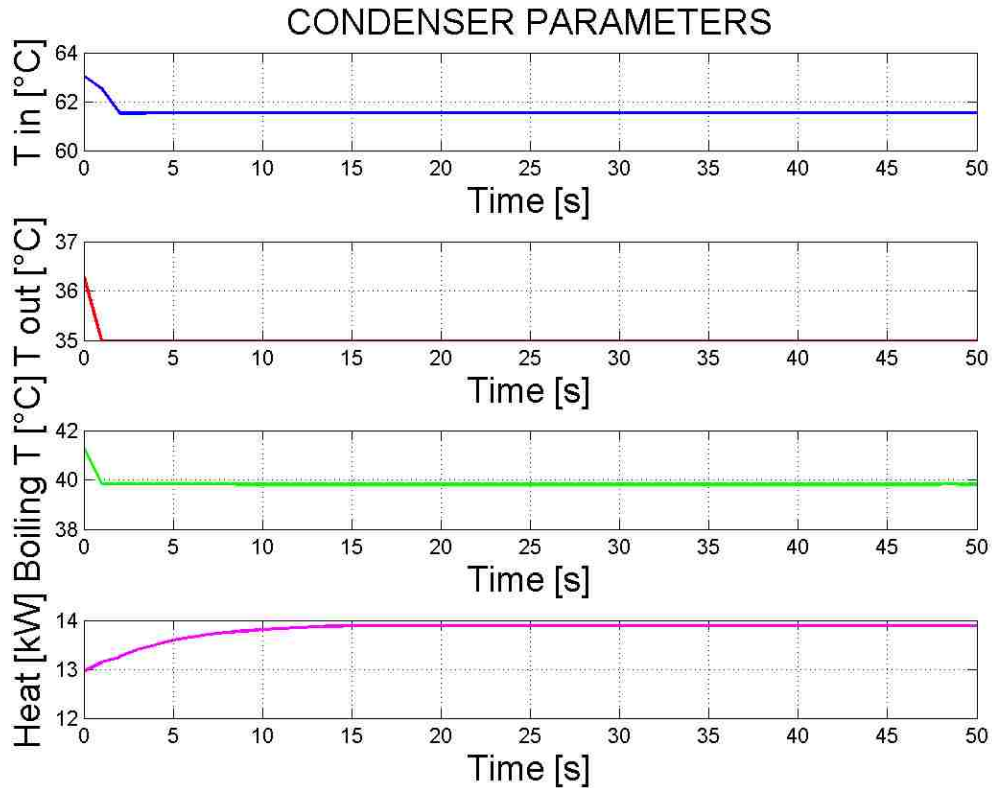


Figure 4.2-13: Condenser operating parameters.

Figure 4.2-12 shows the recuperator operating parameters. In the picture LPS and HPS refer respectively to the High Pressure Side (downstream the pump) and Low Pressure Side (downstream the expander) of the recuperator. The inlet and outlet temperatures for each side are reported. Obviously since no temperature losses in the pipes are taken into account the HPS outlet temperature is equal to the boiler inlet temperature whereas the LPS outlet temperature is equal to the condenser inlet temperature. Anyway the most important output parameter of the recuperator is the heat transfer rate that is equal to 7 kW.

Figure 4.2-13 shows the condenser operating parameters:

- inlet temperature (around 62 °C)
- condensing temperature (around 40 °C)
- outlet temperature (around 35 °C), equal to the condensing temperature minus the target sub-cooling of 5 °C
- heat transfer rate that is slightly less than 14 kW.

On the cold side of the condenser the coolant fluid that flows is the one used in the engine cooling system, that is a 50-50 Ethylene-Glycol mixture (in other vehicle a 50-50 Water- Ethylene mixture might be used). The inlet temperature assumed for this fluid is 30 °C, and it is plotted along with the mass flow rate required and the outlet temperature in Figure 4.2-14.

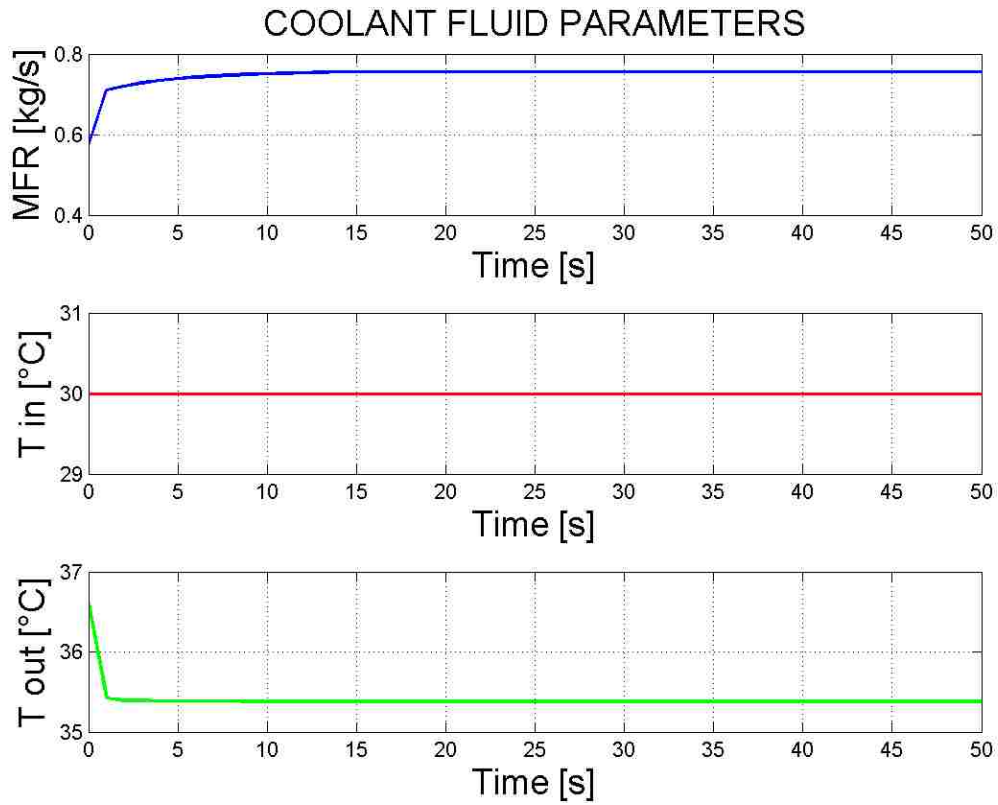


Figure 4.2-14: Coolant fluid parameters.

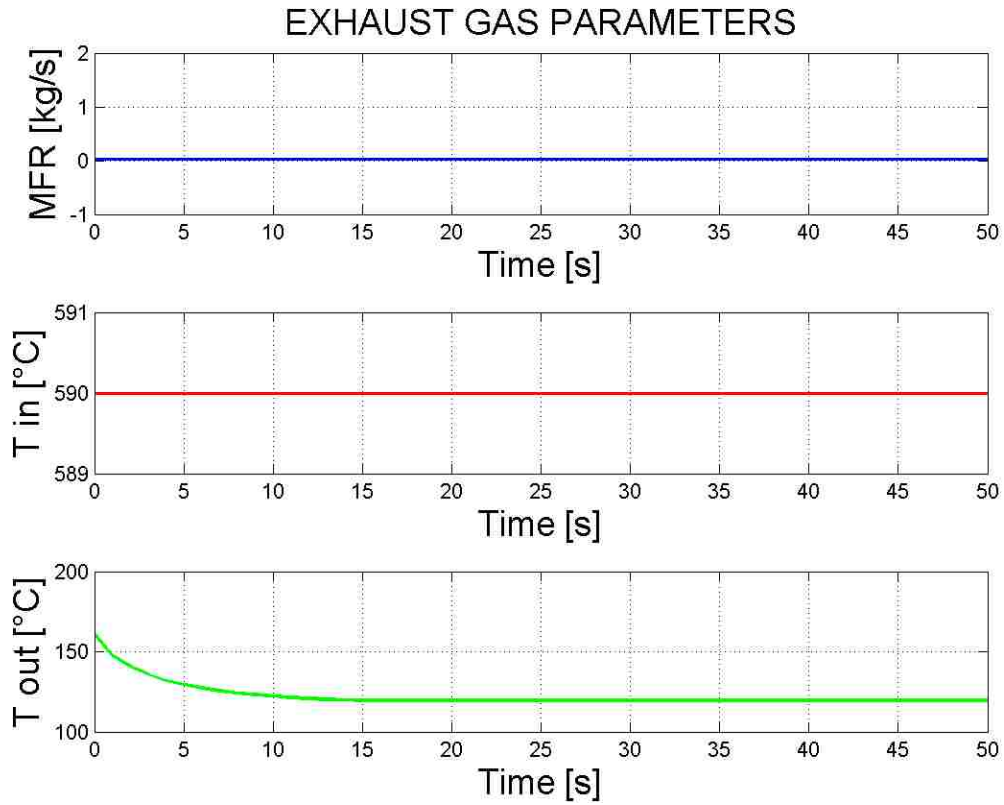


Figure 4.2-15: Exhaust gas operating parameters.

Probably the most important parameter here is the mass flow rate of the coolant fluid necessary. In fact the temperature rise of the coolant fluid is not so high just 5-6 °C whereas the mass flow rate required is definitely higher. It should be noted that the adoption of the coolant fluid of the engine system in the condenser has non-negligible effects on the coolant system of the vehicle such as: increased pumping power necessary, increased area of the radiator in front of the vehicle and others. These effects are not analyzed in the present work, but they are very important to understand the interactions that the WHR unit has with the vehicle, hence the coolant fluid outlet temperature and mass flow rate should be monitored carefully.

Another point in the cycle in which the WHR unit interacts with the vehicle is the boiler, Figure 4.2-15 shows the parameters of the exhaust gas flowing in it. The mass flow rate and the inlet temperature (respectively blue and red lines) are parameters set by the user and in this case of stationary point analysis they are constant. They are entirely function of the engine type, engine load and engine speed. Actually, there might be the possibility that a portion of the exhaust gas mass flow rate bypasses the boiler in order not to heat up too much the working fluid in the cold side of the boiler or not to cool down too much the hot exhaust gases, as already explained in paragraph 3.2.2.4. However, at this operating conditions it does, not happen thus the mass flow rate of the exhaust gas flowing out of the cylinders entirely goes into the boiler. The resulting outlet temperature trend is reported in the green line still of Figure 4.2-15. It is 20 °C above the threshold set at the beginning of the simulation of 100 °C. The exhaust gas have dropped their temperature of 470 °C, that means that, as we will see later, almost all the heat available is extracted and absorbed by the working fluid.

Looking in more details what happens in the heat exchangers Figure 4.2-16 and Figure 4.2-17 show respectively the heat exchanger effectiveness and pressure drop of the heat exchanger so basically in which zone of the maps, shown in Figure 4.2-2 through Figure 4.2-5, the heat exchangers operate. IN particular we can note that the recuperator has an effectiveness almost equal to the initial value assigned 0.8 whereas the condenser actually have a lower effectiveness about 0.17. The most surprising performances are obtained by the boiler whose effectiveness is around 0.96-0.97. If the performance map used for the simulation corresponds to the real performances of the boiler the heat transfer rate taking place in the boiler would be very high and the potential power output of the cycle could be very interesting at least at the operating conditions analyzed in this paragraph.

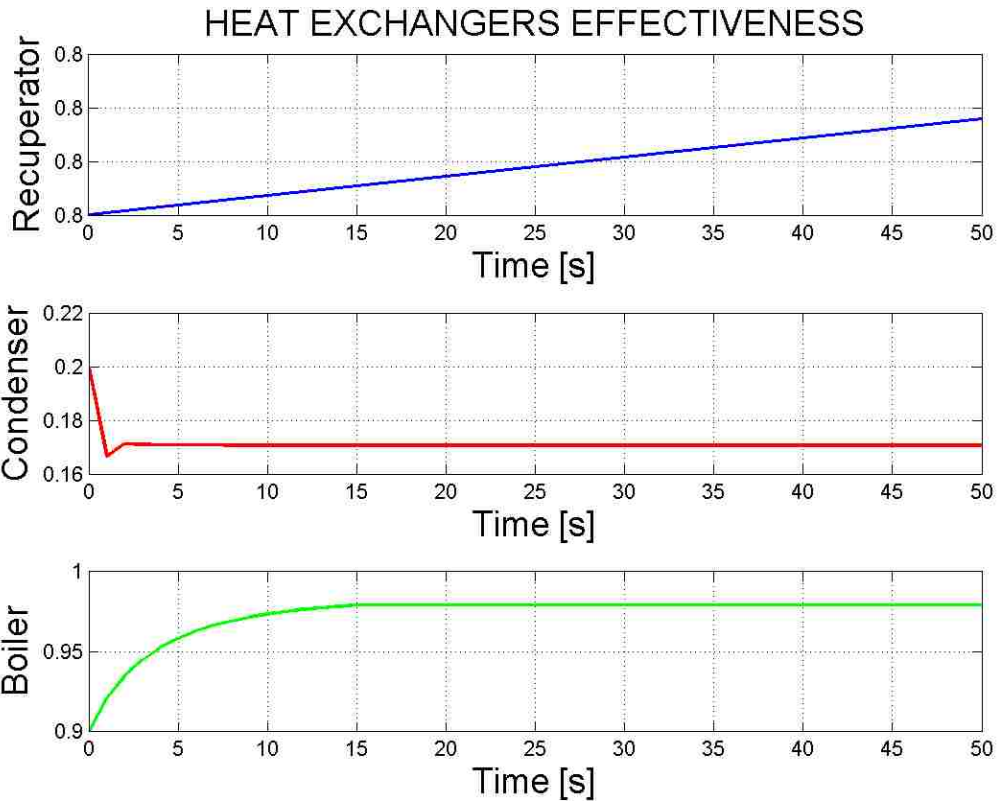


Figure 4.2-16: Heat exchanger effectiveness.

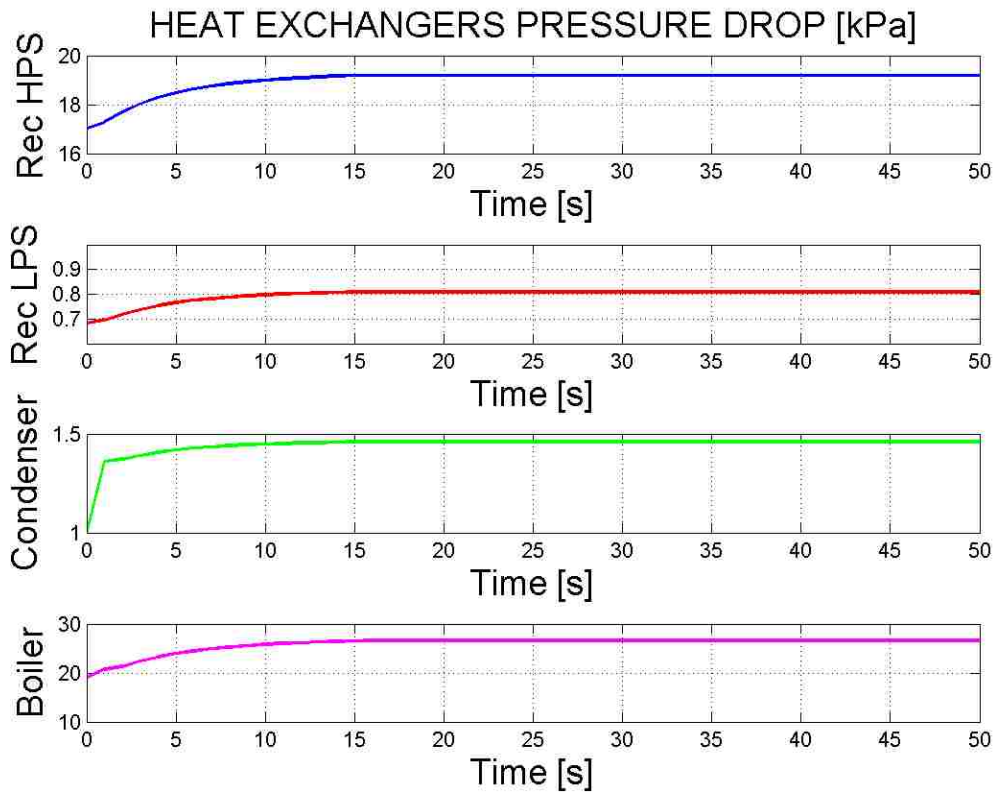


Figure 4.2-17: Heat exchanger pressure drop.

On the other hand, as predictable looking at Figure 4.2-2, the pressure drop in the heat exchangers appears to be greater in the heat exchangers in which the working fluid has high pressure, such as in the boiler, 27 kPa, and in the recuperator high pressure side (HPS), 19 kPa, whereas in the condenser 1.5 kPa and in the recuperator LPS just 0.7 kPa. So the heat exchangers whose pressure drop reduces the most the net power output of the cycle are boiler and the recuperator HPS.

Anyway, as long as the pressure drop in the heat exchanger stays around the value indicated above the net power output is weakly affected by the actual value of the pressure drop. With reference to the nominal values shown in Figure 4.2-17, Table 4.2-21 has been calculated to assess how much a variation of the pressure drop from its nominal values affects the net power output of the WHR unit. It has been found out that even quadrupling the values of the pressure drop inside each heat exchanger the net power output is reduced by just 1.02%, that considering the uncertainty that characterize the model, is an extremely small value. Furthermore, even in the case there was no pressure drop in the heat exchangers the increase of the net power output, with respect to its nominal value, is so small (0.33%) to be considered acceptable and a very good approximation of the nominal value. The rule of thumb suggested here is to roughly estimate the pressure drop inside the heat exchangers and verify that their values are not higher than 100 kPa. If this is the case they can be neglected in the simulation without making mistakes, instead if they are above the threshold it might be better to include them in the computation.

Heat Exchanger Pressure Drop	Net Power Output Percentage Variation
200% increased	-1.02%
100% increased	-0.33%
Nominal	0.00%
50% reduced	+0.12%
Null	+0.33%

Table 4.2-21: Heat exchanger pressure drop effect on the net power output.

To complete the analysis of the pressure losses around the cycle, Figure 4.2-18 shows the pressure drop in each pipe. Those values are low and these losses do not cause a great power output reduction. Only pipe 4 has a pressure loss that goes greater than 10 kPa because in that pipe the Re number is particularly high and especially because it is the longest and has the highest number of concentrated losses. If we compare the values of Figure 4.2-18 with those reported in paragraph 4.2.1, it is clear how the pressure drop in the pipes for this application is lower, even though the bend pressure loss coefficient selected is greater.

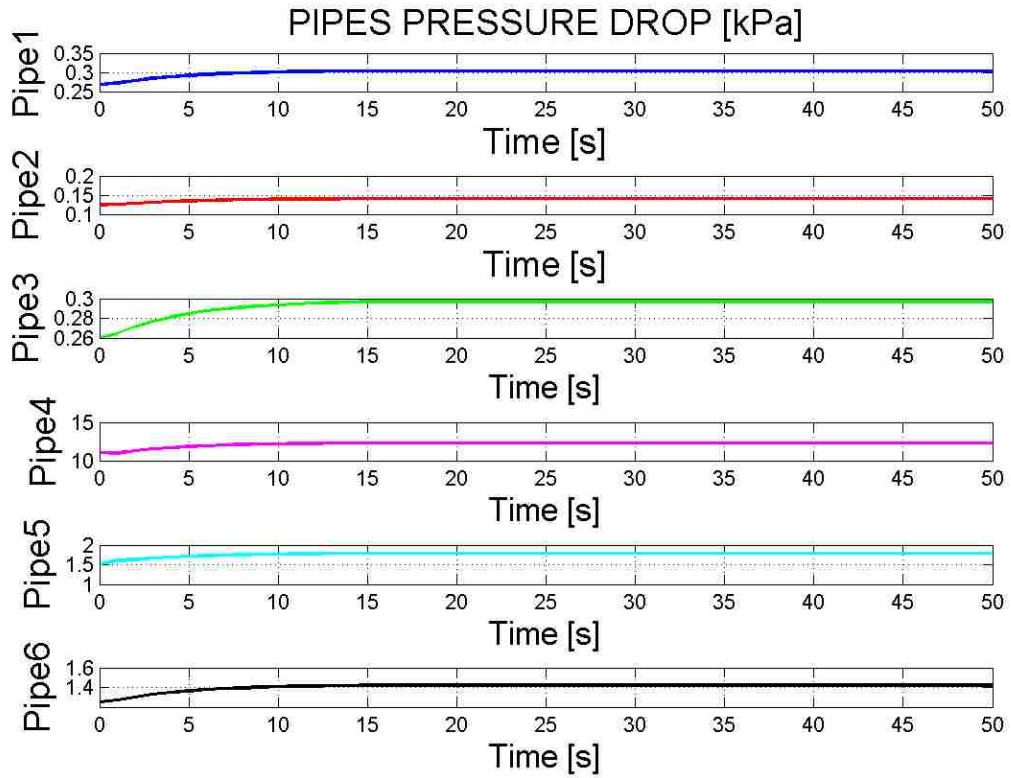


Figure 4.2-18: Pipe pressure drop.

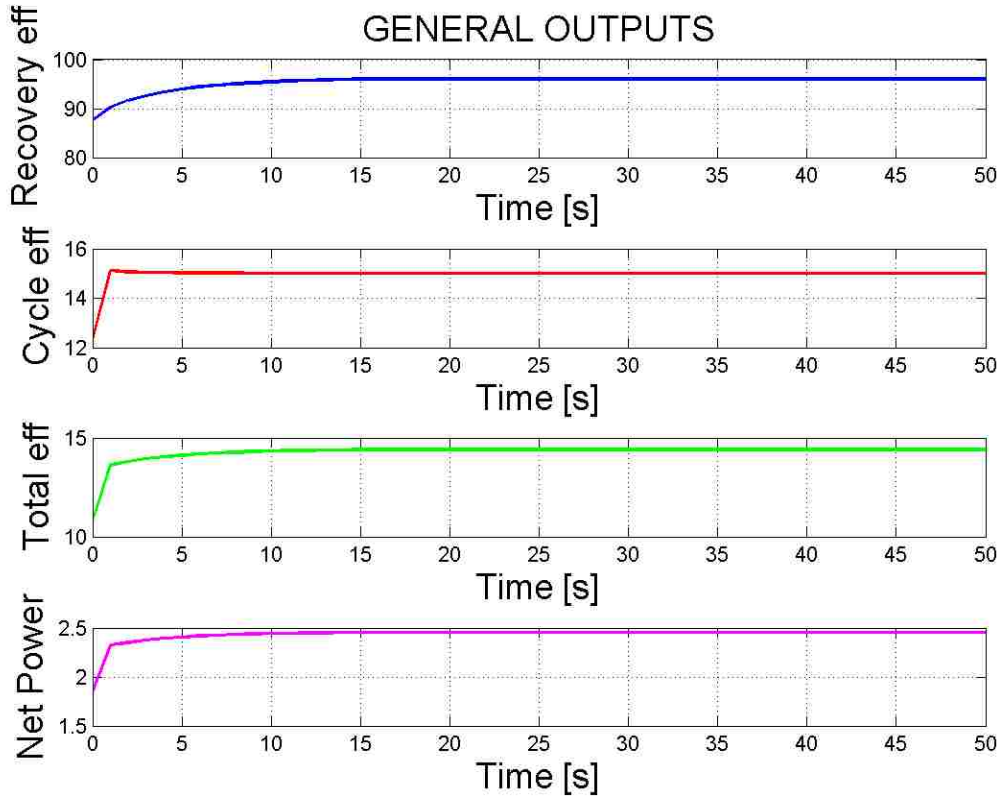


Figure 4.2-19: General output parameters of the WHR unit.

It should be said that the pipes are shorter and there are less concentrated losses however the main causes of this difference might be another: the pipes diameter. To verify this hypothesis another simulation has been performed substituting the pipes diameter reported in Table 4.2-20 with those used in the previous paragraph. Basically pipe 1, 2 and 6 diameter has been changed from 0.0127 m to 0.0125 m (1.5% reduction), while pipe 3, 4 and 5 have been changed from 0.0254 m to 0.0209 m (17.7% reduction). The results obtained are illustrated in Table 4.2-22. In each pipe the pressure drop is increased. Except for pipe 2 whose growth of pressure drop is just of 1.3%, the pressure drop in the pipes in the liquid side is increased by a percentage that is around 10 starting from a diameter reduction of just 1.57%. Instead for the pipes on the vapor side the pipe pressure drop is heavily increased, more than doubled. Such a big increase of pressure drop derived from a small change in pipe diameter has also non-negligible effects on the net power output, that is the parameter of greatest interest, making it drop by 4%. So the designer of the system has to be very careful in choosing a suitable pipe diameter in order to find the right trade-off between size and pressure drop.

	Pipe Diameter Variation	Pressure Drop Variation
pipe 1	1.57%	10.0%
pipe 2	1.57%	1.3%
pipe 3	17.7%	130.0%
pipe 4	17.7%	116.7%
pipe 5	17.7%	127.8%
pipe 6	1.57%	8.6%

Table 4.2-22: Pipe diameter effect on pipe pressure drop.

To conclude the analysis of the results obtained with the simulation at target (stationary) vehicle operating conditions, Figure 4.2-19 shows what have been called the general output parameters, practically the parameters that give an indication of the overall behavior of the WHR unit. The first one presented in the recovery efficiency that is around 98%, it is computed as the heat transfer rate in the boiler divided by the maximum possible heat transfer rate, the one that can occur when the exhaust gas is cooled down to its minimum temperature defined equal to 100 °C. As already anticipated, since the outlet temperature of the exhaust gas is around 120 °C very close to its minimum value, it means that almost all the heat that could be extracted has been actually taken from the exhaust gas. The red line instead represents the cycle efficiency. Its value is around 15%, slightly higher than the 13% found out, for R245fa in a recuperative ORC, with the preliminary model (see Figure 4.1-3 for reference), because the expander and pump efficiencies as well as the boiler effectiveness utilized in the detailed model are higher.

The efficiency of a Carnot cycle operating between the same maximum and minimum temperatures according to Equation 2.1 would be 83%, 5.5 times higher than the 15% reported. The resulting total efficiency defined as the product of the two other efficiencies already defined, is 14.4% that is a very good and promising result, even though the expander and pump performance maps do not correspond to those of the real component that have not yet been provided by the suppliers. Translating the efficiency result obtained into something more concrete, the net power output of the cycle (magenta line of Figure 4.2-19) is 2.455 kW. Considering that the engine at the operating conditions considered, 2465 RPM vehicle speed of 70 MPH and engine torque of 125 Nm delivers 29 kW, the WHR unit could be able to provide an additional 8.47% power that can be used to recharge the vehicle battery, to run some accessory or simply to make the vehicle go faster.

4.2.3 Working fluid comparison at steady state

In the previous paragraph the results obtained with R245fa at target vehicle operating conditions have been illustrated and explained in details. In the present paragraph the results that can be obtained with other three working fluid at the same vehicle operating conditions are reported. Although the components (especially the heat exchangers) have been developed and designed for R245fa the same performance maps used before are also utilized for the other working fluids. The working fluids compared and their critical temperatures and pressures are reported in the table below.

Working fluid	Critical temperature [°C]	Critical pressure [kPa]	GWP	ODP
R245fa	154.05	3651	1030	0
R134a	101.06	4059	1430	0
Water	373.95	22064	0.2	0
Ethanol	240.75	6148	-	-

Table 4.2-23: Working fluid tested list.

Ethanol pollution indicators have not been reported because it is not included in the US EPA classification of refrigerants.

However, the simulations were not run blindly using the same inputs set for R245fa, since, as already anticipated, water and ethanol have pressure and temperature at the critical point significantly higher than those of the other two fluids. These differences have forced the author to define proper values in the input window to make the program run properly. Anyway the results obtained are illustrated in Table 4.2-24 and will be analyzed and explained for each working fluid except for R245fa that is used as reference.

Fluid	WF MFR [Kg/s]	Pump power [kW]	Expander power [kW]	Boiler heat [kW]	Condenser heat [kW]	Cycle eff [%]	Total eff [%]	Net power [kW]
R245fa	0.066	0.15	2.61	16.4	14.0	15.0%	14.4%	2.45
R134a	0.061	0.09	0.42	10.2	9.9	3.3%	2.0%	0.33
Water	0.006	0.02	1.42	15.48	14.1	9%	8.2%	1.4
Ethanol	0.016	0.09	1.41	14.8	13.47	8.9%	7.75%	1.32

Table 4.2-24: Main outputs of the cycle, working fluids comparison.

4.2.3.1 R134a

As already mentioned in the preliminary analysis and highlighted in Table 4.2-23, R134a is a wet fluid with low critical temperature. Nonetheless its critical pressure is not that low so the nominal pressure rise in the pump has been kept high in order that at the expander inlet the maximum the working fluid pressure was the highest possible 2100 kPa. The small saturation curve of the R134a has allowed to operate far from the saturation curve in the vapor zone.

Looking at the mass flow rate column of Table 4.2-24 it is evident how it is very close to that obtained for the R245fa. Practically it means that even though the density of the R134fa is slightly lower, its volume flow rates are almost equal to those obtained with R245fa and so pump and expander of the same dimensions can be used. Investigating better what happens in the boiler one can see that the heat exchanged by the R134a is the lowest among the working fluids analyzed, so the expected mass flow rate should be the lowest as well. However, since the saturation curve of the R134a is so small if compared to that of the other, its ability of absorbing heat is strongly limited, so the working fluid mass flow rate necessary to absorb 10.2 kW in the boiler is 0.061 kg/s. On the other hand since the mass flow rate in the boiler is the same as the R245fa one, but the specific heat of R134a is lower, the heat capacity rate ratio (C^*) in the boiler obtained with the R134a is higher. Looking at Figure 4.2-3 it is clear that the boiler effectiveness decreases for increasing values of C^* at a given NTU. In turns the low boiler effectiveness, around 0.75, makes the heat transfer rate in the boiler very low. Anyway despite these consideration the net power output of the cycle rightmost column of Table 4.2-24 is the lowest, so low to discourage an application of the working fluid in a WHR unit. The low net power output (0.33 kW) is the reflection of a very low cycle efficiency (3.3%) due to the fact that the expander inlet pressure is far from the critical one (condition that maximizes the cycle efficiency). Moreover, considering that the input heat transfer rate in the boiler that is constitutes the power input of the cycle is very low the net power output obtained is more than justified.

4.2.3.2 Water

Water is the most safe and environmental friendly working fluid that can be used. It has a very strong ability in absorbing heat, so a small amount of mass flow rate is enough to recover the amount of heat available in the exhaust gas. However, its high critical temperature and pressure, the big shape of its saturation curve makes this working fluid unfeasible for the application in the WHR industry of low grade heat source such as the exhaust gas. Anyway before drawing conclusions the modifications necessary to make the simulation run are summarized in the bullet list below:

- The target condensing temperature has been risen to 100 °C in order to have a pump inlet temperature equal to the ambient pressure and avoid air infiltration.
- The nominal pressure rise in the pump (pump head) is equal to 1650 kPa. The problem is that if a higher pressure rise were selected at the expander inlet the fluid would have been in the double phase zone of the Mollier diagram. This condition has to be avoided and the only way to that was to reduce the pressure because the expander inlet temperature cannot be risen above the expander limit.
- The pump and expander so far adopted are machines not dimensioned to operate with water, so the pump volume flow rate limit has been lowered below the limit previously assumed of ($3 \cdot 10^{-5} \text{ m}^3/\text{s}$). So since pump performance maps are not available for volume flow rates below this threshold the expander and pump efficiency had to be assumed constant and equal to the input value.
- The adoption of the recuperator was not possible since at the expander outlet the working fluid is already in the two-phase (some liquid droplets are already formed) zone.
- The heat exchangers so far adopted were not meant to operate at the combination of NTU and C^* that are achieved with water and so proper effectiveness maps were not available. Also heat exchangers effectiveness are assumed constant and equal to the initial value.

All these modifications were necessary to run the simulation properly without generating errors. The risk of liquid droplets left at the expander inlet with the constraint of not surpassing 210 °C and 2100 kPa is too high. The control part of the system would be very complex. Given all the limitations done to make at least the WHR unit run properly, the net power output obtained is even high 1.4 kW. However, it is clear how the considerations done in sections 2.2 and 2.3 hold; water cannot effectively operate in a WHR unit with a low grade heat source (heat available smaller than 20 kW) for two main reasons: low efficiency and complexity of the control system.

4.2.3.3 Ethanol

Ethanol has thermodynamic properties at the critical point that are intermediate between those of water and those of R245fa. In fact, the mass flow rate of the required is between that of the other two fluids just mentioned. However, also for ethanol some modifications had to be done because the volume flow rate at the pump inlet is below the limit of that of the map available. So the expander and pump efficiency have been assumed constant. Furthermore the heat exchanger effectiveness have been assumed constant and equal to the initial value for the same reason explained in the paragraph dedicated to the water. Moving on the results obtained with ethanol, still reported in Table 4.2-24, are substantially equal to those obtained with water. The only difference is in the power absorbed by the pump that is slightly higher for ethanol, making the net power output slightly lower.

4.2.3.4 Conclusion on the working fluid comparison

In this short paragraph it has been demonstrated that R245fa is the most suitable working fluid for this application, the power output achieved with this fluid is around 75% greater than that of water and ethanol. Nevertheless it must be said that the components of the system were designed appositely for R245fa, giving to this working fluid a significant advantage. However, the range of operating temperature and pressure make difficult to control the WHR unit if water is used. On the other hand, ethanol appears to be a valid alternative if a slightly higher amount of heat were available and especially if components were customized to its thermodynamic properties. These results are in contrast to those shown by Bosch GmbH in [28], where the reported net power output of the WHR system with water and ethanol is three times greater than that for R245fa. This difference can be in part explained by the fact that in this work the heat exchangers, whose maps were uploaded in the detailed model, were specifically designed for R245fa and not further optimized for water and ethanol as working fluids. Moreover, the Bosch GmbH study has considered an engine three times bigger than the 3.6L considered in this thesis. A bigger engine means a greater amount of heat available in the exhaust gas; the problem of liquid droplets formation upstream and downstream the expander is avoided for both water and ethanol. Finally it should be pointed out that R245fa has a very large GWP. However, it will be replaced by a new working fluid that has the same thermodynamic properties but a GWP of two magnitudes lower.

4.2.4 WHR unit integration with the engine and creation of the net power output map

The simulations of paragraphs 4.2.2 and 4.2.3 were carried out at what has been denominated target vehicle operating conditions:

- 70 Mph, vehicle speed
- 2465 RPM, engine speed
- 125 Nm, engine torque
- 29 kW of power delivered by the engine.

The speed transmission ratio between the engine shaft and the expander has been optimized in order to make the expander operate at the highest efficiency when the engine rotates at the speed aforementioned. However, when the WHR unit has to be integrated with the engine and set up to work in a wide range of engine operating conditions there are different constraints that have to be considered and that guide the choice of the gear ratio.

- The expander operates at faster speeds with respect to the engine, so a speed multiplier is necessary.
- The expander has to operate at speeds lower than its maximum one.
- The expander has to operate at speeds higher than its minimum one.

Even though the expander, at least the one adopted in the current application, can safely operate at a wider range of speeds (from 6000 RPM to 24000 RPM) with respect to that of the engine (from 550 RPM to 6500 RPM) the expander cannot be activated at every engine speed no matter what kind of speed ratio is selected. Supposing for instance to select the speed ratio in order that at the maximum engine speed the expander operates at its maximum possible speed, the speed ratio would be 3.7 (equal to the ratio between the two maximum speeds). However, at the lowest engine speed (500 RPM) the expander would rotate at a speed lower than its minimum one (2960 RPM). On the other hand if the opposite approach is used and the speed ratio is calculated assuming that at the minimum engine speed the expander rotates at its slowest speed, the speed ratio would be 10.9, but again when the engine speed is 6500 RPM the expander would rotate at a velocity higher than its maximum one. So, unless a transmission with variable speed ratio is adopted that is a too complex solution, a clutch is necessary in order that the expander operates only under safe conditions. Given that, the designer has to decide in which engine speed range wants the expander, hence the overall WHR unit, to operate and generate additional power. The smartest solution appears to be that of selecting the speed window at which the engine operates more often. To this purpose two considerations arise:

- The engine very rarely operates at speeds higher than 5000 RPM and, if it does, it is just for few seconds.
- At low engine speeds, typical of an urban driving style, the temperature of the exhaust gas is usually low and there is less heat ejected (in absolute value not in percentage) with the exhaust gas that can potentially be recovered.

That said, the selected engine speed range, at which the WHR system works, is within 1200 RPM and 4700 RPM. The speed ratio resulting is around 5.1. Table 4.2-25 shows the minimum and maximum speeds at which the expander can operate given that speed ratio; they are within the range in which the expander can safely operate.

	Minimum speed [RPM]	Maximum speed [RPM]
Engine	1200	4700
Expander	6120	23970

Table 4.2-25: Minimum and maximum engine and expander rotational speeds with a speed ratio of 5.1.

Whenever the engine speed is outside the interval just defined, the clutch is virtually activated, the WHR unit is switched off and the exhaust gas bypasses the boiler. Actually there is another condition set by the author at which the WHR unit is switched off: when the exhaust gas temperature at the boiler inlet is below 220 °C. Otherwise the specification about minimum temperature difference between the exhaust gas and the working fluid inside the boiler is not even respected at the working fluid outlet section, where the temperature of the working fluid should be around 210 °C. Anyway the results obtained will justify this restriction imposed by the author.

Beside the speed ratio and the minimum temperature at which the WHR unit is turned on, no other input parameters of the simulation have been changed from paragraphs 4.2.2 and 4.2.3. The final objective of the analysis reported in this paragraph was to assess how much net power the WHR unit can generate at different engine operating conditions.

So starting from the maps of the engine that give the mass flow rate and the temperature of the exhaust gas as a function of the engine speed and throttle position, shown in Figure 4.2-20 and Figure 4.2-21, a similar map has been built by means of the detailed model reporting the net power output of the WHR unit still as a function of the engine speed and throttle position. However, it should also be clarified that few results may be non-physical because maps have been extrapolated using "griddata" in Matlab to cover entire range given by inputs. Looking Figure 4.2-21 we can see that the exhaust gas temperature falls below the threshold of 220 °C in two cases:

- Engine speed close to the minimum one, condition already excluded from the net power output map since the selected range of engine speed goes from 1200 RPM to 4700 RPM.
- Throttle slightly open even at engine speeds as high as 2000 RPM.

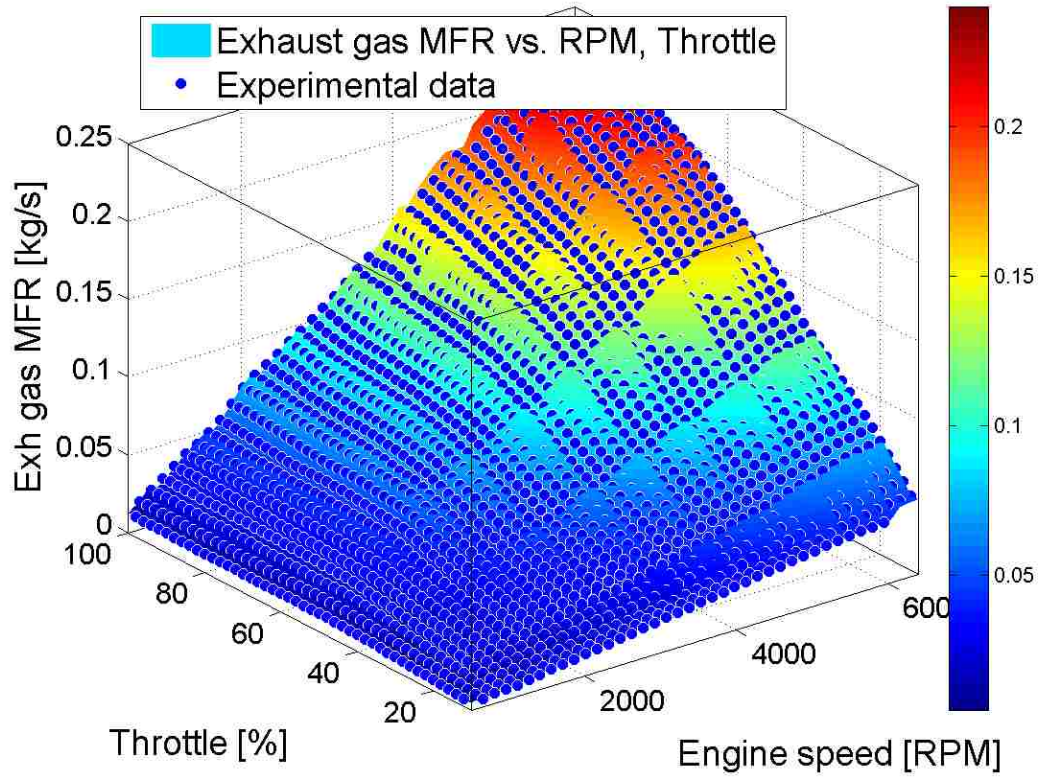


Figure 4.2-20: Exhaust gas mass flow rate map.

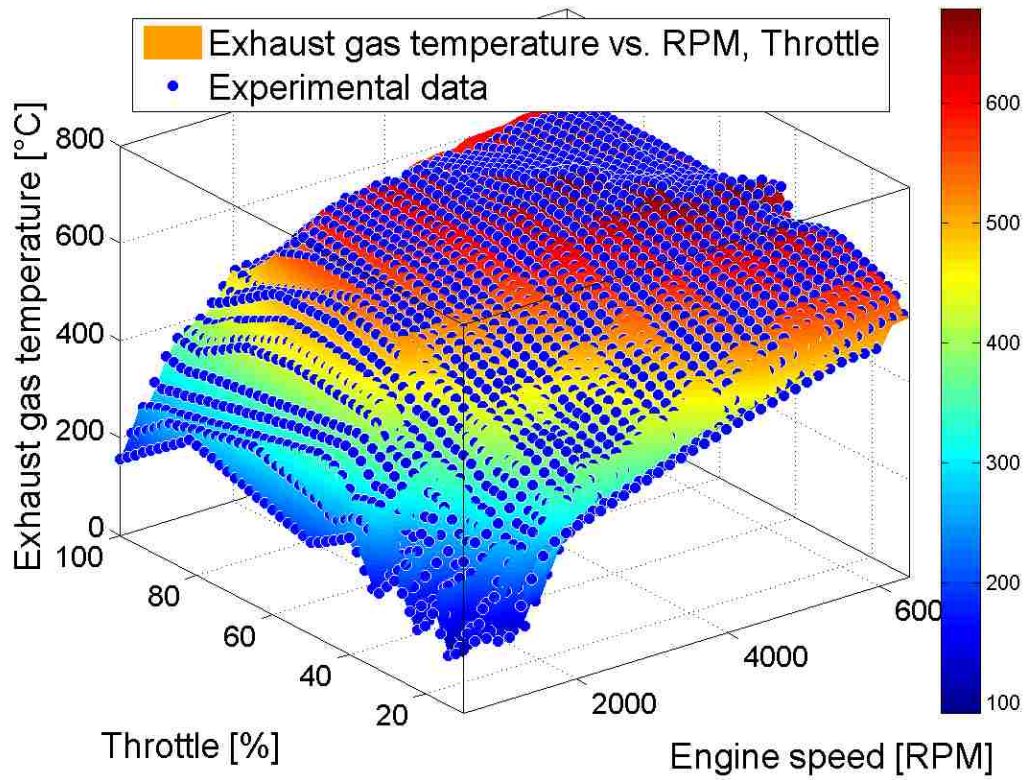


Figure 4.2-21: Exhaust gas temperature map.

The detailed model has been run for all the possible combinations of engine speed, between the limits aforementioned, and throttle position. The outcomes are illustrated in Figure 4.2-22. The first thing that should be noticed is that the net power output of the cycle dramatically drops when the throttle is almost close until it achieves a limit in which, even though engine speed is inside the defined range, the WHR unit is switched off because the exhaust gas temperature is below the threshold. The higher the engine speed the closer is the position of the throttle at which this limit occurs, look at Figure 4.2-23 that is the top view of Figure 4.2-22. Actually the throttle position defines the limit for each engine speed:

- If the throttle is less open than the limit the net power output is low and drops significantly for small changes of throttle position.
- If the throttle is more open than the limit the net power output is high and it is almost not affected at all by the throttle position.

That said, the area in which the WHR unit performs in the best way is the portion of the map in yellow and red of Figure 4.2-22. There, the net power output is well above 2 kW. In particular a peak is achieved at 3500 RPM where the net power output is as high as 2.69 kW for a throttle position of 34% open. The reasons why the peak occurs there are not so simple to explain.

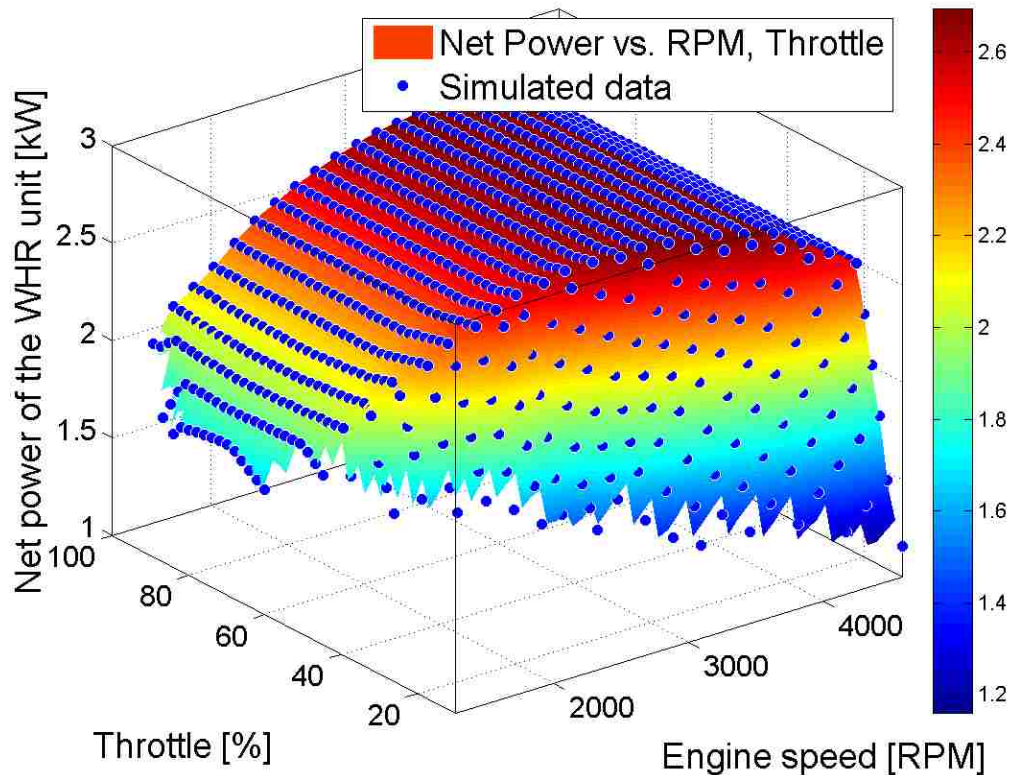


Figure 4.2-22: Net power output of the WHR unit map, speed ratio: 5.1.

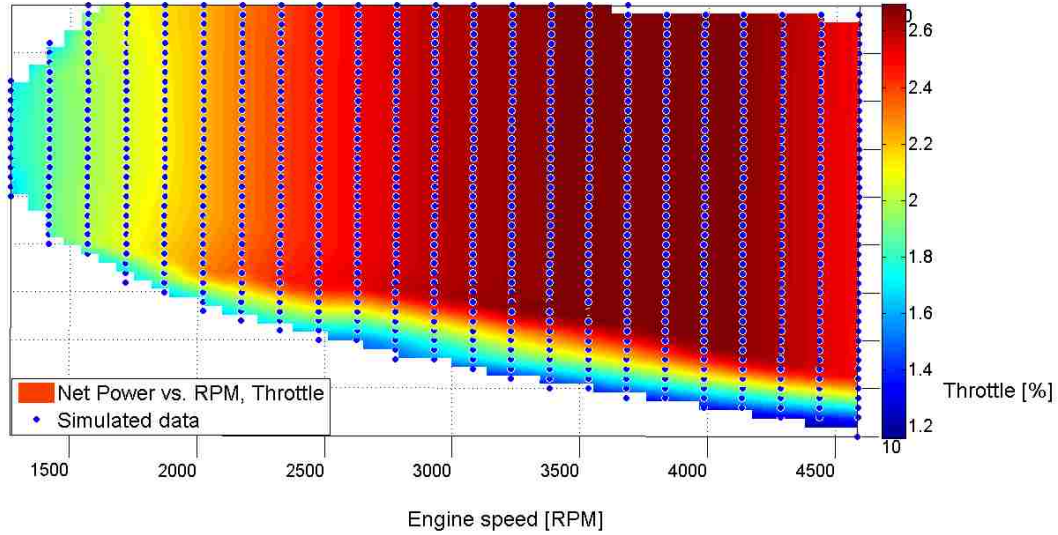


Figure 4.2-23: Top view of the net power output map, speed ratio: 5.1.

Table 4.2-26 summarizes the conditions of the exhaust gas that maximize the net power output of the WHR unit. As a matter of fact the exhaust gas temperature is not particularly high, however the mass flow rate of the exhaust gas is great, and the heat potentially available is 22.4 kW, 30% greater than the 17 kW available at target vehicle operating conditions. Moreover, the combination of expander efficiency, heat exchanger effectiveness and working fluid mass flow rate is the one that gives the maximum net power output. Anyway, the thing that counts the most is that for engine speeds between 1800 RPM and 4700 RPM the WHR unit gives outputs of more than 2 kW.

Engine speed [RPM]	Throttle position [%]	Exhaust gas temperature [°C]	Exhaust gas MFR [kg/s]	Net power output [kW]
3531	34	492.7	0.0575	2.69

Table 4.2-26: Exhaust gas condition that maximize the power output of the WHR unit.

At speeds lower than 1800 RPM the power output starts to decrease quickly even though it remains greater than 1.5 kW. So the choice of selecting these range of engine speed in which the WHR unit is turned on appears justified because even at slow engine speeds the WHR unit can still provide a significant contribution to the power delivered by the engine. Someone might point out that at engine speeds higher than 4700 RPM there still were the conditions to obtain power outputs greater than 2 kW and hence greater than that obtained around 1200 RPM. Nevertheless, in the case the range is shifted towards higher speeds, the WHR unit would be active for a shorter amount of time so the total energy that it can deliver would be lower.

To conclude the analysis of Figure 4.2-22 the smallest net power output is obtained with high engine speeds and close throttle positions, only because the exhaust gas temperature is high enough (higher than 220 °C) not to turn off the WHR unit. The minimum net power output reported is equal to 1.16 kW at 4600 RPM and with throttle open by 10%.

To sum up the analysis computed in this paragraph showed that the WHR unit is able to provide good net power outputs even at engine operating conditions far from the target one, provided that a suitable speed ratio is selected between the engine and the expander. The criteria used to select this ratio have been also presented and discussed.

4.2.5 WHR unit simulation on a standard driving cycle

The final analysis performed was to simulate the behavior of the WHR unit on a standard driving cycle. In particular the US Environmental Protection Agency (EPA), in 2008 has defined a series of four tests to measure tailpipe emissions and fuel economy of passenger cars. In the current paragraph the additional power output that the WHR unit can produce in the city driving (FTP-75) and highway driving (HWFET), the two main tests, is simulated. Starting from the data of engine speed and throttle position of the 3.6L V-6 gasoline engine throughout the two driving cycles joint together a net power output map similar to the one shown in Figure 4.2-22 is interrogated to assess the net power output of the cycle. In this case the WHR unit produces a surplus of energy that is not used to run the vehicle but that can be used to run accessories. In the future design stages, when more data will be available, simulation will be carried out to see how much the power generated by the engine can be reduced in a driving cycle, using the additional power generated by the WHR unit to run the vehicle. As a matter of fact, with the simulation reported here the engine power cannot be reduced by the amount of power generated by the WHR unit, because if the engine produces less energy its exhaust gas mass flow rate and temperature will be different, the inputs of the WHR unit change as well and so very likely the power output of the WHR will be different. In order to make a very complete analysis of the fuel savings the Matlab/Simulink model of the WHR unit created by the author has to be integrated in a global Matlab/Simulink model of the vehicle. However, the objective of the thesis is a step behind this phase, since it is the creation of the Matlab/Simulink “block” of the WHR unit that will be integrated in future in the overall vehicle model. Nonetheless the simulation results reported here can give an important indication about how much energy can be produced by the WHR unit in the standard driving cycle considered.

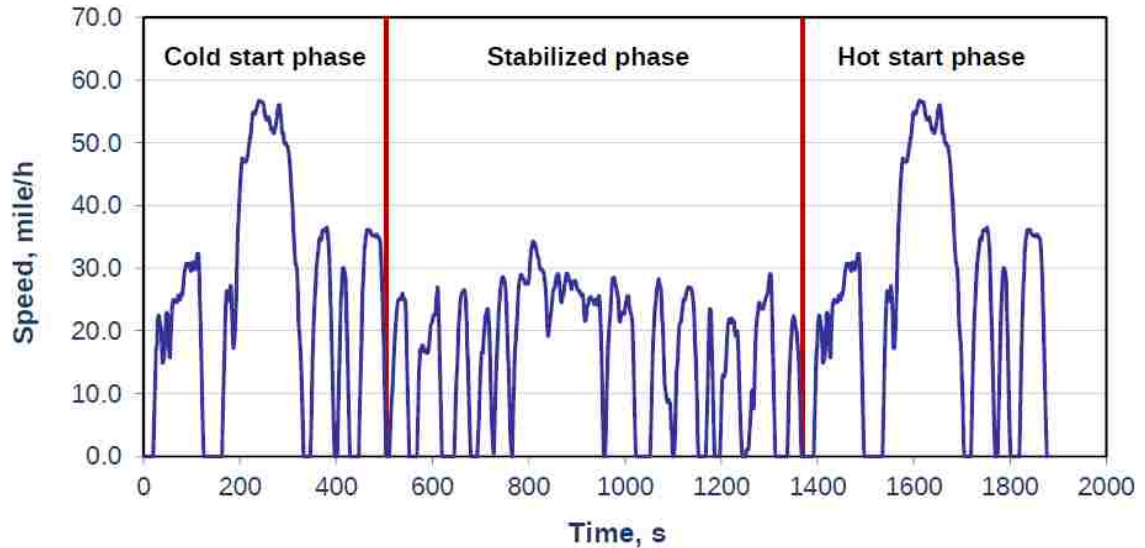


Figure 4.2-24: FTP-75 driving speed schedule [67].

Anyway, Figure 4.2-24, [67], shows the velocity profile of the FTP-75 urban driving cycle. As depicted in the figure the driving cycle is divided into three phases:

- cold start transient phase 0-505 s
- stabilized phase 506-1372 s
- hot soak (around 600 s)
- hot start transient phase 1373-1877 s.

The last phase is equal to the first one with the exception that the engine is started after being stopped for ten minutes, what it is usually called a hot start. The other parameters that summarize the cycle are:

- travelled distance: 17.77 km
- average speed: 34.12 km/h
- maximum speed: 91.25 km/h.

To this urban cycle the highway driving cycle HWFET, whose velocity profile is shown in Figure 4.2-25, [67], has been connected, with a connection period of 45 seconds where the engine is runs at idle speed. The characteristics of this second driving cycle that replicates highway driving conditions, there is a different test called US 06 for the aggressive highway driving conditions, are summarized in the bullet list below:

- total distance: 16.45 km
- average speed: 77.7 km/h
- maximum speed: 97 km/h.

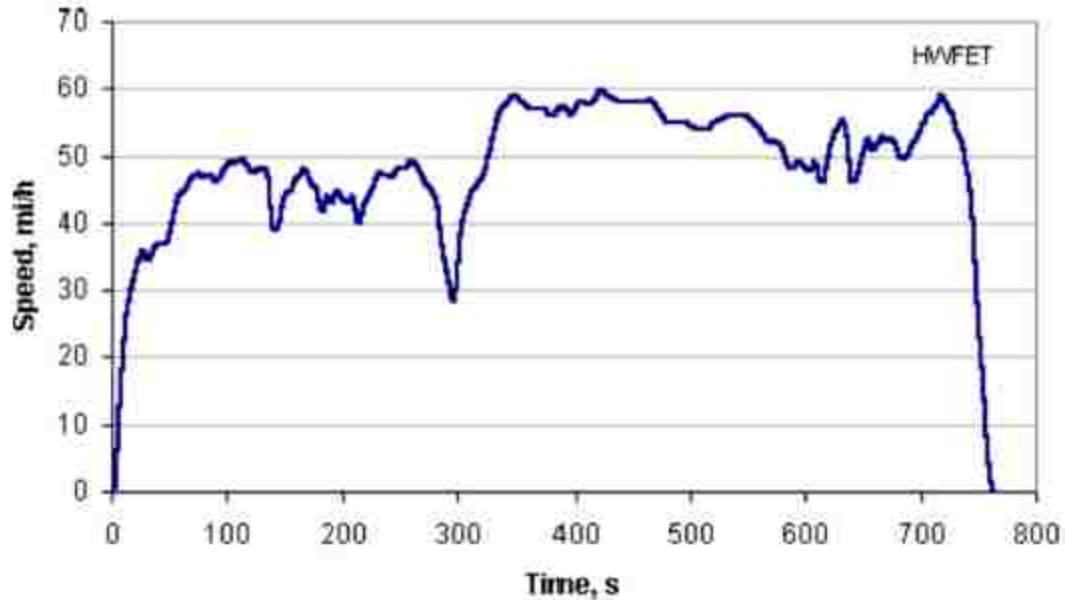


Figure 4.2-25: HWFET driving speed schedule [67].

While in the urban cycle there are 23 stops over a period of 31 minutes, in the HWFET there are no stops in a period of ten minutes. So the WHR unit is expected to be active for a longer period of time during the HWFET than in the FTP-75.

The two driving cycles just presented have been joint together making a single driving cycle with a total duration of 2696 s. The engine speed and throttle position profiles correspondent to this driving cycle are illustrated in Figure 4.2-27 and Figure 4.2-28 where the red vertical line divides the FTP-75 from the HWFET. In paragraph 4.2.4 the speed ratio between the engine speed and the expander speed selected (5.1) allowed to activate the WHR unit in an engine speed range that goes from 1200 to 4700 RPM. However, looking at the chart, it is evident that for a significant period of time (30% of the total testing time) the WHR does not work only for the limitation on the expander minimum and maximum speed. Since the objective is to have the WHR unit active as long as possible the speed ratio selected was of 7.5, the resulting engine speed range goes from 800 to 3200 and during 83% of the testing time the engine speed falls within this range. Although the speed ratio, once defined, cannot be changed, the author has decided to change it in order to optimize the WHR unit for this particular kind of application. Then, when the system will be installed in production vehicles, the speed ratio that makes the WHR unit generate power in the most frequently used operating conditions, will be selected by the automaker. Taking into account the real driving style of the users the speed ratio of 5.1 selected in the previous paragraph appears to be the right one. However, only for the purpose of obtain the best possible performances in the driving cycle considered here, the speed ratio selected is equal to 7.5. The new net power output map employed is shown in Figure 4.2-26.

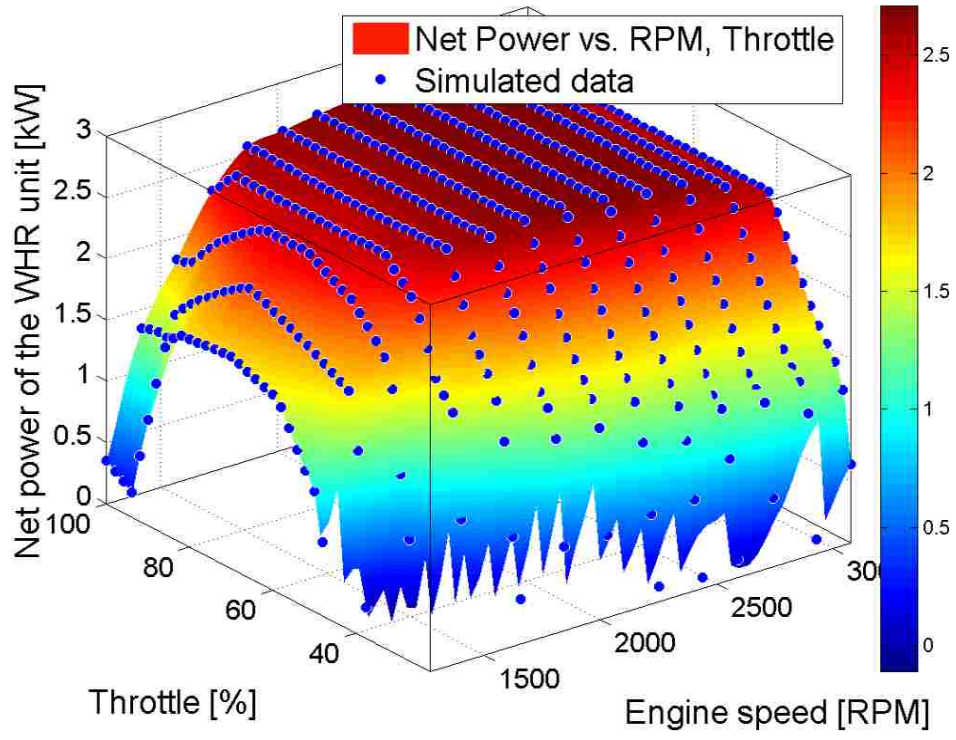


Figure 4.2-26: Net power output of the WHR unit map, speed ratio: 7.5.

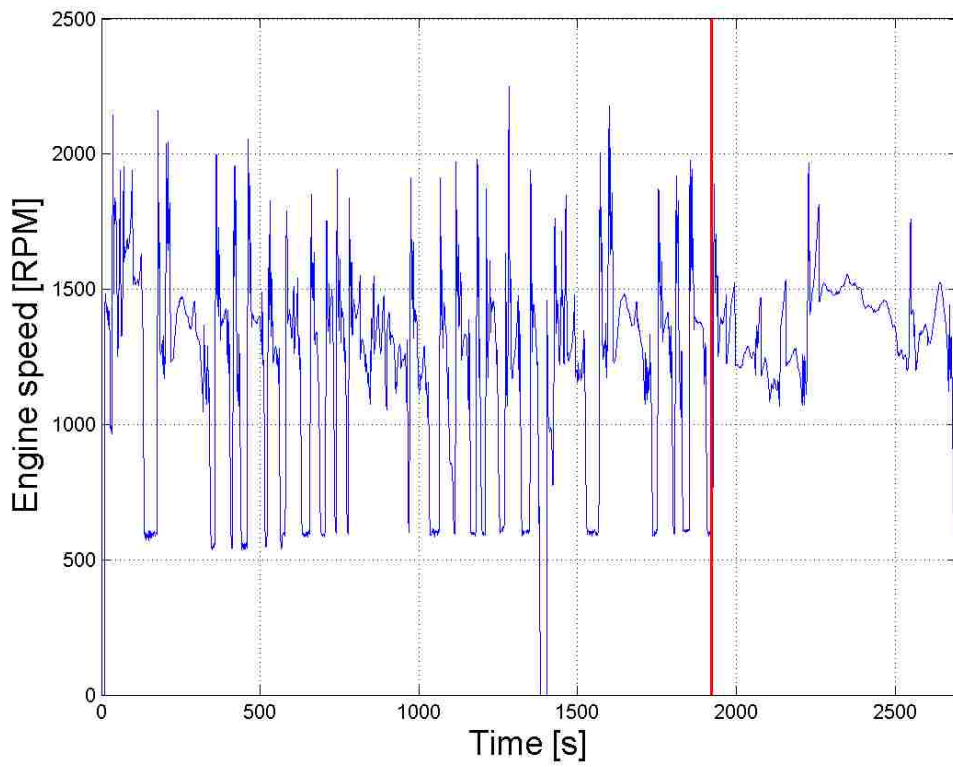


Figure 4.2-27: Engine speed profile, FTP-75 + HWFET.

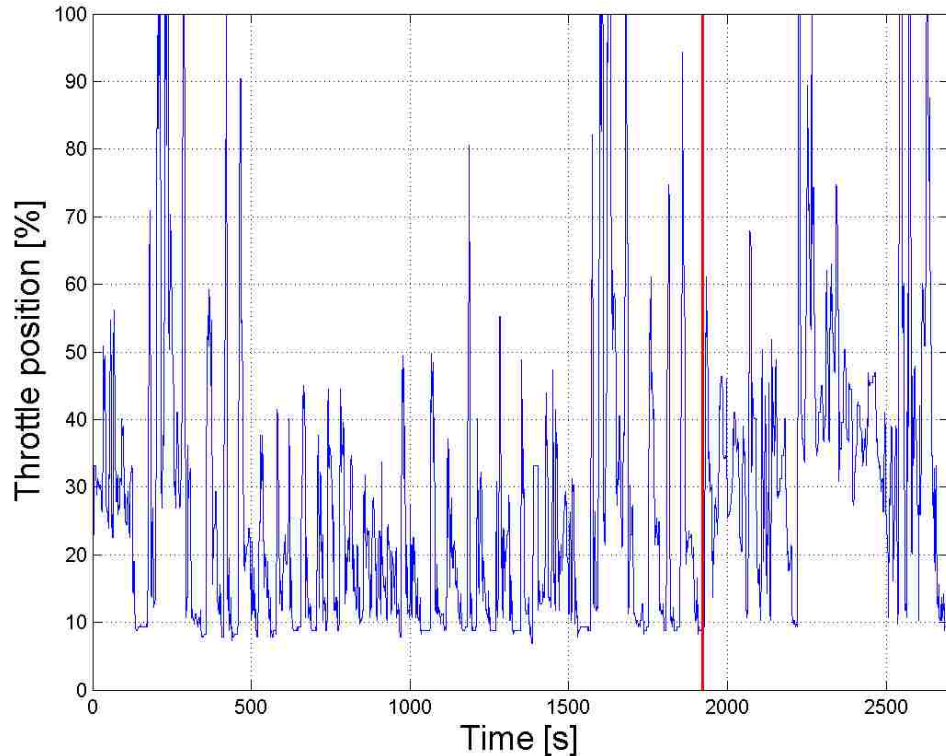


Figure 4.2-28: Throttle position profile, FTP-75 + HWFET.

Still for the same reason the lower limit of the exhaust gas temperature at which the WHR unit is turned on has been lowered of 40 °C to 180 °C. In the previous paragraph the limit was set to 220 °C because it is the minimum temperature necessary to eventually have the working fluid expander inlet temperature equal to 210 °C respecting the pinch point specification of the boiler. Despite of that, even if the temperature at the expander inlet is lower than the optimal one (210 °C), the WHR unit generates power. So in it is better to recover also this power lowering the limit of the exhaust gas temperature. A threshold of 180 °C has been selected because at the expander inlet temperature the working fluid can reach a temperature of 170 °C (180 – 10 °C of pinch point minimum temperature difference) that is higher enough than the saturated vapor temperature, that for the R245fa at 2100 kPa is equal to 124.3 °C, to operate away from the two-phase zone and high enough to obtain a expander outlet temperature higher than the pump outlet one end hence justify the presence of the recuperator. This feature adopted has not brought significant improvement to the total time in which the WHR unit is turned on during the cycle, however it appears to be the right control strategy also for future applications. Figure 4.2-29 and Figure 4.2-30 illustrate respectively the exhaust gas temperature and mass flow rate, whereas Figure 4.2-31 shows the heat available in the exhaust gas, so basically the heat that can be recovered if the exhaust gas was expanded down to a temperature of 100 °C.

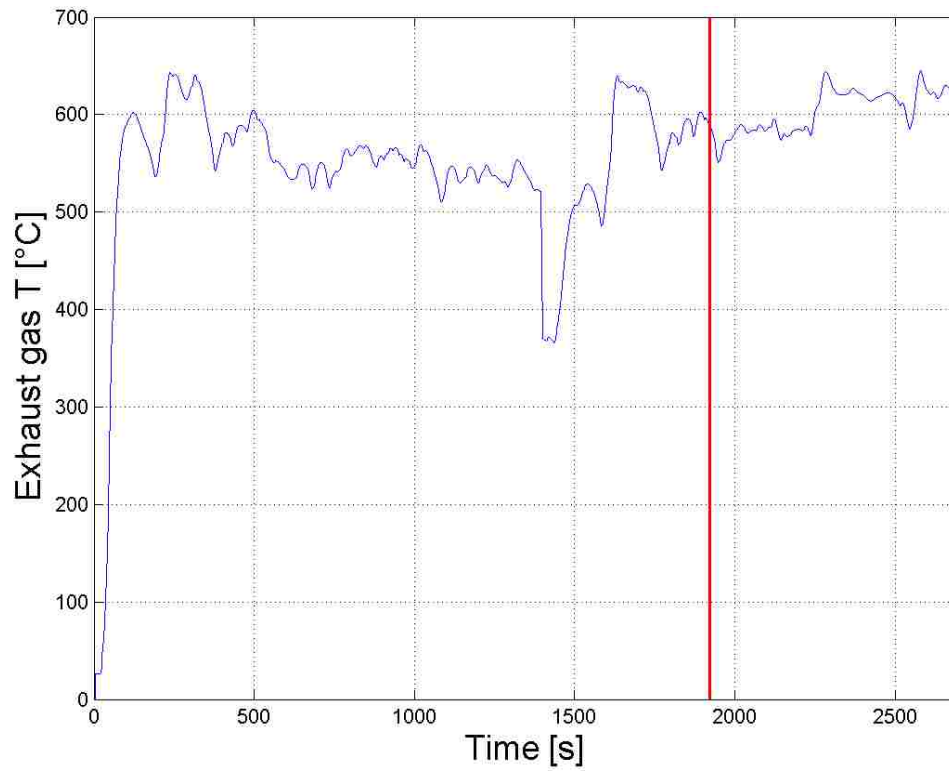


Figure 4.2-29: Exhaust gas temperature profile, FTP-75 + HWFET.

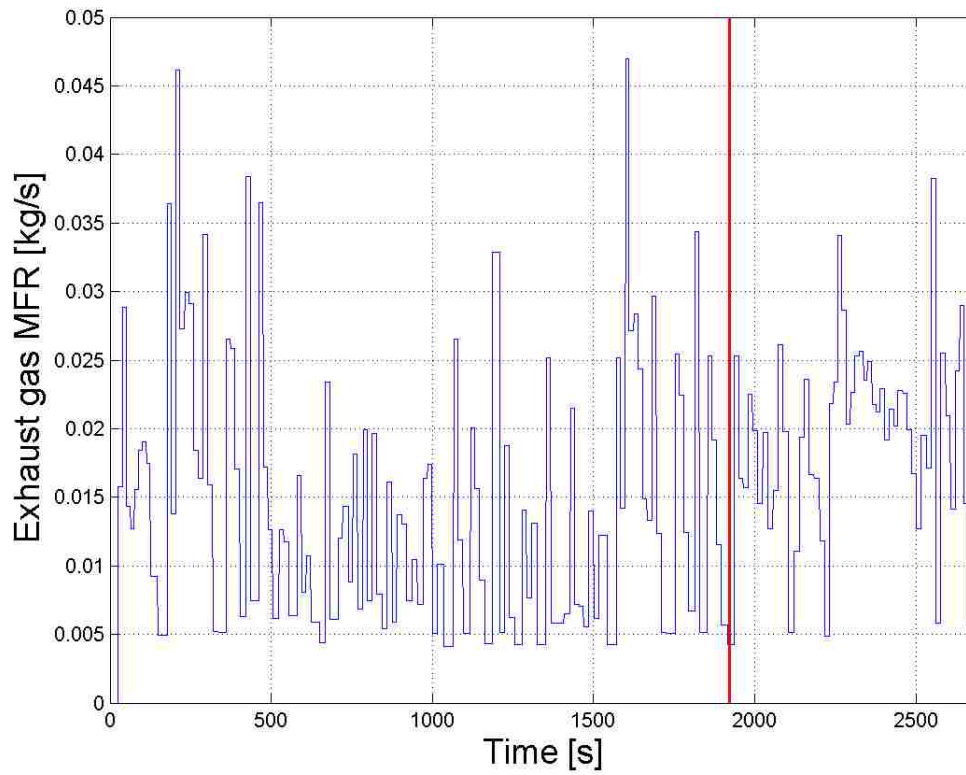


Figure 4.2-30: Exhaust gas mass flow rate profile, FTP-75 + HWFET.

In particular the exhaust gas temperature is below the threshold assigned to the model, only for few seconds at the beginning of the FTP-75 driving cycle.

The simulation results gathered are plotted in Figure 4.2-32 and Figure 4.2-33. As we can see from the net power plot very rarely the net power output goes above 2.5 kW as someone could think from the maps presented above (see Figure 4.2-22 and Figure 4.2-26). This happens because in transient conditions the exhaust gas temperature does not strictly follow the map (see Figure 4.2-21) obtained at stationary operating conditions. Moreover, the mass flow rate of the exhaust gas is low if compared to the 0.035 kg/s used in the stationary analysis of paragraph 4.2.2. That said the WHR unit generates useful power for 921 seconds out of the total 2696 seconds correspondent to 34% of the total testing time. The average net power, averaged on the whole testing period, is 0.5492 kW. This and other information are grouped in Table 4.2-27. In the first two columns the time in which the WHR unit generates power and the total time of the test. The third is simply the ratio between these two values expressed as a percentage.

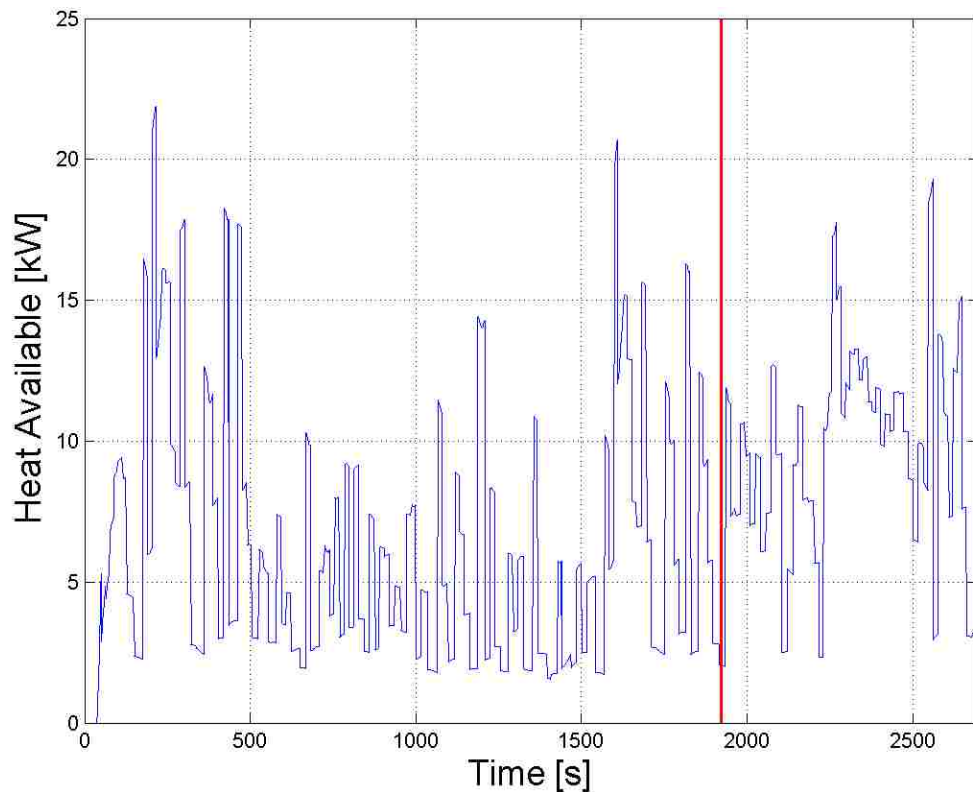


Figure 4.2-31: Exhaust gas heat available profile, FTP-75 + HWFET.

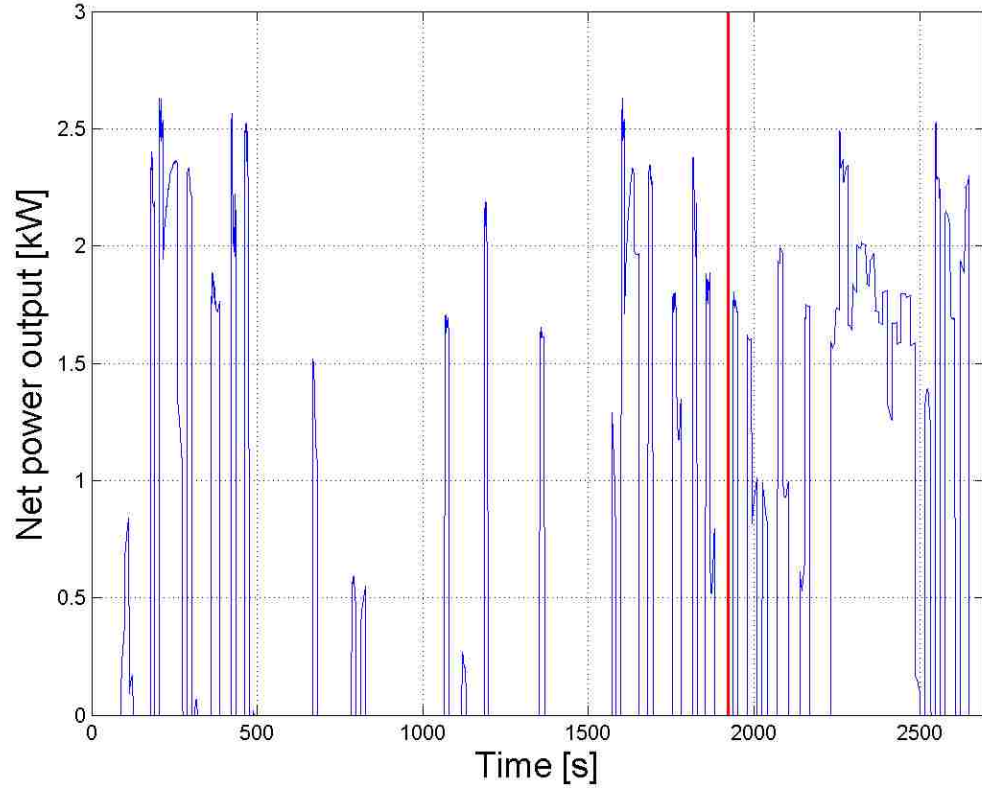


Figure 4.2-32: Net power output of the WHR unit, FTP-75 + HWFET.

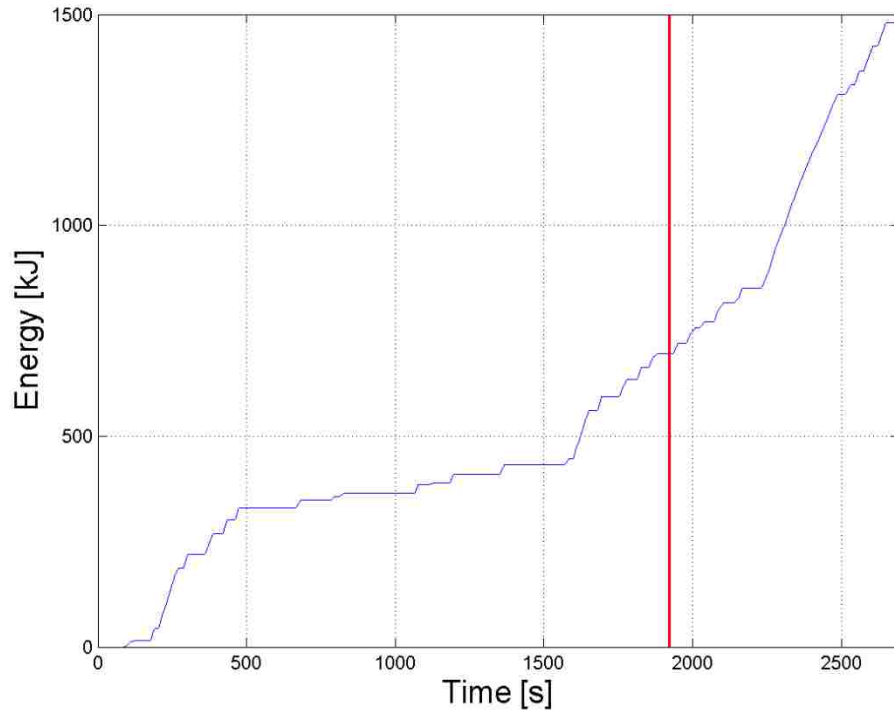


Figure 4.2-33: Total energy recovered by the WHR unit, FTP-75 + HWFET.

The fourth column is the energy produced by the system in the cycle so basically summing the net power outputs of the system at each second. At last the fifth and sixth columns are the net power output of the cycle averaged respectively on the time in the WHR unit was activated (ON) and on the total testing time.

	Time WHR unit ON [s]	Total time [s]	Time WHR unit ON [%]	Energy produced [kJ]	Average net power on time ON [kW]	Average net power on total time [kW]
FTP-75	442	1922	23%	695.2	1.57	0.36
HWFET	479	774	62%	785.4	1.64	1.01
Total	921	2696	34%	1480.6	1.61	0.55

Table 4.2-27: Driving cycle simulation results summary.

As appears evident during the high way drive the performances obtained with the WHR unit are significantly better than those obtained in the urban driving cycle (FTP-75). The WHR unit is “ON” 62% of the total time in the HWFET cycle whereas only for 23% of the total FTP-75 cycle time. So even though the FTP-75 lasts more than twice longer than the HWFET the energy produced by the WHR unit during the latter cycle is greater (look at the fourth column of the table above). Moreover, also considering only the period of time in which the WHR unit is “ON” the average net power output is higher in the HWFET cycle, mainly because the average exhaust gas heat available is higher as depicted in Figure 4.2-31. In short, the much better performances, in absolute terms, obtained during the HWFET cycle have shown that during highway driving the energy that can be recovered is higher and the time in periods in which the WHR can operate are longer.

Now, looking at the energy plot of Figure 4.2-33, it can be seen how in the period that goes from second 500 to about second 1500 the energy produced is very low. This period corresponds to the second of the three parts in which the FTP-75 test is divided. On the other hand the low point of the exhaust gas temperature, see Figure 4.2-29, right before second 1500 corresponds to the hot start of the engine after it was stopped by 10 minutes. It is also interesting to compare the energy generated by the WHR unit in the first part of the FTP-75, called “cold start”, to the one generated in the third part, “hot start”. The vehicle velocity profile, as previously mentioned, of these two parts is equal. The fuel consumption is in general greater in the first part, “cold start”, because there is a warm up period in which the engine efficiency is lower. A lower engine efficiency means a greater heat ejected with the exhaust gas, in fact during the “cold start” period the average heat available in the exhaust gas is 7.9 kW whereas during the “hot start” period it is 6.4 kW.

However, the heat available is converted by the WHR unit into useful power, so a greater amount of heat available means a greater net power output, and once again this statement is confirmed by the result:

- energy produced during the “cold start” phase of the FTP-75 test: 330 kJ
- energy produced during the “hot start” phase of the FTP-75 test: 263 kJ.

This finding, although it seems trivial, demonstrates how much the WHR unit could potentially reduce the fuel consumption. At given vehicle operating conditions it supplies more power when the efficiency of the engine is lower, so in the most critical condition from a fuel saving test perspective.

Finally simply dividing the net power output by the heat available the WHR (total) efficiency is obtained. The maximum values of the total efficiency are the same as those found in the previous paragraphs for R245fa, around 15%. Globally the efficiency is high, meaning that the net power output of the system is simply function of the heat available. However, there are few points in which the total efficiency is low, even close to only 3%. In these few points the system operates beyond the limit of throttle position and engine RPM already encountered in paragraph 4.2.4.

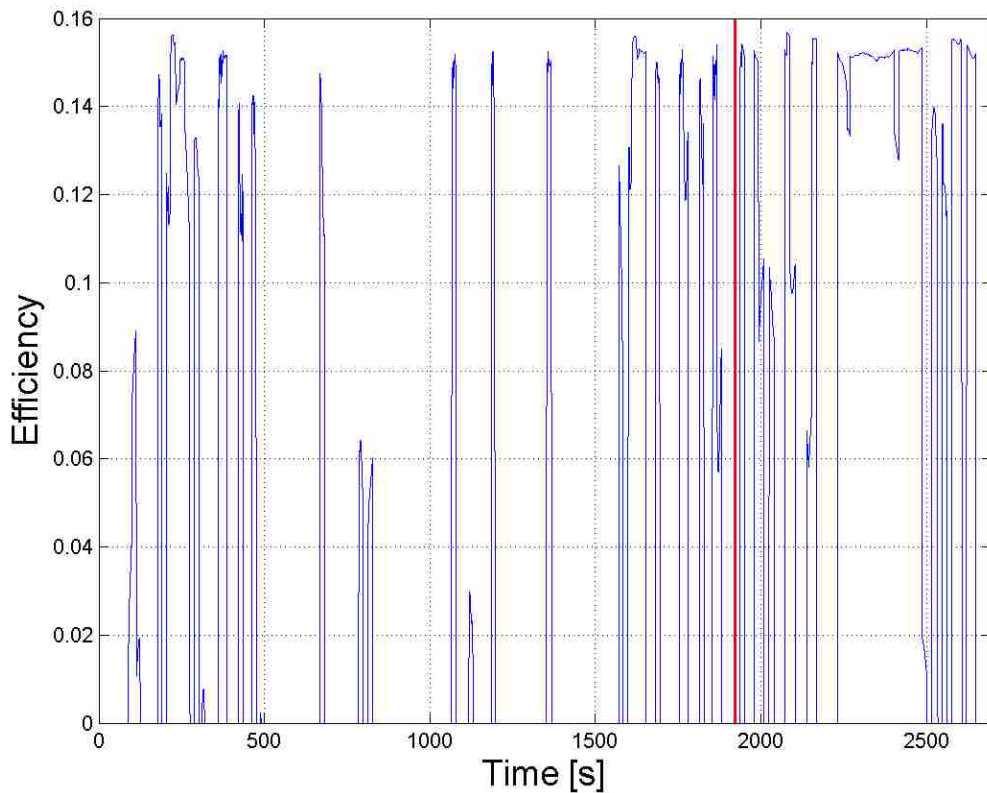


Figure 4.2-34: WHR unit total efficiency profile, FTP-75 + HWFET.

5. CONCLUSIONS AND RECOMMENDATIONS

5.1 Methodology summary

This thesis has assessed the feasibility of using a WHR unit based on an ORC in passenger vehicles. In order to do that two simulation software created by the author have been employed:

- The first one, called preliminary model, was developed entirely in Matlab environment and had several limitations. However, it has been utilized to understand the ORC parameters and alternatives that maximize the power output.
- The second model, called detailed model, was developed in Simulink/Matlab environment from the indications obtained with the preliminary analysis. The majority of the simulations and the results illustrated come from this model. After being calibrated with the results of experimental tests already carried out on a test rig, it has been used to accurately predict the net power output that the Waste Heat Recovery unit can provide in different operating conditions, stationary and non-stationary. A short comparison of the results achievable with working fluids that were not treated in the preliminary model has been also done.

5.2 Preliminary model findings

The findings obtained with the preliminary model are summarized in the following bullet list:

- The higher the expander inlet pressure of an Organic Rankine Cycle the greater the net power output. However, there are three limitations to such pressure: pump maximum pressure rise (pump head), working fluid critical pressure, and expander maximum pressure (usually the most stringent).
- The higher the expander inlet temperature, the higher the net power output of a recuperative ORC. Whereas in a standard ORC the optimal amount of superheat depends on the slope of the isobaric curves in the superheated region of the T-s diagram. If a fluid exhibits a steeper slope for the isobaric curve in the high-pressure region than in the low-pressure region, the net power output increases as the expander inlet temperature rises [3].

- The maximum net power output achievable with a recuperative ORC is always greater than that achievable with a standard ORC, no matter the working fluid utilized. Although it costs more, a greater amount of working fluid mass flow rate is usually required and the complexity of the system is increased.
- Six criteria to compare the working fluids have been established: thermodynamic properties, chemical compatibility, safety, environmental aspects, costs and performances. Among those considered, the best working fluid appears to be R245fa. It has good thermodynamic properties, which allow it to generate a great amount of power. In addition to that it is not being classified as dangerous (safety group B1), it has an ODP equal to zero so it will be not phased out, as other refrigerants, in the next few years.

5.3 Detailed model findings and results

The detailed model has been set up and calibrated using the available experimental test data. The simulated net power output, cycle efficiencies and power exchanged deviate less than 5% from the measured values. The simulations performed with this model provided the following outcomes:

- The exhaust gas temperature and mass flow rate, evaluated at reference vehicle operating conditions (constant speed 70 MPH, engine speed 2465 RPM and a torque of 125 Nm), have been used as input of the model to analyze the system in steady state conditions. Detailed performance maps of the components adopted were employed to make the simulation even more accurate. A recuperative ORC, with R245fa as working fluid, operating at maximum possible pressure and temperature at the expander inlet gives a net power output of 2.44 kW that corresponds to 8.47% of the power provided by the engine.
- At the same exhaust gas conditions of the previous point, three other working fluids have been tested: R134a, water and ethanol. R134a returned a very low power output of 0.33 kW. On the other hand water and ethanol provided an acceptable net power output, respectively of 1.4 kW and 1.32 kW. However, with both working fluids, especially water, there was the risk to have liquid droplets formation at the expander inlet and outlet. Moreover, it was not even possible to utilize the recuperator with water because the expander outlet temperature was too close to the pump outlet one. The exhaust gas does not contain enough energy to bring water and ethanol from a liquid state to a vapor state. R245fa remains the optimal working fluid.

- The considerations that have to be made to connect the WHR unit to a real engine and make it operate in a wide range of engine speeds and throttle positions have been discussed. By means of the detailed model a map with the net power output achievable by the WHR unit with different combinations of engine speeds and throttle positions has been drawn. In particular when the throttle is partially open and the engine speed is slow the net power output of the cycle significantly drops. For high engine speeds (between 2000 and 5000 RPM) the net power output achievable increases and stays between 2.4 to 2.6 kW even when the throttle is partially open. However, the vehicle is most frequently operated with engine speeds that are within 1000 and 3500 RPM. So the range in which the expander operates has to be selected making a trade-off between the two aspects considered: frequency of usage of the engine speed and potential net power output of the system.
- The net power output of the WHR unit has been estimated, using the engine speed, exhaust gas temperature and mass flow rate profiles generated by an engine during a standard driving cycle commonly employed to assess fuel consumption. This cycle is made up of two different parts that replicate respectively urban and highway driving conditions. The heat available in the exhaust gas, the net power output of the WHR unit and the energy generated by the WHR unit were assessed. For this particular kind of application a different speed ratio was selected in order to recover energy even at engine speeds as low as 800 RPM. The results obtained showed how the WHR unit was active for 34% of the total testing time generating an average power of 0.55 kW. However, if only the highway driving portion of the driving cycle is considered the time in which the WHR unit is ON increases to 62% and the mean net power output goes up to 1.01 kW. Moreover, it has been shown how at given vehicle operating conditions, basically at a given vehicle speeds, the net power output of the WHR is greater for lower engine efficiencies, simply because more heat is available to be recovered in the exhaust gases.

5.4 Recommendations

The application of a WHR system appears particularly suitable for vehicle models that travel a lot of miles (or kilometers) in highways at constant speed. In fact it should be underlined, that the controls of a real WHR unit based on ORC is the most critical aspect of this technology. Especially if the expander is mechanically connected to the engine shaft, it is very difficult to turn on and off the WHR unit suddenly and frequently.

As a matter of fact the connection between engine and expander still has to be studied accurately, and it is a very critical aspect too. Anyway, it is correct to state that the WHR unit should be set up in order that once it is turned ON it can operate for a period of time longer than few seconds. Nevertheless the results obtained through simulation in the early design stages of the system have strengthened the conviction that such a WHR system is a very effective solution to generate additional power. Further investigations addressing estimates of the actual fuel savings, including also the added mass of the components, should be performed in future works.

If the necessary data are available, the simulations should be repeated for varying exhaust gas specific heat and for a system designed to accommodate properties of water and ethanol, because in this investigation the design of the heat exchangers was optimized for R245fa and not water and ethanol.

Finally, the features that an ideal WHR unit must have, according to what has been found out in this work, are summarized. It should be made up by a recuperative ORC with R245fa operating at the maximum possible expander inlet temperature and pressure, and at the lowest possible condensing temperature (usually 40 °C). Moreover, the WHR system should operate in driving conditions where the exhaust gas mass flow rate and temperature are almost constant, such as those typical of a highway drive. Hence, if a direct connection between crank shaft and expander is chosen, a speed ratio, that allows the expander to safely operate at the engine speeds typical of a highway drive, has to be selected.

Bibliography

- [1] M. Saad, *Thermodynamics for Engineers*, Englewood Cliffs, NJ: Prentice-Hall, 1966.
- [2] M. O. Bamgbopa, "Modeling and performance evaluation of an organic Rankine cycle (ORC) with R245fa as working fluid," Middle East Technical University, 2012.
- [3] T. C. Hung, T. Y. Shai and S. K. Wang, "A review of organic rankine cycles (ORCs) for recovery of low-grade waste heat," *Energy*, vol. 22, no. 7, pp. 661-667, 1997.
- [4] N. Hall and W. Ibele, *Engineering Thermodynamics*, Englewood Cliffs, NJ: Prentice-Hall, 1960.
- [5] B. Saleh, G. Koglbauer, M. Wendland and J. Fischer, "Working fluids for low-temperature organic Rankine cycles," *Energy*, vol. 32, pp. 1210-1221, 2007.
- [6] I. Vaja and A. Gambarotta, "Internal Combustion Engine (ICE) bottoming with Organic Rankine Cycles (ORCs)," *Energy*, vol. 35, pp. 1084-1093, 2010.
- [7] A. Schuster, S. Karellas and R. Aumann, "Efficiency optimization potential in supercritical Organic Rankine Cycles," *Energy*, vol. 35, pp. 1033-1039, 2010.
- [8] A. Bracco, *Study and simulation of an exhaust gas heat recovery system of a vehicle*, Turin, Italy: Polytechnic of Turin, Master thesis, 2008.
- [9] G. Wall, "Exergy - a useful concept.," Physical Resource Theory Group, Chalmers University of Technology, Goteborg, Sweden, 1986. [Online]. Available: <http://exergy.se/goran/thesis>. [Accessed 28 10 2013].
- [10] K. Harada, "Development of a Small Scale Scroll Expander," Oregon State University, 2010.
- [11] J. Larjola, "Electricity from industrial waste heat using high-speed organic Rankine cycle (ORC)," *International Journal of Production Economics*, vol. 41, no. 1 - 3, pp. 227 - 235, 1995.
- [12] C. Invernizzi, P. Iora and P. Silva, "Bottoming micro-Rankine cycles for micro-gas turbines," *Applied Thermal Engineering*, vol. 27, pp. 100-110, 2007.
- [13] M. Yari and S. M. S. Mahmoudi, "A thermodynamic study of waste heat recovery from GT-MHR using organic Rankine cycles," *Heat Mass Transfer*, vol. 47, pp. 181-196, 2011.
- [14] C. Song, "Fuel processing for low-temperature and high-temperature fuel cells: Challenges, and opportunities for sustainable development in the 21st century," *Catalysis Today*, vol. 77, no. 1-2, pp. 17-49, 2002.

- [15] "IPCC Fourth Assessment report, WG III," 2007.
- [16] European Commission,
 "http://ec.europa.eu/clima/policies/transport/vehicles/cars/faq_en.htm," [Online]. [Accessed 28 10 2013].
- [17] A. Mittica, "Combustion engines and their application to vehicle course notes," Department of Energy, Polytechnic of Turin, Turin, Italy, 2012.
- [18] R. Stobart and R. Weerasinghe, "Heat Recovery and Bottoming Cycles for SI and CI engines - A perspective," *SAE Technical Paper 2006-01-0662*, 2006.
- [19] T. Endo, S. Kawajiri, Y. Kojima, K. Takahashi, T. Baba, S. Ibaraki, T. Takahashi and M. Shinohara, "Study on Maximizing Exergy in Automotive Engines," *SAE Technical Paper 2007-01-0257*, 2007.
- [20] X. Zhang, K. Zeng, S. Bai, Y. Zhang and M. He, "Exhaust Recovery of Vehicle Gasoline Engine Based on Organic Rankine Cycle," *SAE Technical Paper 2011-01-1139*, 2011.
- [21] H. Teng, J. Klaver, T. Park, G. L. Hunter and B. van der Velde, "A Rankine Cycle System for Recovering Waste Heat from HD Diesel Engines - WHR System Development," *SAE Technical Paper 2011-01-0311*, 2011.
- [22] Q. E. Hussain, D. R. Bringham and C. W. Maranville, "Thermoelectric Exhaust Heat Recovery for Hybrid Vehicles," *SAE Technical Paper 2009-01-1327*, 2009.
- [23] C. Baker and L. Shi, "Experimental and Modeling Study of a Heat Exchanger Concept for Thermoelectric Waste Heat Recovery From Diesel Exhaust," *SAE Technical Paper 2012-01-0411*, 2012.
- [24] E. F. Doyle and P. S. Patel, "Compounding the Truck Diesel Engine with an Organic Rankine-Cycle System," *SAE Technical Paper 760343*, 1976.
- [25] E. Doyle, L. DiNanno and S. Kramer, "Installation of a Diesel-Organic Rankine Compound Engine in a Class 8 Truck for a Single-Vehicle Test," *SAE Technical Paper 790646*, 1979.
- [26] H. Teng, J. Klaver, T. Park, G. L. Hunter and B. van der Velde, "A Rankine Cycle System for Recovering Waste Heat from HD Diesel Engines - Experimental Results," *SAE Technical Paper 2011-01-1337*, 2011.
- [27] H. Teng and G. Regner, "Improving Fuel Economy for HD Diesel Engines with WHR Rankine Cycle Driven by EGR Cooler Heat Rejection," *SAE Technical Paper 2009-01-2913*, 2009.

- [28] D. Seher, T. Lengenfelder, J. Gerhardt, N. Eisenmenger, M. Hackner and L. Krinn, "Waste Heat Recovery for Commercial Vehicles with a Rankine Process," in *21st Aachen Colloquium Automobile and Engine Technology 2012*, Stuttgart, Germany, 2012.
- [29] C. Nelson and Cummins Research and Technolgy, "Exhaust Energy Recovery," in *Diesel Engine-Efficiency and Emissions Research (DEER) Conference*, Deaborn, MI, USA, 2008.
- [30] R. El Chammas and D. Clodic, "Combined Cycle for Hybrid Vehicles," *SAE Technical Paper 2005-01-1171*, 2005.
- [31] A. Boretti, "Recovery of exhaust and coolant heat with R245fa organic Rankine cycles in a hybrid passenger car with naturally aspirated gasoline engine," *Applied Thermal Engineering*, vol. 36, pp. 73-77, 2012.
- [32] S. Bae, H. Heo, H. Lee, D. Lee, T. Kim, H. Lee, J. Park and C. Kim, "Performance Characteristics of a Rankine Steam Cycle and Boiler for Engine Waste Heat Recovery," *SAE Technical Paper 2011-28-0055*, 2011.
- [33] J. Ringler, M. Seifert, V. Guyotot, W. Hubner and BMW Research and Technology, "Rankine Cycle for Waste Heat Recovery of IC Engines," *SAE Technical Paper 2009-01-0174*, 2009.
- [34] Hypercat ACP, "<http://www.hypercat-acp.com/non-selective-catalytic-reduction.html>," Metalico Inc. [Online]. [Accessed 28 10 2013].
- [35] "Car Diesel Selective Catalytic Reduction," 30 April 2009. [Online]. Available: <http://vehicletransport.blogspot.it/2009/04/car-diesel-selective-catalytic.html>. [Accessed 28 10 2013].
- [36] A. Boretti, "Transient operation of internal combustion engines with Rankine waste heat recovery systems," *Applied Thermal Engineering*, vol. 48, pp. 18-23, 2012.
- [37] K. M. Lee, S. F. Kuo, M. L. Chien and Y. S. Shih, "Parameters analysis on organic Rankine cycle energy recovery system," *Energy Conversion and Management*, vol. 28, no. 2, pp. 129 - 136, 1988.
- [38] ASHRAE, *Designation and Safety Classification of Refrigerants standard 34 2007*.
- [39] H. Chen, Y. Goswami and E. Stefanakos, "A review of thermodynamic cycles and working fluids for the conversion of low-grade heat," *Renewable and Sustainable Energy Reviews*, vol. 14, pp. 3059-3067, 2010.
- [40] R. P. Scaringe and L. R. Grzyll, "An Explanation of the Refrigerant Designation Numbering System," [Online]. Available:

- <http://www.rogersrefrig.com/Refrigerant%20Designation%20Numbering%20System.htm>.
[Accessed 28 10 2013].
- [41] B. Liu, K. Chien and C. Wang, "Effect of working fluids on organic Rankine cycle for waste heat recovery," *Energy*, vol. 29, pp. 1207-1217, 2004.
- [42] V. Maizza and A. Maizza, "Working fluids in non-steady flows for waste energy recovery systems.," *Applied Thermal Engineering*, vol. 16, pp. 579-590, 1996.
- [43] T. Yamamoto, T. Furuhashi, N. Arai and K. Mori, "Design and testing of the Organic Rankine Cycle," *Energy*, vol. 26, pp. 239-251, 2001.
- [44] S. Quoilin, "Experimental study and modeling of a low temperature Rankine cycle for small scale cogeneration. Thesis," University of Liège (Belgium), 2007.
- [45] L. Calderazzi and P. C. Paliano, "Thermal stability of R-134a, R-141b, R-131I, R-7146, R-125 associated with stainless steel as a containing material," *International Journal of Refrigeration*, vol. 20, no. 6, pp. 381-389, 1997.
- [46] W. C. Andersen and T. J. Bruno, "Rapid screening of fluids for chemical stability in organic Rankine cycle applications," *Industrial and Engineering Chemistry Research*, vol. 44, pp. 5560-5566, 2005.
- [47] "OZONE DEPLETION and Global Environmental Change," CIESIN Thematic Guides, [Online]. Available: <http://www.ciesin.org/TG/OZ/odp.html>. [Accessed 28 10 2013].
- [48] "IPCC Fourth Assessment Report: Climate Change 2007," IPCC intergovernmental panel on climate change, [Online]. Available: http://www.ipcc.ch/publications_and_data/ar4/wg1/en/tssts-2-5.html. [Accessed 28 10 2013].
- [49] S. Quoilin, "Sustainable Energy Conversion Through the Use of Organic Rankine Cycle for Waste Heat recovery and Solar Applications. Thesis," University of Liège (Belgium), 2011.
- [50] H. Wang, R. B. Peterson and T. Herron, "Experimental performance of a compliant scroll expander for an organic Rankine cycle," *J. Power and Energy*, vol. 223 Part A, pp. 863-872, 2009.
- [51] J. S. Baek, E. A. Groll and P. B. Lawless, "Piston-cylinder work producing expansion device in a transcritical carbon dioxide cycle. Part I: experimental investigation," *International Journal of Refrigeration*, vol. 28, no. 2, pp. 141-151, 2005.
- [52] M. b. Mohd. Tahir, N. Yamada and T. Hoshino, "Efficiency of Compact Organic Rankine Cycle System with Rotary-Vane-Type Expander for Low-Temperature Waste Heat

- Recovery," *International Journal of Civil Environmental Engineering*, vol. 2, no. 1, pp. 11-16, 2010.
- [53] G. Haiqing, M. Yitai and L. Minxia, "Some design features of CO swing piston expander," *Applied Thermal Engineering*, vol. 26, no. 2-3, pp. 237-243, 2006.
- [54] X. Wang, L. Zhao, J. Wang, W. Zhang, X. Zhao and W. Wu, "Performance evaluation of a low-temperature solar Rankine cycle system utilizing R245fa," *Solar Energy*, vol. 84, no. 3, pp. 353-364, 2010.
- [55] V. Lemort, S. Quolin, C. Cuevas and J. Lebrun, "Testing and modeling a scroll expander integrated into an Organic Rankine Cycle," *Applied Thermal Engineering*, vol. 29, pp. 3094-3102, 2009.
- [56] E. Oralli, A. Tarique, C. Zamfirescu and I. Dincer, "A study on scroll compressor conversion into expander for Rankine cycles," *International Journal of Low-Carbon Technologies*, vol. 6, pp. 200-206, 2011.
- [57] N. P. Halm, Y. Chen, E. A. Groll and J. E. Braun, "Mathematical modeling of scroll compressors-part I: compression process modeling," *International Journal of Refrigeration*, vol. 25, no. 6, pp. 731-750, 2002.
- [58] B. Aoun and D. Clodic, "Theoretical and experimental study of an oil-free scroll type vapor expander," in *In Proceedings of the 19th International Compressor Engineering Conference*, Purdue, 2008.
- [59] T. Yanagisawa, Y. Fukuta, T. Ogi and T. Hikichi, "Performance of an oil-free scroll-type air expander," *In Proceedings of the IMechE Conference Transactions on Compressors and their systems*, pp. 167-174, 2001.
- [60] A. Schuster, S. Karellas, E. Kakaras and H. Spliethoff, "Energetic and economic investigation of Organic Rankine Cycle applications," *Applied Thermal Engineering*, vol. 29, no. 8, pp. 1809-1817, 2009.
- [61] E. Wang, H. Zhang, B. Fan, M. Ouyang, Y. Zhao and Q. Mu, "Study of working fluid selection of organic Rankine cycle (ORC) for engine waste heat recovery," *Energy*, vol. 36, pp. 3406-3418, 2011.
- [62] S. Quolin, V. Lemort and J. Lebrun, "Experimental study and modeling of an Organic Rankine Cycle using scroll expander," *Applied Energy*, vol. 87, pp. 1260-1268, 2010.
- [63] K. K. Srinivasan, P. J. Mago and S. R. Krishnan, "Analysis of exhaust waste heat recovery from a dual fuel low temperature combustion engine using an Organic Rankine Cycle,"

- Energy*, vol. 35, pp. 2387-2399, 2010.
- [64] R. K. Shah and D. P. Sekulic, *Fundamentals of Heat Exchanger Design*, John Wiley & Sons, 2003.
- [65] M. McLinden, "Development of the REFPROP Database and Transport Properties of Refrigerants," Physical and Chemical Properties Division National Institute of Standards and Technology, Boulder, CO, USA, 1998.
- [66] American Society of Heating, Refrigerating and Air, *ASHRAE Handbook, Fundamentals*, Atlanta, 1997.
- [67] "Emission Test Cycles: FTP-75 and EPA Highway Fuel Economy Test Cycle," [Online]. Available: <http://www.dieselnet.com/standards/cycles>. [Accessed 28 10 2013].
- [68] D. Wei, X. Lu, Z. Lu and J. Gu, "Performance analysis and optimization of organic Rankine cycle (ORC) for waste heat recovery," *Energy Conversion & Management*, vol. 48, pp. 1113-1119, 2007.
- [69] F. Incropera and D. DeWitt, *Introduction to Heat Transfer*, New York: John Wiley & SONS, 1996.
- [70] A. Hobson, "Energy Flow Diagrams for Teaching Physics Concepts," *The Physics Teacher*, vol. 42, pp. 113-117, 2004.

VITA AUCTORIS

NAME: Gianmarco Capano

PLACE OF BIRTH: Bordighera, Italy

YEAR OF BIRTH: 1989

EDUCATION: Liceo Scientifico A. Apro시오, Diploma di Maturità Scientifica, Ventimiglia, Italy, 2003 – 2008.

Politecnico di Torino, B.Sc. in Automotive Engineering, Torino, Italy, 2008 – 2011.

Politecnico di Torino, Master in Automotive Engineering, Torino, Italy, 2011 - 2012.

University of Windsor, M.A.Sc. in Mechanical Engineering, Windsor, ON, 2012 - 2013.

COMPANY EXPERIENCES (stages): Polytechnic of Turin, Department of Materials Science and Chemical Engineering, Turin, Italy, April 2011 – June 2011.

Chrysler Group LLC., Auburn Hills, Michigan, U.S.A., September 2012 – September 2013.

Fiat S.p.A., Turin, Italy, September 2012 – September 2013.

PUBLICATIONS: “Investigation of the Electric Power Balance in a Vehicle for the Choice of the Battery”. Gianmarco Capano, Maurizio Mozzone, Narayan Kar. ITEC 2013, Dearborn, Michigan, U.S.A., Conference Proceeding.